REPEATED MILD TRAUMATIC BRAIN INJURY IS ASSOCIATED WITH ACUTE MICROVASCULAR DAMAGE IN JUVENILE MALE AND FEMALE RATS

by

Juan Sebastian Triviño Paredes
BSc, Universitat de Barcelona, 2013
MSc, Universitat de Barcelona, 2014

A Dissertation Submitted in Partial Fulfilment

of the Requirements for the Degree of

DOCTOR OF PHILOSOPHY

in the Division of Medical Sciences (Neuroscience)

University of Victoria

We acknowledge with respect the Lekwungen peoples on whose traditional territory the university stands and the Songhees, Esquimalt and W̲SÁNEĆ peoples whose historical relationships with the land continue to this day.

Supervisory Committee

REPEATED MILD TRAUMATIC BRAIN INJURY IS ASSOCIATED WITH ACUTE MICROVASCULAR DAMAGE IN JUVENILE MALE AND FEMALE RATS

by

Juan Sebastian Triviño Paredes
BSc, Universitat de Barcelona, 2013
MSc, Universitat de Barcelona, 2014

Supervisory Committee

Dr. Brian R. Christie, Division of Medical Sciences
Co-supervisor

Dr. Patrick C. Nahirney, Division of Medical Sciences
Co-supervisor

Dr. Craig Brown, Division of Medical Sciences
Departmental Member

Dr. Hector Caruncho, Division of Medical Sciences
Departmental Member

Dr. Jodie R. Gawryluk, Department of Psychology
Outside Member

Abstract

Supervisory Committee

Dr. Brian R. Christie, Division of Medical Sciences
Co-supervisor

Dr. Patrick C. Nahirney, Division of Medical Sciences
Co-supervisor

Dr. Craig Brown, Division of Medical Sciences
Departmental Member

Dr. Hector Caruncho, Division of Medical Sciences
Departmental Member

Dr. Jodie R. Gawryluk, Department of Psychology
Outside Member

Traumatic Brain Injury (TBI) is a growing global health problem. Mild forms of TBI (mTBI) such as concussions, represent the most common manifestation of this type of injury with children and youth (< 20 years old) among the most likely to sustain mTBI. There is growing evidence for the cumulative effects of repeated mTBI (rmTBI) suggesting that while a single concussion may not cause evident or long-lasting brain alterations, the summation of multiple mTBI may lead to more severe consequences. In contrast to severe TBI, lesions in mTBI patients are challenging to detect. Despite this, mTBI patients may still present with cognitive and emotional deficits. Cerebral microbleeds (CMBS), a subtle form of vascular damage, have been identified as an early hallmark in brain trauma and several neurodegenerative diseases. The cumulative effects of subtle but sustained microvascular damage could explain the persistent long-term functional deficits observed in mTBI. In this study, the awake closed-head injury (ACHI) model was used to investigate the association between rmTBI and microvascular damage in different brain regions in both male and female juvenile rats at one and seven days after the last injury. The results indicate that the injury paradigm used in this study (i.e. 8 impacts over 4 days) using the ACHI model is associated with an acute increase in sings of microvascular damage in both sexes that is no longer evident at a longer time point. These study is the first to describe the negative impact of rmTBI on CMBs in the juvenile using an awake animal model, and provides evidence for the potential involvement of this subtle form of vascular damage in the development of neurological deficits after rmTBI.

TABLE OF CONTENTS

LIST OF TABLES

LIST OF FIGURES

LIST OF ABBREVIATIONS

ACA	Anterior Cerebral Artery
ACHI	Awake Closed Head Injury
AD	Alzheimer's Disease
ADP	Adenosine Diphosphate
ATP	Adenosine Triphosphate
BBB	Blood Brain Barrier
BSA	Bovine Serum Albumin
CA1	*Cornu Ammonis* 1
CA3	*Cornu Ammonis* 3
CCI	Controlled Cortical Injury
CT	Computed Tomography
CTE	Chronic Traumatic Encephalopathy
CMB	Cerebral Microbleeds
CMR	Cerebral Metabolic Rate
CNS	Central Nervous System
CR3	Complement Receptor 3
CSF	Cerebrospinal Fluid
DAB	3,3′-diaminobenzidine
DAMPs	Damage Associated Molecular Patterns
DAPI	4′,6-diamidino-2-phenylindole
DiI	1,1′-dioctadecyl-3,3,3′,3′-tetramethylindocarbocyanine perchlorate
DNA	Deoxyribonucleic acid
EtOH	Ethanol
Fe^{3+}	Ferric Ion
FPI	Fluid Percussion Injury
GCS	Glasgow Coma Score
H_2O	Dihydrogen Oxide (water)
HCl	Hydrochloric Acid
HR	Hazard Ratio
IBA1	Ionized Calcium-Binding Adaptor Molecule 1
ICH	Immunohisto Chemistry
IgG	Immunoglobulin G

K^+	Potassium
MCA	Medial Cerebral Artery
MRI	Magnetic Resonance Imaging
mRNA	Messenger Ribonucleic acid
MS	Multiple Sclerosis
mTBI	Mild Traumatic Brain Injury
NAP	Neurological Assessment Protocol
NAPDH	Nicotinamide Adenine Dinucleotide Phosphate
PBS	Phosphate Buffered Saline
PCA	Posterior Cerebral Artery
PCS	Post-Concussive Syndrome
PD	Parkinson's Disease
PFA	Paraformaldehyde
PID	Post-Injury Day
PND	Post Natal Day
RBC	Red Blood Cell
rmTBI	Repeated Mild Traumatic Brain Injury
RNA	Ribonucleic acid
ROI	Region Of Interest
ROS	Reactive Oxygen Species
RT	Room Temperature
SCAT	Sports Concussion Assessment Tool
TAI	Traumatic Axonal Injury
TBI	Traumatic Brain Injury
TDE	Thiodiethanol
TMEM119	Transmembrane Protein 119
WD	Weight Drop
WGA	Wheat Germ Agglutinin

Acknowledgments

First, I would like to thank my co-supervisors Dr. Brian Christie and Dr. Patrick Nahirney for taking a chance on me and helping me grow both academically and personally. Your support and guidance has made the past six years in the Division of Medical Sciences an incredible opportunity to expand my technical and scientific toolbox. This thesis would not have been possible without you, thank you! And thank you for all the lab meetings at Fel's too!

I would also like to thank my supervisory committee members, Dr. Craig Brown, Dr. Hector Caruncho and Dr. Jodie Gawryluk for your feedback and suggestions on my research and your support and enthusiasm in shaping this thesis into what it is today.

To the Neuroscience Graduate Program administrative staff members, for their endless support. I can say without hesitation that I would be years behind in my studies without your incredible support. Evelyn Wiebe, Erin Gogal, Heather Alexander, Chii Kong, Nicole Coutts, Lori Aasebo and Sara Ohora, I am forever grateful for all the help you have provided me throughout my graduate studies.

To the Animal Care Staff for always being there looking after the wellbeing of the animals. Thank you! And thank you for teaching me everything I know about rats and ethics, you have been an amazing support and I consider myself very lucky to have had you throughout my graduate studies.

To the Christie lab family, past and present, thanks for everything! Dr. Anna Patten and Dr. Joanna Gil-Mohapel, thanks for opening the lab doors to me and kicking off my neuroscience adventure by teaching me *in vivo* electrophysiology and helping me publish my first paper. Thanks for being there as mentors during my initial steps, you are amazing. To Dr. Christine Fontaine, for always being there to provide feedback and help in every single step of this journey and dissertation. All the experimental planning, document edits and all your thorough presentation notes. And for putting up with me and my microscope invading your little room. To Ryan Wortman for all your help in my first steps in the TBI model and project, and for introducing me to Saint Frank's and the Drake. And for visiting us in Barcelona, can't wait to see you again soon, I promise I won't use all the hot water next time. To Katie Neale, for introducing me to the world of pens and notebooks. I had no idea I had such strong feelings about these. And for your help in the TBI project. To Melissa Clarkson for adding dad jokes to lab meetings agendas, and for making the confocal tutorial, it definitely save me a lot of time! To Dr. Luis Eduardo Bettio De Sousa, for all your duck and immunostaining expertise and always being down for a Fels evening (or afternoon, let's be honest). And remember, as the Spice Girls say, "You got it, you got it". To Erin Grafe, for being awesome. You are an amazing person and scientist; I am sure that you will accomplish anything you aim for. To Dr. Jon Thacker for all our interminable science and projects conversations. And for all the games nights, in person or online. I wish you the best of luck out east! Also thank you to all the new incorporations to the Christie and Nahirney labs, Taylor, Hannah, Stan, Irene, Charlotte. Best of luck on your endevaours.

To the Neuroscience Graduate Program student and trainee body – thank you for all the memories! To the Caruncho's OG, especially Raquel, for bringing all us together and for all the chicken stories. To Ben, Carla, Jenessa, Josh, Juan SA, Laura H, Mo and Luis for all the "What does the fox says", "Chum Drum Bedrum" and "Hasta el amanecer".

To the outside of the lab family, thanks for making Victoria feel like home! To Josh and Niki, you have always been there for us. Who would have thought that a weird conversation about Jennifer Aniston neurons would start our very special relationship? Thanks for coffees, beers and dances. You are family. To your first born Diego, for all the loving howls and fluffy fur. To Thalia, for all her hugs and kisses and for learning to say "kikiriki" before "cock-a-doodle-doo". And of course to Maisie, for always having something to say and for the cutest frown face I have ever seen.

To Melissa and Shaq for their lessons on everything: from how to build furniture and make sausages, to how to operate a boat with no gas on your way to Bamfield. To Boof, for all the drools and loving hugs. Christine, Ryan and Penny for the countless rides home and ear cleanings and for all the knowledge on weird diets, we miss you on the west coast! Laura and Chris, for opening your families and allowing us to be part of your special moments. For encouraging dips in frozen lakes and for all the peaches. I hope we can keep sharing experiences regardless of where we all end-up. – To all of you, thank you! I could not have asked for a better family!

And to my Colombian/Spanish family. My parents and brother, thank you so much for everything you do. Your never-ending support have got me to where I am today and nothing in my life would be possible without your love pushing me forward. I couldn't have done it without you. Gracias mis amores! To the Pinar Cabeza de Vaca family, thanks for welcoming me into your family, for all the visits and trips and thank you for all the pop-corn moments. Gràcies! To Dr. Amanda Fernandez for all the visits, mojitos and "cotorras" moments, and for all your stats master classes. To Alexia and Katxe for being our Spanish family in Canada. For all those weekend camps in Gordon Head or View Street, you really were the pillar of our first 2 years here and we miss you everyday! Gracias!

And finally to the person I am most indebted to: Cristina Pinar. Thank you for your endless support in the laboratory and outside. Thank you for helping me pushing my PhD project forwards and for constantly setting some fire under my butt. Without you, I would have taken 20 years to finish my PhD. Thanks for celebrating victories with me and pulling me up from the mud during hard times. Thank you for giving balance to my life, standing all my nerdy stuff, "forcing" Zoey into our lives, and anchoring me to reality by reminding me of the important things in life and by synchronizing my Juan's Standard Time (JST) zone to the rest of the world. You are also the best partner in crime I could have asked for.

Dedication

This work is dedicated to my parents and brother, whose constant love and support keeps pushing me forward.

CHAPTER 1: GENERAL INTRODUCTION

For centuries, humans have known that receiving impacts to the head can lead to immediate consequences that range from subtle physical, cognitive or emotional impairments to death. These consequences of these impacts were primarily caused by damage to one of our most important organs, the brain.

In cases of severe head trauma, it is easy to identify the features and location of what is often focal brain damage, and these events have always been treated as what they are, immediate life-threatening injuries. Although the nature of these types of injuries is diverse and the severity spectrum wide, to date the majority of our understanding on traumatic brain injury (TBI) comes mainly from severe cases. However, in the last 15 years, there has been growing evidence of the long-term consequences of milder forms of TBI. This fact in combination with the difficulty identifying associated brain damage in this milder type of brain injury has encouraged a deeper investigation on subtler pathophysiological manifestations of TBI. In this dissertation my aim is to advance our understanding of the pathophysiology of mild TBI (mTBI) by providing tangible evidence of subtle structural changes that accompany this injury. I want to help grow the promising and growing body of scientific knowledge in this field with the ultimate goal of helping increase the life quality of those affected by these brain injuries.

I will start this dissertation by providing background information that will help contextualize the research presented in this study. First of all, I will provide an overview

of the definition, epidemiology and classification of TBI. Next, I will review the evidence around the pathophysiological events that happen during TBI and the cognitive and emotional consequences including the relevance of repeated mTBI (rmTBI). Subsequently, I will provide a description of the animal models currently used to investigate head trauma and I will introduce the model used in this dissertation: the awake closed-head injury (ACHI) model. I will follow with an overview of the brain vascular system and finally, I will review how the brain reacts to vascular injuries of different severities and how maladaptive responses can lead to prolonged brain damage. Regarding this last part, I will focus on the relevance of cerebral microbleeds (CMBs) in several central nervous system (CNS) diseases and their potential critical role as early events in mTBI pathophysiology. This general introduction will end with a proposed mechanistic link between rmTBI and neurodegenerative diseases with fibrinogen as the putative common factor. Following this I will review the general methods used for this dissertation ("**2. General Materials & Methods**"), then I will present and discuss my results ("**3. How can we measure cerebral vascular damage?"** and "**4. Is rmTBI associated with increased cerebral microvascular damage and microglia reaction?"**) and I will end this dissertation with a general discussion (**"5. General Discussion"**).

1.1. Traumatic Brain Injury

1.1.1. Definition, Epidemiology and Classification

The most common causes of brain injuries are cerebrovascular accidents and external mechanical forces. TBI is defined as a sudden change in brain position induced

by external mechanical forces transmitted to the head that results in damage to this organ. TBI has received increasing attention due to recent reconsiderations of its epidemiology, the variables affecting its severity and the long-term consequences of this type of brain injury (Saatman et al., 2008; Voss et al., 2015; Mayer et al., 2017; McInnes et al., 2017; Greco et al., 2019). It is estimated that every year, over 160,000 individuals in Canada experience some form of TBI and currently ~1.5 million Canadians have their lives affected by this type of brain injury with an estimated annual cost of ~$3 billion (Fu et al., 2015). The biophysical mechanisms that cause brain damage in TBI are usually presented as penetrating forces (e.g. sharp object piercing the skull), acceleration-deceleration forces (e.g. car accident or aggressive tackle in a rugby game) blast waves (e.g. explosions) or a combination of these. The leading causes of non-fatal TBI are falls (35%), motor vehicle-related injuries (17%) and strikes or blows to the head from or against an object (17%) such as in sport injuries (Faul et al., 2010).

TBI severity is classified as mild, moderate and severe depending on the patient's history and clinical manifestations. Although potentially broad, the clinical history provides important context on the circumstances leading to the injury (e.g. patient was in a serious car accident; patient was tackled in a rugby game, etc.). Clinical manifestations include presence and duration of loss of consciousness, presence and duration of mental confusion/disorientation, presence and location of abnormal structural brain imaging and the Glasgow Coma Scale (GCS) (Teasdale and Jennett, 1974), a set of behavioural tests that evaluate ocular, motor and verbal responses. All these

parameters are taken into account when evaluating a TBI patient (O'Neil et al., 2013). **Table 1** summarizes the criteria used for each type of TBI severity. In addition, common imaging techniques such as Computed Tomography (CT) and Magnetic Resonance Imaging (MRI) scans are routinely performed in TBI patients to rule out severe lesions like meningeal hemorrhages or skull fractures that would require immediate attention. Although some imaging techniques have shown promising improvements in the last 5 years (Wu et al., 2016), they are still mainly used to detect macroscopic damage and are not sensible enough to identify subtler forms of brain alterations.

Mild TBI represents the most common type of TBI in the population (~80%) (NCIPC, 2003; Thomas R. Frieden, Debra Houry, 2015). In contrast to more severe forms of TBI, lesions in mTBI patients are challenging to detect and show negative results in common diagnostic imaging techniques. Mild forms of TBI are consensually defined as an injury to the head resulting in loss of consciousness for < 30 min and/or confusion and disorientation for < 24 hrs, a GCS of 14 or greater and normal structural imaging (Belanger et al., 2007; Petchprapai and Winkelman, 2007; Iverson, 2010; Gao and Chen, 2011) (**Table 1)**. It is important to note that although some studies use interchangeably mTBI and concussions, there are inconsistencies in the field and a large body of literature classifies concussion as a mild form of mTBI (Mayer et al., 2017). Despite not showing overt signs of brain damage, mTBI individuals may still present with cognitive, emotional, sensory and motor impairments (Cicerone and Kalmar, 1995; Carroll et al., 2004; Cole and Bailie, 2015). The lack of evident brain lesions in mTBI patients makes

diagnosis and prognosis of this injury primarily a response to a myriad of potential behavioural symptoms at presentation rather than a physical injury. As a consequence, despite efforts to create standardized behavioural measures like the GCS (Teasdale and Jennett, 1974) and the Sports Concussion Assessment Tool (SCAT) (Echemendia et al., 2017), there is not yet a reliable objective test to diagnose mTBI, assess the severity of the lesion, or determine the prognosis of concussion patients. Consequently, the need for reliable indicators of the resulting mTBI pathology has become a health research priority (Saatman et al., 2008; Blennow et al., 2012a; Jeter et al., 2013).

Although the elderly (> 64 years old) is the population that present with more severe and long-lasting effects following mTBI, it is important to note that children and youth (≤ 20 years old) are among the most likely to sustain this type of brain injury. (Susman et al., 2002; CIHI, 2006; Fu et al., 2015; Thomas R. Frieden, Debra Houry, 2015; Taylor et al., 2017). Indeed, high school athletes commonly experience this type of brain injury and 15% of these sport-related concussions are recurrent injuries (Castile et al., 2012; Marar et al., 2012). In addition, this age group can be particularly susceptible to the effects of mTBI, because during this period, the sensory and motor systems responsible for head stability are not fully established (e.g. development of neck muscle strength and tone, head positioning, etc.) and the brain is undergoing significant synaptic reorganization and myelination (Verger et al., 2000; Carmody et al., 2004; Koizumi, 2004; Haynes et al., 2005). Therefore, mTBI has the potential to impair the normal brain development of children and adolescents producing long-lasting cognitive effects that could critically affect the

quality of life during adulthood. Moreover, there are documented sex differences in mTBI (Bazarian et al., 2010), with young males more frequently sustaining mTBI, but young females more likely to experience persistent symptoms. However, this observation is still under debate and the causes of these sex differences remain unclear. Surprisingly, despite the epidemiological evidence of age and sex distribution in mTBI, juvenile and female individuals are still underrepresented in experimental models of this injury (Bazarian et al., 2010; Bodnar et al., 2019; Merritt et al., 2019).

	Mild TBI	Moderate TBI	Severe TBI
Structural brain imaging	Normal	Normal or abnormal	Normal or abnormal
Loss of consciousness	0-30 min	30 min to 24 hrs	> 24 hrs
Altered mental state	≤ 24 hrs	> 24 hrs	> 24 hrs
Post-trauma amnesia	≤ 1 day	1 – 7 days	> 7 days
Glasgow Coma Scale score	13-15*	9-12*	< 9*

Table 1. Classification of TBI Severity. Mild forms of TBI or concussions are consensually defined as an injury to the head resulting in loss of consciousness for < 30 min and/or confusion and disorientation for < 24 h, a GCS of 14 or greater and normal structural imaging. Adapted from Traumatic Brain Injuries Review (Blennow et al., 2016). *Best score obtained in the first 24 hr following the injury.

1.1.2. Pathophysiology

1.1.2.1. Primary Injury

The damaging effects induced by TBI are classified into two main phases: primary and secondary injury **(Fig. 1)**. The initial impulsive forces that produce the head trauma are the cause of the primary injury. In this initial phase, the brain tissue sustains a sudden

mechanical stress that may induce necrosis, diffuse axonal injury and diffuse vascular injury (Ray et al., 2002; Werner and Engelhard, 2007; Pekna and Pekny, 2012).

Understanding the biomechanics of energy transmission from external forces to the brain and the effects of this physical stimulus on the brain tissue and its cellular components is critical for understanding TBI in all its severity types. There have been several efforts on this with both animal models and computational simulations using finite element models (Lamy et al., 2011; Yang et al., 2014; Shultz et al., 2016; Wu et al., 2017). The current understanding is that despite the protection that the skull and cerebrospinal fluid (CSF) provide, a head injury that occurs even without skull fractures, can damage the brain tissue via acceleration and deceleration forces. The physical properties of the brain tissue show that this organ has a non-linear behaviour in response to applied loading rate. This means that the brain is resistant to shape changes when subjected to pressure forces but it can deform easily in response to shear forces compared to other biological tissues (Arbogast et al., 1997; Donnelly and Medige, 1997; Miller and Chinzei, 1997; Prange-Kiel et al., 2003; Takhounts et al., 2003). A growing number of studies have evaluated the impact of shear deformation and rotational forces in comparison to other forces and their results suggest that shear deformation could be the main injury trigger in concussions (Unterharnscheidt and Higgins, 1969; Adams et al., 1982; Gennarelli et al., 1982; Ivancevic, 2009; Cloots et al., 2013). In addition, the anatomical location and structure of different brain regions can make certain areas more susceptible to the shearing forces. For instance, it has been observed that those areas with

abrupt changes in tissue composition like grey-white matter interfaces are particularly vulnerable to this sheer stress (Kotapka et al., 1992; Tate and Bigler, 2000; Bigler et al., 2002; Tomaiuolo et al., 2004; Serra-Grabulosa et al., 2005; Cloots et al., 2013; Bigler, 2018).

1.1.2.2. Secondary Injury

The initial events in the primary injury can subsequently trigger a secondary injury phase that is characterized by a myriad of changes that include alterations in energetic metabolism, redox status, neuronal structure, inflammation and homeostasis of glutamate and calcium **(Fig. 1)** (Fineman et al., 1993; McIntosh et al., 1997; Sun et al., 2008; Pekna and Pekny, 2012; Weber, 2012; Walker and Tesco, 2013). However, in human mTBI patients, these alterations are difficult to detect and as a result concussions are described as "silent injuries". It is possible that the current diagnostic tools lack sufficient power to detect subtle structural alterations in brains of mTBI patients, or that due to our incomplete understanding of the pathophysiology of milder forms of TBI we do not know what to look for to pinpoint these subtle alterations. Vascular damage and inflammation are factors that have been identified as early hallmarks both in brain trauma (Hay et al., 2015) and in several CNS diseases including Alzheimer disease (AD)(Wyss-Coray and Rogers, 2012; Zamolodchikov and Strickland, 2016), multiple sclerosis (MS) (Davalos et al., 2012; Ryu et al., 2015a), and chronic traumatic encephalopathy (CTE) (Mckee et al., 2018), a neurological disorder triggered by repeated impacts to the head. This suggests a potential common triggering mechanism and provides with possible pathological indicators and therapeutic targets in initial phases of these CNS alterations. In this

dissertation the focus will be centered on the vascular damage and inflammatory aspects of rmTBI, because even subtle forms of damage to blood vessels in the brain, when accumulated over time have the potential to trigger or exacerbate subsequent events in the secondary injury phase (e.g. inflammation) and lead to long-lasting structural and functional deficits **(Fig. 1)**.

Because of the nature of mTBI, the damage caused in the primary injury is only partially avoidable by reducing the exposure to such events and taking safety precautions. On the other hand, events in the secondary injury phase occur over time and initiate a variety of signalling cascades that can last hours to years after the injury and contribute to long-lasting disabilities. Therefore, preventing or mitigating the effects of the damaging processes in the secondary injury phase may be critical to improving the lives of mTBI patients (Salehi et al., 2017)

1.1.3. Cognitive and emotional deficits and synergistic effects of rmTBI

While most mTBI patients recover quickly from their injuries (days to weeks), up to one fifth may continue to have prolonged symptoms like learning and memory problems, gait disturbances, epilepsy, sleep patterns modifications, and emotional alterations (McMahon et al., 2013). Commonly in the literature, the term "Post-Concussive Syndrome" (PCS) is used to describe these long-term neurobehavioral sequelae that some individuals experience after mTBI (Hall et al., 2005; Hsu et al., 2015; Voormolen et al., 2018). Some risk factors associated with PCS have been identified in recent years. These factors include advanced age, female sex, prior history of head injury, lower education,

personality disorder 13 and pre-existing cognitive dysfunction (Bazarian et al., 2005, 2010; Scopaz and Hatzenbuehler, 2013; Polinder et al., 2018).

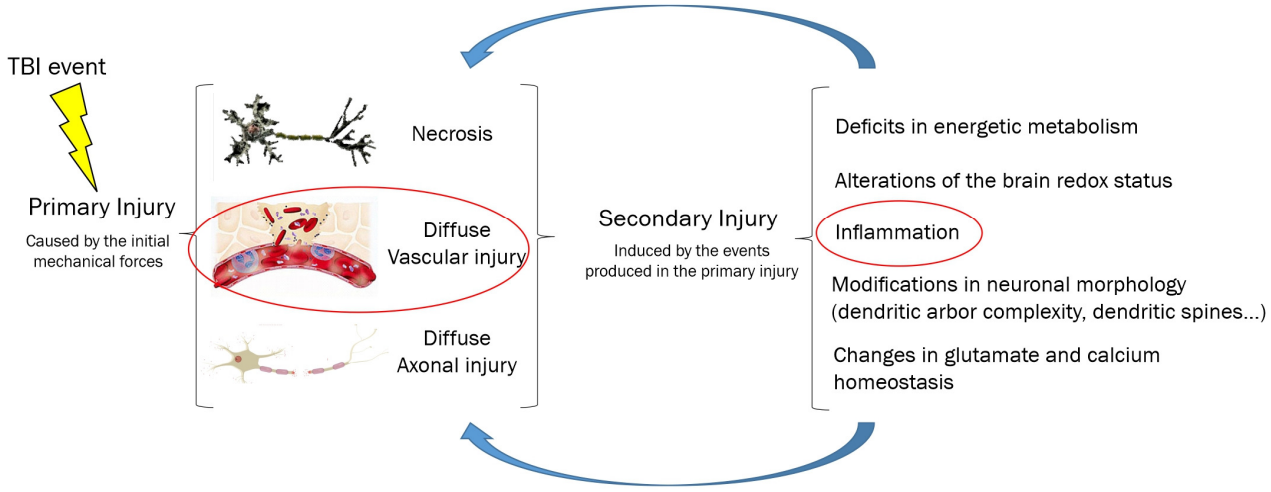

Figure 1. TBI Pathophysiology. TBI pathophysiology is classified into two main phases: primary and secondary injury. The initial impulsive forces that produce the head trauma are the cause of the primary injury. In this initial phase, the brain tissue sustains a sudden mechanical stress that may induce necrosis, diffuse axonal injury and diffuse vascular injury. The initial events in the primary injury trigger the secondary injury phase, characterized by a myriad of changes that include alterations in energetic metabolism, redox status, neuronal structure, inflammation and homeostasis of glutamate and calcium. Preventing or mitigating the effects of the damaging processes in the secondary injury phase may be critical to improving the lives of TBI patients. This study will focus on the vascular damage and inflammatory aspect of repeated mTBI, because even subtle forms of damage to blood vessels in the brain, when accumulated over time, have the potential to trigger or exacerbate subsequent events in the secondary injury phase (e.g. inflammation), create a pathological loop and lead to long-lasting structural and functional deficits.

There is a growing body of literature providing evidence for a correlation between history of multiple concussions and increased learning and memory disabilities (Bijur et al., 1996; Matser et al., 1998; Wall et al., 2006), anxiety, personality changes, depression and post-traumatic epilepsy (Lowenstein et al., 1992; Jorge et al., 2004; Agrawal et al., 2006; Hart et al., 2011). In addition, it has been reported that rmTBI increases the risk of developing

dementia (Guskiewicz et al., 2005; Lee et al., 2013) and other neurodegenerative diseases (McKee et al., 2009; Masel and DeWitt, 2010). For instance, a recent large-scale study of nearly 13,000 patients reported that TBI increases the pathogenic hazard ratio (HR) for neurodegenerative diseases by a factor greater than 3 (Chu et al., 2016). This data highlights the cumulative implications that concussions may have. Indeed, in the last decade the synergistic deleterious effect of rmTBI has been identified as a key element in injury severity (Guskiewicz et al., 2003; Prins et al., 2012; Fehily and Fitzgerald, 2017; Greco et al., 2019). This means that, while a single concussion may not cause evident or long-lasting structural and functional deficits, it may render the brain vulnerable to subsequent injuries, creating a window of susceptibility where the accumulation of multiple mild concussive events may lead to more severe injuries and long-term cognitive dysfunction (Guskiewicz et al., 2003; Prins et al., 2012; Fehily and Fitzgerald, 2017). This cumulative non-linear effect of mild but sustained brain damage driven in part by vascular lesions and inflammation could explain the persistent functional deficits observed in this type of injury and sudden complications like second impact syndrome. In addition, this phenomenon could provide a putative mechanistic link between repeated concussions and its reported correlation with the development of tauopathies such as AD and CTE (Guskiewicz et al., 2003; McKee et al., 2009; Johnson et al., 2010; Masel and DeWitt, 2010; Blennow et al., 2012b; Mckee et al., 2018).

Finally, it is important to note that the effects of rmTBI can manifest in pediatric and juvenile populations as academic failure, chronic behavioural problems, social isolation

and difficulty with employment, relationships and in some cases problems with the law (Hendryx and Verduyn, 1995; Ewing-Cobbs et al., 2004; Gerrard-Morris et al., 2010; Huw Williams et al., 2010). Because this behavioural pattern is commonly observed in populations of this age range, potential changes caused by rmTBI can be mistakenly attributed to other causes like lack of motivation, laziness, adolescent-like behaviour and even bad parenting (Wade et al., 2006). This makes the proper diagnosis and monitoring of this type of injury in the juvenile population an even harder challenge.

1.1.4. Preclinical models of TBI

Several pre-clinical models of TBI have been developed to better understand the fundamentals of this biomechanical injury and provide translational advances to improve the diagnosis, treatment and prognosis of brain trauma patients. Given the wide severity spectrum and the heterogeneity of TBI, different models have been developed to this day (Shultz et al., 2016). Some of these models include the weight drop (WD) model (Feeney et al., 1981; Foda and Marmarou, 1994), the fluid percussion injury (FPI) model (Dixon et al., 1987; Gennarelli, 1994), the controlled cortical impact (CCI) model (Dixon et al., 1991; Lighthall, 1988; Lindner et al., 1998), the blast injury model (Cernak et al., 1996; Leung et al., 2008), the CHIMERA model (Namjoshi et al., 2014; Cheng et al., 2019), the lateral impact model (Mychasiuk et al., 2014) and the ACHI model (Petraglia and Huang, 2013; Meconi et al., 2018a; Pinar et al., 2020). These models are predominantly used in rodents, however models for animals with gyrencephalic brains like ferrets, pigs, cats, rabbits, sheep and others have also been developed (Vink, 2018). Experimental TBI

can induce focal or diffuse injuries, and can be delivered on an open or closed head (i.e. brain exposed or intact skull). If the reader is interested in a more extensive review of different animal models of TBI please see (Petraglia et al., 2014a; Xiong et al., 2014; Shultz et al., 2016; Bodnar et al., 2019). It is important to consider that even within the same model, small adjustments can be adopted by different research groups (e.g. changes in piston velocity, presence of helmet, type of impact tip etc.), so it is crucial to carefully assess the methodology of the studies when evaluating TBI literature.

In this dissertation, the ACHI model was used. Compared to other models, the ACHI model does not need craniotomy surgery or skull exposure. This allows to avoid potential confounding factors introduced by chronic systemic inflammation (Shultz et al., 2015; McDonald et al., 2016). In this model, the impacts are delivered to restrained but fully conscious animals without the need of anesthesia. This point is important given that anesthesia has been reported to be neuroprotective (Seto et al., 2014; Jiang et al., 2017) and therefore could mask some of the manifestations triggered by mTBI. The lack of anesthesia also allows to perform an immediate evaluation of sensory-motor functions following mTBI, a common practice in the human population. In addition, in the ACHI model in order to help target the piston tip and to distribute the impact forces and prevent skull fractures, animals are provided with a 3D printed plastic helmet. Indeed, previous studies published by our research group show that our model does induce acute and short-lived sensorimotor alterations without evident brain tissue damage (Meconi et al., 2018a; Pinar et al., 2020). All these factors can be considered an improvement over

previous models as they likely make the ACHI model more representative of clinical rmTBI. More details about this mTBI model will be described in "Chapter 2: General Methods".

1.2. General organization of the cerebral vascular system and response to damage

1.2.1. Characteristics of brain circulatory system, function and blood supply

Despite evident differences between species, the structures and functions of the circulatory system responsible of maintaining brain homeostasis and supporting the high energetic demand of this organ are remarkably conserved. In humans, while being only 2% of the body mass, the brain is responsible for ~20% of energy demand. This is not surprising given the continuous information processing and interpretation that this organ performs to make sense of both our internal and external environments. Rodent and human brains have limited glycogen reserves, so this organ relies heavily on constant and proper energy and oxygen transport provided by the circulatory system. Interruption of cerebral blood flow very quickly results in neuronal death and for instance, after cardiac arrest, apoptosis of neurons begins almost immediately, and irreversible brain damage occurs after about only 5 min (Hossmann, 2006). Most of the energy consumed by the brain is used by neurons to generate nerve impulses and to maintain ion gradients (Attwell and Laughlin, 2001; Shulman et al., 2004; Raichle and Mintun, 2006). Across several species, the circulatory system is also responsible for clearing by-products generated in normal brain metabolism and for preventing the passage and removing potential harmful molecules from the brain.

The blood supply to the human and rodent brains arises form two primary sources: the internal branches of the carotid arteries and the vertebral arteries. These arteries fuse at the base of the brain and form the circle of Willis, an important vascular structure that provides redundant blood flow routes that can be used in case of vessel blockades **(Fig. 2)**. From there, the internal branches of the carotids become the anterior cerebral arteries (ACA) and middle cerebral arteries (MCA), providing blood supply to most midline portions of the frontal lobes and superior parietal lobes and to temporal lobes, insular cortex and deep subcortical structures (e.g. basal ganglia) respectively **(Fig.2)**. Before merging into the circle of Willis, the vertebral arteries are joined together to form the basilar artery that in turn gives rise to the posterior cerebral artery (PCA), pontine arteries and cerebellar arteries. These vessels provide blood supply to the occipital lobes, inferomedial surface of the temporal lobes (including hippocampal formation), midbrain, thalamus and choroid plexus, and to the pons and cerebellum, respectively. From the circle of Willis, cerebral and pial arteries are distributed along the surface of the brain within the subarachnoid space from which arteries and arterioles penetrate into the brain parenchyma perpendicular to the brain surface. However, on their path to the brain surface, several vascular branches such as the lenticulostriate, hippocampal or choroidal arteries arise providing blood supply to deeper brain structures **(Fig. 2)**.

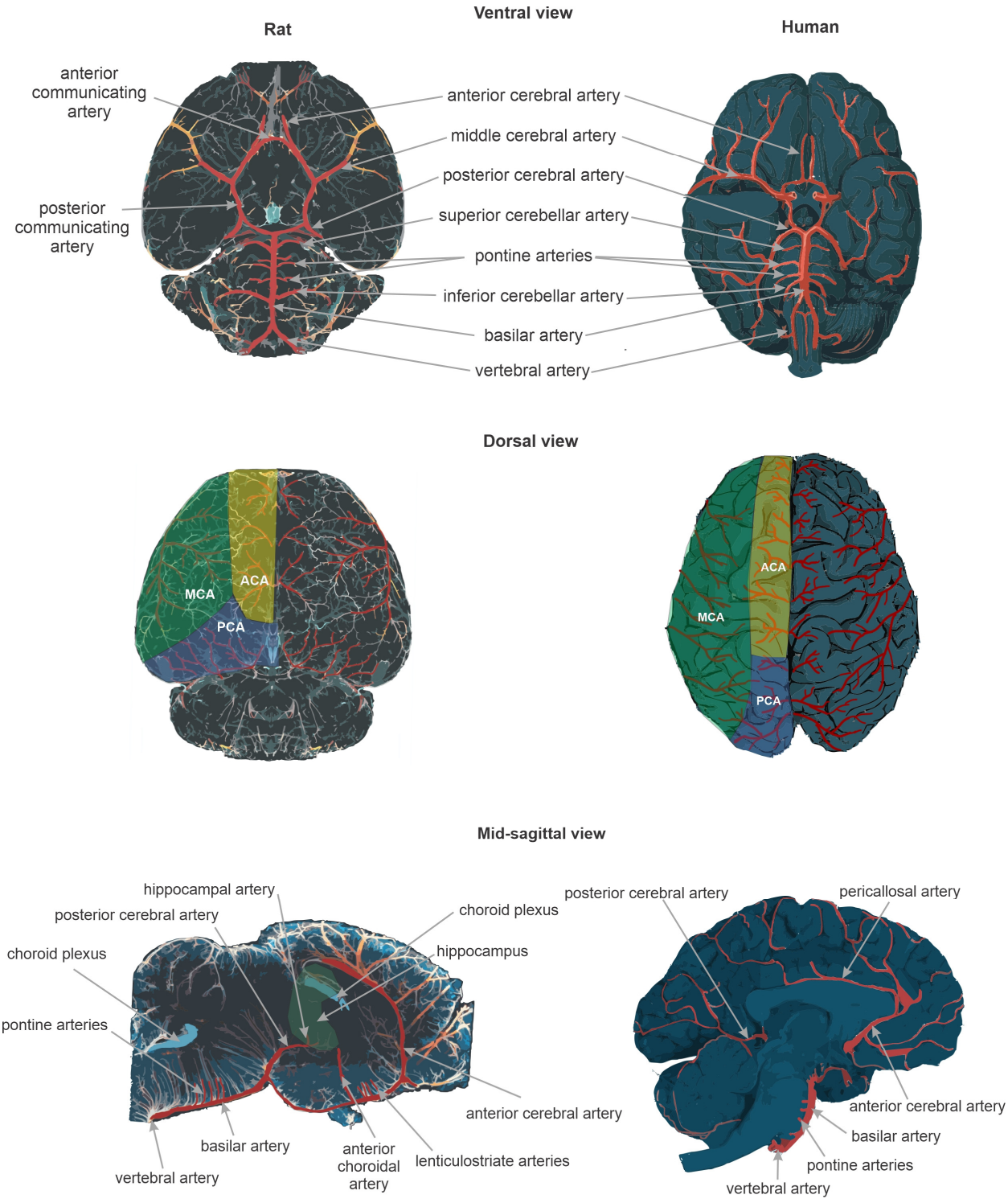

Figure 2. Overview of brain vascularization in the rat brain. Major arteries (red) in the rat and human brains are displayed in a ventral, dorsal and mid-sagittal views. Approximate vascular territories supplied by the posterior cerebral artery (PCA), middle cerebral artery (MCA) and anterior cerebral artery (ACA) are indicated in the dorsal view with blue, green and yellow respectively. The location of the hippocampus

is provided in the mid-sagittal view of the rat brain to provide an anatomical reference. Images inspired by the excellent brain vascular mapping work reported in (Kirst et al., 2020).

In order to reach every cell in the brain, the circulatory system has a highly ramified and vast capillary network **(Fig. 3)**. Capillaries in the human brain may be as small as 5-10 μm in diameter and the average intercapillary distance is about 40 μm. As a consequence, the cell body of a neuron is typically about 10-20 μm from the nearest capillary (Cipolla, 2009; Zlokovic, 2009; Smith et al., 2019). Indeed, this mesh of capillaries is so extensive that the total microvessel length in the adult human brain has been estimated to be at about 600 km (Wong et al., 2013). Capillaries form numerous connections (known as capillary beds) before merging into venules and veins, and the blood flows out of the brain through various venous sinuses and finally through the internal jugular veins. While arteries, arterioles, veins and venules are ensheathed in one or more layers (e.g. smooth muscle, connective tissue) and have a perivascular space, capillaries are tightly surrounded by pericytes and astrocyte end-feet. Indeed, these two cell types are part of the blood-brain barrier (BBB), a highly specialized barrier that controls what gets in and out the brain and that will be described in more detail in a subsequent section.

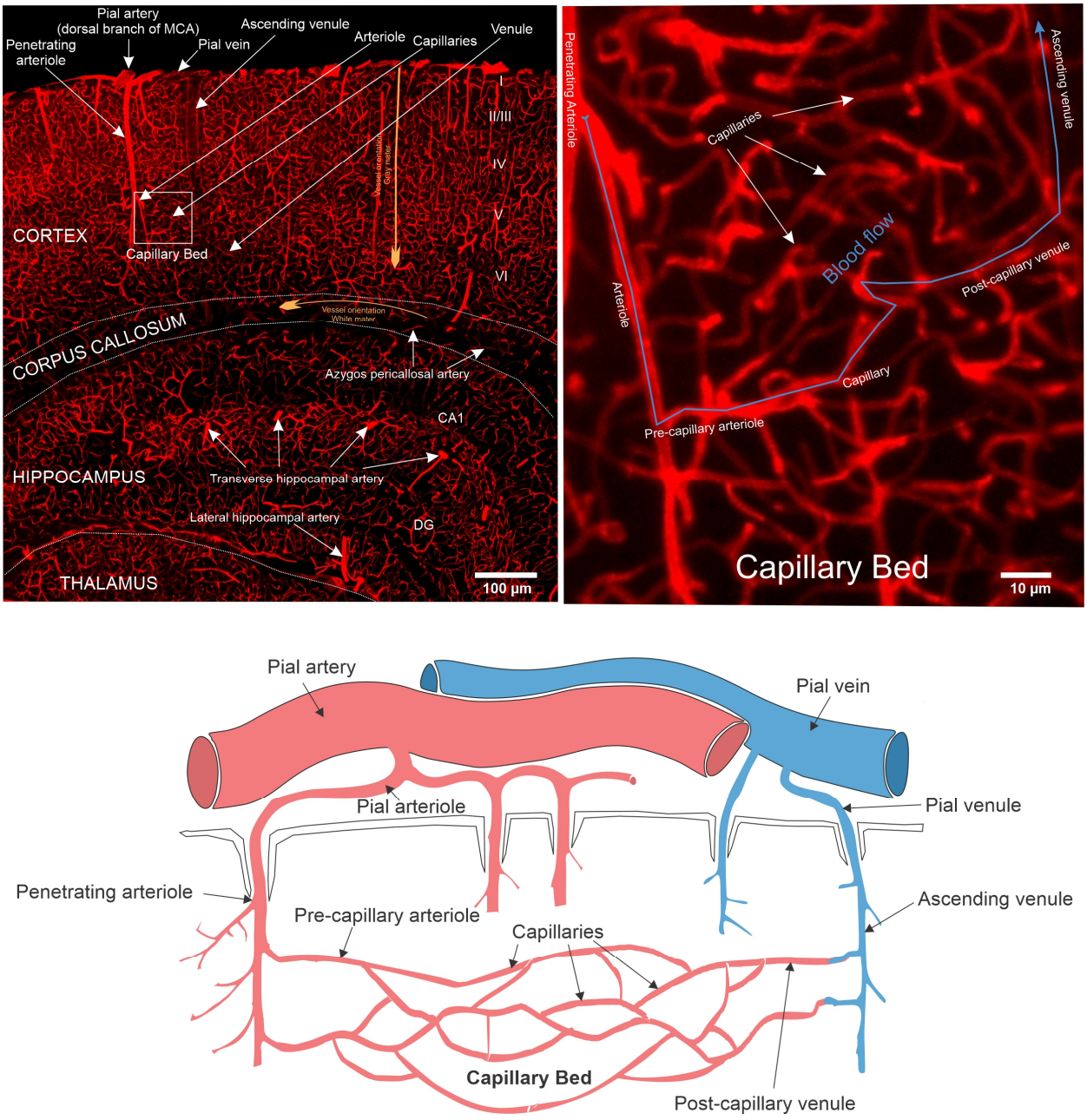

Figure 3. Vessel hierarchical organization and gray-white matter differences. Top panel shows an example of brain vasculature stained with wheat germ agglutinin (WGA) conjugated with AlexaFluor-555 and acquired with epifluorescence microscopy. We can observe the vessel hierarchy starting with pial arteries that descend into the brain parenchyma becoming penetrating arterioles. These vessels continue their ramification and give rise to smaller caliber arterioles and finally to pre-capillary arterioles. After this

we can see the formation of capillaries, and capillary beds (mesh of capillaries) were the majority of nutrient and other molecule exchanges occurs. After this, capillaries converge into post-capillary venules that in turn drain into small caliber venules, ascending venules and then to pial veins that guide blood flow out of the brain thorough diverse sinuses and finally through the jugular veins. Differences in gray and white matter can be observed in this image including vessel orientation and vascular density.

1.2.2. Brain vasculature across species

Brain vasculature in humans and rats have many common features and therefore this animal model has been very helpful to increase our understanding of the circulatory system in the human brain. Initial vascularization of the human and rat brains share a similar pattern, with sprouting angiogenesis populating the cortex from a pial network of vessels (Walls et al., 2008; Marín-Padilla, 2012). This is reflected in the fact that the gross vascular anatomy is similar between species. The brains of both rats and humans are supplied by the same major arteries that also share similar perfusion territories in each species (Kandel et al., 2013; Xiong et al., 2017). The vascular architecture consisting of penetrating vessels arising from pial vessels in the subarachnoid that feed and drain a network of capillaries back to pial vessels is also similar between these two species. Moreover, the architecture of the brain microvasculature across these species is also remarkably similar. One difference reported between these species is that humans have more penetrating arterioles than penetrating venules, while the opposite pattern is observed in rats (Hartmann et al., 2018). It is worth noting that these similarities in brain vasculature extend beyond these two species. The cerebral metabolic rate (CMR) increases with brain volume with an exponent of ~0.83 across species (Karbowski, 2007, 2011), a value that is higher than the ~0.75 reported in relationship with body mass and resting metabolic rate (Kleiber, 1947). This indicates that the brain is a major energy

consumer. To sustain this resource-demanding organ, the circulatory system also has to scale. The neuron density and the capillary length density in the brain scales with brain volume with a value of -0.167, showing that the number of neurons is proportional to the total length of capillaries across species but also reflecting the difficulty in connecting and sustaining a growing 3-dimensional brain cytoarchitecture (Karbowski, 2011; Wong et al., 2013). On the other hand, the average capillary diameter is only weakly dependent on brain volume, increasing from ~4 μm in the rat brain to ~7 μm in the human brain. The fact that cerebral blood flow is directly proportional to CMR and that the capillary length density per neuron is relatively constant across species provides evidence that the architecture of the human brain microvasculature is not unique (Wong et al., 2013). In summary, because neural function is constrained in part by energy demands and the spatial distribution of capillaries is closely correlated with metabolic function, the microvasculature organization across species (including humans and rats) is similar. In addition, the neurovascular unit and the BBB are made up of the same cell types and subcellular components like tight junctions, receptors and transporters across different species, including humans and rodents (O'Brown et al., 2018). This information indicates that rats are an adequate model to study the brain vascular system.

1.2.3. Regional differences in brain vasculature

There are several reports that provide evidence of regional heterogeneity in brain vasculature. For instance, it has been reported that vessel caliber, vessel structure, vascular redundancy, capillary density cerebral blood flow, and the mechanisms involved in neurovascular coupling vary depending on the brain region (Cavaglia et al.,

2001; Iadecola, 2017; Noumbissi et al., 2018; Schmid et al., 2019). A crucial determinant of the brain microvasculature architecture is local energy demands by neurons. About 77% of the brain's energy consumption is in cortical gray matter, which represents about 50% of the brain volume (Zhu et al., 2012). The gray matter consists of neurons, dendrites, unmyelinated axons, glial cells, and capillaries, whereas white matter is mostly myelinated axons, glial cells, and capillaries. Due to the increased energy demands caused by this higher density of synapses and higher levels of neural activity, the capillary density in the gray matter is 2–4 times higher than in the white matter **(Fig. 3)** (Borowsky and Collins, 1989; Cavaglia et al., 2001; Heinzer et al., 2008). In addition, the spatial arrangement of blood vessels between gray and white matter also differs. While vessels in the gray matter are arranged perpendicular to the pyramidal cell layers, white matter vessels are longer and oriented parallel to axonal fibers **(Fig. 3)** (Cavaglia et al., 2001; Noumbissi et al., 2018). Besides variances in overall structure and organization of brain vasculature, there are also gray–white matter differences in endothelial barrier function caused by variations in expression of occludin, claudin-5 and α-catenin (higher in white matter than in gray matter) and in gene expression along the length of the cerebral vasculature tree (i.e. arteriole, capillaries, venules) (Hanske et al., 2017; Noumbissi et al., 2018).

Aside from strictly gray or white matter distinctions, similar vascular variations such as vessel density exist between and even within specific brain regions. For instance, in the rodent brain, the thalamus and dorsal areas of the cortex tend to have higher

vascular densities, while the hypothalamus, lateral cortical areas, and the white matter tend to display the opposite pattern (Cavaglia et al., 2001; Xiong et al., 2017). Furthermore, there are reported differences in vascular density between striate and extra-striate visual cortex and between *Cornu Ammonis* 1 (CA1) and *Cornu Ammonis* 3 (CA3) of the hippocampus (Cavaglia et al., 2001). Although brain vasculature in subcortical regions has been profoundly understudied (outside of the hippocampus) some groups have identified other differences in vasculature between cortical and subcortical areas (Rieke, 1987; Devonshire et al., 2012; Xiong et al., 2017; Schager and Brown, 2020) and it is very possible that more differences between and within brain regions are likely to exist. This information suggests that regional differences in microvasculature in the brain can contribute to susceptibility to injury and for instance, damage in areas with lower capillary density and reduced blood supply redundancy, such as the corpus callosum, could have a higher impact in brain function.

1.2.4. Blood-brain barrier (BBB)

The BBB is a tightly regulated interface that maintains brain homeostasis by controlling molecule and cell movements between the brain parenchyma and the circulatory system **(Fig. 4)**. It is composed primarily of endothelial cells, basement membrane, pericytes, and astrocytes (Nahirney et al., 2016; Nahirney and Tremblay, 2021). Some of the key components of this barrier are 1) tight junctions between endothelial cells that control paracellular transport; 2) a rich number of specialized transporters, receptors and pumps that regulate transcellular transport; 3) the presence

of pericytes, a cell type embedded in the endothelial basement membrane that helps stabilize and monitor endothelial maturation, survival and functioning, coordinate blood supply with metabolic activity and clearance of debris; and 4) a close relationship with astrocytic end-feet and microglia that provides and extra layer of processing and protection before anything reaches neurons. Loss of some, or most, of these barrier properties during neurological diseases including stroke, multiple sclerosis, brain trauma, and neurodegenerative disorders, is a major component of the pathology and progression of these diseases (Zlokovic, 2008; Daneman and Prat, 2015; Nahirney et al., 2016; Nahirney and Tremblay, 2021). BBB dysfunction can lead to ion dysregulation, altered signaling homeostasis, as well as the entry of immune cells and molecules into the CNS, processes that lead to neuronal dysfunction and degeneration. There are, however, special regions in the brain that do not share this special vasculature organization and a more permeable BBB allows direct communication between the brain and the vascular system. These regions are called circumventricular organs and they are located at the surface of the third and fourth ventricles. Neurons and glial cells at these sites can sense changes in the concentration of various molecules, such as hormones, and secrete neurotransmitters, cytokines or hormones into the circulation (Ganong, 2000; Duvernoy and Risold, 2007; Benarroch, 2011).

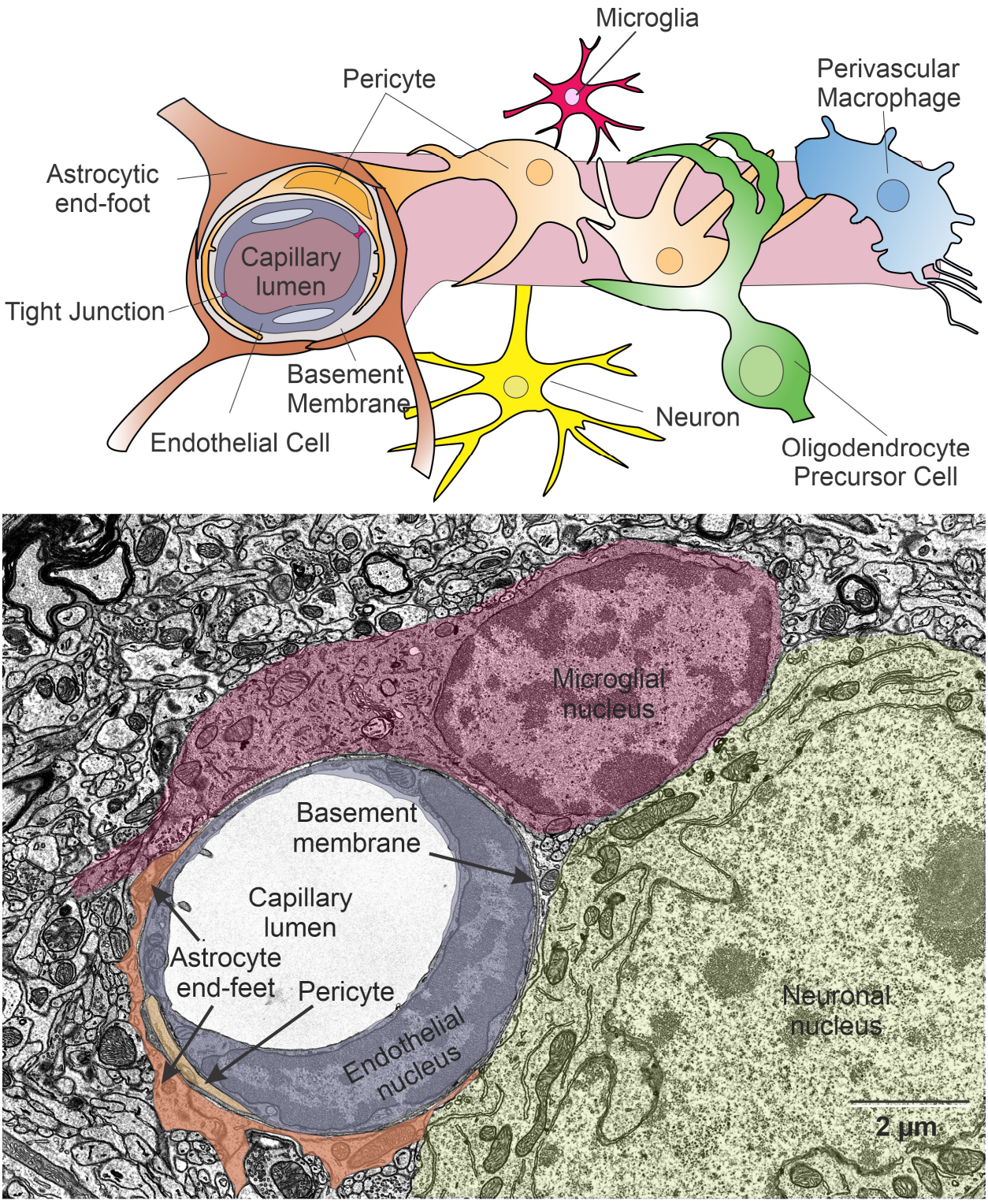

Figure 4. Blood-brain barrier components. The BBB controls molecule and cell movements between the brain parenchyma and the circulatory system. Key components of this barrier are 1) tight junctions between endothelial cells; 2) a rich number of specialized transporters, receptors and pumps; 3) the presence of

pericytes; and 4) a close relationship with astrocytic end-feet and microglia cells. Transmission electron microscopic image kindly provided by Dr. Patrick Nahirney.

1.2.5. Brain response to cerebral vascular damage

The disruption of the BBB allows the release of harmful molecules from the blood vessel into the surrounding microenvironment such as iron, reactive oxygen species and other biomolecules that should not reach the brain parenchyma under physiological conditions. Such molecules trigger an inflammatory response that, if not well managed, can lead to persistent brain damage. BBB disruption typically returns to its normal status by several weeks, but in some patients, it has been reported to last months and years even after mild injuries (Tomkins et al., 2008). It is worth noting that BBB disruption can happen in a broad spectrum of severities ranging from subtle increases in vascular permeability (i.e. increased paracellular and transcellular transport) to complete rupture of vessels. In this section, the events that occur in cases of ruptured vessels as those reported in traditional animal models of hemorrhage, such as infusion of whole blood or injection of bacterial collagenase will be presented. Reports in these models indicate that the injury mechanisms leading to brain damage are initially caused by an acute increase in intracranial pressure and compression of brain tissue resulting from hematoma formation that can mechanically injure cells, crush surrounding blood vessels, reduce cerebral blood flow and cause ischemic pathology (Salehi et al., 2017). In addition, the high concentration of glutamate in the blood plasma that leaks into the brain can cause excitotoxic injury to neurons. During the several days after an intracerebral hemorrhage (ICH), additional injury to brain cells can be caused by oxidative stress and free radical

damage from, for example, the by-product of red blood cell (RBC) lysis. Hemorrhage also drives an inflammatory cascade that leads to microglia response and invasion of neutrophils and macrophages, which may exacerbate the initial injury (Rosidi et al., 2011). The next paragraph provides a more detailed temporal progression of the events occurring after vascular injury **(illustrated in Fig. 5)**.

Under normal physiological conditions, when the brain vasculature is damaged and it allows the passage of blood cells and/or plasma to the brain parenchyma, a contingency and reparatory response is activated (Gadani et al., 2015; Lou et al., 2016). Some of the blood contents that leak outside the vessels after the rupture of endothelial cells act as Damage Associated Molecular Patterns (DAMPs) to signal the initiation of this response. These DAMPs include DNA, RNA, ATP, ADP and some proteins (Gadani et al., 2015). After the initial vascular damage event there is usually an immediate cell death in the lesion site that depends on the severity of the injury. Then, there is a release of ATP at the injury site that is rapidly amplified by astrocytes through connexin channels during the initial moments (Davalos et al., 2005a). Astrocytes and microglia become one of the first line of defense in vascular damage. Astrocytes assimilate the majority of the leaked water from the circulatory system and excess potassium and glutamate, thus reducing edema and excitotoxicity spread (Chen and Swanson, 2003; Scimemi, 2018). Microglial cells that are constantly assessing their environment with its characteristic highly ramified morphology and highly dynamic processes are also first responders during vascular injury. The astrocytic ATP-triggered release of ATP plays a critical role by

attracting these surveilling microglia to the vicinity of the injury site through the P2Y12 purinergic receptors (Lou et al., 2016). Microglial processes respond rapidly and move directly towards the site of injury to create a physical barrier consisting of E-cadherin expressing membrane appositions and temporarily assume the function of the lost BBB (Lou et al., 2016). These cells aggregate at the injury site and begin repairing the vascular disruption, and clearing the debris generated in this process after 30-60 min of the damage (Davalos et al., 2005a; Gadani et al., 2015; Lou et al., 2016). During this process, activated microglia cells start transitioning their morphological profile into a more spherical and amoeboid shape indicating increased phagocytic activity (i.e. ingestion of cells and subcellular components), and also start releasing several cytokines and chemokines (Karperien et al., 2013; Davis et al., 2017). Additionally, this microglia activation and cytokine release also leads to further astrocytic activation and, over time, to the attraction of circulating immune cells like monocytes (Liddelow et al., 2017). Concurrently, the blood-clot cascade is rapidly triggered after vascular injury to seal the vessel rupture. In this process, leaked fibrinogen is converted into fibrin by the cleaving action of thrombin. Fibrin then polymerizes and, in coordination with Factor XIII and activated platelets forms a stable blood clot (Kattula et al., 2017; Petersen et al., 2018). Once hemostasis is restored and debris cleared, endothelial cells restore the vessel wall and basement membrane, astrocytes end-feet reconnect to the vessel again and microglia return to their basal highly ramified surveilling status.

It is important to note that if microglial cells do not revert back to their surveilling status and are chronically stimulated by certain signals, like insoluble fibrin, they can develop into a chronic pro-inflammatory phenotype that not only may cause failure to fully repair the lesion, but can also lead to inflammation-induced alterations and persistent brain damage (Block et al., 2007; Ryu et al., 2010, 2015b, 2018; Davalos et al., 2012; Saijo et al., 2013; Petersen et al., 2017; Rice et al., 2017; Merlini et al., 2019). In addition, this chronic inflammation can create a deleterious feedback loop by continually disrupting the BBB and allowing further leakage of blood contents into the brain parenchyma.

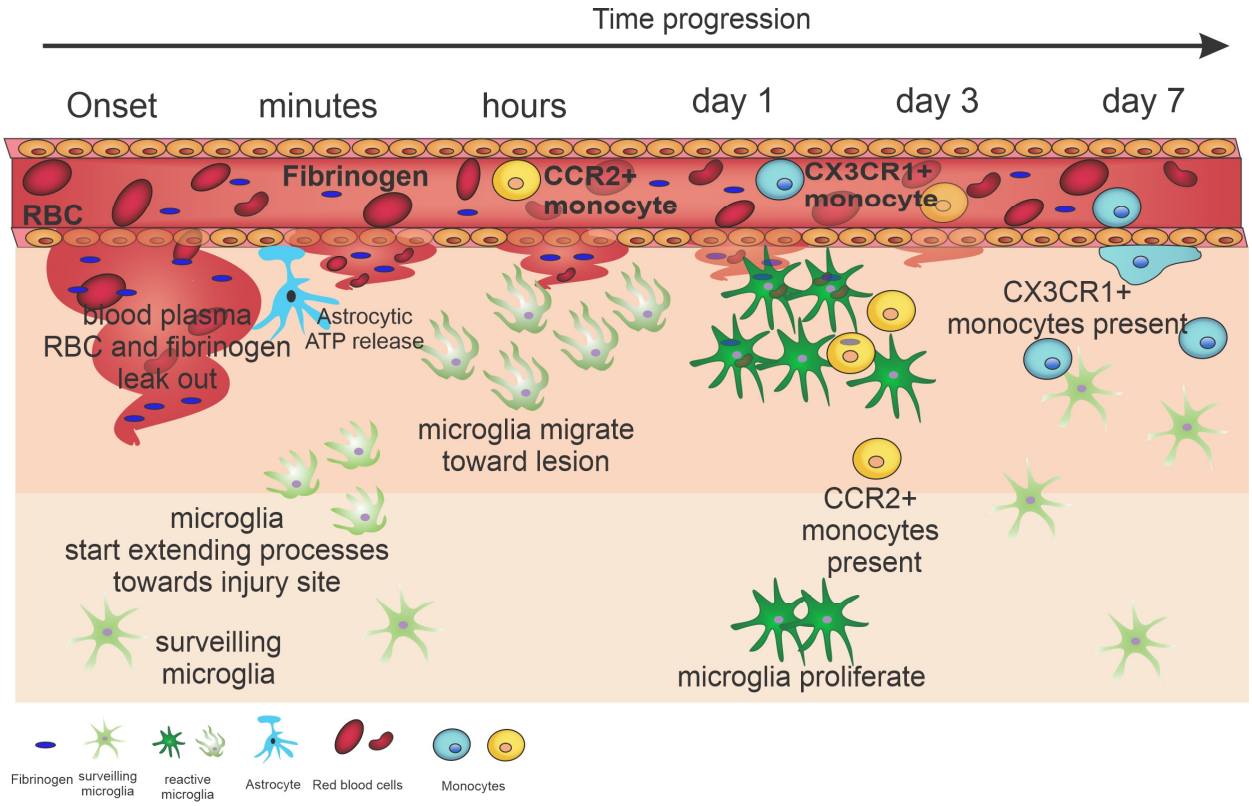

Figure 5. Simplified version of the temporal events occurring after rupture of a blood vessel. Onset: After the initial vascular damage event and leakage of blood contents (e.g. RBCs, fibrinogen, etc.) there is an immediate cell death in the lesion site that depends on the severity of the injury. **Minutes:** Release of ATP at the injury site is rapidly amplified by astrocytes. This astrocytic ATP-triggered release of ATP plays a critical role attracting surveilling microglia to the vicinity of the injury site through purinergic receptors. Microglial processes respond rapidly and move directly towards the site of injury in the first 30-60 min.

Concurrently, the blood-clot cascade is rapidly triggered after vascular injury to seal the vessel rupture **Hours:** Microglia aggregate at the injury site and begin repairing the vascular disruption, and clearing debris. **Days:** Over time, circulating monocytes are also attracted to the injury site. Once hemostasis is restored and debris cleared (in ~7 days), endothelial cells restore the vessel wall and basement membrane, astrocytes end-feet reconnect to the vessel again and microglia return to their basal highly ramified surveilling status. If this process is altered or not resolved properly, maladaptive responses can lead to chronic aggregation of immune cells and persistent deficits.

Indeed some studies have reported that although at 7 days most of the activated microglia within a few hundred micrometers of the hemorrhage return to normal shape, a dense cluster of microglia or perhaps cells derived from blood-borne monocytes can remain packed around the lesion (Rosidi et al., 2011; Davalos et al., 2012; Nishimura and Schaffer, 2013) and remain at the lesion site for several weeks. Moreover, recent data indicates that microglia can develop a primed pro-inflammatory phenotype with a characteristic mRNA, protein and morphological profile in TBI, neurodegenerative disease and aging (Norden et al., 2015). This results in primed microglia exhibiting an exaggerated inflammatory response to secondary and sub-threshold challenges. Consequences of exaggerated inflammatory responses by microglia could contribute to the development of cognitive deficits, impaired synaptic plasticity and accelerated neurodegeneration providing a putative injury mechanism in rmTBI. Furthermore, impairments in regulatory systems in these circumstances may make microglia more resistant to negative feedback and important functions of these cells can become compromised and dysfunctional (Norden et al., 2015)

In the last year, some groups have provided more evidence that injurious and reparative responses in the brain diverge based on time and cellular origin (Mastorakos

et al., 2021). They found that resident microglia initially stabilize damaged vessels in a purinergic receptor–dependent manner. This is followed by an influx of myelomonocytic cells that cause severe edema. The same group reported that prolonged blockade of myeloid cell recruitment with anti-adhesion molecule therapy prevents severe edema but also promotes neuronal destruction and fibrosis by interfering with the vascular repair orchestrated by pro-inflammatory monocytes and proangiogenic repair-associated microglia (Mastorakos et al., 2021). These results highlight the importance of how fine-tuned this process is and how temporally distinct myeloid cell responses can contain, exacerbate and ultimately repair a cerebrovascular injury.

Our current understanding of brain response to vascular damage mainly comes from moderate and severe cases like the one described above. However, these models are unable to reproduce subtler but potentially critical forms of vascular damage like the occurrence of microhemorrhages. This type of vascular damage stems from the rupture of single small arterioles or capillaries, and a growing body of evidence suggest that these microvascular events may underlie aspects of cognitive decline (Wiegman et al., 2014; Ungvari et al., 2017; Ahn et al., 2018). Although there have been very interesting studies in this field in the last 10 years, there still remains an incomplete understanding of the acute and chronic cellular dynamics and pathophysiological events following microhemorrhage due in part to lack of good small vessel injury models. However, a paper published by Dr. Brown's research group in 2018 provides a great explanation of this process (Taylor et al., 2018). It would be interesting to see an increase in in research

publication in this field to progress in elucidating more therapeutic strategies for this type of vascular injury.

1.2.6. Relevance of cerebral microbleeds (CBMs) in neurological conditions

Cerebral microbleeds are a manifestation of cerebral small vessel disease and are currently a major topic in clinical cerebrovascular research (Ungvari et al., 2017). Several studies have shown that CBMs cause neither the death of nearby neurons nor the degeneration of their dendritic arbors (Rosidi et al., 2011). In addition, although neurons near the injury site initially lose their ability to respond to a stimulus, they recover within hours. However, while studies show that CMBs do not produce acute stroke-like symptoms, clinical evidence suggests that the presence of CMBs is highly correlated with cognitive impairment, cognitive decline and dementia (Wiegman et al., 2014; Ungvari et al., 2017; Ahn et al., 2018). Indeed, epidemiological findings show that CMB occurrence may increase dementia risk by a factor of at least ~1.7 (Lee et al., 2013; Romero et al., 2017). These characteristics would fit with the nature of mTBI, where clear signs of brain damage are challenging to identify but individuals still manifest cognitive deficits.

CMBs vary in size from tens of micrometers to several millimeters and occur at increasing frequency with age (Wiegman et al., 2014), hypertension (Wakisaka et al., 2010; Gao et al., 2014), cerebral amyloid angiopathy (Vinters and Gilbert, 1983; Ni et al., 2014) anticoagulant treatment (Charidimou et al., 2012) and with some genetic conditions (Vitali et al., 2014; Ungvari et al., 2017; Ahn et al., 2018). One proposed mechanism of CMBs formation is thought to involve diapedesis, whereby RBCs transiently cross the

BBB to form hemosiderin deposits in the cerebral parenchyma. The time rate of diapedesis is strongly dependent on BBB permeability, which is typically greater in males (Pakulski et al., 2000), begins to increase significantly after age 45 (Blennow et al., 1993), and may be two to three times higher after age 60 compared to age 30 (Rosenberg, 2014; Irimia et al., 2018). However, CBMs can also happen in a less regulated process such as in the case of a vessel rupture.

While typically thought of as acutely asymptomatic, several case reports document CMBs leading to transient neurological episodes that include symptoms such as paresthesia, weakness, and dysphasia in patients with cerebral amyloid angiopathy (Charidimou et al., 2012) or with cerebral autosomal dominant arteriopathy with subcortical infarcts and leukoencephalopathy (Vitali et al., 2014; Ahn et al., 2018). The cellular mechanisms by which CMBs affect the health and function of cells in the brain microenvironment, however, remain poorly understood. From 2006 to 2018 a research group explored the impact of CMBs on neurons and surrounding cells using a laser-based approach to induce these lesions in the cortex of rodents (Rosidi et al., 2011; Cianchetti et al., 2013; Nishimura and Schaffer, 2013; Ahn et al., 2018). A common finding in these investigations was that microhemorrhages do not lead to nearby cell death or degeneration of dendritic arbors (Rosidi et al., 2011) or to long-term loss of neural responsivity (Cianchetti et al., 2013). However, they observed an increase in the density of inflammatory cells near the lesion that was sustained for 7 days (Rosidi et al., 2011). In a follow-up study by the same group, they found similar results and discovered that the

initial inflammatory response was dominated by brain resident microglia, which exhibited a coordinated action that led to an increased density of microglia near the lesion over hours to days by migration from the surrounding tissue. This migration caused a decrease in microglia density in the surrounding tissue that was later (~40 hrs post-injury) recovered by local microglia proliferation (Ahn et al., 2018). Rosidi and coworkers (2011) also reported the presence of reactive astrocytes over a similar spatial region as microglia but with the response delayed by a few days relative to microglia. The authors mention that this delayed astrocyte activation could be explained by recent findings showing that activated microglia induce astrocyte activation through cytokine release (Liddelow et al., 2017). Finally, they reported that a small number of $CCR2^{+}$ Monocyte/Macrophages were found in the brain near the lesion in the first couple of days, and $CX3CR1^{+}$ Monocyte/ Macrophages were found later, over days to weeks after the injury (Ahn et al., 2018). Consistent with these findings, postmortem studies of CMBs in the literature tend to report increased presence of inflammatory cells rather than significant tissue infarction (Fazekas et al., 1999; Dichgans, 2002; Schrag et al., 2010).

1.2.7. Evidence of CMBs in mTBI

Over the last decade, TBI research has focused almost exclusively on neuroprotective strategies that reduce neuronal cell loss. Unfortunately, this approach has failed to develop any meaningful therapeutics for clinical treatment. One less explored potential target has been the brain vasculature and its impact on TBI outcomes (Salehi et al., 2017). TBI often results in significant injury to the vasculature in the brain

with subsequent cerebral hypoperfusion, ischemia, hypoxia, hemorrhage, vasospasms, BBB disruption and edema (Salehi et al., 2017). While these signs of vascular damage are very clear in severe and moderate types of TBI, they are usually absent or hard to identify in mTBI. A growing number of studies are starting to highlight the relevance of subtler forms of vascular damage in TBI that occurs at the microvascular level. CMBs constitute an ubiquitous manifestation of TBIs of all severities and their presence is strongly associated with that of traumatic axonal injury (TAI) (Glushakova et al., 2014; Tian et al., 2014). A 2015 study (Hay et al., 2015) found that 40% of patients dying in the acute phase of TBI and 47% of those who survive TBIs to live for one year or more showed multifocal, perivascular and parenchymal CMBs in the gray matter where long-range axonal connections terminate. Interestingly, preclinical studies demonstrated that delayed microbleeds following TBI are associated with white matter damage. This highlights that these type of locations in the brain tissue are subjected to a substantial gradient of physical momentum during traumatic events and could therefore be more susceptible to damage. Simultaneously, mTBI survivors who exhibit CMBs during the acute stage of injury are ~1.5 times more likely to suffer from Parkinson's disease (PD) (Gardner et al., 2015; Gardner et al., 2014) and their mortality rate is much higher than that of the general population, with an associated HR of ~1.5 (Fuller et al., 2016). Similar to larger hemorrhages, microbleeds also cause the deposition of hemosiderin in the brain parenchyma, a sign that could be detected by special types of MRI (e.g. susceptibility-weighted imaging). These iron deposits formed after BBB breakage typically result from the phagocytosis of RBCs, whereby heme iron (i.e. iron bound to heme cofactors within

certain proteins, including hemoglobin) is degraded and deposited in the form of hemosiderin. Accumulation of hemosiderin is known to be toxic to brain cells and can elicit an inflammatory response.

Even though CMBs themselves are localized, research indicates that the effects triggered by RBC extravasation can extend far outside the immediate CMB neighborhood (Simard et al., 2009; Patel et al., 2013). Although penumbral microvasculature may receive damage during impact that could be insufficient to rupture the BBB, subsequent maladaptive molecular response mechanisms can cause a delayed structural failure of these debilitated capillaries. This phenomenon may lead to the delayed formation of CMBs that can come together to form iron deposits and then lead to more serious complications (Kurland et al., 2012; Irimia et al., 2018).

1.2.8. The fibrinogen hypothesis: a possible common mechanism

Common to several CNS diseases is the presence of extravasated fibrinogen in the brain (Petersen et al., 2018). This plasma protein has been classically involved in the formation of stable blood clots, however, a growing number of reports have also identified fibrinogen as a key factor in the inflammatory cascade induced by vascular damage in the brain (Davalos et al., 2012; Ryu et al., 2015b; Petersen et al., 2018). Indeed, in MS and AD, it has been reported that when this protein leaks repeatedly into the brain parenchyma due to vascular damage, it interacts with the microglial receptor, Complement Receptor 3 (CR3), and initiates a series of events that lead to the generation of clusters of chronically activated pro-inflammatory microglia around these areas (Paul

et al., 2007; Davalos et al., 2012; Petersen et al., 2018). These clusters, in turn, induce progressive demyelination and neurodegeneration through: 1) release of a myriad of pro-inflammatory cytokines (Ryu et al., 2015a); 2) signalling to circulating phagocytes and adaptive immune cells to infiltrate into the injury site (Ryu et al., 2015a); 3) inhibition of remyelination and neurite outgrowth through the blockade of oligodendrocyte progenitor cell differentiation and activation of premature glial scar formation (Jones et al., 2007; Ryu et al., 2010, 2015a; Petersen et al., 2017), 4) induction of excessive reactive oxygen species (ROS) generation by activating the nicotinamide adenine dinucleotide phosphate (NADPH) oxidase (Block et al., 2007; Ryu et al., 2018), and 5) promoting microglia-mediated elimination of dendrites and dendritic spines (Merlini et al., 2019). Given these reasons, in this dissertation the presence of fibrin/fibrinogen in rmTBI will also be assessed.

1.3. Summary, hypothesis and project objectives

TBI has received increasing attention due to recent reconsiderations of its epidemiology, the variables affecting lesion severity and the long-term consequences of this injury (Saatman et al., 2008; Voss et al., 2015; Mayer et al., 2017; McInnes et al., 2017; Greco et al., 2019). mTBI, also commonly referred to as "concussion", does not involve evident damage to the brain but represents the most common type of TBI in the population (NCIPC, 2003; Thomas R. Frieden, Debra Houry, 2015). In contrast to more severe forms of TBI, lesions in mTBI patients are challenging to detect using current diagnostic techniques such as MRI and CT scans (Eierud et al., 2014; Bigler, 2018). Despite this fact, mTBI individuals may still present with cognitive, emotional, sensory and motor

impairments (Cicerone and Kalmar, 1995; Carroll et al., 2004; Cole and Bailie, 2015). As a result, the need for reliable indicators of the resulting pathology has become a health research priority (Saatman et al., 2008; Blennow et al., 2012a; Jeter et al., 2013). The difficulty detecting consistent, objective and evident alterations in early phases of mTBI has made diagnosis, treatment and prognosis of this injury a tedious task. In addition, in the last decade the synergistic deleterious effect of rmTBI has been identified as a key element in injury severity (Guskiewicz et al., 2003; Prins et al., 2012; Fehily and Fitzgerald, 2017; Greco et al., 2019). This means that, while a single concussion may not cause evident or long-lasting structural and functional deficits, the summation of multiple mTBI events is a non-linear process that may lead to more severe injuries and long-term cognitive alterations.

In this dissertation, the focus will be centered on the vascular damage and inflammatory aspect of rmTBI, because even subtle forms of damage to blood vessels in the brain, when accumulated over time, have the potential to trigger or exacerbate subsequent events in the secondary injury phase and lead to long-lasting structural and functional deficits. The experiments presented here will try to shed light on the biomechanics of this type of head injury, help to provide a better understanding of the pathophysiology of rmTBI and attempt to identify reliable early markers associated with concussion.

Based on the background information provided and prior research described above, I hypothesize that the repetitive mechanical forces generated during multiple mTBI

events induce damage to the microvasculature and a sustained pro-inflammatory environment triggered by the chronic activation of microglial cells through fibrin interaction.

Objective 1: Evaluate and validate the most adequate approach to assess brain microvascular damage in juvenile rats

Objective 2: Investigate the effects of rmTBI on microvascular damage and microglia reaction in juvenile male and female rats using the ACHI model.

CHAPTER 2: GENERAL MATERIALS & METHODS

2.1. Animal generation and ethics

Long Evans dams at post-natal day (PND) 80-150 with pups were purchased from Charles River (Charles River Laboratories, St. Constant, PQ, Canada). Pups were requested to arrive at PND14 to give enough time for acclimation to a new environment before weaning at PND21 when they were then separated into same-sex cage groups of 2-3 animals. A total of 60 animals were used in this dissertation. The number of animals per experiment is indicated in each section. In addition, three 5 month-old mice (C57BL/6J background) were donated by Dr. Craig Brown and used for the study of vascular damage in some of my experiments. All procedures used in this study have been approved by the University of Victoria Animal Care Committee and in compliance with Canadian Council for Animal Care guidelines.

2.2. Awake closed-head injury model

mTBI events were induced using the ACHI procedure as described in Meconi et al. (Meconi et al., 2018a). The ACHI model was designed to produce reliable repeated mild closed head injury in non-anesthetized rats and was modeled from that of Petraglia et al. (Petraglia et al., 2014b). In the ACHI procedure, rats are immobilized using a soft plastic restraint cone (Model DC-200, Braintree Scientific, Braintree, MA) which is open at the nostrils to allow adequate ventilation, and is held closed behind the haunches using a plastic claw clip **(Fig. 6B)**. A 3D printed plastic helmet is then placed over the head and

secured using a rubber elastic under the chin and two sided tape under each arm of the helmet. The back of the helmet is aligned with the interaural line and the front is 2-3 mm caudal to the eye, centering the impact site over the left parietal cortex **(Fig. 6C).** The purpose of the helmet is to help target the impact and to reduce the risk of skull fracture by diffusing the force of the impact across the skull. The animal is then placed on a soft foam platform (3 inch thick Super-Cushioning Polyurethane Foam Sheet, McMaster-Carr, OH) below the impact apparatus. A modified controlled cortical impact device (Impact One, Leica Biosystems Inc., ON, Canada) mounted on a stereotaxic frame is used to produce the impact **(Fig. 6A)**. The device has been modified with the addition of a 7 mm diameter flat rubber impact tip. To produce the injury, the impact tip is aligned vertically over the impact site on the subject's helmet. Impact parameters are adjusted using the device's control box to an impact speed of 6 m/s and impact depth to 10 mm. The dwell time is 0.1 sec, meaning the impactor is retracted after 0.1 sec in order to prevent secondary injury from ricochet. Once the animal is motionless and the helmet and impactor properly aligned, the impact is delivered using the control box. The subject is removed from the restrain bag immediately after the impact to check for apnea, loss of consciousness and to begin subsequent neurological assessment.

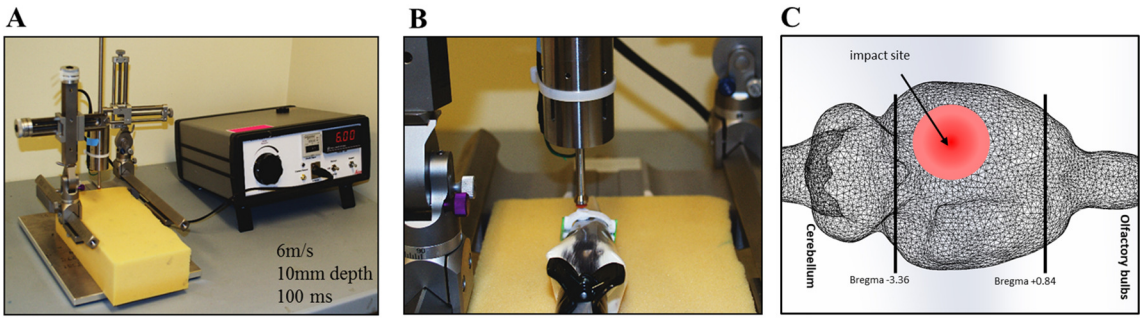

Figure 6. Awake closed head injury (ACHI) model description. (A,B) A modified Leica Impact One controlled cortical impactor was used to produce a closed head injury. The control unit sets the velocity (6 m/s) and dwell time (10 ms) of an electromagnetic piston that is affixed to a stereotaxic frame. The piston drives a customized impact tip with a 7 mm diameter rubber tip. (B) The subject is placed in a soft plastic restraint bag, and a 3D printed helmet is placed on the head so the impact target is centred over the left parietal cortex. The impact is initiated using the control unit, and then the subject is immediately moved from the platform and from restraint so that assessment can begin. (C) Location of the impact over the left parietal cortex. (Figure adapted from Meconi et al 2018)

2.3. Neurological Assessment Protocol (NAP)

Short-term changes in neurological function are a defining feature of a concussion. Confusion, dizziness, disorientation, and impaired balance are common immediately after a concussive head impact. In clinical populations, standardized assessment tools like the GCS (Teasdale and Jennett, 1974) and the SCAT(Echemendia et al., 2017) are used to rapidly assess these types of neurologic changes in order to help diagnose a potential concussion. Similar to what is done in other models, we use an adapted version of these tests for rodents: the NAP **(Fig. 7)**. In our lab, we have been able to show acute and short-lived changes in sensory and motor functions using the ACHI model (Meconi et al., 2018a), mimicking clinical acute deficits after concussions in humans. The animals in this study went through the NAP immediately after after each impact or sham procedure. The state of consciousness was assessed by examining potential post-impact apnea, the

toe pinch reflex and the righting reflex. Apnea was examined immediately after removing the animal from the bag. If apnea was present, the latency to recover breathing was recorded. The toe pinch reflex was then assessed by extending the subject's ipsilateral (to injury hemisphere) hind limb and pinching. Again, latency to retract the limb was recorded. The last of the consciousness assessment test was the righting reflex, which was determined by placing the subject on their back and measuring the time the animals took to right themselves. After this, animals went through a set of 4 simple sensorimotor tasks that were scored on a 4-point scale (0-3) depending on their performance. These 4 tasks were startle response, limb extension, balance beam and rotating beam. The specific scoring is shown in **Figure 7.** Briefly, after receiving the ACHI or sham procedure, animals were placed in the center of a standard housing cage and the response to a researcher's clap was assessed to measure the startle reflex. Then, the limb extension response was evaluated by holding the rat by the base of its tail and raising it 30-50 cm in the air to observed their reaching behaviour. After this, a balance beam test was performed. In this task, animals were placed on the center of a flat balance beam (100 cm long x 2 cm wide x 0.75 cm thick) that was situated 22 cm above a cushioned surface (to prevent potential injury from failing from the beam) and their ability to balance and walk in the beam was assessed. Finally, the same beam was used to evaluate the animal's ability to navigate a slowly rotating beam. In this test subjects were placed on the center of the beam at a height of 50 cm above a cushioned surface and the beam was rotated once per second for 4 rotations. A composite score based on these 4 tasks was computed to reflect the overall performance for each animal with 12 points indicating no deficits

and 0 failure in all tasks. A pre-injury measurement of the NAP was performed to ensure equal behavioral performance on these tasks prior to the ACHI procedure.

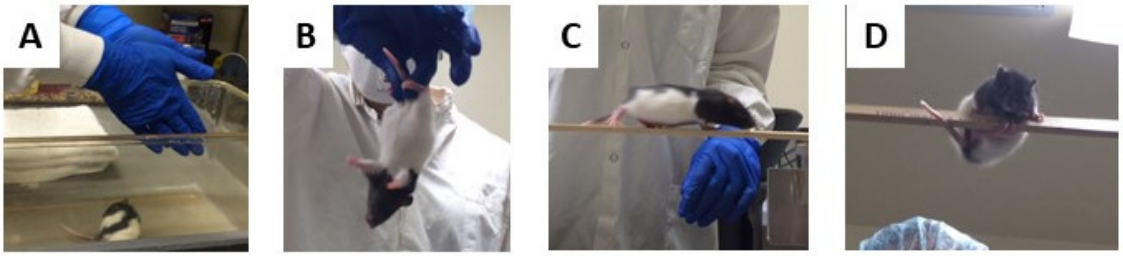

Test	0	1	2	3
A. Startle Response	No reaction to clapping sound	Only ears react to clapping sound	Slow reaction or slight freezing reaction to clapping sound	Ears react quickly and whole body jumps and freezes
B. Limb Extension	Absence of limb extension; limp body	Intermittent retraction/extension of limbs	Only one limb properly extends	Full extension of both paws, animals grasps beam successfully
C. Beam Walk	Complete absence of movement, with all limbs hanging off beam	Non-locomotive movement ("swimming" or "rowing" motion of limbs without movement across the beam)	Animal walks on beam, but more than 2 limb slips are observed	Animal walks across beam to home cage with 2 or fewer foot slips
D. Rotating Beam	Animals falls during the 1st rotation	Animal falls during 2nd or 3rd rotation	Animal falls during 4th rotation	Animal successfully completes 4 rotations

Figure 7. Neurological Assessment Protocol. Photographic depictions of the main sensory motor tasks, showing: **(A)** Startle reflex, **(B)** Forelimb extension, **(C)** Beam walk, and **(D)** Rotating beam. The scoring system used for each task is presented in the associated table. All tests were scored on a scale from 0-3 with 0 being the lowest score (greatest impairment) and 3 being the highest score (no impairment). Prior to these tasks, measures of loss of consciousness and breathing (apnea, toe pinch and righting reflex) were performed, and the latency to respond was recorded on the scoring sheet. Used with permission from (Christie et al., 2019).

2.4. Post-ACHI animal monitoring

To ensure animal welfare, all subjects used in this study underwent rigorous pain assessment after each impact. First, animals were placed in a cage alone to evaluate gross locomotion, skin turgor and pain in the impact zone. Then, after their physical pain examination, the animals were placed back at their home-cages with 1-2 littermates and their social behaviour was evaluated. Animals with a pain score of ≥ 2 in a single category or ≥ 3 as combined score was provided with supportive care and increased monitoring until pain score reverted back to 0.

2.5. Study design & Injury paradigm

Subjects were randomly assigned to one of 3 groups: Naïve control, Sham or rmTBI. In all experiments both sexes were included. At PND 25-28, animals in the rmTBI group received 2 impacts per day for 4 days (8 impacts in total). Sham subjects underwent the exact same procedure as the injured subjects, including being placed in the restrain bag and on the injury platform, wearing the helmet and hearing the piston sound, but without receiving the impact **(Fig. 8)**. Naïve controls were age-matched to sham and rmTBI animals for the short-term time-point (i.e. 1 day after the last hit). Animal tissue was collected at post-injury day (PID) 1 and PID 7 (i.e. 1 or 7 days after the last injury) for histological analysis of microvascular damage.

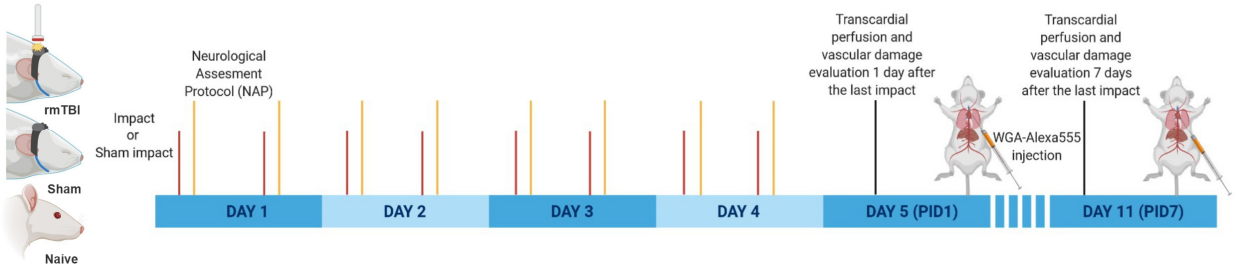

Figure 8. Experimental design. Animals were randomly assigned to rmTBI or sham group. Animals in the rmTBI group received 8 impacts over 4 days (2 impacts/day). Animals in the sham group did not receive an impact, but underwent the exact same procedure as the injured subjects, including being placed in the restrain bag and on the foam platform, wearing the helmet and hearing the piston sound. All the animals in this study went through the neurological assessment protocol (NAP) immediately after every impact or sham procedure. At post-injury day (PID) 1 or 7 animals received an injection in the left ventricle of the heart of wheat germ agglutinin to label the vasculature followed by a standard transcardial perfusion. After tissue processing and staining the corresponding histological analysis was performed. In addition, age-matched naïve controls were used to analyze potential procedural induced vascular damage at PID1.

Product	Company	CAT#	Other details
Wheat germ agglutinin-Alexa555	Invitrogen	W32464	1ml injected in left ventricle. 0.2 mg/ml
Rabbit anti-fibrinogen	DAKO	A0080	1:1000
Mouse anti-Iba1	EMD Millipore	MABN92	1:1000; requires antigen retrieval
Anti-CD68	EMD Millipore	MAB1435	1:1000
Bovine serum albumin	Sigma	A4503	3% or 1% diluted in PBS
Phosphate buffered saline	N/A	N/A	0.8% Nacl 2.7 mM KCl 10 mM $Na_2HPO_4*7H_2O$ 1.8 mM KH_2PO_4 pH: 7.4
Heparin	Sigma	H3149-100KU	one pinch (~0.0001%)
Goat anti-rabbit 488	Life technologies	A11034	1:500
Donkey anti-mouse 647	EMD Milipore	AP1925A6	1:500
Thiodiethanol	Sigma	166782-500G	60% diluted in H_2O
Nuclear Fast Red	Sigma	N-8002	
Citrosolv	Decon Labs	1601	
Cytoseal 60	Thermo Scientific	8310-4	
Evans blue	Sigma	E-2129	2% in 0.9% filtered saline
Harris hematoxylin	Sigma	HHS16-500ML	
Eosin	BDH	B34027	1% aqueous solution
30 gauge neddle	BD PrecisionGlide,	#305106	

Table 2. Details of reagents used in this dissertation. Product, company, catalogue number and additional details are indicated.

CHAPTER 3: HOW CAN WE MEASURE CEREBRAL MICROVASCULAR DAMAGE?

3.1. Introduction

Before jumping into the evaluation of microvascular damage in the ACHI model of rmTBI, the validity of different approaches to measure this outcome was tested and those more appropriate for this study according to the resources available were selected.

3.1.1. How can we label the brain vasculature?

When evaluating fine details of vascular damage, it is important to use a labelling method that allows the visualization of the blood vessels that permits the differentiation between the intravascular and extravascular space. Nowadays, this is normally accomplished by injecting in the circulatory system a fluorescent dye or by immunolabeling endothelial proteins. The nature of the experimental question will guide the type of compound needed. For instance, for *in vivo* live imaging, inert and non-toxic compounds like florescent dextrans would be needed, and for post-mortem histological evaluations lectins conjugated with fluorophores (FITC, AlexaFluors etc.) or labelling of vascular proteins like Acta2, Podocalyxin or CD31 or the use lipophilic molecules like DiI can be employed. Below some of the most common methods used to label the brain vasculature will be described.

3.1.1.1. Dextrans

Dextrans are a common inert and non-toxic injectable molecule used to label brain vasculature and can also be employed to evaluate vascular integrity. This complex branched polysaccharides derived from the condensation of glucose can be produced in several molecular sizes and it is combined with fluorophores to test vascular permeability with a high degree of precision (i.e. using dextrans with different molecular weights and/or conjugated with different fluorophores). These compounds are very common in live imaging studies that use 2-photon microscopy. Although this is a great compound to label blood vessels, it can get cleared form the system relatively fast and requires additional injections in longitudinal studies. If this approach is used to evaluate vascular integrity post-mortem, one of its limitations is that after leaking into the brain parenchyma, dextrans keep diffusing overtime and can lose signal intensity, making it difficult to identify the source of the initial vascular injury or even getting completely washed out. This is problematic if a post-mortem analysis is desired after the *in vivo* imaging. One modification on dextrans designed to overcome the continuous diffusivity problem is the covalent addition of lysine residues. This permits the conjugation of dextrans to surrounding biomolecules by aldehyde-mediated fixation. A big advantage of this approach is the ability to select dextrans with a specific molecular size and the use multiple fluorophores for post-mortem analysis. A fact to consider with this approach is that the intravenous injection procedure can potentially produce some vascular stress than may introduce vascular damage artifacts, however, experienced personnel can

greatly reduce this risk. Finally, an important limitation of this technique is the elevated cost of this product.

3.1.1.2. Lectins

Lectins are carbohydrate-binding proteins that are highly specific for sugar groups in other molecules and can cause agglutination of particular cells or precipitation of glycoconjugates and polysaccharides. They function as recognition molecules involved in protective mechanism in different organism. For instance, wheat germ agglutinin (WGA) is a type of lectin that protects wheat from insects, yeast and bacteria. This agglutinin protein binds very specifically to N-acetyl-D-glucosamine and sialic acid. The ability of WGA to bind to glycoconjugates in endothelial cell membranes in combination with its conjugation with fluorophores is used to label the lumen of blood vessels. This approach allows differentiating intra- and extravascular locations. Lectins can also be used to evaluate vascular integrity, however their strong binding to endothelial molecules may not make it the most ideal approach. In addition, lectins can also bind to post-translational modifications in macrophage/microglial cells, making the analysis of leakages more complex. This approach is commonly used in post-mortem evaluations because this molecule can stand common transcardial perfusion-fixation methodologies used in histological studies. Similarly, to dextrans, a limitation of this approach is its elevated cost.

3.1.1.3. DiI

DiI, also defined as 1,1′-dioctadecyl-3,3,3′,3′-tetramethylindocarbocyanine perchlorate is a lipophilic carbocyanine dye that was initially used by cell biologists to study the structure and dynamics of cell membranes and artificial lipid bilayers (Schlessinger et al., 1977; Jacobson et al., 1981; Vaz et al., 1984; Honig and Hume, 1986) and to visualize the morphology of neurons and interaction with other cells in live cultures (Schwartz and Agranoff, 1981; Honig and Hume, 1986, 1989). Later, carbocynaide dyes have been used as both anterograde and retrograde tracers of axonal fibers (Godement et al., 1987; Harris et al., 1987; Thanos and Bonhoeffer, 1987; O'Leary and Terashima, 1988; Stuermer, 1988; Burkhalter and Bernardo, 1989) and more recently to visualize and analyze dendritic spines (Kim et al., 2008; Skrzypiec et al., 2013; Cheng et al., 2014; Atkin et al., 2015; Mahmmoud et al., 2015; Batista et al., 2016; Trivino-Paredes et al., 2019). In the last 10 years, DiI has also started to be used as a marker of brain vasculature with several interesting approaches yielding different success rates (Li et al., 2008; Konno et al., 2017, 2020). Long-chain dialkyl carbocyanines are very affordable compounds that have become a useful tool for labeling the plasma membranes of several cell types including the endothelium. They can be constructed to contain both a charged amphiphilic fluorophore that allows visualization of the plasma membrane surface and a lipophilic aliphatic tail that anchors this molecule in this cellular location (Wiederschain, 2011). To date, the literature indicates that the best approach using DiI for vascular labelling consist of using neutral liposomes and DiIC12 (Konno et al., 2017).

3.1.2. How can we evaluate vascular damage in brain tissue?

There are several approaches used to evaluate vascular damage in humans and other animals with varying strengths and limitations. In humans these approaches are mainly non-invasive imaging techniques like CT and MRI scans. While these techniques are also available for animals and provide a great translational advantage when combined with more classical histological techniques, the acquisition and maintenance costs of this type of equipment is not affordable for most laboratories. Several more invasive and usually post-mortem approaches are commonly used in animal models. These techniques include intravascular injections of dyes like Evans blue, detection of extravasated plasma proteins like fibrinogen or immunoglobulins, and iron detection using Prussian blue reaction.

3.1.2.1. Evans Blue

Evans blue is an azo dye that has a high affinity for serum albumin and it can be visualized both with light microscopy as a blue dye and under fluorescence microscopy in the far red spectrum that excites around 600-620 nm and emits at around 680 nm. Because it is mainly bound to serum albumin, it will not leak into the brain parenchyma unless there is an increase in vessel permeability (including vessel rupture) large enough to allow the passage of a relatively large protein like albumin. This approach has the advantage that it is a non-lethal molecule that can be used in live animals for longitudinal studies and it is a very affordable compound. However, one of the limitations of this technique is that similar to non-fixable dextrans, Evans blue also continually diffuses after

leaking into the brain parenchyma and makes the identification of initial sources of vascular damage a challenging task, especially in post-mortem analysis. Another fact to consider is that, again similar to dextrans, the intravenous injection procedure can potentially produce some vascular stress and introduce vascular damage artifacts. There is an interesting non-microscopy way of using Evans blue to evaluate vascular damage. In this approach, animals are injected with Evans blue and then a transcardial perfusion is performed to flush out the intravascular presence of this compound while keeping the extravasated traces locked in the brain parenchyma. The brain is then homogenized after extraction and the extravasated levels of Evans blue can be evaluated using a spectrophotometer. Although this approach is good to quantify overall effects on vascular damage, all the spatial information is lost.

3.1.2.2. Detection of extravasated plasma proteins

Another approach used to evaluate vascular damage is the detection of plasma proteins that do not cross the blood-brain barrier unless there are alterations in vascular permeability that allow their infiltration into the brain parenchyma. A very common protein used on this approach is immunoglobulin G (IgG). The immunolabeling of this protein is a relatively affordable approach that is typically used in DAB (3,3'-diaminobenzidine) staining.

In addition, in recent years, fibrinogen, a plasma protein classically involved in the blood-clot cascade has emerged as a novel marker that can be used to both detect alterations in vascular permeability but also provide a mechanistic explanation of

vascular damage induced neuroinflammation. This approach provides a mean to identify active vascular damage and depending on the clearance rate of this protein from the brain parenchyma it could potentially be used for traces of recently solved vascular damage.

3.1.2.3. Prussian Blue

All the methods explained above are good approaches when studying the acute effects of active vascular damage. However, depending on the severity of the vascular damage this acute visualization will take more or less to be resolved and at that point it may be undetectable. Therefore, it is very useful to use a technique that allows the detection of the "signature" or traces left by vascular injuries or to stain RBCs (e.g. immunostaining TER119). The traces left by vascular injuries are hemosiderin deposits and a common technique used to detect them is the histochemical stain Prussian blue (Parry, 2017). When RBCs extravasate into the brain parenchyma they slowly start to degrade. Once they deplete their ATP reserves these RBCs can not maintain their osmotic pump and end up suffering an osmotic shock that induces the release of its cytosolic contents. One of these cytosolic components is hemoglobin. This iron-containing metalloprotein is responsible for oxygen transportation in almost all vertebrates and some invertebrates. When hemoglobin degrades, it releases the iron bound to its heme group. This iron is then picked up by phagocytic cells like microglia and macrophages and stored intracellularly as hemosiderin deposits. Hemosiderin deposits are a good proxy for vascular damage because they are mainly caused by RBC extravasation in the brain parenchyma. Alternative causes of iron deposits in the brain other than bleeds are

possible but they are very minimal unless the model of study has a pre-existing modification of iron metabolism (e.g. transgenic model of iron overload). Furthermore, an iron overload phenotype takes a long time to develop, so in experiments with short experimental timelines there is a high degree of certainty that the source of hemosiderin deposits are vascular injuries. Prussian blue is used to label non-heme iron such as ferritin and hemosiderin. Heme iron like that in hemoglobin or myoglobin is not detected using this approach. In this histochemical stain, hydrochloric acid is used to increase the availability of Ferric iron (Fe^{3+}) in the tissue and the reaction with potassium ferrocyanide creates a bright blue precipitate (ferric ferrocyanide) that can then be detected with light microscopy.

3.1.2.4. Cellular response to vascular damage

An indirect way to detect and evaluate vascular damage is to observe the cellular events that occur after this type of brain injury. The most common way to do this is by assessing the reaction of microglial cells. These cells respond very rapidly to vascular damage and are attracted to the source of injury within 30-60 min. The most common microglial marker is the ionized calcium-binding adaptor molecule 1 (Iba1). Although not exclusively expressed in microglia (this marker is also expressed in macrophages), the morphological characteristics of these resident immune cells provide a clue of the cellular origin of Iba1 positive cells. More specific microglial markers have been identified over the last years, including transmembrane protein 119 (TMEM119) and purinergic receptor P2Y12 (Bennett et al., 2016; Van Wageningen et al., 2019). This approach can be used in conjunction with the direct methods described previously to provide

confirmation of the specificity of the vascular damage observed (i.e. to rule out acute methodological-induced vascular damage artifacts).

3.1.3. Features of ideal methodologies to be used to address aims on this dissertation.

In summary, given the experimental questions in this study (i.e. analysing the relationship between microvascular damage and rmTBI) the ideal methodology should include 1) a way to evaluate acute and active vascular damage post-mortem that is easy to localize, stays closer to the initial source of vascular damage, can be clearly identified as being in the extravascular space, and is not a product of a methodological artifact, and 2) because vascular injuries resolve over time, a technique that allows to easily visualize evidence of past vascular injuries, also in a post-mortem approach would be needed. In this chapter the methodologies tested in this study and how the were validated using two models of positive control for vascular damage (stab wound injury and laser ablation of microvessel) will be present before proceeding to the specific research question.

3.2. Materials & Methods

3.2.1. Animal generation

Control rats used for in vivo electrophysiology experiments (PND30) were used after electrophysiological recordings as vascular damage positive controls for histological analysis. Briefly, animals were anesthetized with urethane (1.5 g kg^{-1}) and placed in a Kopf stereotaxic apparatus. Body temperature was maintained at $37^{o}C \pm 0.5^{o}C$ throughout the experiment with a grounded homeothermic temperature control unit (Harvard Instruments, MA). Extracellular field potentials were recorded by inserting a

125-µm stainless-steel recording electrode into the hilus of the DG (3.5 mm anterior, 2.0 mm lateral to bregma). This procedure provides a similar model to a stab wound injury that can be used as a positive control of brain vascular damage (Lin et al., 2005; Schachtrup et al., 2010) **(Fig. 9).** A total of 3 animals were generated using this injury model.

To test less severe vascular damage and longer time points, 5 month old mice (C57BL/6J background) with a chronic cranial window used for 2-photon microscopy live imaging were used **(Fig. 10)**. These animals received a laser-induced vascular microablation to generate positive controls for brain microvascular damage (Rosidi et al., 2011; Ahn et al., 2018; Taylor et al., 2018).

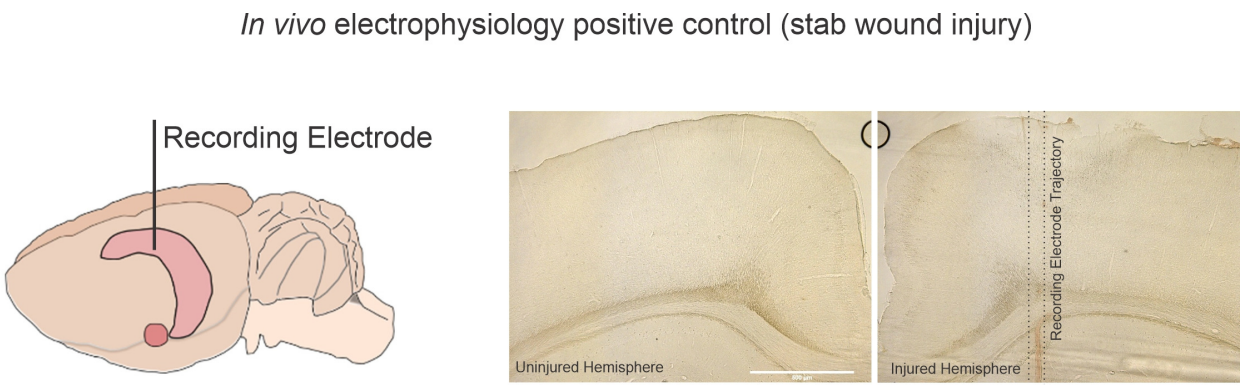

Figure 9. Stab wound injury model as a positive control for moderate and active vascular damage. Control rats used for in vivo electrophysiology were used as positive controls for vascular damage. A recording electrode was position in one hemisphere (injured hemisphere) at 3.5 mm anterior, 2.0 mm lateral to bregma and lowered 1-1.5 mm below pial surface to be in the hilus of the DG. The penetrating trajectory of the 125 µm-thick stainless steel electrode created an evident path of vascular damage that was used to validate different histological methods described in this chapter. Images on the right panel display unstained uninjured and injured brain sections where the approximate electrode trajectory is indicated.

Briefly, to visualize the brain vasculature, mice received an intravenous injection of 2% Evans blue in a sterile 0.9% saline solution. Animals were anesthetized (~1% isoflurane in air) and *in vivo* 2-photon imaging of fluorescently labelled blood vessels in the somatosensory cortex was performed with a 40× objective (NA = 0.8) using an Olympus FV1000MPE laser scanning microscope coupled to a mode-locked Ti:sapphire laser. Microvessels (~5-10 µm in width), 50–100 µm below the pial surface were selected for laser-induced microablation. The microbleed was induced using focal high-power illumination on microvessels (850 nm, ~220 mW at back aperture, ~5-µm-diameter circle centered on vessel) for 5–6 s. The rupture of the microvessels was confirmed by the appearance of extravascular fluorescence signal from the circulating Evans blue at the site of the bleed. We want to thank Dr. Craig Brown for donating these animals and Benjamin Schager for assisting with the laser ablation injuries in this study. A total of 2 animals were generated using this injury model.

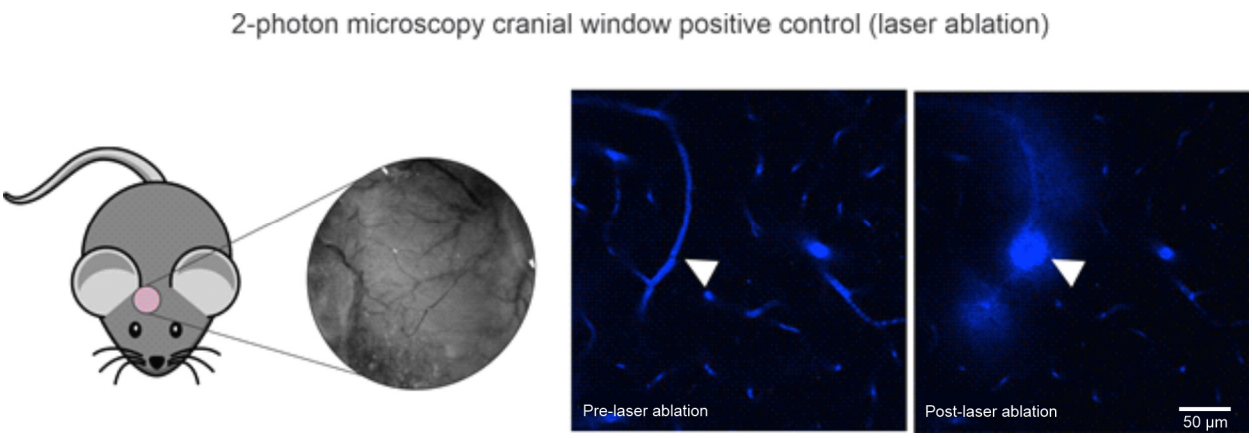

Figure 10. Laser microablation injury model as a positive control for microvascular damage. Control mice with chronic cranial window used for 2-photon microscopy imaging were used as positive controls for microvascular damage. Focal high-power illumination of the microvessel was employed to produce a laser-

induced microablation. Vessels were visualized using an intravascular injection of Evans blue (blue) and cerebral microbleeds were confirmed by the extravasation of this dye. The vascular damage induced in this model was used to validate different histological methods described in this chapter in less severe forms of vascular injury and also at longer time points (5 days after initial injury). We want to thank Benjamin Schager for his assistance in this procedure.

3.2.2. Histology

3.2.2.1 Tissue preparation

Positive control animals from *in vivo* electrophysiology experiments were transcardially perfused after the experimental recordings were concluded. These animals were perfused with ~150 ml of heparinized 0.1 M phosphate buffered saline (Hep-PBS) followed by the same volume of 4% paraformaldehyde (PFA) diluted in 0.1M PBS. After brain extraction, samples were post-fixed overnight in the same fix solution. Brains were then sliced using a vibratome (Leica VT1200S) into 50 µm-thick sections and collected in a 12 well plate. One of every 12 sections was collected into the same well. Sections with clear signs of vascular damage (i.e. close to location of recording electrode and with traces of blood) were selected for histological analysis. Some of these animals received injections of Evans blue, DiI or WGA depending on the experiment.

Positive control animals from laser microablations were monitored for 5 days after microbleed induction and then perfused in a similar way as the *in vivo* electrophysiology positive controls (perfusion volumes were adjusted to mice with 50 ml Hep-PBS and 50 ml 4% PFA in PBS). Sections were also post-fixed overnight in 4% PFA and then sliced into 50 µm-thick sections using a vibratome (Leica VT1200S)

3.2.2.2. DiI staining

To label the vasculature with DiI we followed the instructions described in a previous report by Li et al. (Li et al., 2008). Briefly, we diluted 100 mg of DiI crystal in 16.7 ml of 100% ethanol to a final concentration of ~6 mg/ml. Then, during transcardial perfusion we injected 1 ml of this DiI solution diluted in Hep-PBS (DiI final concentration of 0.1 mg/ml) directly into the perfusion lines while flushing with Hep-PBS. We also tried injecting this DiI solution directly into the left ventricle while performing the transcardial perfusion. This labelling was only performed in *in vivo* electrophysiology control rats.

3.2.2.3. Wheat germ agglutinin

To label the lumen of blood vessels with a fluorophore-conjugated lectin we followed the methodology described in the report by Roberston et al. (Robertson et al., 2015). Briefly, animals received a 1 ml intraventricular injection of 0.2 mg/ml WGA conjugated with AlexaFluor-555 (Invitrogen, #W32464). WGA-Alexa555 was diluted in Hep-PBS to avoid the potential formation of blood clots while performing the injection. Several concentrations were tested and 0.2 mg/ml provided the best balance for signal intensity to the amount of WGA-Alexa555 used. A 30-gauge needle (BD PrecisionGlide, #305106) was used to inject this solution directly in the left ventricle of the heart slowly over a period of ~30 sec. After this, the WGA-Alexa555 was allowed to circulate for ~20 sec more before starting the transcardial perfusion with Hep-PBS and 4% PFA. Injecting the WGA-Alexa555 solution directly in the gravity feed perfusion lines during the transcardial perfusion was also tested but yielded suboptimal results.

3.2.2.4. Evans blue

To visualize the cerebral vasculature and visualize vascular damage (including microbleeds), some rats and mice received an intravenous injection (tail vein) of 0.1 ml of 2% Evans blue (Sigma-Aldrich, E-2129) in sterile 0.9% saline solution. For both types of models of vascular damage (i.e. stab wound injury and laser microablation), Evans blue was administered 30 min before inducing vascular injury. Mice monitored for 5 days after laser microablation did not received additional injections of Evans blue.

3.2.2.5. Immunofluorescence

To evaluate vascular damage, we used extravasation of fibrinogen and reaction of perilesional microglia to this injury. This staining required an initial antigen retrieval step. Briefly, sections were placed in 1.5 ml Eppendorf tubes containing 1.4 ml of 10 mM sodium citrate (pH 6.0). These tubes were place in a water bath at 75°C for 30 min. After this tubes were allowed to cool down in a bench at room temperature (RT) for ~20 min. Next, sections were transferred to a 24-well plate and blocked using a solution of 5% bovine serum albumin (BSA), 0.3% Triton-X 100 and 0.01% sodium azide diluted in 0.1 M PBS on a belly dancer for 1 hr at RT. Following this step, sections were incubated at 4°C overnight (on a belly dancer) with primary antibodies diluted in 1% BSA, 0.1% Triton-X 100 and 0.01% sodium azide diluted in 0.1M PBS. Antibodies used were rabbit anti-fibrinogen 1:1000 (DAKO, A0080), mouse anti-Iba1 1:1000 (EMD Millipore, MABN92), and mouse anti CD68 1:1000 (EMD Millipore, MAB1435). After this, sections were washed 3 times for 10 min with 0.1% Triton-X 100 diluted in 0.1 M PBS and then incubated with secondary antibodies diluted in 1% BSA, 0.1% Triton-X 100 diluted in 0.1

M PBS for 1 hr at RT. Secondary antibodies used were goat anti-rabbit AlexaFluor488 at 1:500 (Life Technologies, #A11034), goat anti-mouse AlexaFluor488 at 1:500 (Thermo Fisher, A-11001) and donkey anti-mouse AlexaFluor647 at 1:500 (EMD Milipore, #AP1925A6). Next, sections were washed twice with 0.1% Triton-X 100 diluted in 0.1 M PBS for 10 min each, counterstained with 1 microgram/ml of DAPI (Sigma) diluted in PBS for 8 min and washed once for 10 min with 0.1 M PBS. After this, sections were incubated with 63% thiodiethanol (TDE) (Sigma, N-8002) diluted in dH_2O overnight and next day mounted and coverslipped using also 63% TDE. Finally, coverslips were sealed using clear nail polish. The antigen retrieval step was essential for Iba1 staining but introduced a significant amount of background fluorescence noise. We used TDE to overcome this issue since this refractory index matching compound greatly reduced the background noise.

3.2.2.6. Prussian blue

Sections with evident signs of vascular damage (presence of Evans blue or blood) were mounted on glass slides and allowed to air dry for 4-5 days. After this, sections were rehydrated for 10 min in distilled water and then covered with Prussian blue stain composed of 5% hydrochloric acid and 5% potassium ferrocyanide (aq) in a 1:1 ratio. This staining solution was made fresh every time because potassium ferrocyanide oxidizes fast when exposed to light and turns into a dark solution. Sections were incubated in a dark wet chamber for 30 min and then quickly rinsed 3 times with dH_2O and 1 time for 10 min. After this, sections were counterstained with nuclear fast red for 10 min. Then,

sections were quickly rinsed in distilled water 3 times and dehydrated by placing them in a 95% ethanol (EtOH) solution for 1 min followed by 1 min in 100% EtOH and finally 2 min in CitriSolv (Decon Labs, 1601). Sections were then coverslipped using Cytoseal 60 (Thermo-Scientific, 8310-4) and allowed to cure for 24 hrs.

3.2.2.7. Hematoxylin & Eosin

The Harris method for hematoxylin & eosin staining (H&E) was used for staining vibratome sections. Sections with evident signs of vascular damage (presence of Evans blue or blood) were mounted on glass slides and allowed to air dry for 4-5 days. After this, sections were rehydrated in dH_2O for 2 min and then incubated in Harris hematoxylin (Sigma, HMS1160-500ML) for 2-2.5 min. Next, sections were rinsed 3 times with dH_2O (3 sec each) and then incubated in differentiation solution (1% HCl in 70% EtOH) for 30 sec. After this, sections were rinsed again in dH_2O 3 times and blued in Scott's tap water for 30 sec. Next, slides were incubated in 95% EtOH for 30 sec before placing them in Eosin Y (1% aqueous solution) for 15 sec counterstaining. Finally, sections were serially dehydrated by placing them in ascending concentrations for 1 min in 50%, 70%, 95% and 100% EtOH. Sections then were cleared with a 2 min incubation in CitriSolv and coverslipped using Cytoseal 60.

3.2.3. Imaging

3.2.3.1. Brightfield microscopy

Sections stained with Prussian blue, H&E and unstained sections were imaged using a motorized Olympus BX51 microscope (Olympus) at different magnifications

using Olympus UPlanFLN objectives (Olympus). Sections were examined for the presence of vascular damage and then images were acquired using the StrereoInvestigator software (MBF Bioscience). Exposure and white balance were adjusted automatically using software assistance.

3.2.3.2. Fluorescence microscopy

Immunolabelled sections were imaged using Olympus FV-1000 confocal laser microscope (Olympus, Toronto, ON) and FV10-ASW 4.2 software. A 405 nm laser was used to visualize cell nuclei with DAPI. A 488 nm laser was used to visualize immunolabelled fibrinogen and CD68 with an AlexaFluor488 secondary antibody. A 561 nm laser was used to visualize blood vessels stained with WGA-Alexa555 or DiI. Finally, a 647 nm laser was used to visualize immunolabelled Iba1 or Evans blue. Different UPlanSApo objectives (Olympus) with diverse numerical apertures were used to obtain low- and high-magnification image stacks of regions with vascular damage. Images were acquired at 1024x1024-pixel frame size, 2-µs/pixel and different step sizes depending on the magnification (e.g. for 20x a 1-µm-step size was used). Since multiple channels were imaged, the sequential acquisition option was selected. Laser power and high voltage (HV) settings were adjusted to obtain optimal images and were maintained consistent between samples that needed to be compared.

3.2.4. Image processing and analysis

3.2.4.1. Evans blue

Evans blue stained sections were analyzed by creating a mask of the dye-filled blood vessels. This allowed measuring only the fluorescence signal present outside of the blood vessels. The ImageJ trainable WEKA (Waikato Environment for Knowledge Analysis) segmentation tool was used to accurately generate a blood vessels mask. Using ImageJ's "Image calculator", this mask was added to the original image and then only extravascular Evans blue signal was measured. Results are presented as florescence intensity with arbitrary units.

3.2.4.3. Fibrinogen

Fibrinogen stained sections were also analyzed by creating a mask using the WGA-labelled blood vessels. This mask was similarly generated using the ImageJ "Trainable WEKA segmentation tool". This mask was added to the fibrinogen florescence channels to ensure that only extravascular fibrinogen signal was measured. Results are presented as florescence intensity with arbitrary units.

3.2.4.2. Prussian blue

Qualitative visual analysis of Prussian blue-stained sections was performed initially on sections to identify bright blue hemosiderin deposits, and once identified, an image was acquired. Validation of the specificity of the Prussian blue staining was accomplished by doing serial staining of an adjacent section and assessing the presence of Evans blue.

3.3. Results

3.3.1. Brain vasculature labelling

DiI was initially tested to visualize the blood vessels **(Fig. 11)**. This lipophilic molecule was injected into the animal's circulatory system in two different ways: In the perfusion lines during transcardial perfusion and directly in the left ventricle of the heart before this procedure. Although direct injection in the heart provided better staining, neither approach yielded satisfactory results. DiI labelling of blood vessel provided a non-homogeneous staining of the brain vasculature and showed localized patches of vessels labelled in both cortical and subcortical structures. In addition, even though brains were fixed with 4% PFA, DiI continued to diffuse out of some of the vessels, creating overstained regions where the extended labelling of brain parenchyma made it impossible to pinpoint the exact location of blood vessels. Interestingly, this continuous diffusion of DiI allowed for the potential identification of vascular structures associated with blood vessels (e.g. astrocytic end-feet). However, since this was not the goal of this study, these results ruled out the use of DiI as a marker of brain vasculature.

The use of WGA conjugated with AlexaFluor-555 was then tested to label blood vessels in the brain **(Fig. 12)**. Given that in the DiI experiments direct ventricular injection provided better results this route was used to inject a 0.2 mg/ml solution of WGA-AlexaFluor555. The results revealed a homogeneous labelling of brain vasculature with a high degree of detail in both cortical and subcortical structures. This labelling approach withstood the procedural steps used in a transcardial perfusion (both flushing of Hep-

PBS and fixation with 4% PFA) and therefore was deemed superior as a vasculature marker for post-mortem analysis.

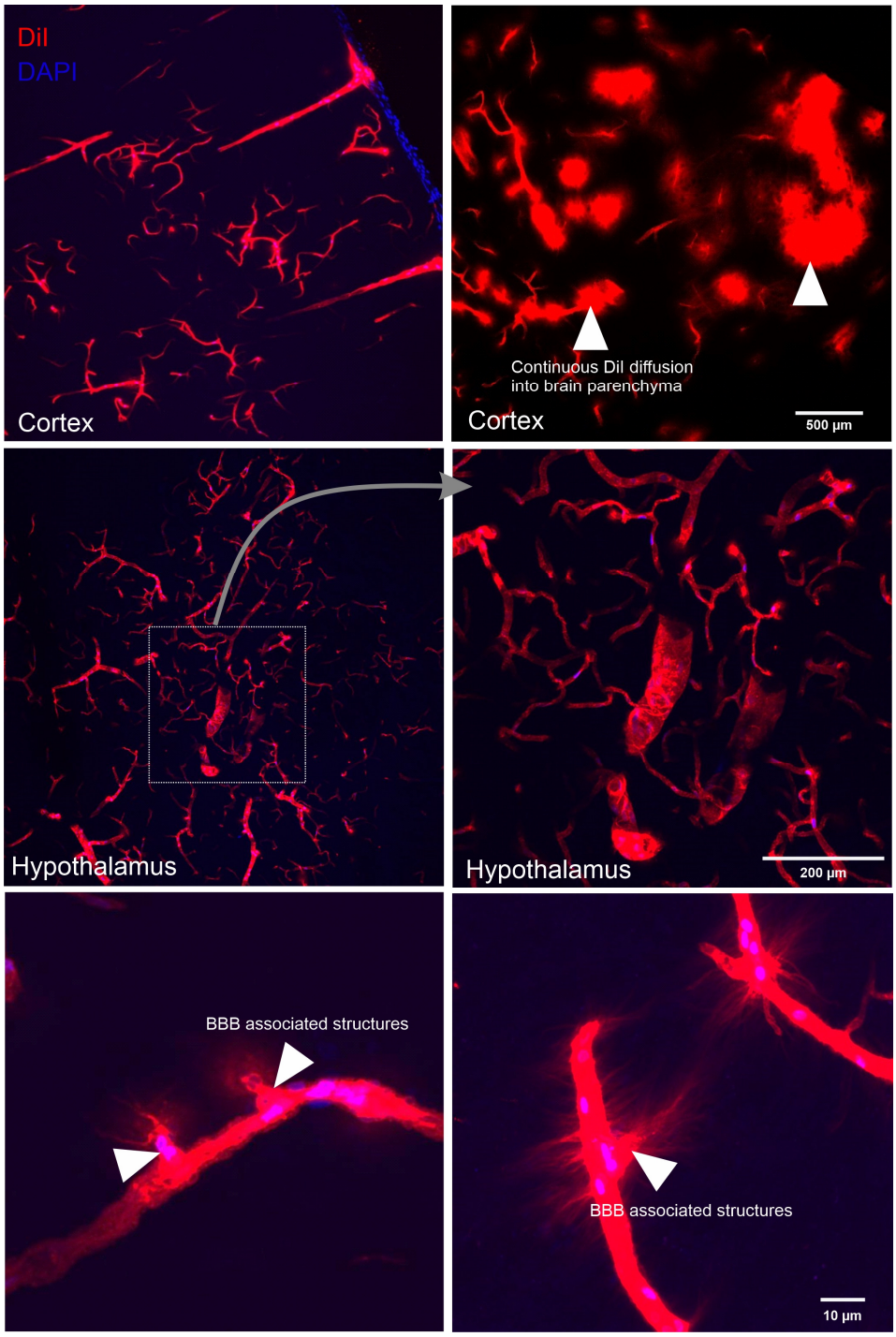

Figure 11. DiI labeling of brain vasculature. Animals were injected with a solution of DiI during transcardial perfusion. DiI provided a non-homogeneous staining of the brain vasculature producing a

"patchy" pattern of staining. In addition, even though the tissue was fixed with 4% PFA, DiI kept diffusing into the tissue generating regions of overstained vessels and labelled structures associated with blood vessels compatible with astrocytic end-feet. DAPI (blue); DiI (red). Therefore, DiI was not a suitable method to label the vasculature in this study.

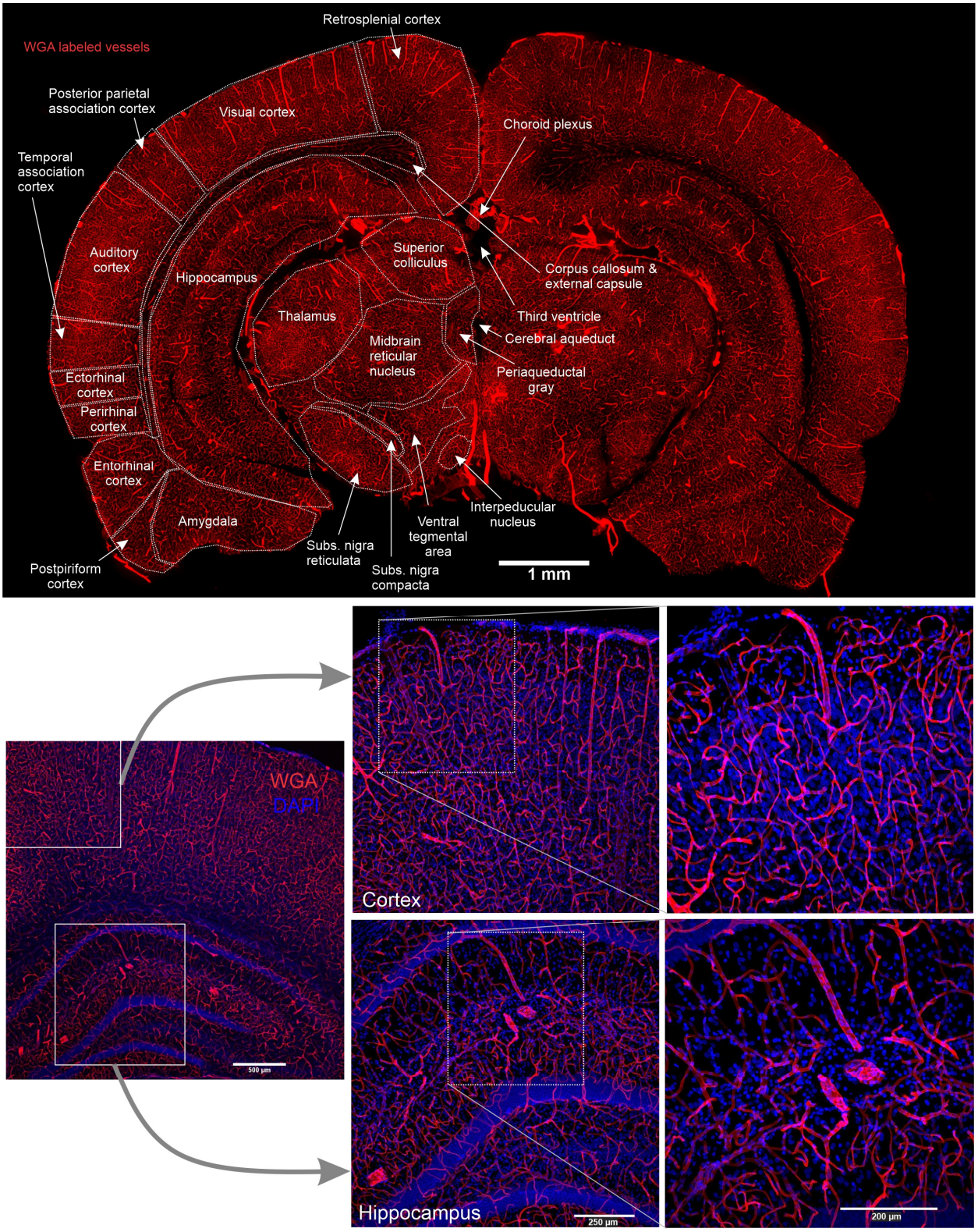

Figure 12. Labeling of brain vasculature with WGA. A solution of WGA-AlexaFluor555 was injected in the left ventricle of the heart before starting the transcardial perfusion. This approach produced optimal and reproducible results by providing a homogeneous staining and high level of detail in labeled vessels.

WGA (red); DAPI (blue). Image at the top panel was created by stitching together 28 images in ImageJ acquired with a 10x objective on an epifluoresence microscope. Lower panels are cortex and hippocampus maximum intensity projection stacks acquired with confocal microscopy using 4x, 10x and 20x objectives, respectively indicating the great level of detail obtained using this approach.

3.3.2 Stab wound injury positive control

First, the vascular damage in the stab wound injury model **(Fig. 9)**, a paradigm of active moderate vascular damage, was evaluated. Initially, Evans blue was tested for this purpose. Evans blue (2%) was injected in the circulatory system of rats (tail vein injection) prior to starting in vivo electrophysiology recordings. A 125 μm-thick stainless steel recording electrode was inserted in the brain at approximately 3.5 mm anterior, 2.0 mm lateral to bregma. The electrode was lowered so the tip was positioned in the hilus of the dentate gyrus (DG) and was then kept in this location for 1 hr. Afterwards, the brain was extracted and directly submerged in a 4% PFA solution in PBS for overnight fixation. Subsequently, the brain was sliced and analyzed for vascular damage **(Fig. 13)**. The fluorescent signal of Evans blue-filled vessels was used to generate a mask to block the intravascular signal and only extravasated Evans blue was analyzed. This approach successfully identified the presence of vascular damage and provided a quantitative measure of injury severity **(Fig.13)**. However, the methodology required to generate the intravascular vessel mask was tedious, time-consuming and not very scalable.

Then, the validity of using extravascular fibrinogen detection to identify vascular damage was tested. In this case, after electrophysiological recordings, animals were prepared for standard transcardial perfusion. Once the cavity chest of urethane anesthetized animals was opened and the heart exposed, a solution of WGA-

AlexaFluor555 was injected in the left ventricle of the heart and allowed to circulate for ~30 sec to label the brain vasculature. Following this, a regular transcardial perfusion was performed. The brain was extracted, post-fixed in 4% PFA and then vibratome sliced into 50 µm-thick sections which were then immunolabelled to detect fibrinogen extravasation. The presence of extravascular fibrinogen in regions that were injured by the penetration of the recording electrode was evident in both cortical and hippocampal areas **(Fig. 14)**. The same procedure to quantify the severity of vascular damage by masking the WGA-labelled blood vessels and measuring the extravascular fibrinogen fluorescent signal was followed in this experiment. The results indicate that fibrinogen extravasation is also a good approach to evaluate active moderate vascular damage.

To further validate this approach and confirm microglia reaction to vascular damage, Iba1 immunolabeling was performed in combination with fibrinogen staining **(Fig. 15).** Again, extravasated fibrinogen signal at the injury site and the physiological reaction of microglia in the perilesional zone (extending their processes towards the injury site) was observed. These results validated the use of fibrinogen and Iba1 in detecting vascular damage in the brain.

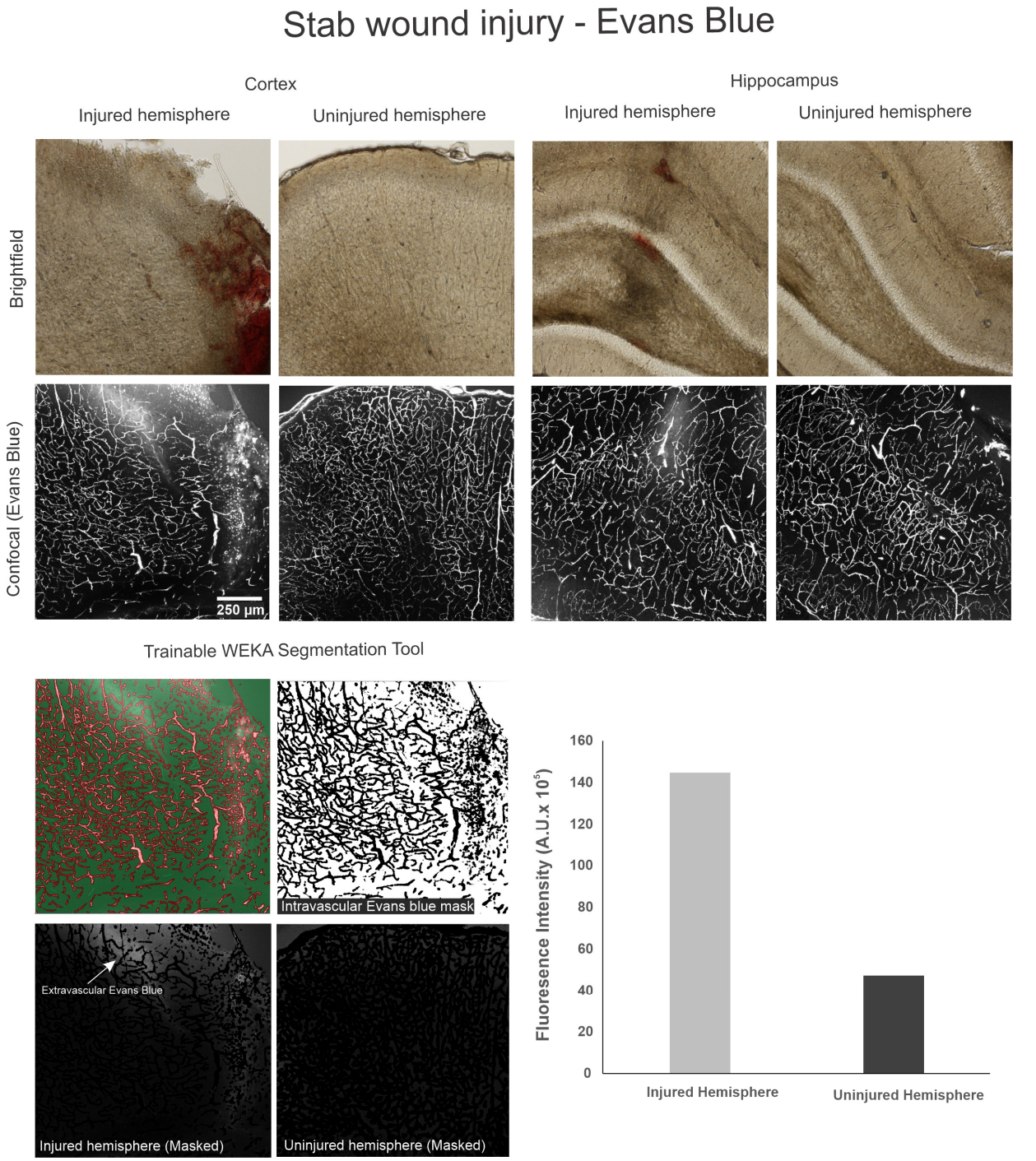

Figure 13. Example of vascular damage in stab wound injury model using Evans blue. Top row shows unstained sections of injured and uninjured hemispheres of stab wound injury animals. Both cortex and hippocampus exhibit vascular damage produced by the penetrating injury. Corresponding confocal images below the top row show Evans blue florescent signals. Left bottom panel shows an example of Evans blue-filled vessels mask creation. These masks were superimposed on original images to measure only extravascular Evans blue signal. Right bottom panel shows quantification of these cortical examples and confirm that Evans blue is a valid method to assess active moderate vascular damage.

Stab wound injury - Fibrinogen

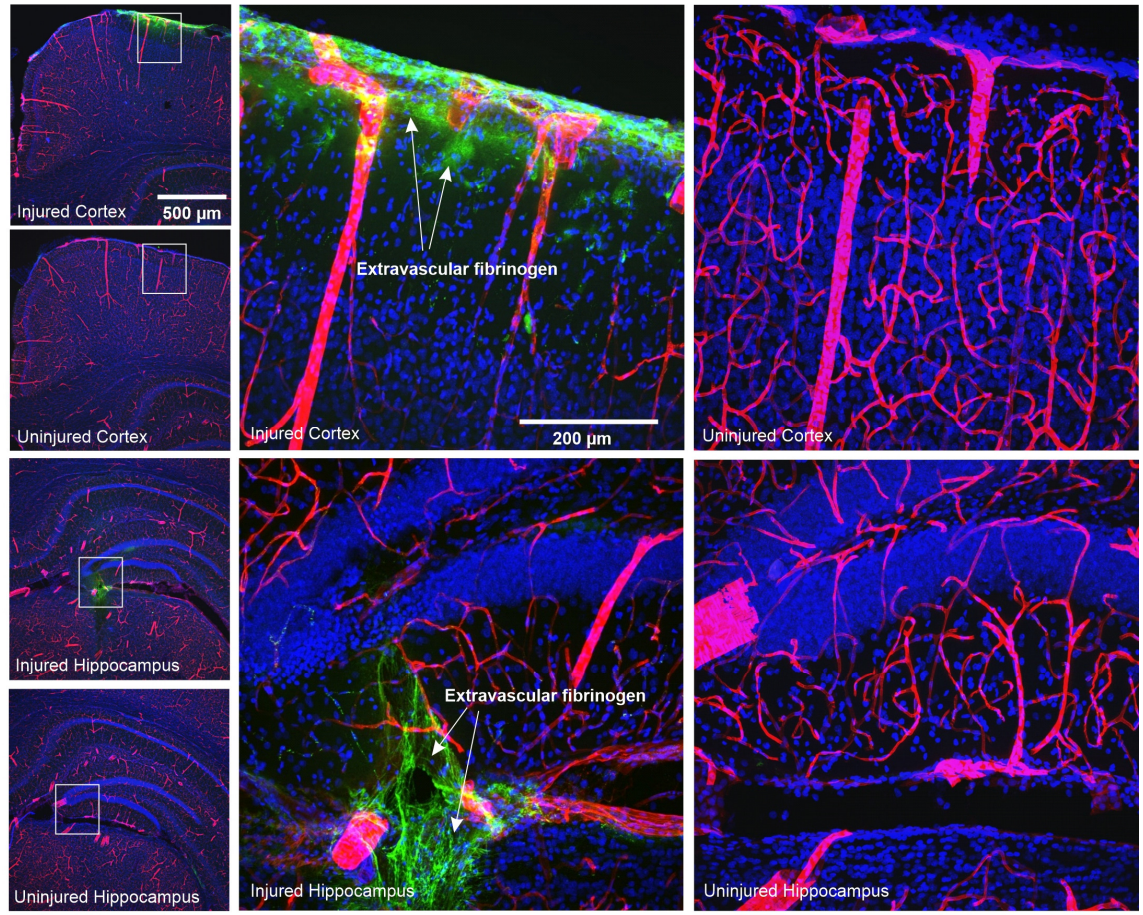

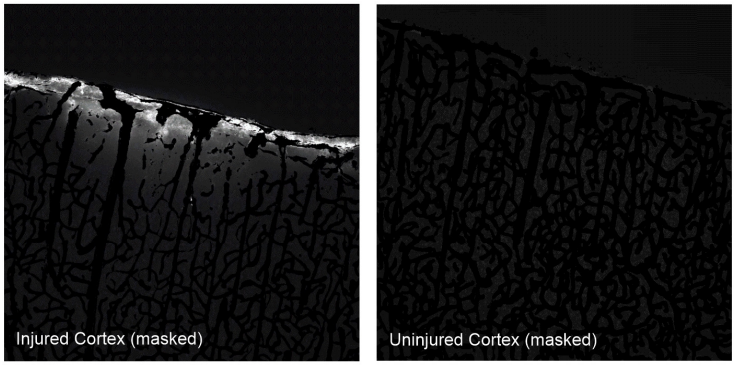

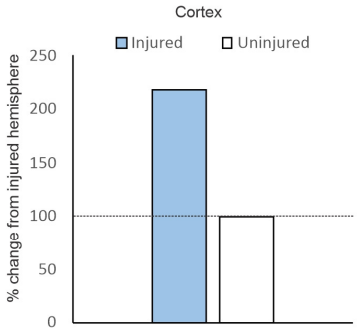

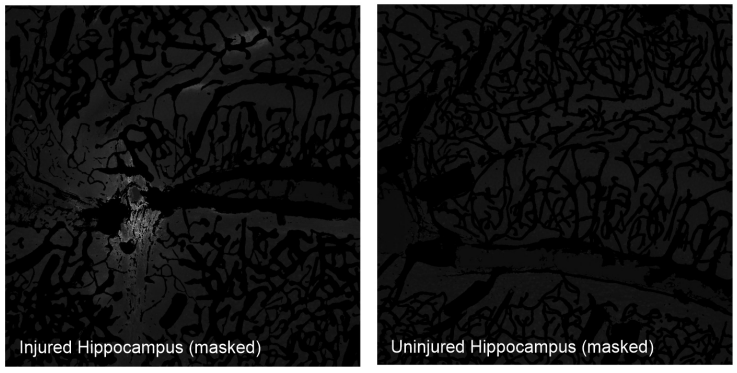

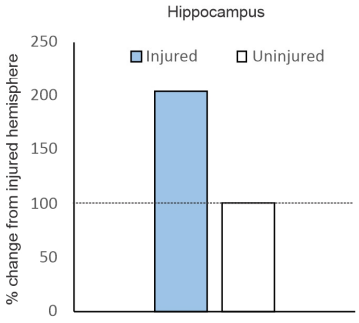

Figure 14. Example of vascular damage in stab wound injury model using fibrinogen. Top left panel shows low magnification (4x objective) max intensity projections of confocal microscopy acquired stacks of stab wound injury animals. Injured and uninjured hemispheres and brain region (cortex or hippocampus) are indicated. Top center and right panel show higher magnifications (10x and 20x objectives, respectively) of these images. The location of extravascular fibrinogen is indicated in the images. Bottom panel shows an example of image analysis. Quantification of extravascular fibrinogen was performed in the same way as Evans blue. Bottom left panel shows example of masked images. Blood vessel masks were superimposed on the original fibrinogen florescent channel to ensure only extravasated fibrinogen was measured. Quantification of cortical and hippocampal damage in the example images is shown in the bottom right panel. These examples reveal that fibrinogen is a valid marker of active moderate vascular damage. DAPI (blue); WGA (red); Fibrinogen (green).

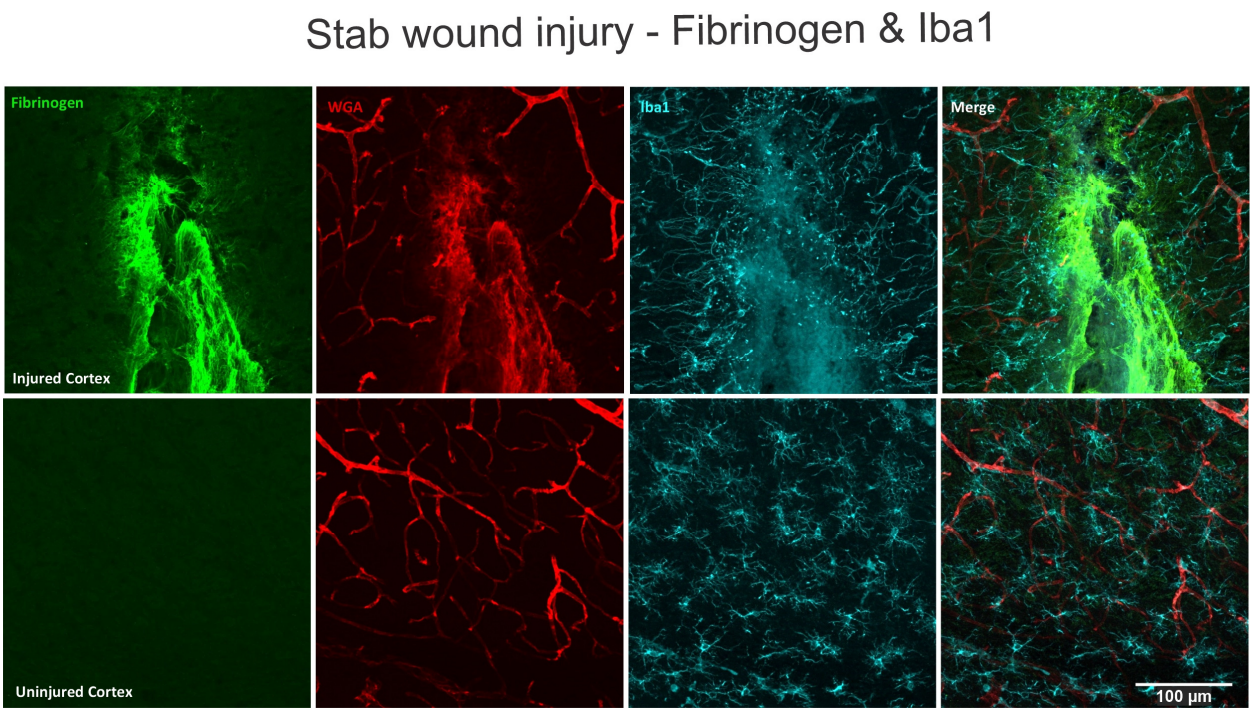

Figure 15. Vascular damage 1 hr after stab wound injury. Examples of fibrinogen (green) leakage and microglia (cyan) reaction in the perilesional area (i.e. along stab wound path) 1 hr after injury (top panel). The uninjured contralateral hemisphere (bottom panel) is presented as control. This data shows that fibrinogen accumulates following vascular damage and that microglia rapidly react to this damage. WGA (red).

It is important to note that the use of WGA to label the lumen of the blood vessels was very important since it was noted that some residual fibrinogen can remain inside the vessels after transcardial perfusion **(Fig. 16).** Therefore, WGA is critical to analyze only fibrinogen that has leaked into the brain parenchyma.

The stab wound injury model provided valuable information regarding approach validation to detect acute moderate vascular damage. However, for the main research questions in the rmTBI model, we expect to see less severe types of vascular damage (i.e. microbleeds) and longer time points. For this reason, a model allowing to test these conditions was needed.

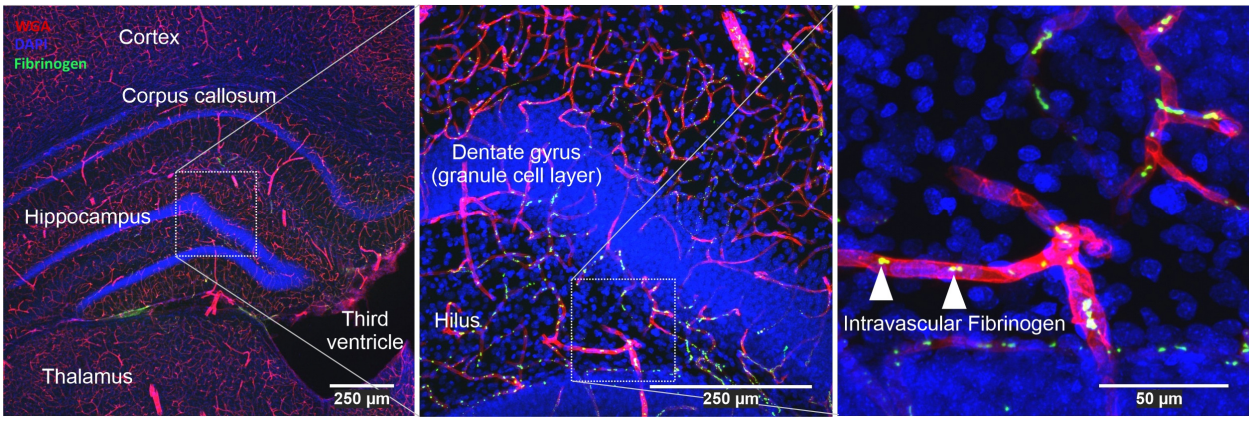

Figure 16. Residual fibrinogen in vasculature after transcardial perfusion. Some residual fibrinogen can remain inside blood vessels after transcardial perfusion. It is critical to label the brain vasculature with WGA-Alexa555 to differentiate the intra and extravascular spaces to ensure that only fibrinogen leaked into the brain parenchyma is measured. DAPI (blue); WGA (red); Fibrinogen (green).

3.3.3. Laser microablation positive control

To assess less severe forms of vascular damage and longer time-points, animals with a cranial window that received microvessel ablation with a laser were used **(Fig. 10)**. These animals received an injection of Evans blue to label the blood vessels and to confirm the induction of microbleeds (i.e. Evans blue leakage). After inducing microbleeds, animals were monitored for 5 days and then transcardially perfused to obtain tissue for post-mortem histological analysis.

The first step in this analysis was locating post-mortem the microbleeds induced 5 days before. To do this, sections were stained with H&E and visually inspected to find Evans blue traces. It was unclear if Evans blue would remain in the system 5 days after the initial leakage, however, the data showed that indeed there were still some traces of Evans blue extravasation both when evaluated with brightfield and confocal microscopy **(Fig. 17)**. To make sure that the presence of Evans blue was caused by vascular damage and not a methodological artifact, staining of phagocytic cells such as reactive microglia and macrophages was performed by immunolabeling with anti-CD68, a lysosomal marker that is expressed in these cells. The results indicated that the leakage of Evans blue was associated with aggregation of CD68 positive cells, confirming the specificity of microvascular damage detection **(Fig. 18)**.

Next, fibrinogen immunolabeling was employed to see if it was a suitable marker for detecting 5-day old microvascular lesions, and if present, what was its staining pattern in comparison to Evans blue (i.e. do fibrinogen and Evans blue co-localize). The results

showed that fibrinogen labeling was present in the same region as leaked Evans blue with fibrinogen located closer to the source of the vascular injury and Evans blue diffusing further away **(Fig. 19)**. These results indicated that both Evans blue and fibrinogen are good markers of microvascular damage and that they could be detected some time after the occurrence of the initial vascular injury (in this case 5 days after). The possibility to detect fibrinogen and Evans blue extravasation 5 days after the initial vascular injury is important given our mTBI injury paradigm (i.e. 8 impacts over 4 days) and the specific relevance will become clearer in the next chapter. Although Evans blue remains relatively close to the original injury site, it diffuses more than fibrinogen, making it probably not the best approach to study vascular injuries at longer time points.

Finally, since the previous positive control model for vascular damage (stab wound injury) was confined to an acute time point (i.e. ~30-60 min post-injury), it was impossible to test the validity of the Prussian blue staining to detect traces of 2/3-day-old vascular damage. However, animals that received laser microablations were euthanized 5 days after the initial vascular injury allowing the possibility to test Prussian blue staining for hemosiderin deposit visualization. As expected, with Prussian blue staining it was possible to identify 5-day-old hemosiderin deposits caused by the laser microablation procedure **(Fig. 20)**. To confirm that indeed the identified hemosiderin deposits were cause by microbleeds, the same brain location was examined in a serial section (50 μm apart) and it was found that this region also showed extravasation of Evans blue **(Fig. 20)**.

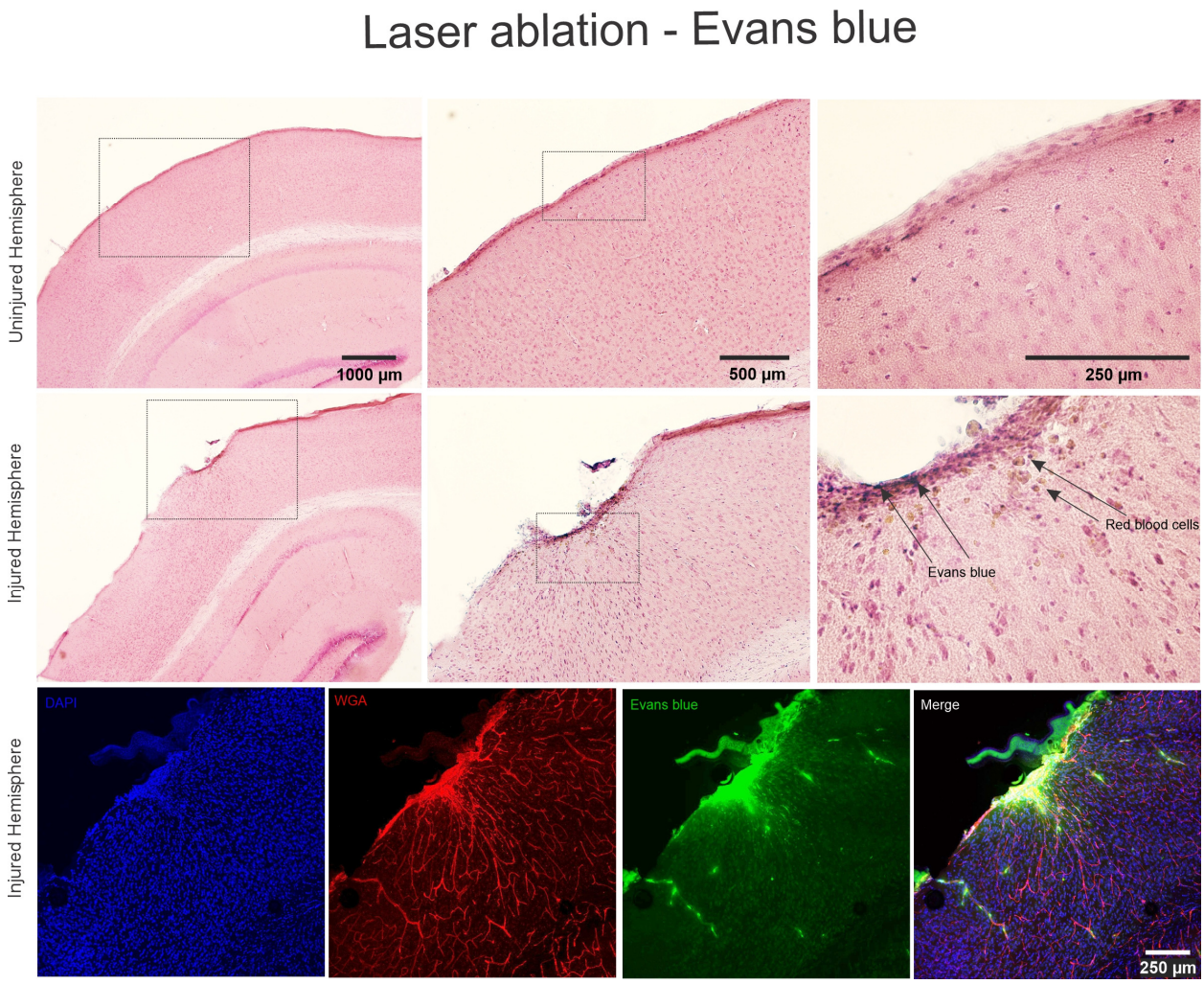

Figure 17. Example of Evans blue leakage 5 days after laser microablation. Top and middle panel show H&E stained sections of the uninjured (top) and injured (middle) hemispheres of a mouse that received laser microablation injury in the primary somatosensory cortex. Animals were monitored for 5 days after induction of microvascular damage and then processed for post-mortem histological analysis. In the injured hemisphere (middle panel) we can see the cortical region showing signs of microvascular damage as traces of Evans blue and degrading RBCs with their characteristic blue and brown pigments, respectively. Bottom panel shows the corresponding confocal max intensity projections of a serial section showing extravasation of Evans blue in this area. These results confirm that Evans blue is a valid method to assess microvascular damage 5 days after the initial lesion.

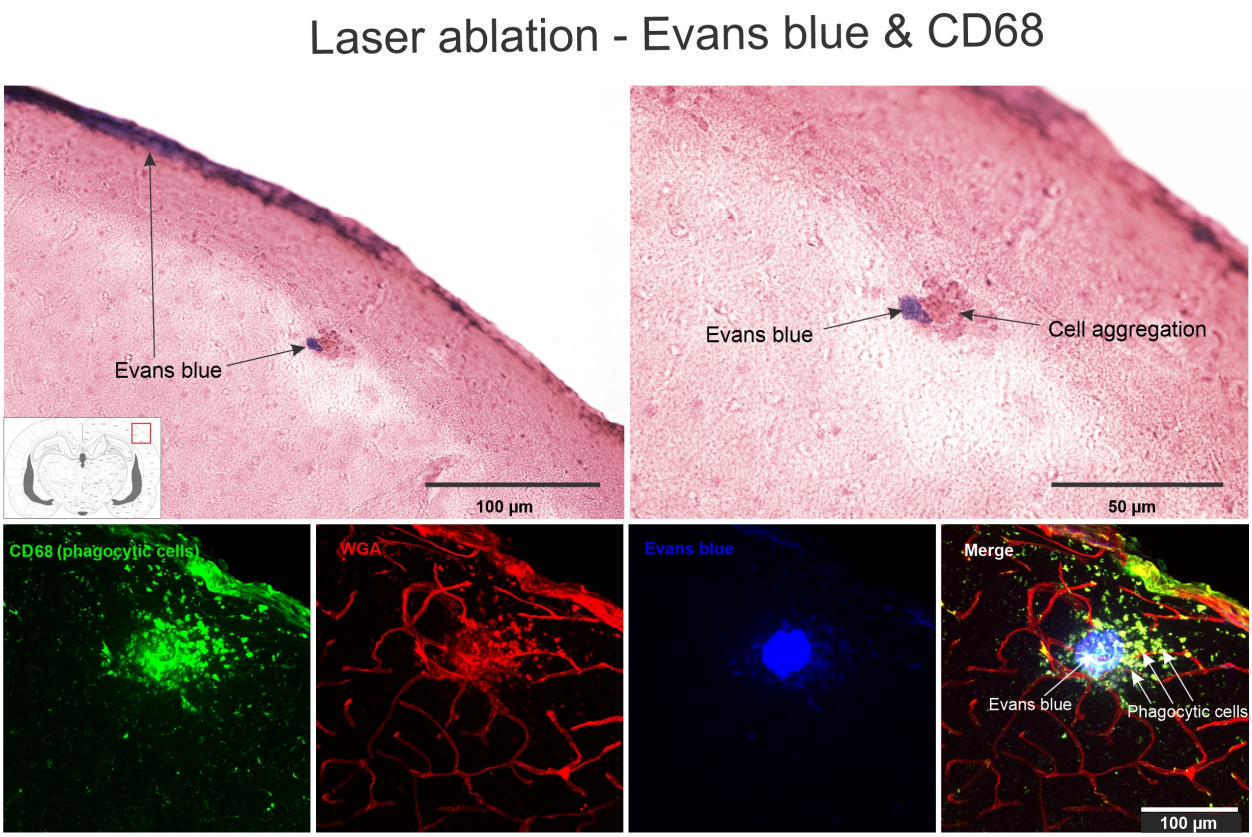

Figure 18. Evans blue co-localizes with CD68 positive cells following laser microablation. Top panel shows H&E stained section of a mouse that received a laser microablation injury in the primary somatosensory cortex and was processed for post-mortem histological evaluation 5 days after the initial vascular injury. The location of Evans blue (blue) is indicated in the images as well as cluster of cells in close proximity. Bottom panel shows the corresponding confocal max intensity projection images of a serial section labelled with CD68 to visualize phagocytic cells, blood vessels with WGA, and Evans blue to locate the vascular damage. Confocal microscopy confirmed that the cell aggregation was a cluster of CD68+ cells, indicating that phagocytic cells such as reactive microglia or macrophages were clustered in the vicinity of leaked Evans blue. This suggests that indeed the presence of leaked Evans blue was caused by the laser microablation and not by methodological manipulation and that this microvascular damage induced a physiological response of immune cells that was still visible 5 days after the initial injury.

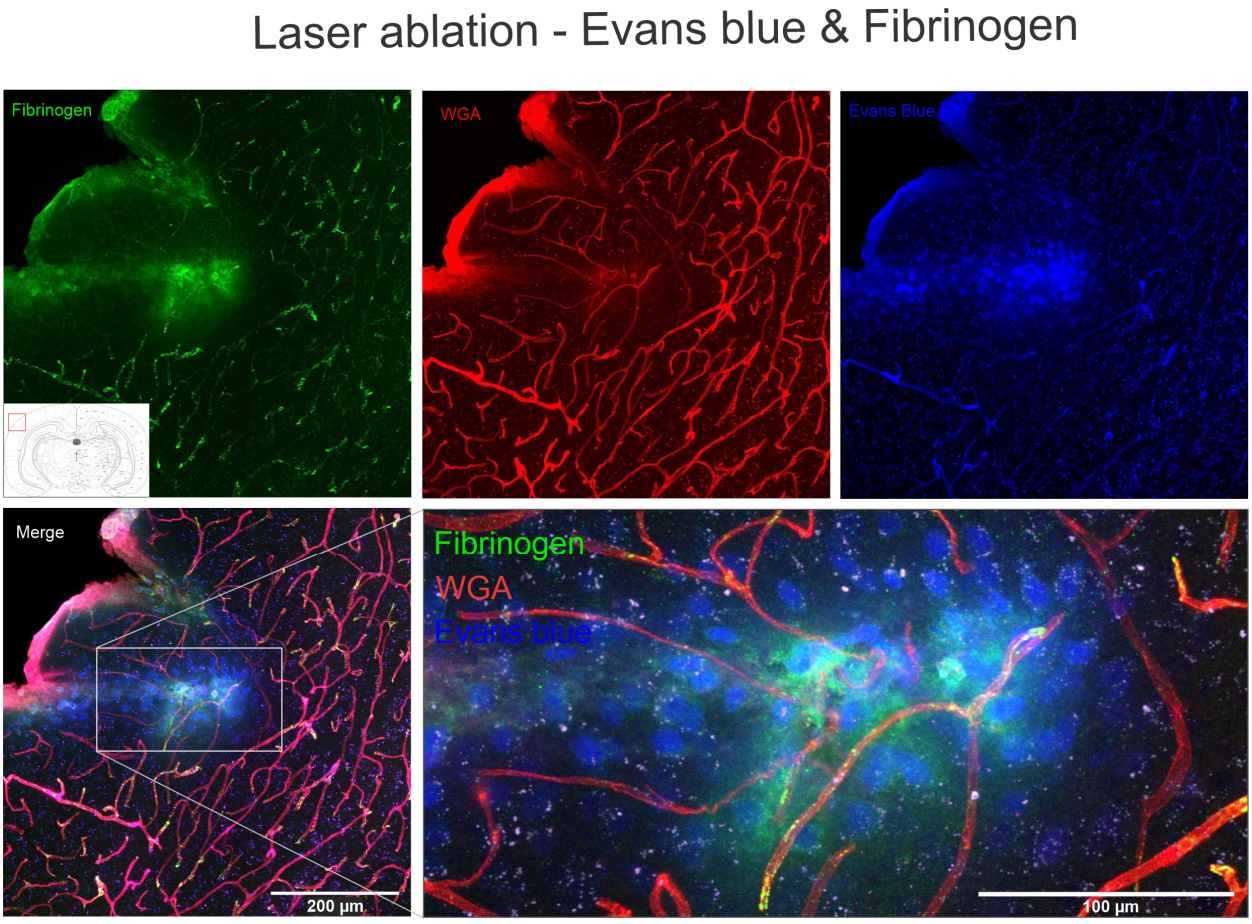

Figure 19. Fibrinogen extravasation co-localizes with Evans blue leakage following laser microablation. Representative images from a mouse that received a laser microablation injury in the cortex and was processed for post-mortem histological evaluation 5 days after the initial vascular lesion. Confocal max intensity projection images of brain sections immunolabelled to visualize fibrinogen (green), blood vessels with WGA (red) and Evans blue (blue). The intention of this staining was to 1) confirm that fibrinogen was still detectable 5 days after the initial injury, 2) validate that fibrinogen was indeed located in a microbleed site (using Evans blue as a reference) and 3) compare the staining pattern of these two markers of microvascular damage. This staining revealed that fibrinogen was detectable at a microbleed site 5 days after initial injury and that this protein stayed at the source of the vascular damage while Evans blue diffused away from the original lesion.

.

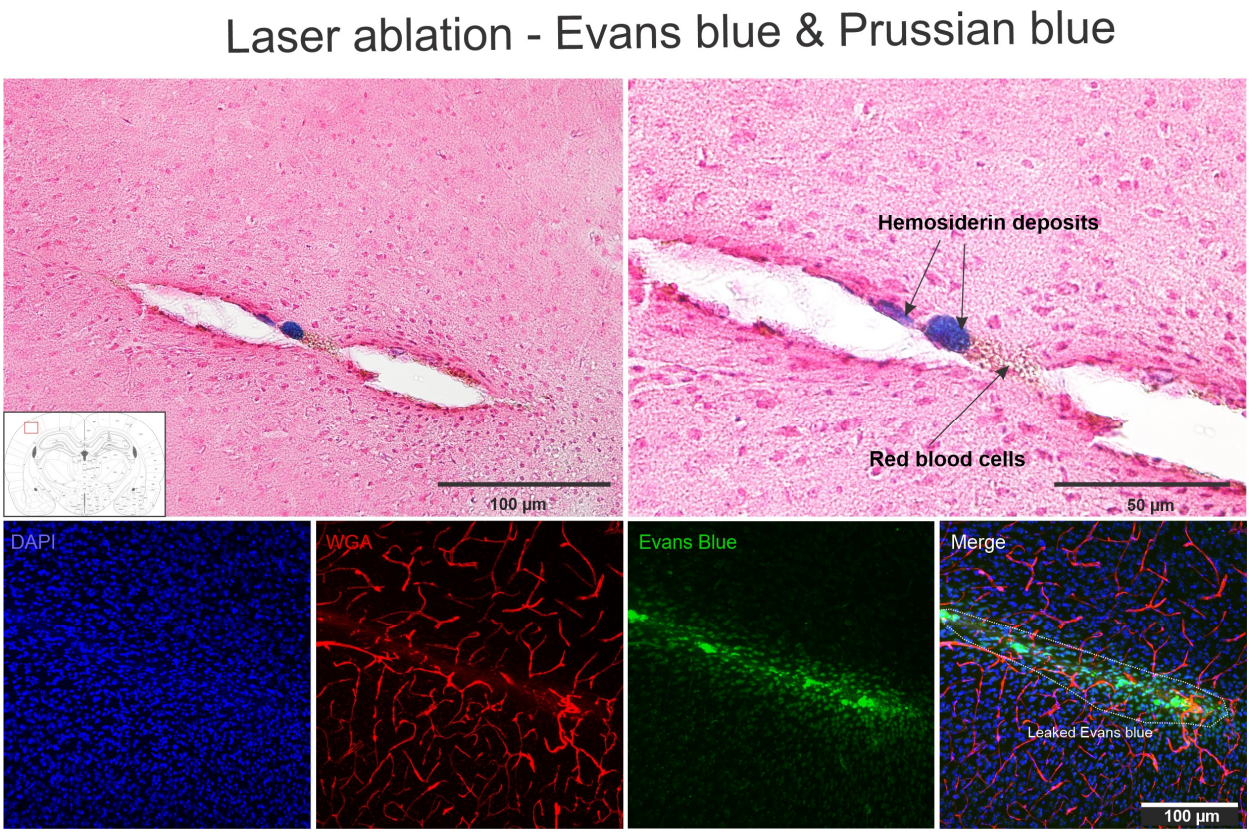

Figure 20. Hemosiderin deposits can be detected in 5-day-old microbleeds using Prussian blue staining. Hemosiderin deposits were detected using the Prussian blue reaction (top panel) 5 days after the laser microabalation injury. In addition, confocal evaluation of leaked Evans blue in the corresponding brain location in a serial section (50 µm apart) confirmed the presence of microvascular damage (bottom panel) and, therefore, specificity of the Prussian blue staining.

3.4. Discussion

In this chapter, an overview of the most common methods used to label the brain vasculature and evaluate vascular damage in rodents was provided, and then different approaches were evaluated with the intention to identify and validate the most appropriate methodology to use in the main research questions using the ACHI model of rmTBI. Two models of vascular damage were used as positive controls to validate these approaches on different injury severities and time points. Specifically, a model of stab wound injury in rats was used to test active short-term moderate vascular damage (Lin et al., 2005; Schachtrup et al., 2010), and then a model of cerebral microbleeds (laser microablation) was used to evaluate microvascular damage (Rosidi et al., 2011; Ahn et al., 2018; Taylor et al., 2018) at a longer time point. A critical part in evaluating vascular damage with a high degree of precision is having a reliable method to label the vasculature. These results showed that similar to what has been reported in other studies, WGA is an excellent method to label the lumen of blood vessels (Robertson et al., 2015) and superior to DiI staining. Nevertheless, it is worth mentioning that other studies have demonstrated optimal results using this lipophilic molecule, although with a different approach as the one used in this study (Konno et al., 2017).

Then, it was shown that detection of extravasated Evans blue and fibrinogen are both good approaches to detect active vascular damage in both moderate and mild severities as reported in previous studies (Davalos et al., 2012; Nahirney et al., 2013; Petersen et al., 2018; Taylor et al., 2018; Wu et al., 2021). However, the continuous

diffusion of Evans blue after leakage combined with a slightly more technical expertise required in some steps (e.g. tail vein injection) favoured deciding on fibrinogen labelling as microvascular damage marker for the main rmTBI research questions that will be presented in the following chapter. In addition, since the hypothesis of the rmTBI study states that "insoluble depositions of fibrin caused by vascular damage may play an important role in rmTBI", it made more sense to analyze this protein instead of Evans blue.

In the rmTBI study, the intent is to evaluate not only active vascular damage, but also traces of past vascular injuries that may be already resolved. Prussian blue staining allows detection of the iron traces (hemosiderin deposits) left by vascular injuries as blue particles (Liu et al., 2014; Sumbria et al., 2016). To validate this approach, animals that received laser microablation injuries were processed for post-mortem histological analysis 5 days after the initial injury. The results indicated that indeed, in accordance with previous reports (Liu et al., 2014; Sumbria et al., 2016), Prussian blue staining was able to detect the presence of hemosiderin deposits caused by this microbleeds. This was confirmed with leakage of Evans blue in close proximity of the hemosiderin deposits.

In addition, the reaction of microglial cells in the vicinity of vascular injuries was assessed to confirm the specificity of these signs of vascular damage (i.e. confirm that the staining was not caused by perfusion artifacts). The images showed that these cells displayed a regular physiological response to vascular damage by extending their processes towards the injury site ~30-60 min after initial damage (Davalos et al., 2005b;

Lou et al., 2016), and also showed aggregation of phagocytic cells (i.e. CD68 positive) in perilesional sites 5 days after initial injury.

The data presented here has provided evidence to select the most optimal and available approach to use given the goal of evaluating the association between rmTBI and microvascular damage in the ACHI model. It was decided that using a combination of WGA labeling for blood vessels, and fibrinogen and Iba1 immunolabeling to evaluate the presence of microvascular damage was optimal because these labels provide a way to evaluate acute and active vascular damage post-mortem that is easy to localize, remains closer to the initial source of vascular damage, can be clearly identified as being in the extravascular space and can be confirmed as not being a product of a methodological artifact. In addition, Prussian blue was selected for the rmTBI study because vascular injuries resolve over time, and this staining technique reveals iron traces left by past vascular injuries in a post-mortem scenario. It is worth mentioning that a dextran conjugated with FITC was also tested to assess alterations in vascular permeability (data not shown). Unfortunately, since this molecule was not fixable, the dextran signal was not detected because it presumably got cleared from the system during the transcardial perfusion or lost florescence over time. For future studies, it would be interesting to evaluate the possibility of using fixable dextrans conjugated with different fluorophores to assess vascular permeability overtime (e.g. how long does a vascular injury remains active) or study the contributing effects of different conditions (e.g. what is the vascular damage caused by impact 1, impact 2, etc.).

Finally, it is important to mention that the methodology described in these experiments to quantify vascular damage (i.e. vasculature masking, visual inspection, etc.) was tailored to get fast but non-thorough and non-easily scalable measurements. This methodology was deliberately used to be able to validate quickly and with a low number of animals the approaches proposed to be used in the rmTBI study. Therefore, the specific methodology employed in the evaluation of microvascular damage in rmTBI that will be described in the following chapter will differ to allow a more thorough and sensitive assessment of microvascular damage.

CHAPTER 4: IS rmTBI ASSOCIATED WITH INCREASED CEREBRAL MICROVASCULAR DAMAGE AND MICROGLIA REACTION?

4.1. Introduction

TBI often results in significant injury to the vasculature in the brain that often leads to cerebral hypoperfusion, ischemia, hypoxia, hemorrhage, vasospasms, BBB disruption and edema (Salehi et al., 2017). Signs of vascular damage are very clear in severe and moderate types of TBI but they are usually absent or hard to identify in mTBI. However, there is increasing evidence showing that subtler forms of vascular damage at the microvascular level can have an important role in injury severity in head trauma. While studies show that CMBs do not produce acute stroke-like symptoms like nearby cell death, degeneration of dendritic arbors (Rosidi et al., 2011) or long-term loss of neural responsivity (Cianchetti et al., 2013), several studies have reported that there is an increase in the density of inflammatory cells near the lesion that can be sustained for weeks (Rosidi et al., 2011). Even without the presence of severe stroke-like signs, clinical evidence suggests that CMBs are highly correlated with cognitive impairment, cognitive decline and dementia (Wiegman et al., 2014; Ungvari et al., 2017; Ahn et al., 2018). The formation of CMBs is thought to involve diapedesis, whereby RBCs transiently cross the BBB to form hemosiderin deposits in the brain parenchyma (Zhang et al., 2014). It is important to note that microbleeds have been reported to occur spontaneously in healthy

individuals and this phenomenon increases with age. Therefore, since there is a basal level of microvascular events, signs of microvascular damage can be observed in healthy individuals and this should be taken into consideration when analysing this phenomenon.

CMBs have been reported to occur to a certain extent in all severities of TBIs and their presence is strongly associated with that of traumatic axonal injury. Even though CMBs themselves are localized, research indicates that the effects triggered by RBCs extravasation can extend far outside the vicinity of the initial vascular lesion. (Simard et al., 2009; Patel et al., 2013). This information hints to a potential mechanism of how sustained, repeated and multifocal microvascular damage can lead to alterations in synaptic transmission in part through axonal disruption and ultimately can cause changes to brain function in areas located far from initial damage.

Common to several CNS diseases is the presence of extravasated fibrinogen in the brain (Petersen et al., 2018). This plasma protein, involved in the formation of stable blood clots, has received increasing attention due to growing evidence highlighting the importance of this protein in the inflammatory cascade induced by vascular damage in the brain (Petersen et al., 2018). Indeed, in MS and AD, it has been reported that when this protein leaks repeatedly into the brain parenchyma due to vascular damage, it interacts with the microglial receptor CR3, and initiates a series of events that lead to the generation of clusters of chronically activated pro-inflammatory microglia (Paul et al., 2007; Davalos et al., 2012; Petersen et al., 2018). This in turn can result in progressive

demyelination and neurodegeneration. These data indicate that even subtle forms of damage to blood vessels in the brain, when accumulated over time, have the potential to trigger or exacerbate subsequent deleterious events and lead to long-lasting structural and functional deficits.

Based on this information, I hypothesize that the repetitive mechanical forces generated during multiple impact (rmTBI) events induce damage to the microvasculature and promote a sustained pro-inflammatory environment triggered by the chronic activation of microglial cells through the continuous interaction with fibrin deposits.

In the previous chapter, common techniques used to evaluate vascular damage in rodents were shown, and their use to detect microbleeds at different time points was validated. In this chapter, these approaches (i.e. detection of hemosiderin deposits and fibrinogen extravasation) will be employed to evaluate the presence, location and severity of microbleeds associated with the ACHI model of rmTBI. Two time points (i.e. PID1 and PID7) will be selected to assess the overall and regional effects of this injury paradigm on microvascular damage in juvenile males and females. Five different brain areas will be explored to assess potential regional susceptibility to head trauma. In addition, the specificity of microvascular damage will be confirmed by evaluating the microglia response to vascular injury, and the possibility of differences in the reaction of these immune cells to microbleeds will be explored.

4.2. Methods

4.2.1. Animal generation & Experimental design

In this study, two main experimental groups for each sex were used. These groups were sham control and rmTBI. Also, two time-points were selected: PID1 (i.e. 1 day after the last impact) and PID7 (i.e. 7 days after the last impact). In addition, for PID1, one more experimental group (naïve control) for each sex was used to evaluate potential procedural-induced vascular damage. A total of 5 animals per experimental group, sex and time point were used. Therefore, a total of 50 Long Evans rats were used in this study. For a more detailed explanation on animal generation and the ACHI model please see section "2. General Materials & Methods".

4.2.2 Histology

4.2.2.1. Tissue preparation

Before proceeding to transcardial perfusion, animals were anesthetized with an intraperitoneal injection of urethane at a dose of 1.5 mg/kg. Once animals reached a deep status of anesthesia (~30-45 min; evaluated by toe pinch reflex) the cavity chest was opened and the heart was exposed. One ml of a 0.2 mg/ml solution of WGA-Alexa555 diluted in Hep-PBS was injected directly into the left ventricle of the heart using a sterilized syringe (Henke Saas Wolf, #4010-200U0) and a 30-gauge needle at a constant rate over 30 sec. This WGA-Alexa555 solution was allowed to be distributed by the still pumping heart throughout all the animal's circulatory system for ~20 sec. After this, ~120 ml of Hep-PBS was perfused through the left ventricle (with right atrium cut) followed

by the same volume of 4% PFA diluted in 0.1 M PBS. The full time length of the transcardial perfusion was ~20 min. After this, the brain was carefully extracted and post-fixed in the same 4% PFA solution for 24 hrs and then stored in PBS with 0.02% sodium azide. After this, brains were sliced into 50-µm-thick sections using a vibratome (Leica VT1200S) and 1 every 12 sections was collected in a 12-well plate. Contiguous wells were used for Prussian blue staining **(Fig. 21)** and immunofluorescence labeling **(Fig. 22)**.

4.2.2.2. Prussian blue staining

A total of 12 sections per animal from the same well were mounted on glass slides (Fisher Brand, #12-550-15) (3 sections per slide) and allowed to air dry for 4-5 days. After this, sections were rehydrated for 10 min in dH_2O and then covered with Prussian blue solution consisting of 5% hydrochloric acid and 5% potassium ferrocyanide in a 1:1 ratio. This mix solution was made fresh every time because potassium ferrocyanide oxidizes rapidly when exposed to light and turns into a dark solution. Sections were incubated in a dark wet chamber for 30 min and then quickly rinsed 3 times with dH_2O and 1 time for 10 min. After this, sections were counterstained with nuclear fast red for 10 min. Then, sections were quickly rinsed in dH_2O 3 times. Next, slides were serially dehydrated by placing them in a 95% ethanol (EtOH) solution for 1 min followed by 1 min in 100% EtOH and finally 2 min in CitriSolv. After this, sections were coverslipped using Cytoseal 60 and allowed to cure for 24 hrs.

4..2.2.3. Immunofluoresence

A total of 12 slices per animal from the same well were selected for immunostaining. First, an antigen retrieval step was performed. Briefly, sections were placed in 1.5 ml Eppendorf tubes containing 1.4 ml of 10 mM sodium citrate (pH 6.0). These tubes were placed in a water bath at 75°C for 30 min. After this, tubes were allowed to cool down at RT (~20 min). Next, sections were transferred to a 24-well plate and blocked a solution of 5% BSA, 0.3% Triton-X 100 and 0.01% sodium azide diluted in 0.1M PBS. Following this step, sections were incubated at 4°C overnight with primary antibodies diluted in a solution of 1% BSA, 0.1% Triton-X 100 and 0.01% sodium azide diluted in 0.1 M PBS. Antibodies used were rabbit anti-fibrinogen at 1:1000 (DAKO, A0080) and mouse anti-Iba1 at 1:1000 (EMD Millipore, MABN92). After this, sections were washed 3 times for 10 min with 0.1% Triton-X 100 diluted in PBS and then incubated with secondary antibodies diluted in 1% BSA, 0.1% Triton-X 100 diluted in PBS on a belly dancer for 1 hr at RT. Secondary antibodies used were goat anti-rabbit AlexaFluor 488 (1:500) and donkey anti-mouse Alexa 647 (1:500). Next, sections were washed twice with 0.1% Triton-X 100 diluted in PBS for 10 min each, counterstained with DAPI for 8 min and washed one more time for 10 min with PBS. After this, sections were incubated with 63% TDE diluted in dH_2O overnight and the next day mounted and coverslipped using the same TDE solution. Finally, coverslips were sealed using clear nail polish.

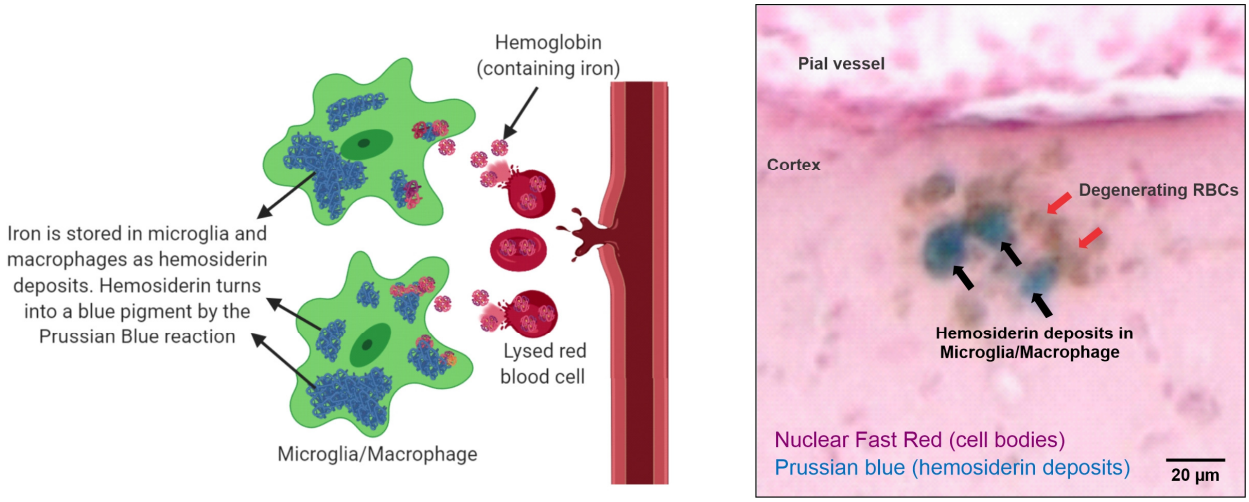

Figure 21. Detection of microbleed hemosiderin deposits by Prussian blue. Left panel shows a schematic of the events following a cerebral microbleed that causes the leakage of RBCs. When RBCs deplete their energy reserves they eventually release their cytosolic components. Among these components is hemoglobin, an iron-containing molecule that is processed by microglia and macrophages to recycle the iron and store it intracellularly as hemosiderin deposits. This process takes ~2-3 days. Hemosiderin deposits can be identified as blue particles with the Prussian blue staining. Right panel shows an example of Prussian blue stained hemosiderin deposits in the primary somatosensory cortex of a rmTBI animal. Some RBCs are still undergoing degeneration and their iron has not yet been converted into hemosiderin deposits.

4.2.3 Imaging & Image analysis

4.2.3.1. Evaluation of hemosiderin deposits

A total of 4 slides per animal (3 slices per slide) were imaged and analyzed by an investigator blind to the experimental condition of the animal **(Fig. 23)**. Images were acquired using a motorized Olympus BX51 (Olympus). The virtual scanning module of StereoInvestigator (MBF Bioscience) was utilized to obtain a whole-slice image for each of the 12 stained slices per animal. Whole slice analysis was attempted but due to computational-intensive requirements, a segmentation approach was used. For this, 5 brain regions (cortex, corpus callosum, hippocampus, thalamus and striatum) were

segmented from each section (if the region was anatomically present) **(Fig. 24)**. Approximately 88 segmented images for each animal were obtained. The exact methodology for regional segmentation is included in **Appendix A**. The presence of hemosiderin deposits and the features of these deposits were evaluated using an ImageJ macro that combined the "color threshold"and the "analyze particles" modules of ImageJ **(Fig. 25)**. Also, another simple macro to evaluate the total area analyzed in each segmented image was used (these macros can be obtained in **Appendix B**). These macros were used to select particles of at least 5 μm^2 within the blue spectrum (specific parameters used are provided on **Appendix B**), and then this selection was used to obtain: 1) total number of hemosiderin deposits per segmented image; 2) density of hemosiderin deposits per segmented image; 3) total area and percentage area occupied by hemosiderin deposits per segmented image; and 4) average size of hemosiderin deposit per segmented image. These values were grouped by brain region and added (number and area) or averaged (density and size) and results are presented as total number of hemosiderin deposits per animal, total percentage area occupied by hemosiderin deposits per animal, average hemosiderin deposit density per animal and average hemosiderin deposit size per animal **(Fig. 23).** Both an overall analysis (i.e. all regions combined) and regional analysis were preformed taking into account experimental group and sex.

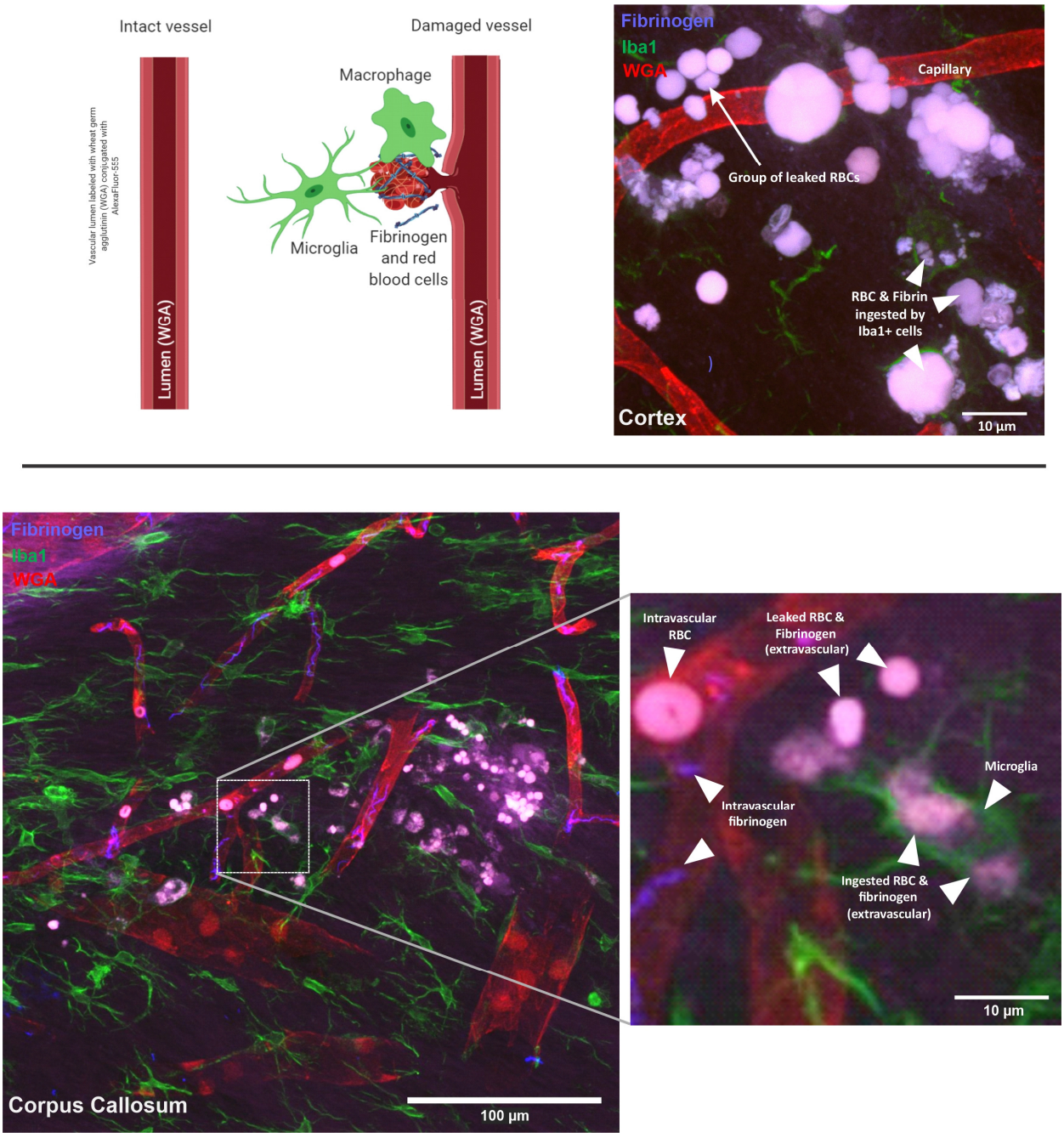

Figure 22. Detection of microbleeds with confocal microscopy by immunolabelling for fibrinogen leakages and microglia reaction. (Top left panel) Fibrinogen leaks after a blood vessel ruptures in conjunction with other blood components like RBCs, and this initiates a reparatory response that includes the attraction of microglia to the injury site. (Top right panel) Part of this reparatory process involves clearing of these blood components by microglia through phagocytosis. (Bottom panel) Confocal images highlighting what can be observed in the vicinity of a microbleed. This includes microglia ingesting leaked blood components, surveilling microglia, and also intravascular fibrinogen and RBCs (not included in microbleed analysis).

4.2.3.2. Evaluation of extravasated fibrinogen

Twelve stained slices per animal were systematically scanned using an epifluorescence microscope **(Fig. 26)**. Every time fibrinogen positive signal was identified, its validity as microbleed was tested by evaluating the other channels for extravascular location (WGA) and microglia reaction (Iba1) using an Olympus FV-1000 confocal microscope (Olympus) and FV10-ASW 4.2 software. For a candidate microbleed site to be confirmed as an actual microbleed it had to be: 1) located outside of a WGA-stained vessel lumen, and 2) show signs of microglial cells interacting with the extravasated fibrinogen. This microglia interaction included a fibrinogen positive signal inside microglia (i.e. phagocytosed fibrinogen) or microglia processes in contact with extravasated fibrinogen (i.e. microglia approaching fibrinogen) **(Figs. 22 and 27)**. In cases of doubt, 3D reconstructions were generated to confirm this interaction. If a microbleed was confirmed, a standard size squared imaging region of interest (ROI) of 317.13 x 317.13 μm (100,571.43 μm^2) was acquired using a 20x UPlanSApo (NA:0.75; W.D. 0.65) objective (Olympus, 1-U2B825) and 2x digital zoom **(Fig. 26)**. This ROI size was picked to resemble imaging with 60x objective but avoiding the sequence of 1) scanning and identifying microbleeds at 10x, 2) adding immersion oil,3) imaging at 60x, 4) cleaning immersion oil, and 5) going back to scanning and identifying microbleeds at 10x. A 488 nm laser was used to visualize immunolabelled fibrinogen with an AlexaFluor 488 secondary antibody. A 561 nm laser was used to visualize blood vessels stained with WGA-Alexa555. Finally, a 647 nm laser was used to visualize immunolabelled Iba1. Image stacks of regions with vascular damage were acquired at 1024x1024-pixel frame size, 2-μs/pixel and 1 μm step size.

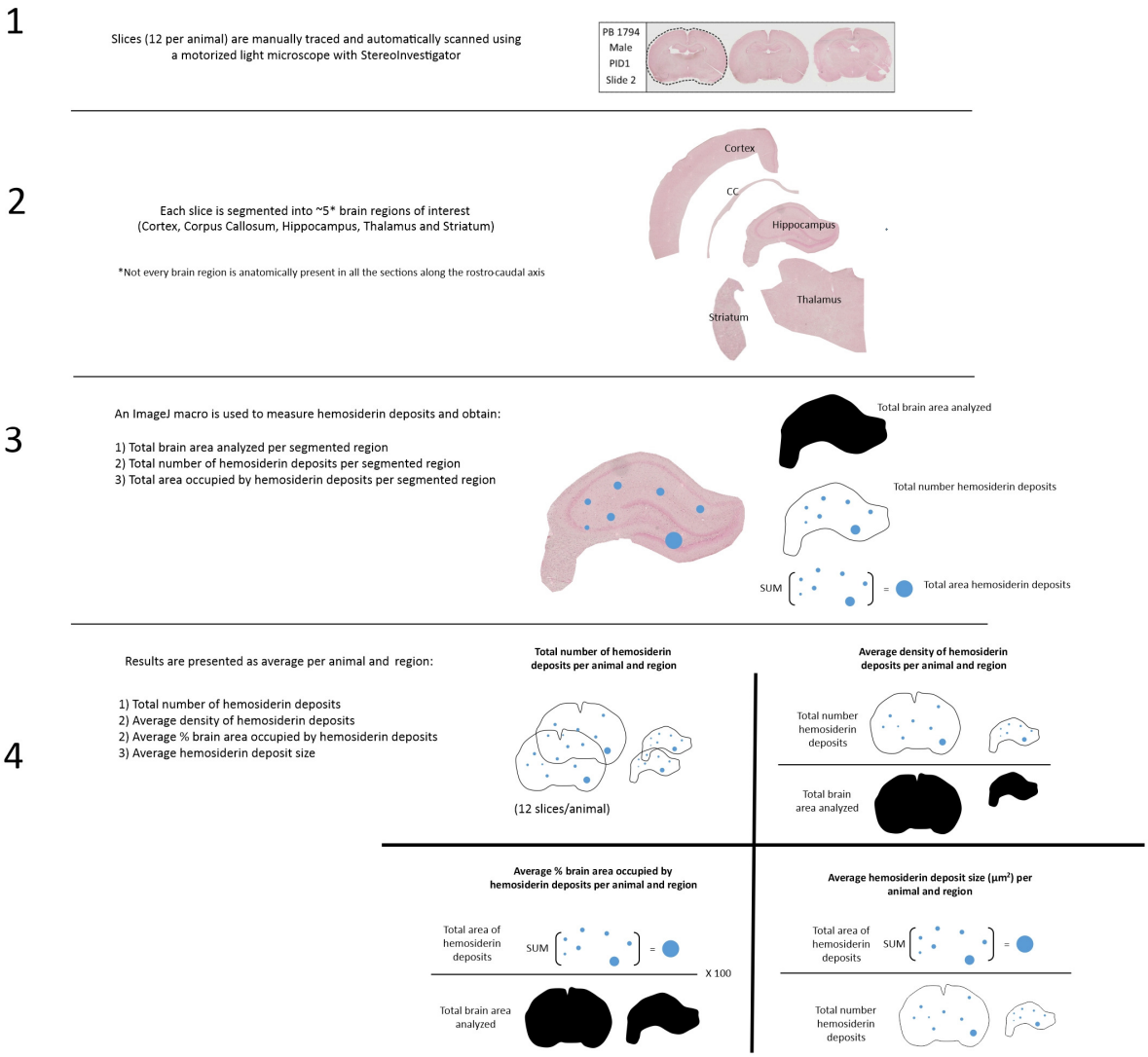

Figure 23. Methodology used to analyze hemosiderin deposits. First, each of the 12 slices stained for each animal were traced to generate whole-slice images with a motorized microscope and StereoInvestigator. These whole-slice images were segmented into 5 brain regions of interest (cortex, corpus callosum, hippocampus, thalamus and striatum). Each segmented image was analyzed using an ImageJ macro based on the "color threshold" and "particle analyzer" tools to obtain number of Prussian blue particles (i.e. number of hemosiderin deposits) and area occupied by these particles. In addition, another ImageJ macro was used to obtain total brain area analyzed for each segmented image. These measurements were used to present results as 1) total number of hemosiderin deposits; 2) average density of hemosiderin deposits; 3) average percentage of area occupied by hemosiderin deposits; and 4) average hemosiderin deposit size.

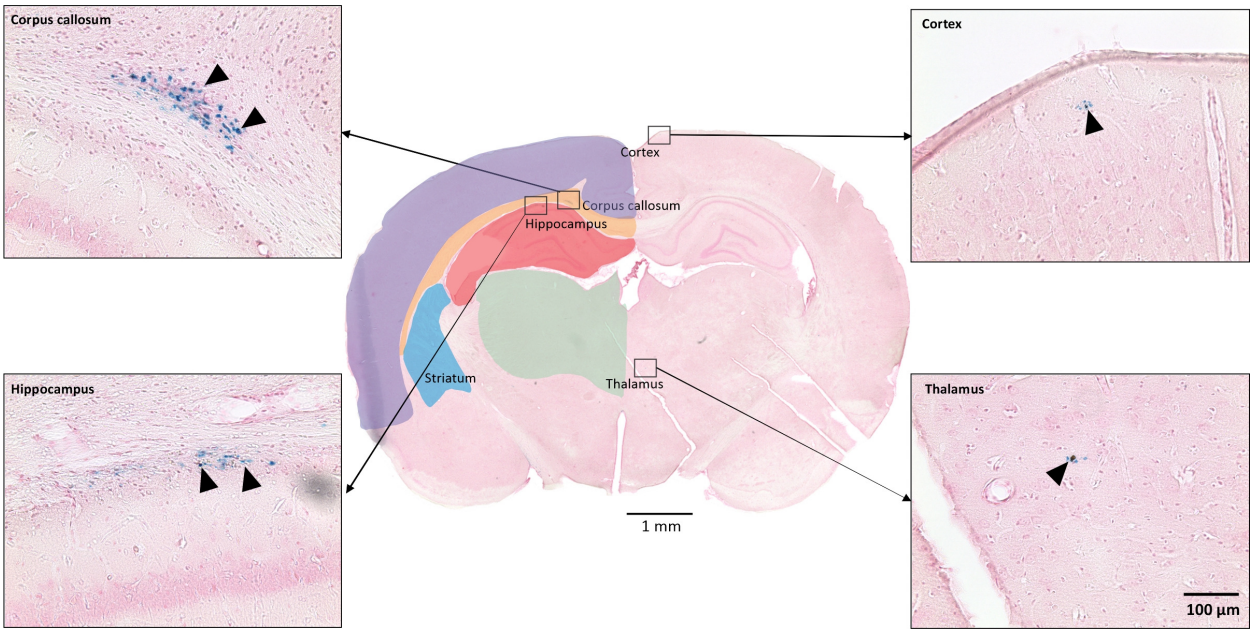

Figure 24. Brain regions selected for analysis and examples of hemosiderin deposits labelled with Prussian blue. Whole section from an rmTBI individual (center). The specific brain regions analysed in this study (highlighted with different colors) were cortex, corpus callosum, hippocampus, thalamus and striatum. Higher magnification examples of hemosiderin deposits in different brain regions are shown with their corresponding location indicated in the center panel. A detailed segmentation protocol is included in Appendix A.

The sequential acquisition option was enabled to avoid signal interference between fluorescent channels. Laser power and HV settings were adjusted to obtain optimal images and were maintained consistent for all experimental groups. Using an ImageJ macro (available in **Appendix B**), the fibrinogen channel was selected for analysis. First, a duplicated image was generated for this channel (analysis image) and the original one was merged with the red channel (i.e. WGA) to validate the extravascular location of the microbleed **(Fig. 28)**. A maximum intensity projection was generated for both analysis

and reference images. Using the merged image for reference, only extravascular fibrinogen signal was selected with the polygon selection tool.

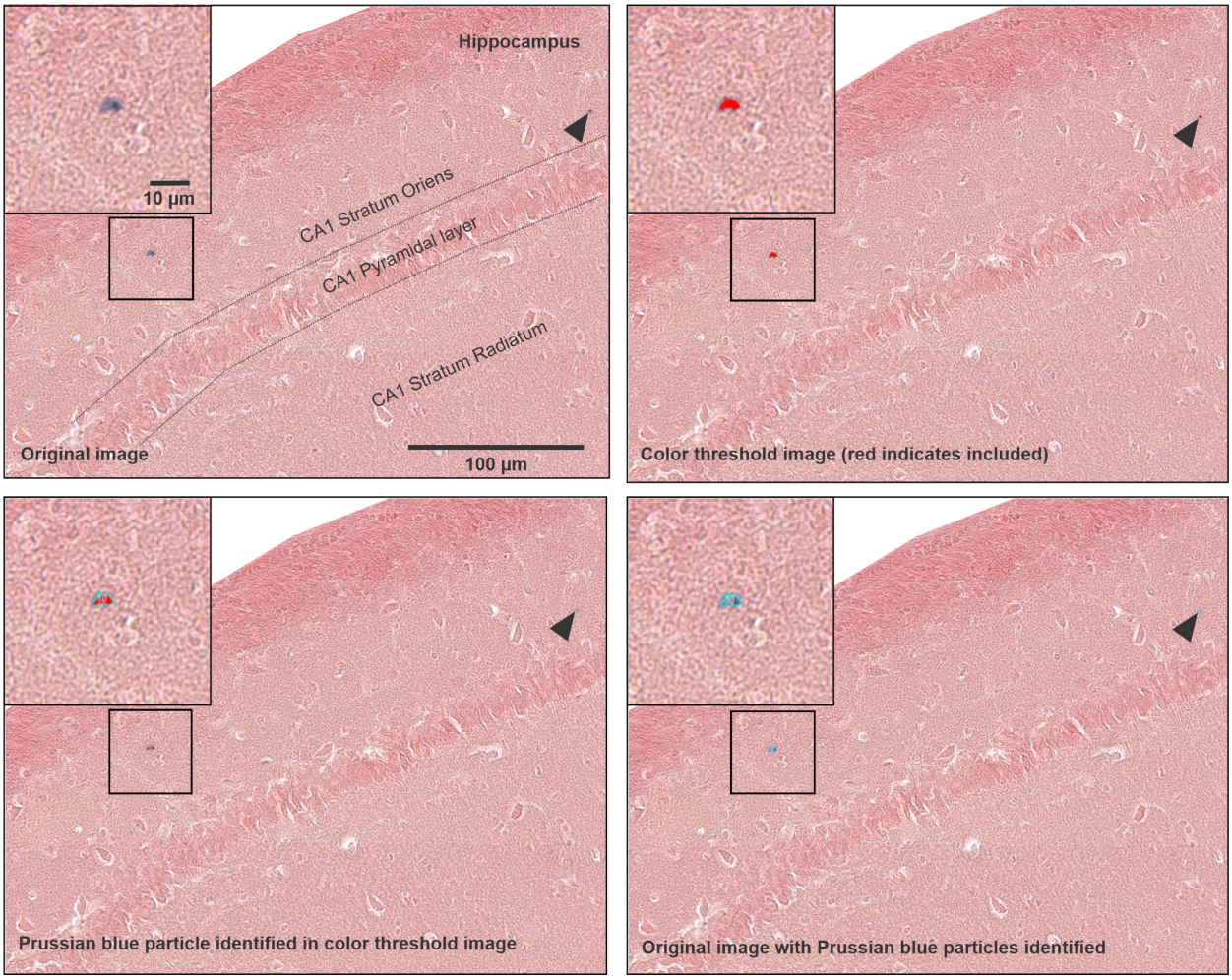

Figure 25. Example of Prussian blue particle analysis flow using ImageJ macro. Prussian blue particles (i.e. hemosiderin deposits) were identified by combining the "color threshold" and "analyze particles" tools of ImageJ. These images show the progression from original image (top left), to blue hue thresholded image (top right), to blue particles selected including its number ID, in this case "10" (bottom left) and finally the original image outlining the analyzed Prussian blue particles (hemosiderin deposits) to ensure appropriate measurement (bottom right). Black arrowhead points to another Prussian blue particle in the vicinity identified using this analysis flow. This example is from the hippocampal CA1 stratum oriens of a sham animal at PID1. Macro code used for this analysis is included in **Appendix B.**

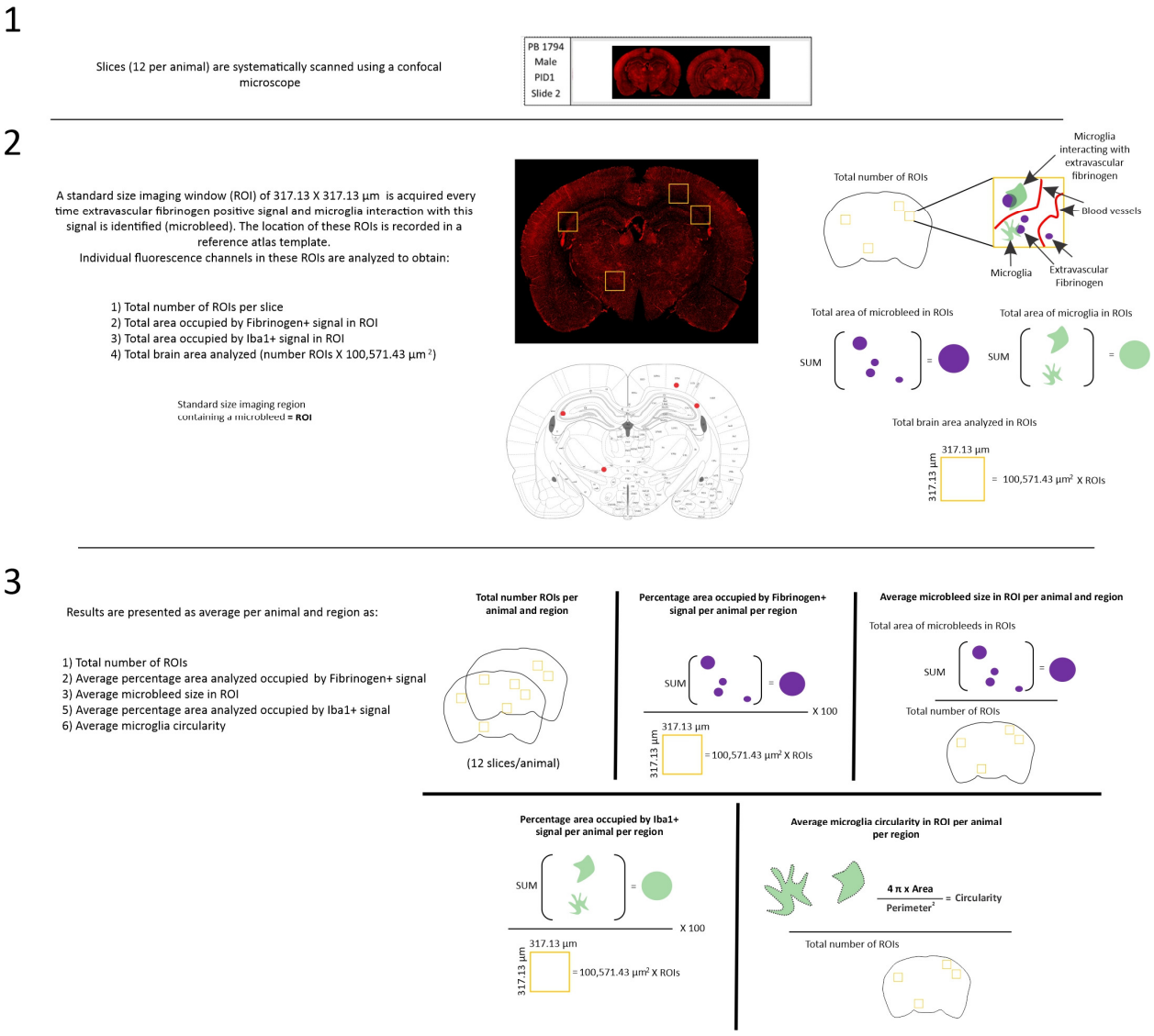

Figure 26. Methodology used to analyze fibrinogen extravasation and perilesional microglia reaction. Each of the 12 slices stained for each animal were systematically analyzed using epifluoresence. Every time a microbleed was spotted, a standard size ROI was acquired by confocal microscopy. These ROIs were a square imaging window of 317.3-µm per side with a total area of 100,571.43 µm². A microbleed was identified using the criteria of fibrinogen positive signal co-localizing with Iba1 positive cells. The location of these microbleeds was recorded in a reference atlas. Individual fluorescence channels in these ROIs obtained from each slice were analyzed to get total number of ROIs (proxy for number of microbleeds), total area occupied by fibrinogen positive signal, total area occupied by Iba1 positive cells, and total brain area analyzed. These measurements were used to present results per animal as overall and regional average per group of: 1) total number of ROIs; 2) average percentage area analyzed occupied by fibrinogen positive signal; 3) average microbleed size; 4) average percentage area occupied by Iba1 positive cells; and 5) average microglia circularity.

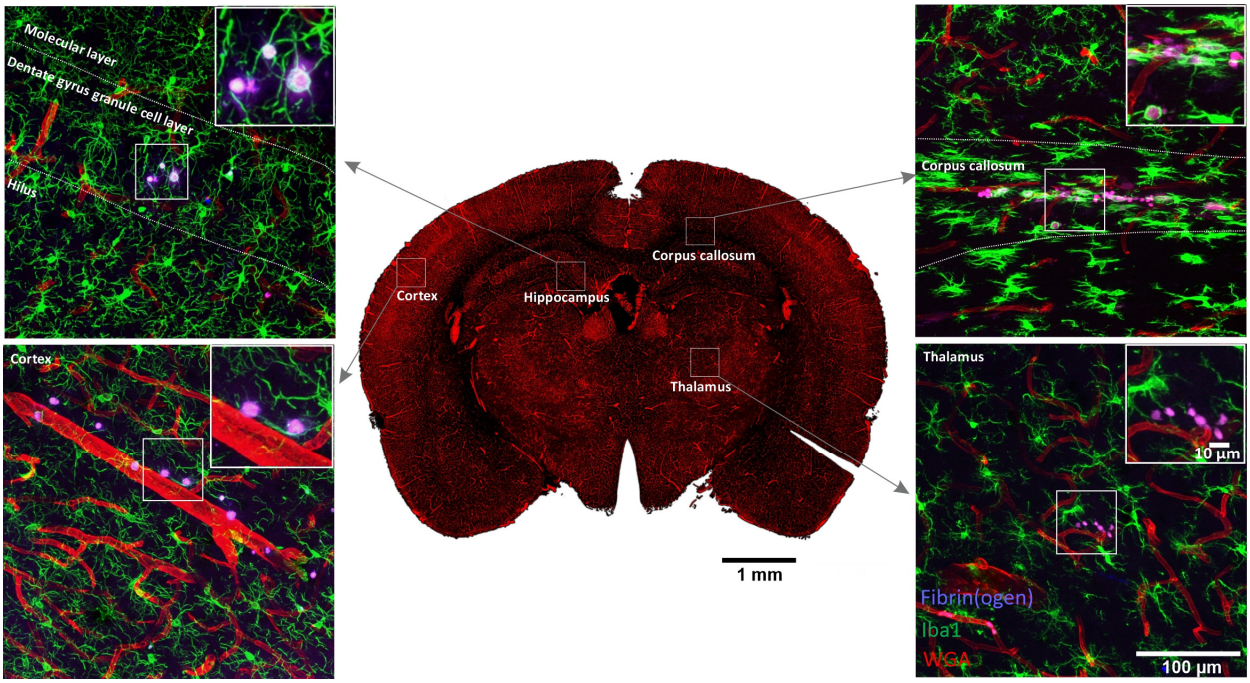

Figure 27. Examples of microbleeds identified by labelling fibrinogen and perilesional microglia reaction. When evaluating fibrinogen extravasation and microglia reaction, cortex, corpus callosum, hippocampus, thalamus and striatum were also the brain regions of interest. In this example, we can see in the center a whole slice displaying vasculature labelled with WGA. Left and right panels show examples of microbleeds imaged in different brain regions and microglia interacting with leaked fibrinogen. These sample images were obtained from a rmTIB animal at PID1.

The selected region was automatically thresholded with the "Default" algorithm and the total area occupied by extravasated fibrinogen in each ROI was measured **(Fig. 28)**. Results are presented as: 1) total number of ROIs per animal and brain region (proxy for number of microbleeds); 2) average percentage area occupied by extravasated fibrinogen signal (i.e. area occupied by microbleeds) per animal and brain region; and 3) average microbleed size (i.e. total area microbleed divided per total number of ROIs) per animal and brain region **(Fig. 26)**.

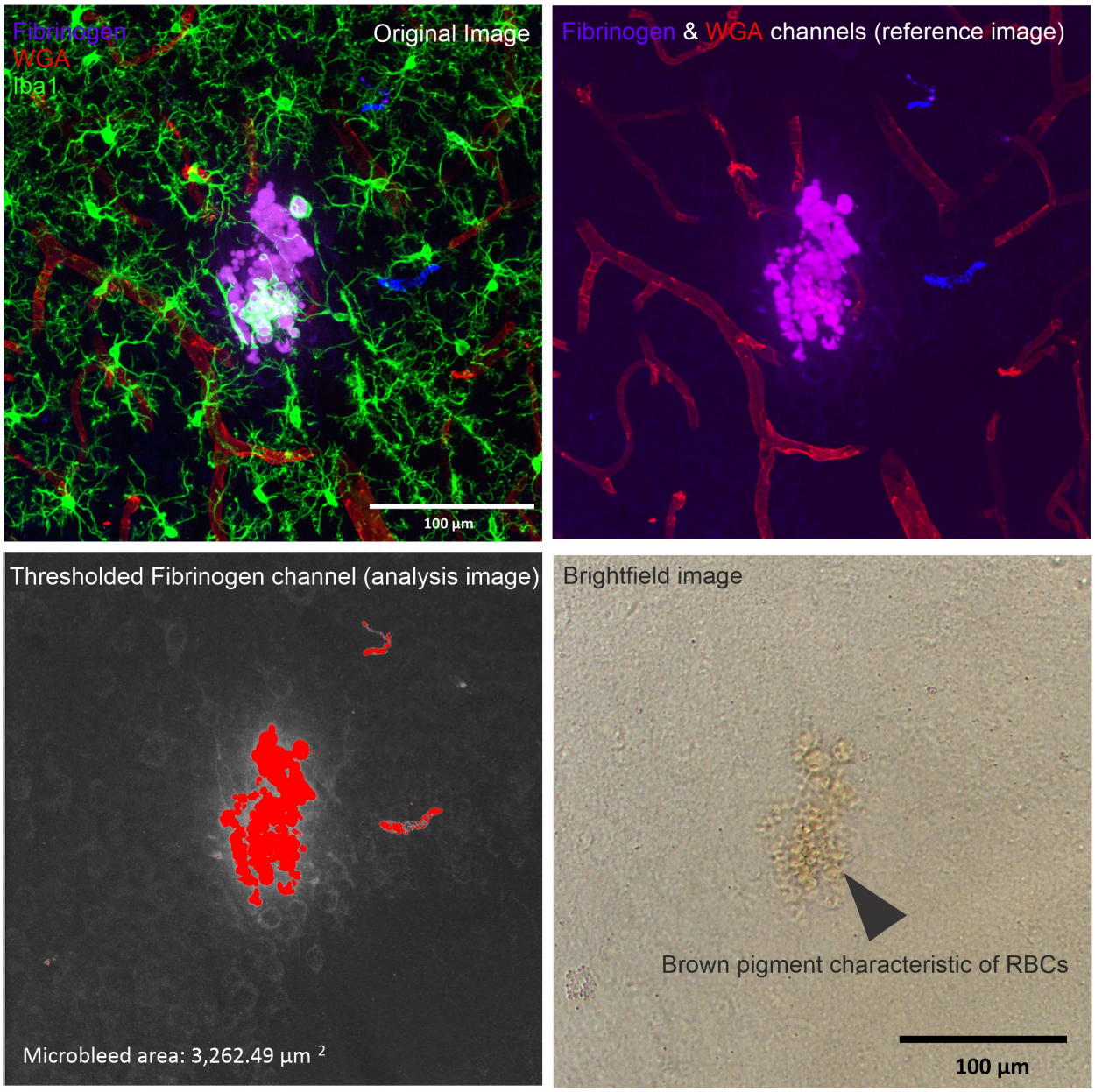

Figure 28. Example of fibrinogen extravasation analysis. Original confocal image of a microbleed ROI displaying fibrinogen (blue), WGA (red) and Iba1 (green) is shown in the top left panel. This image is from the agranular insular area in the orbital frontal cortex of a rmTBI animal at PID1. The fibrinogen analysis macro created a reference image with fibrinogen and WGA signal (top right). This reference image was used to select only extravascular fibrinogen. Bottom left panel shows an example of extravascular fibrinogen signal area measurement and the actual value. Bottom right image shows further confirmation of a valid microbleed by showing a cluster of RBCs with the characteristic brown pigment that this cells display under brightfield microscopy.

To further validate that what was being measured in this immunolabelled sections were indeed microbleeds, a serial section containing a microbleed (confirmed as fibrinogen leakage) was processed for electron microscopy **(Fig. 29).** Indeed, this evaluation confirmed that this approach was detecting RBCs and other blood contents being ingested by microglia **(Fig. 29).**

4.2.3.3. Microglia analysis

To assess the level of microglia aggregation and activation based on morphology, we analysed the far red channel (i.e. 647/Iba1 signal). Using an ImageJ macro **(Appendix B)**, a maximum intensity projection of the Iba1 channel was created and an automatic threshold using the "Li" algorithm was performed. This threshold was then converted into a binary mask and 3 iterations of the "Open" processing method with a count of 5 was performed. This allowed us to separate cells that were too close together and could be mistakenly analyzed as a big fused cell. After this, the "analyse particles" plugin was used to obtain area occupied by the Iba1 positive signal in each ROI to evaluate microglia aggregation, and the area and perimeter of each individual microglia cell to assess the level of activation based on circularity index. The formula used to calculate for circularity index was: $(4\pi \times \text{area})/\text{perimeter}^2$ **(Fig. 30)**. Results are presented as average percentage area occupied by Iba1 positive cells per animal and brain region, and average circularity index per animal and brain region **(Fig. 26).** It is important to note that equipment and resource limitations guided in part the specific methodology used in this study for fibrinogen and Iba1 immunofluorescence analysis.

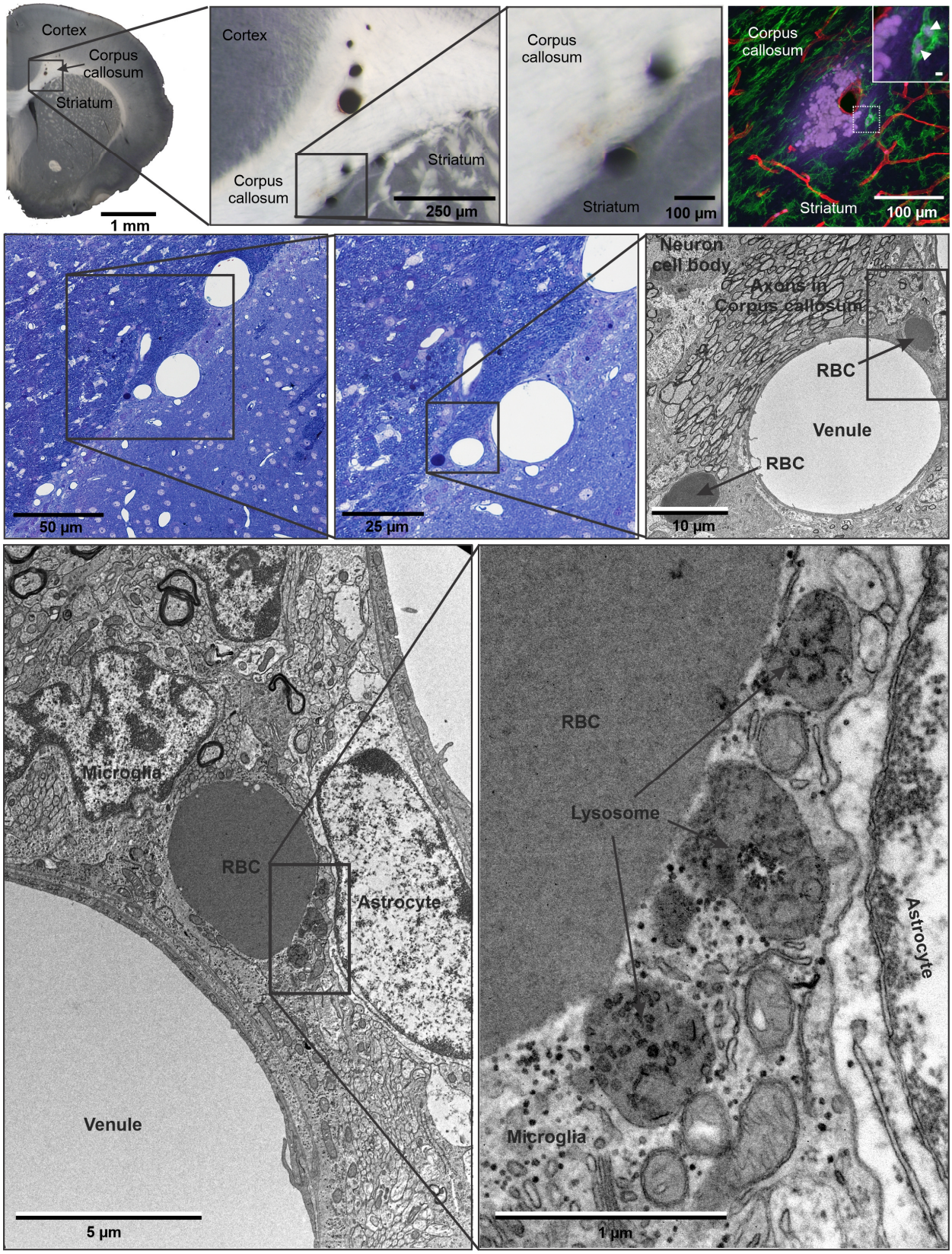
Cortex
Corpus callosum
Striatum
1 mm
Cortex
Striatum
Corpus callosum
250 µm
Corpus callosum
Striatum
100 µm
Corpus callosum
Striatum
100 µm
50 µm
25 µm
Neuron cell body
Axons in Corpus callosum
RBC
Venule
RBC
10 µm
Microglia
RBC
Astrocyte
Venule
5 µm
RBC
Lysosome
Astrocyte
Microglia
1 µm

Figure 29. Microbleed confirmation using electron microscopy. To further confirm that our microbleed analysis indeed was based on extravasation of blood contents we processed a microbleed for electron microscopy visualization. Top row shows images obtained with a stereoscope to highlight a microbleed in the corpus callosum and a serial section stained for fibrinogen, WGA and Iba1. Middle panel shows a toluidine blue stained section and low magnification EM corresponding to this microbleed. Bottom panel shows medium and high magnification EM views providing greater detail of a RBC and likely fibrin depositions being phagocytosed by a microglia cell. I would like to thank Dr. Patrick Nahirney for his assistance in generating these EM images.

As mentioned in the methodology section, the unavailability of a motorized confocal microscope that would have allowed a whole slide analysis similar to the Prussian blue evaluation forced us to use an event-driven analysis. This means that all ROIs contained microbleeds and only if a microbleed was present an ROI was imaged. The implication of this is that there were some animals that showed no microbleeds (and thus no ROIs) in some specific regions theoretically giving missing values for that animal (i.e. 0 μm^2 occupied by microglia / 0 ROIs = error). This had an impact on the regional analysis. For these missing values we decided to use an adapted multivariate normal imputation method (Schafer JL, 1997; Sullivan TR, 2017). Briefly, a value based on the group mean and standard deviation was generated for each missing value using the *rnorm()* and *sample()* functions in R. First, *rnum()* returned a list of random numbers picked from a normal distribution based on the mean and standard deviation provided. We generated 100 values with this function. Then the function *sample()* was used to pick random values from this list (total number depended on the missing values) and that was used as the values for missing data. The number of microbleeds at PID7 was so low (and thus regional missing values high) that this approach for regional analysis was deemed impractical. Therefore, this was only used with the missing values in PID1 data.

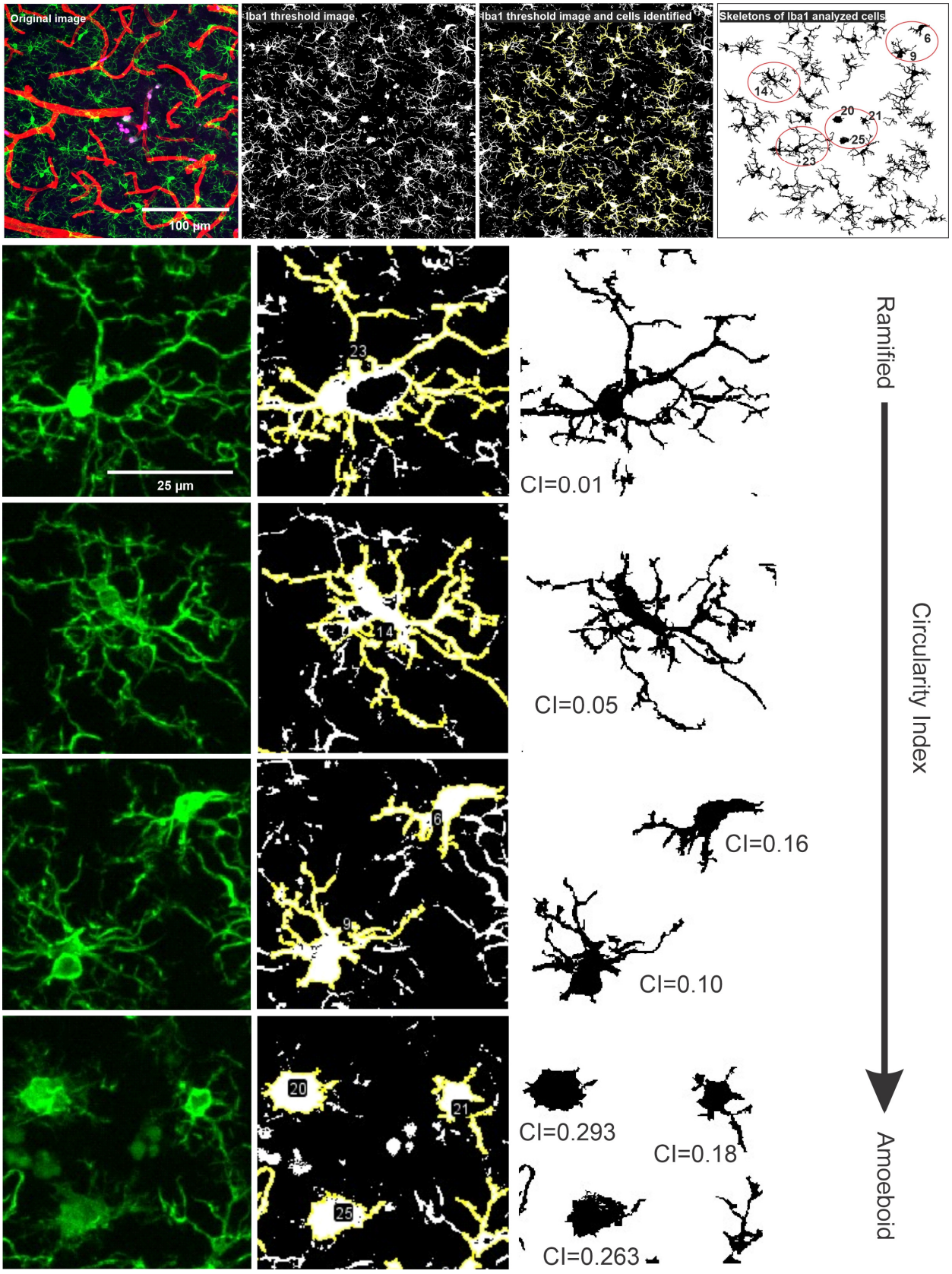
Original image
100 µm
Iba1 threshold image
Iba1 threshold image and cells identified
Skeletons of Iba1 analyzed cells
6
9
14
20
21
25
23
25 µm
CI=0.01
CI=0.05
CI=0.16
CI=0.10
CI=0.293
CI=0.18
CI=0.263
Ramified
Circularity Index
Amoeboid

Figure 30. Analysis of microglia aggregation and circularity index. Top panel shows the image processing carried out to evaluate the microglia reaction in the vicinity of a microbleed. Top left-most image shows the original image labelled with WGA (red), fibrinogen (purple) and Iba1 (green). The Iba1 channel was isolated and thresholded to generate a binary image of Iba1 positive cells. The area occupied by these cells was used to evaluate level of microglia aggregation in the microvascular perilesional regions. This thresholded image was also used to select individual Iba1 positive cells using the "particle analyzer" tool in ImageJ and to obtain the area and perimeter of each cell. Then using the circularity formula ($4\pi \times \text{area}/\text{perimeter}^2$) the circularity index of each cell was computed. An average circularity index was calculated for each ROI. Bottom panel shows different examples of microglia cells in a morphological spectrum ranging from ramified to amoeboid. The circularity index (CI) is indicated for each cell and this value goes from 0 (highly complex shape) to 1 (perfect circle). The closer to 1 the more amoeboid features a cell presented.

It was acknowledged that this data processing can have an influence over the final results but, given the alternatives or just discarding this data, it was considered that overall this approach provided a superior output. However, this fact needs to be taken into account when reaching conclusions.

4.2.4. Statistical analysis

GraphPad Prism was used to perform statistical analysis and generate figures. Specific statistical test used in each experiment are explicitly defined in the figure legends. Results are presented as group mean $\pm$ SEM and the individual animal values are displayed as black dots. The main statistical test employed in this study was a student's t-test. For this dissertation a p-value < 0.1 was considered significant. It is worth considering that a statistical power analysis was performed for sample size estimation based on preliminary data obtained in the laboratory. A general effect size was estimated to be around 1.2-1.3. This is considered to be a large effect using Cohen's and Sawilowsky's criteria. With an alpha = 0.05 and power = 0.8, the projected sample size needed with this effect size (Gpower 3.1.9.4) is approximately N = 9-10/group. Therefore,

when interpreting the results in this study, it is important to consider that the low sample size employed (N= 5/group) may render results underpowered for inferential statistics. However interesting trends worth following up are presented in the results section.

4.3. Results

4.3.1. rmTBI is associated with acute neurobehavioral deficits in both males and females

Concussions in humans are primarily evaluated based on the presence or absence of acute neurobehavioural signs. To evaluate if the ACHI model was also causing similar behavioural deficits, animals were assessed using a set of sensorimotor tests immediately after each impact (the Neurological Assessment Protocol, or NAP) **(Fig. 31)**. This protocol consisted of a battery of simple behavioural tasks aimed at evaluating sensorimotor functions. The NAP initially evaluates presence of post-impact apnea, loss of consciousness with toe pinch reflex, and the animal's righting reflex **(Fig. 31)**. This is followed by performance assessment of startle response, limb extension, balance beam and rotating beam. The animal performance in all these tasks is scored on a 4-point scale (with 0 being complete failure and 3 perfect performance) taking into consideration a set of objective criteria (**Fig. 6**). A final composite score based on these 4 tasks is generated to obtain the overall performance of each animal. In this composite score 0 is worst performance and 12 is perfect performance (**Fig. 31**). The data shows that no animal suffered post-impact apnea. It also indicates that the majority of animals did not show impairments on the toe pinch reflex evaluation, however those that did were on the rmTBI groups. (n=10 per group and sex). When evaluating the righting reflex, all sham

controls in both sexes showed an immediate righting reflex after being placed on their backs. On the other hand, the male and female rmTBI groups showed impairments in this task (n=10 per group and sex; Kruskal-Wallis H = 24.83; p<0.0001; **sham female**: 0 ± 0; **rmTBI female:** 3 ± 0.68; p=0.0005; **sham male:** 0 ± 0; **rmTBI male:** 2.1 ± 0.62; p=0.017). Evaluation of the NAP composite score revealed an acute impairing effect during the initial impacts followed by a temporary recovery and a consistent performance decline of ~33% in the lasts impacts in both sexes (n=10 per group and sex).

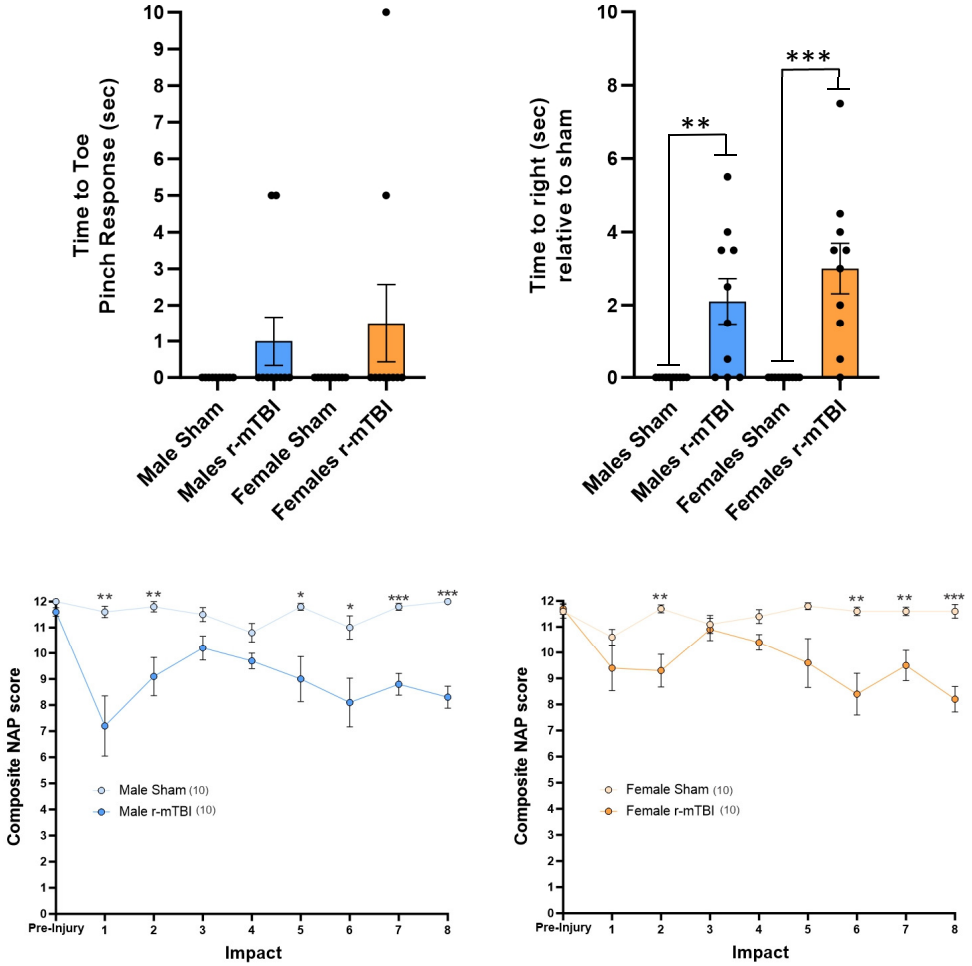

Figure 31. Both males and females show acute sensorimotor deficits after rmTBI. Top panel (left) shows toe pinch response as a measure of loss of consciousness. The majority of animals did not show any impairment in this task. Those that did were in the rmTBI groups (n=10 per group and sex). Top right panel shows righting reflex. All sham controls in both sexes showed an immediate righting reflex after being placed on their backs. Male and females in the rmTBI groups showed impairments in this task (n=10 per

group and sex). Bottom panels shows NAP Composite score. This analysis revealed an acute impairing effect during the initial impacts followed by a temporary recovery and a consistent performance decline (~33%) in the lasts impacts in both sexes. Kruskall-Wallis test and Dunn's for multiple comparisons was used for toe-pinch and righting reflex. Freidman two-way ANOVA and Tukey-HSD test for multiple comparisons analysis was used for the NAP. *p<0.1;**p<0.05;***p<0.01.

4.3.2. No differences in hemosiderin deposits between naïve animals and age-matched sham animals were observed.

In order to rule out the possibility that the sham procedure was deleterious and potentially causing microbleeds ***t***hat could create a confounding element in this investigation, first hemosiderin deposits in naïve non-handled animals with age-matched sham animals were evaluated and compared (n=5 per group and sex; animal age= PND29) (**Fig. 32**).

When evaluating the hemosiderin deposits with all regions combined we saw that there was no difference in the total number of hemosiderin deposits in either males (**naïve**: 621.6$\pm$67.63; **sham:** 395.8$\pm$75.35; p=0.056) or females (**naïve:** 491.8$\pm$46.6; **sham:** 450.2$\pm$128.0; p=0.767). Similarly, no differences were observed in density of hemosiderin deposits in male (**naïve:** $8.59x10^{-7}\pm1.27x10^{-7}$; **sham:** $5.8610^{-7}\pm1.11x10^{-7}$; p=0.145) or females (**naïve:** $6.83x10^{-7}\pm5.74x10^{-7}$; **sham:** $6.39x10^{-7}\pm1.98x10^{-7}$; p=0.837). The evaluation of percentage area occupied by hemosiderin deposits was not significantly different in either males (**naïve:** 0.00227%$\pm$0.00025; **sham:** 0.00167%$\pm$0.00041; p=0.256) or females (**naïve:** 0.00212%$\pm$0.00017; **sham:** 0.00157%$\pm$0.00030; p=0.150). Finally, the average hemosiderin deposit size was equivalent between naïve and shams for both males (**naïve:** 26.98$\pm$1.06; **sham:** 27.69$\pm$1.49; p=0.708) and females (**naïve:** 31.52$\pm$2.76; **sham:** 28.39$\pm$3.17;

p=0.479). In addition, when evaluating every brain region analysed in this study separately, no relevant differences in any of the measurements was evident.

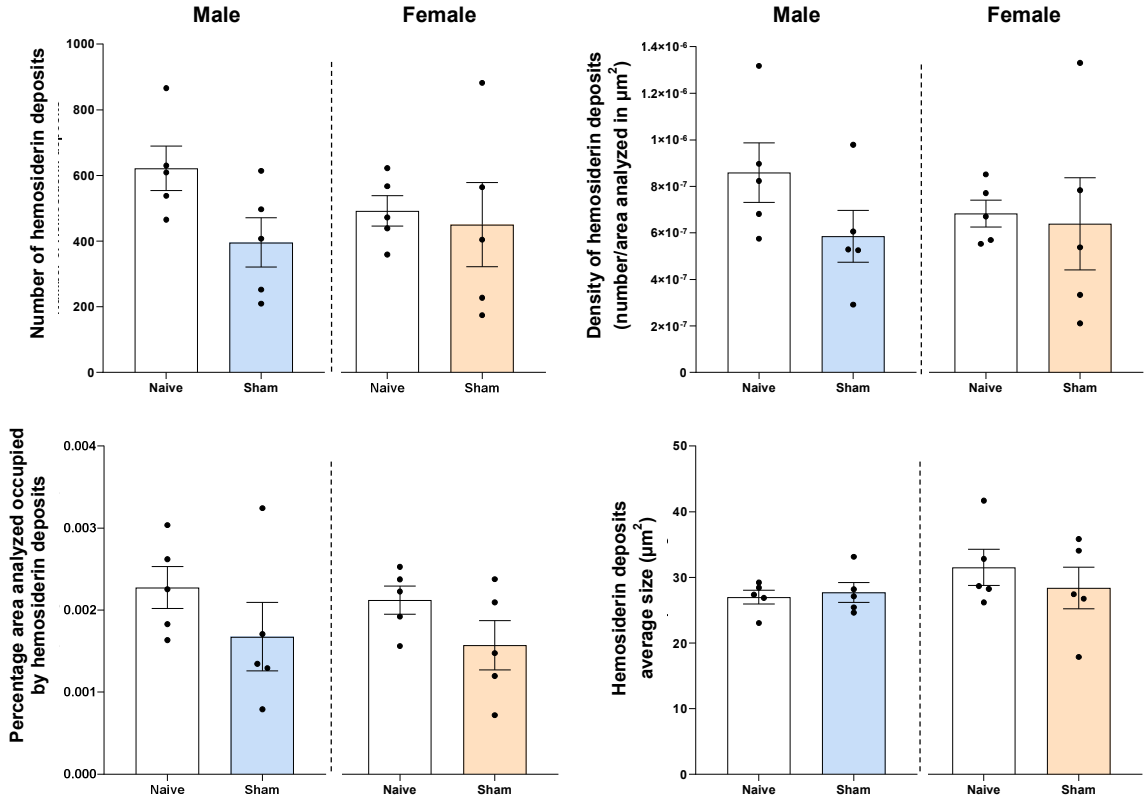

Figure 32. No differences in hemosiderin deposits between naïve and sham animals were observed. None of the hemosiderin deposit measurements evaluated showed group differences in male or female. These data indicate that the basal levels of microvascular damage are not altered by our sham procedure. Unpaired two-tail t-test was performed for group comparison in each sex. N=5 per group and sex.

4.3.3. Higher levels of hemosiderin deposits are associated with rmTBI in both males and females at PID1

Following rmTBI the total number of hemosiderin deposits was increased in males (**sham:** 395.8±75.35; **rmTBI:** 856.8±161.5; p=0.016) but not in females (**sham:** 450.2±128.0; **rmTBI:** 612.2±239.1; p=0.283), when compared to sham animals. The density of

hemosiderin deposits was also increased in males (**sham:** $5.86x10^{-7}\pm1.11x10^{-7}$; **rmTBI:** $11.5x10^{-7}\pm2.60x10^{-7}$; p=0.040) but not in females (**sham:** $6.39x10^{-7}\pm1.98x10^{-7}$; **rmTBI:** $8.70x10^{-7}\pm3.45x10^{-7}$; p=0.289). However, evaluation of the percentage of area occupied by hemosiderin deposits revealed that the rmTBI groups in both sexes displayed an overall increase in microbleed area (**male sham:** 0.00167%±0.00041; **male rmTBI:** 0.00405%±0.00071; p=0.010; **female sham:** 0.00157%±0.00030; **female rmTBI**: 0.00303±0.00090; p=0.082). A similar result in both sexes was observed when measuring the average hemosiderin deposit size (**male sham:** 27.69±1.49; **male rmTBI:** 36.53±3.35; p=0.021; **female sham:** 28.39±3.17; **female rmTBI:** 38.14±2.92; p=0.026). These data indicate that, overall, rmTBI is associated with larger and more extensive microvascular damage area in both sexes. These differences are more clear in males where the number and density of hemosiderin deposits were increased (**Fig. 33**).

Next, to determine if different brain regions were more affected by rmTBI, hemosiderin deposits were evaluated separately in the cortex (**Fig. 34**), corpus callosum (**Fig. 35**), hippocampus (**Fig. 36**), thalamus (**Fig. 37**) and striatum (**Fig. 38**).

Hemosiderin deposit density was initially measured since this allows one to take into account the substantial differences in the area of some of these brain regions (e.g. larger brain areas have a higher probability of having a hemosiderin deposit based on size alone). This regional investigation showed that in males the corpus callosum (**sham:** $11.9x10^{-7}\pm3.75x10^{-7}$; **rmTBI:** $28.0x10^{-7}\pm6.62x10^{-7}$; p=0.033), hippocampus (**sham:** $4.96x10^{-7}\pm0.76x10^{-7}$; **rmTBI:** $9.61x10^{-7}\pm1.74x10^{-7}$; p=0.020) and thalamus (**sham:** $5x10^{-7}\pm6.74x10^{-7}$;

rmTBI: $11.85 \times 10^{-7} \pm 1.97 \times 10^{-7}$; p=0.007) had an increase in hemosiderin deposit density. In the case of females, only the thalamus showed an increase in hemosiderin deposits density (**sham:** $3.79 \times 10^{-7} \pm 0.88 \times 10^{-7}$; **rmTBI:** $8.02 \times 10^{-7} \pm 2.32 \times 10^{-7}$; p=0.063). When measuring the extent of these microbleeds, it was found that in males all studied regions showed an increase in percentage area occupied by hemosiderin deposits compared to sham animals (**sham ctx:** 0.00146%±0.00036; **rmTBI ctx:** 0.00345%±0.00099; p=0.050; **sham cc:** 0.00384%±0.00163; **rmTBI cc:** 0.01206%±0.00406; p=0.048; **sham hipp:** 0.00152%±0.00032; **rmTBI hipp:** 0.00351%±0.00063; p=0.011; **sham thal:**0.00172%±0.00038; **rmTBI thal:** 0.00455%±0.00071; p=0.004; **sham str:** 0.00155%±0.00049; **rmTBI str:** 0.00364%±0.00110; p=0.060). In females, the thalamus (**sham:** 0.00109%±0.00015; **rmTBI:** 0.00365±0.00116; p=0.030) and the hippocampus (**sham:** 0.00162%+0.00046; **rmTBI:** 0.00324%+0.00081; p=0.061) were the only regions that showed an increase in percentage area analyzed occupied by hemosiderin deposits. To define if these changes in microbleed extent were due to more microbleeds or bigger microbleeds, the average size of hemosiderin deposit in each region was measured. Results revealed that in males the cortex (**sham:** 24.40+1.41; **rmTBI:** 32.45+2.57; p=0.012) and striatum (**sham:** 27.83±3.93; **rmTBI:** 42.13±8.37; p=0.080) presented a significant increase in hemosiderin size in the rmTBI group. In the case of females, only the hippocampus showed this increase in hemosiderin deposit size (**sham:** 26.25+2.14; **rmTBI:** 49.04+7.38; p=0.009). This data suggests that the regional increase in hemosiderin deposit area in the rmTBI group can be caused both by presence of larger microbleeds but also by more abundant microbleeds but with similar size as those observed in the

sham group. In males, microbleeds in the cortex and the striatum were larger but not more abundant. In contrast, the corpus callosum, hippocampus and thalamus showed similar-sized but more prevalent hemosiderin deposits compared to the sham group. In females, the hemosiderin deposits in the hippocampus were caused by larger microbleeds and the ones in the thalamus had a similar size to those reported in the sham group, but were more abundant.

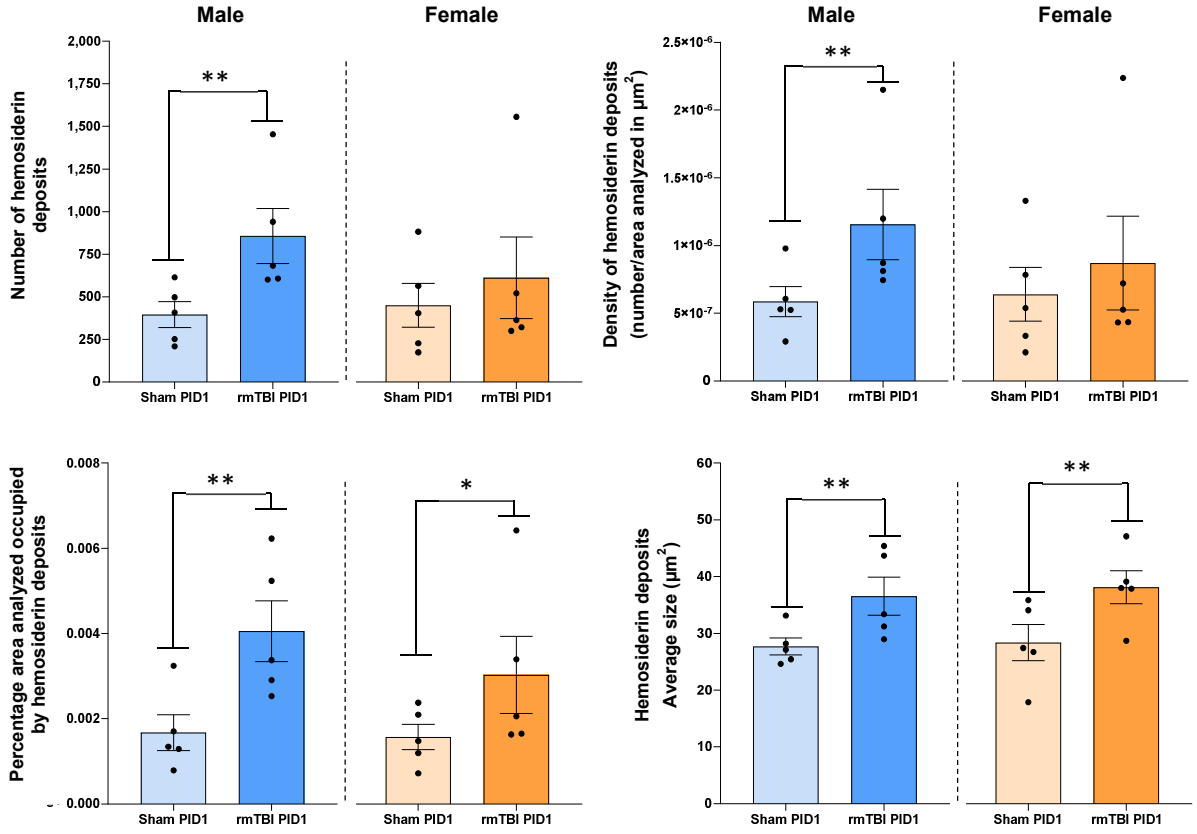

Figure 33. Males and females in the rmTBI group showed increased hemosiderin deposits at PID1. Males showed increases in total number and density of hemosiderin deposits, as well as percentage area occupied and average size of these deposits. Females only show an increase in percentage area occupied by hemosiderin deposits and average size. *p<0.1; **p<0.05. N=5 per group and sex; unpaired one-tailed t-test.

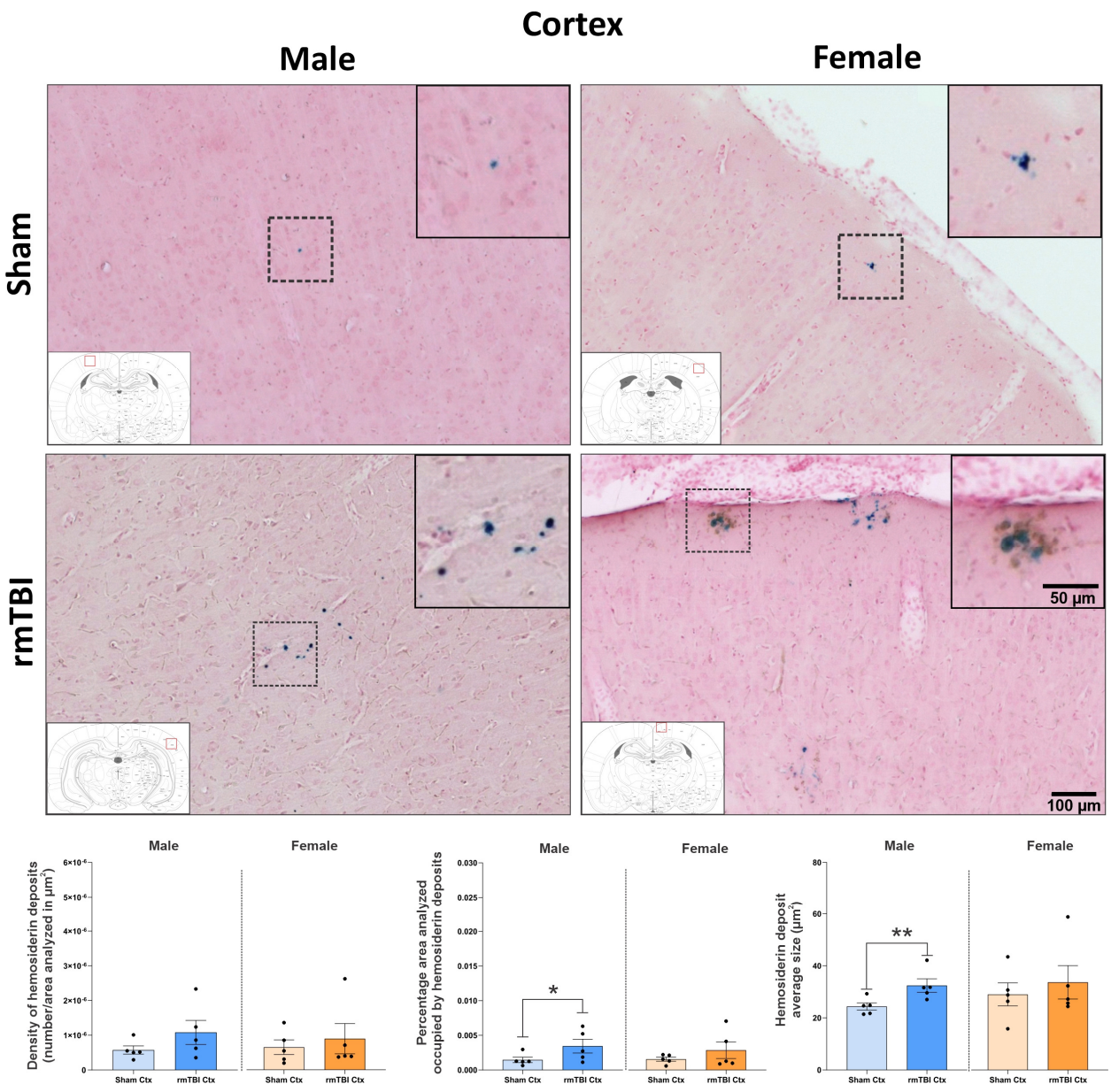

Figure 34. Only males show a larger extension of hemosiderin deposits in the cortex after rmTBI at PID1. Regional assesment of hemosiderin deposits in the cortex showed that males had an increase in percentage area occupied by these deposits and an increase in average size. In contrast, although there were some animals with clear effects, females in the rmTBI group showed no differences compared to sham controls in this region. Unpaired one-tail t-test was used for group comparison in each sex. *p<0.1; **p<0.05. N=5 per group and sex.

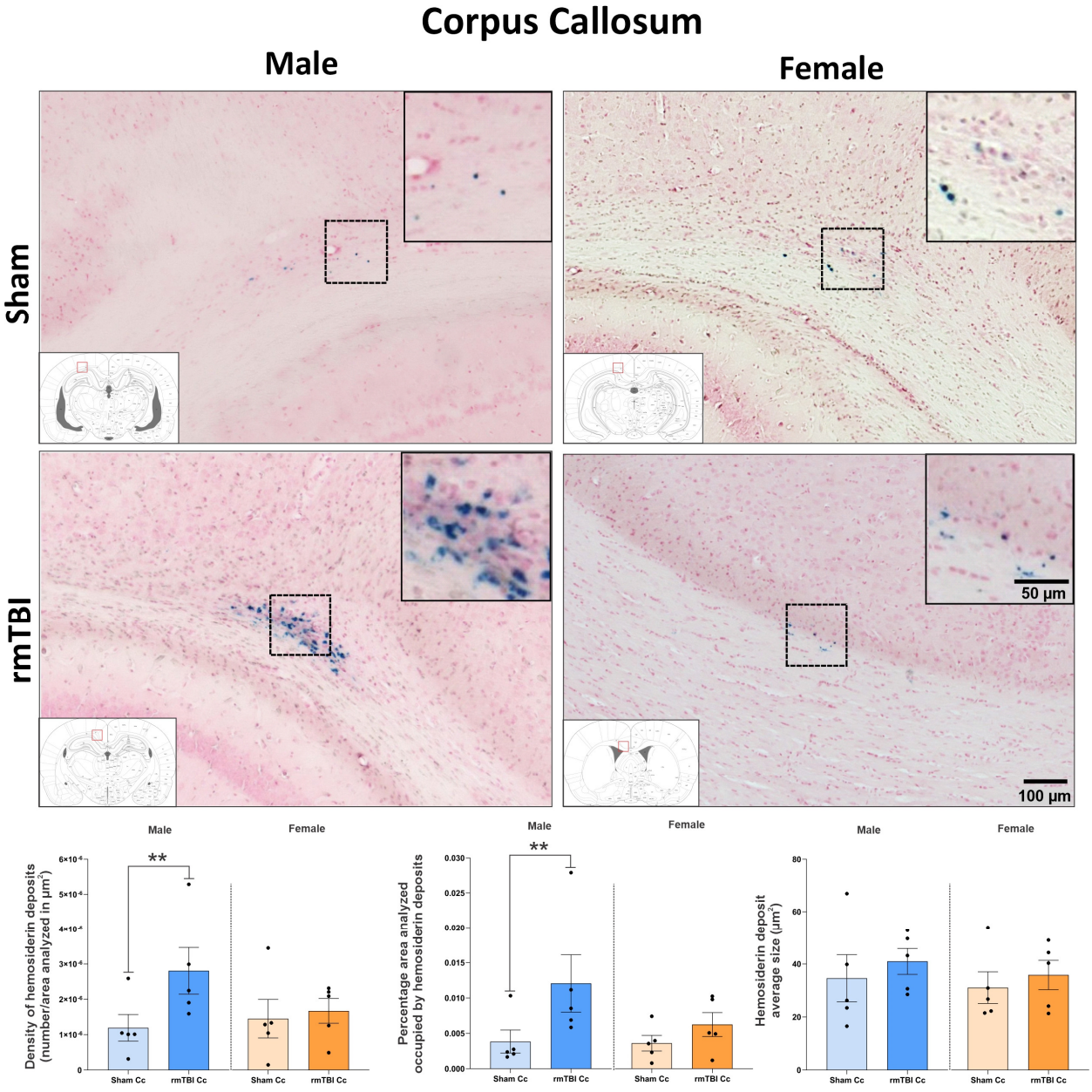

Figure 35. Males but not females showed increases in hemosiderin deposits in the corpus callosum after rmTBI at PID1. Regional analysis of hemosiderin deposits in the corpus callosum showed that males had an increase in density of hemosiderin deposits and percentage area occupied by these deposits but not in hemosiderin deposits average size, suggesting more abundant but not larger microbleeds. Females showed no differences. Unpaired one-tailed t-test was used for group comparison in each sex. *p<0.1; **p<0.05. N=5 per group and sex.

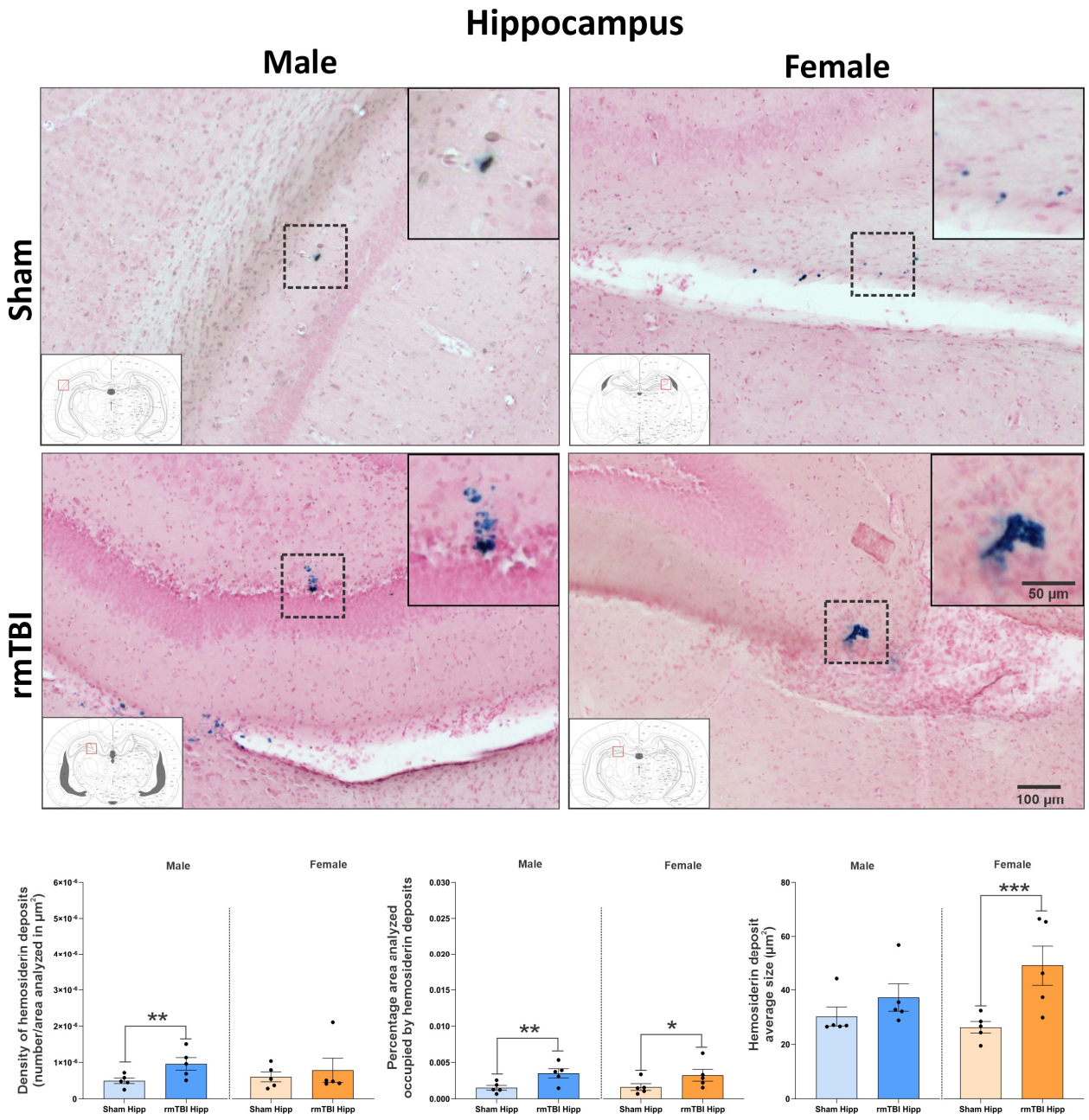

Figure 36. Both males and females showed an increase in hemosiderin deposit in the hippocampus after rmTBI at PID1. Regional evaluation of hemosiderin deposits in the hippocampus showed that males had an increase in density of hemosiderin deposits and percentage area occupied by these deposits but not in hemosiderin deposits average size. Females showed no differences on density, but had an increase in percentage area occupied by hemosiderin deposits and deposit average size. Unpaired one-tailed t-test was used for group comparison in each sex. *p<0.1; **p<0.05; ***p<0.01. N=5 per group and sex.

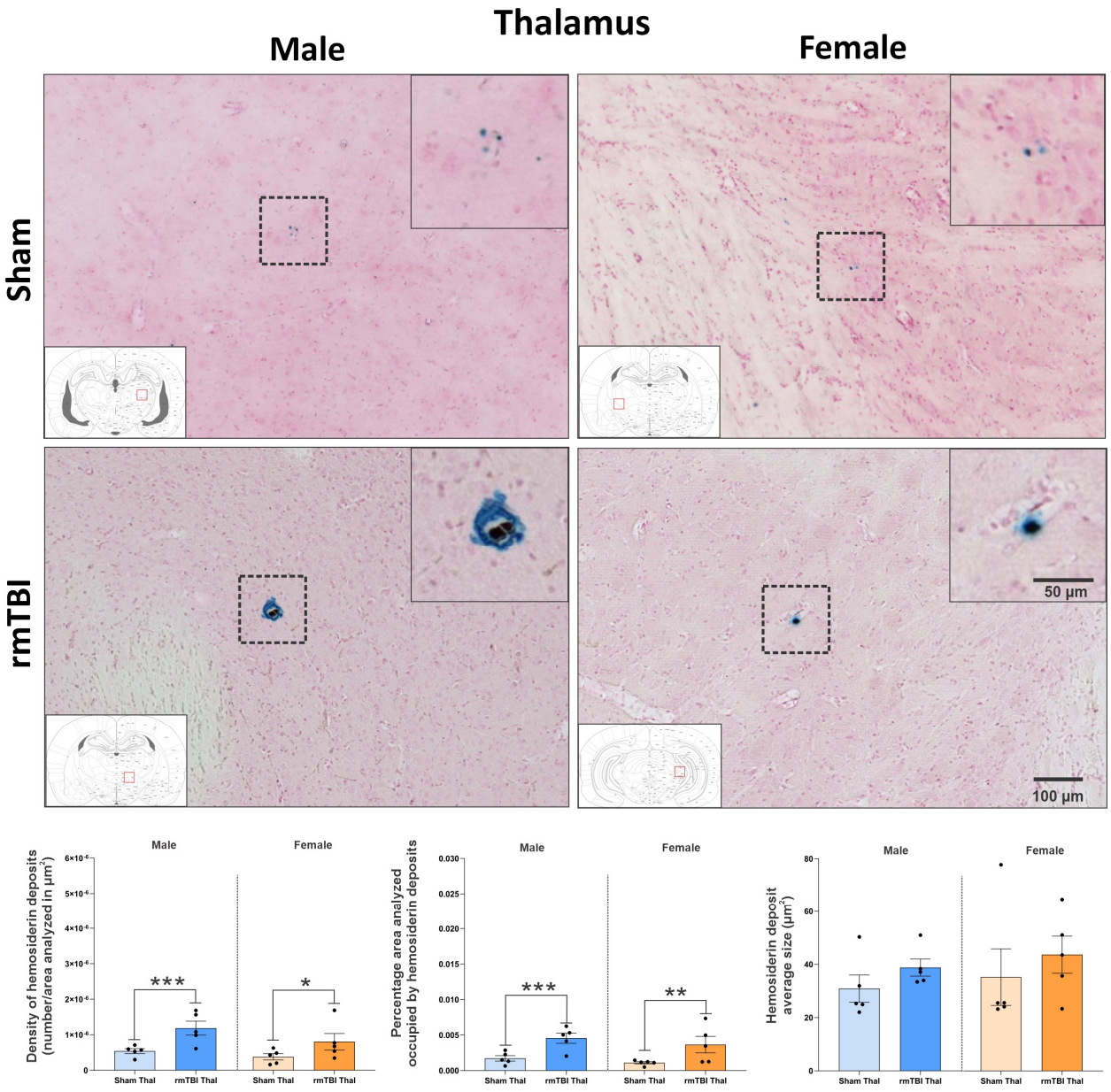

Figure 37. Males and females showed increases in hemosiderin deposits in the thalamus following rmTBI at PID1. Exploration of hemosiderin deposits in the thalamus showed that males had an increase in density of hemosiderin deposits and percentage area occupied by these deposits but not in hemosiderin deposits average size. Females also showed an increase in density and percentage area occupied by hemosiderin deposit but not in average size. Unpaired one-tailed t-test was used for group comparison in each sex. *p<0.1; **p<0.05;***p<0.01. N=5 per group and sex.

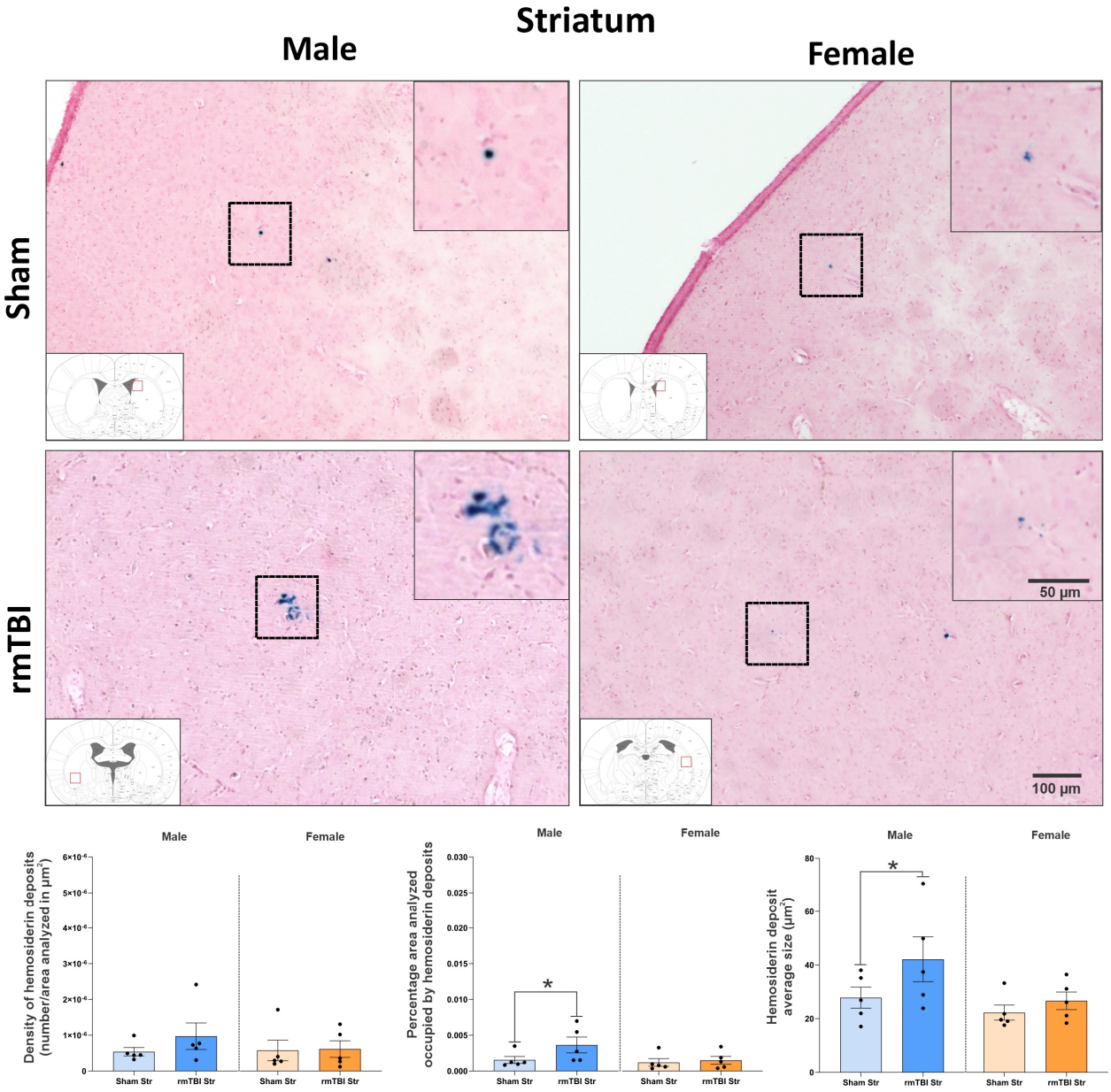

Figure 38. Only males show signs of increased hemosiderin deposits in the striatum after rmTBI at PID1. Analysis of hemosiderin deposits in the striatum showed that males had an increase in percentage area occupied by hemosiderin deposits and in hemosiderin deposits average size but not in density of hemosiderin deposits. Females showed no differences in this brain region. Unpaired one-tailed t-test was used for group comparison in each sex. *p<0.1; **p<0.05;***p<0.01. N=5 per group and sex.

4.3.4. No differences in hemosiderin deposits were detected at PID7 in males or females.

A longer time point (i.e. PID7) was selected to evaluate if changes in hemosiderin deposits observed short-term (i.e. PID1) were still detectable at this later time point. When the overall effects in number of hemosiderin deposits, density of hemosiderin deposits or percentage area occupied by hemosiderin deposits were evaluated, no differences were observed in either males (**sham density:** $4.72x10^{-7}\pm0.50x10^{-7}$; **rmTBI density:** $4.10x10^{-7}\pm0.30x10^{-7}$; p=0.162; **sham % area:** 0.00138%$\pm1.7x10^{-5}$; **rmTBI % area:** 0.00154%$\pm2.2x10^{-5}$; p=0.197) or females (**sham density:** $5.11x10^{-7}\pm0.57x10^{-7}$; **rmTBI density:** $4.82x10^{-7}\pm0.76x10^{-7}$; p=0.162; **sham % area:** 0.00178%$\pm3.3x10^{-5}$; **rmTBI % area:** 0.00211%$\pm6.1x10^{-5}$; p=0.328). Interestingly, males but not females did show an increase in hemosiderin deposits average size (**sham male:** 29.15$\pm$1.52; **rmTBI male:** 38.33$\pm$2.46; p=0.006; **sham female:** 33.90+3.31; **rmTBI female:** 40.77+5.20; p=0.149), indicating a potential sign of persistent damage. However, this data suggests that contrary to what was expected, hemosiderin deposits were not more elevated at PID7 than at PID1, indicating that they do not persist at a longer time-point. Note that scales in PID7 graph are kept consistent with PID1 graphics to allow a direct visual comparison (**Fig. 39**).

In a similar way, the regional evaluation of hemosiderin deposits revealed no changes in either density of hemosiderin deposits or percentage area analyzed occupied by hemosiderin deposits in either sex nor region. Surprisingly, in both sexes there were some regions showing increases in hemosiderin deposit average size. In males, these brain regions were the cortex and the hippocampus and in females only the cortex (**Fig.**

40). This could be an indication of regions that may have some persistent damage or show residual signs of microbleeds, but again this data is not conclusive enough and results may be constrained by a lack of power.

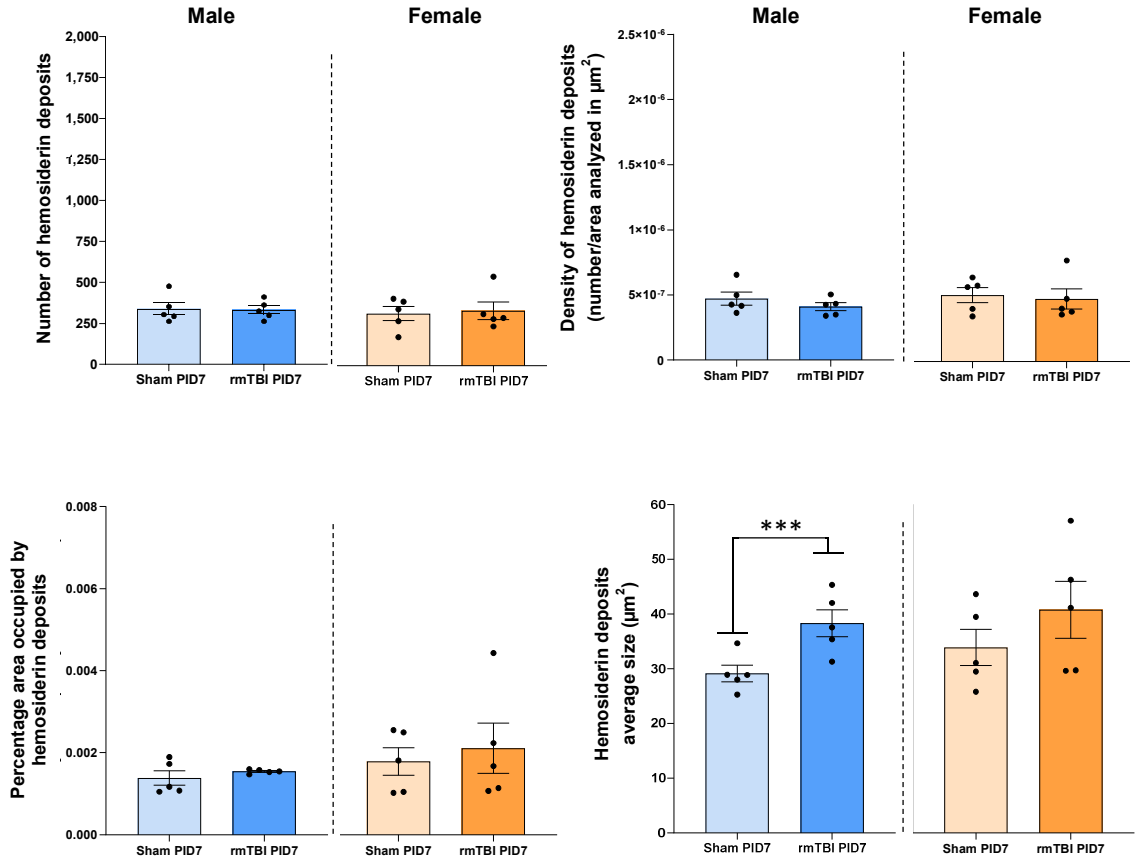

Figure 39. At PID7 rmTBI and sham animals show no differences in hemosiderin deposits in either males or females. At this time point, overall analysis of hemosiderin deposits showed that rmTBI males had no differences compared to sham controls besides an increase in hemosiderin deposit average size. Females showed no differences in any measurement at this time point. Unpaired one-tailed t-test was used for group comparison in each sex. *p<0.1; **p<0.05. N=5 per group and sex.

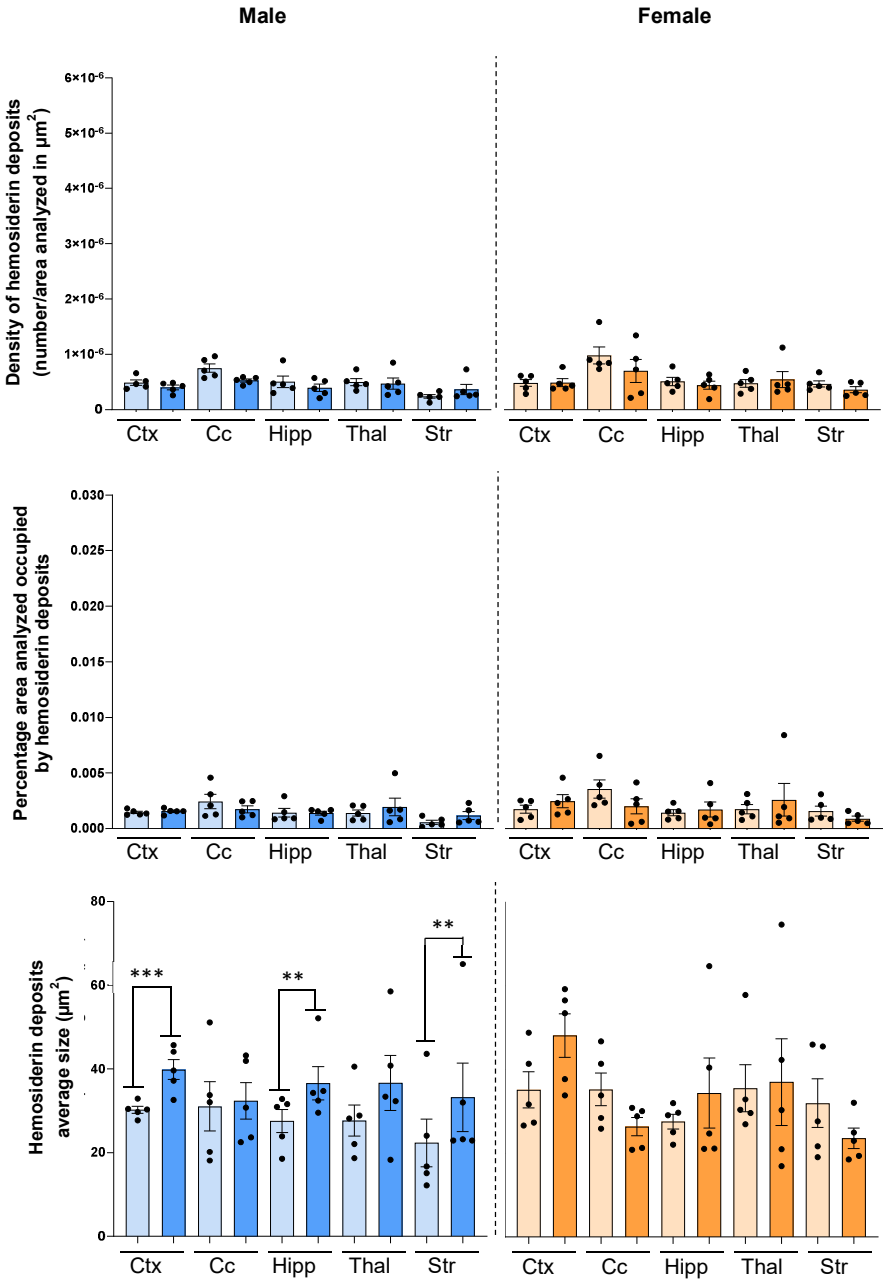

Figure 40. Regional analysis revealed no evident changes in hemosiderin deposits associated with rmTBI at PID7. Neither males or females show differences at this time point except for some discrete differences in hemosiderin deposits average size in males. Unpaired one-tailed t-test was used for group comparison by region in each sex. *p<0.1; **p<0.05; ***p<0.01. N=5 per group and sex.

4.3.5. Males and females in the rmTBI group show increased fibrinogen extravasation at PID1

Evaluating hemosiderin deposits is a good proxy for microbleed detection, however the technique used to label these iron deposits (Prussian blue) has some characteristics that need to be taken into consideration when interpreting results. Briefly, the process that takes hemoglobin-bound iron from extravasated RBCs to hemosiderin deposits (that can then be detected with the Prussian blue reaction) can take between 2-3 days. Therefore, microbleeds that are not older than this, will not be detected using this approach. It is worth noting that even though hemosiderin deposits are thought to remain indefinitely in the brain after they are generated and indeed there are MRI studies suggesting this, to our knowledge there is not a study that systematically evaluates how long these deposits last and if there is some kind of clearing mechanism that can remove them from the brain. Nevertheless, the consensus is that Prussian blue staining allows to visualize the iron traces left by microbleeds that are older than 2-3 days and can be detected long-term. To overcome this "waiting period" limitation and complement the result exposed above, detection of extravascular fibrinogen, a plasma protein involved in the blood-clot cascade, was used as an indicator of active microbleeds. To help confirm the extravascular location of this plasma protein, the vascular lumen of the animals was labeled with wheat-germ agglutinin conjugated with Alexa-555. In addition, to control for any potential artifacts induced by transcardial perfusion when preparing the tissue, the reaction of microglial cells was also evaluated using Iba1 staining. It is worth mentioning that by examining all the measurements together (number ROIs, percentage

area and average size microbleed) simultaneously, it is possible to determine if the size of a microbleed or the number are having a more profound impact on the brain.

When assessing fibrinogen extravasation into the brain parenchyma no overall (i.e. all brain regions combined) differences in the number of standard size regions of interest (i.e. ROIs; proxy for number of microbleeds) was observed between experimental conditions in males (**sham:** 15.60±2.89; **rmTBI:** 23.00±8.19; p=0.209;). However, females in the rmTBI group showed an overall increase in total number of ROIs (**sham:** 12.20+3.69; **rmTBI:** 23.60+6.83; p=0.090). On the other hand, when evaluating the overall percentage area occupied by these microbleeds, an increase in both males and females in the rmTBI group compared to sham animals was detected (**sham male:** 0.293%±0.048; **rmTBI male:** 2.216%±0.696; p=0.012; **sham female:** 0.213%±0.014; **rmTBI female:** 1.219%±0.372; p=0.013) (**Fig. 41**). This indicates that in males, while there were not differences in independent sources of microbleeds (as measure by number of ROIs), there was a larger extension of brain area occupied by extravasated fibrinogen. In females both measurements were elevated. The evaluation of the overall average microbleed size revealed that both males and females in the rmTBI group showed larger microbleeds compared to their sham controls (**sham male:** 294.7±48.29; **rmTBI male:** 2229±699.9; p=0.012; **sham female:** 215.1±14.40; **rmTBI female:** 1226±374.9; p=0.013), confirming that this increase in brain area occupied by extravasated fibrinogen was primarily due to larger but not more abundant microbleeds.

A regional analysis was also performed to individually evaluate fibrinogen extravasation in the cortex (**Fig. 42**), corpus callosum (**Fig. 43**), hippocampus (**Fig. 44**), thalamus (**Fig. 45**) and striatum (**Fig. 46**). This analysis revealed that in males, only the hippocampus showed and increase in number of ROIs in rmTBI compared to sham animals (**sham:** 1.6±0.67; **rmTBI:** 3.8±1.15; p=0.069). Surprisingly, the opposite pattern however was observed in the striatum (**sham:** 3.2±0.66; **rmTBI:** 1.00±0.54; p=0.016). In females, the cortex (**sham:** 2.80±1.15; **rmTBI:** 7.40±1.99; p=0.040) and hippocampus (**sham:** 1.6+0.67; **rmTBI:** 5.6±2.54; p=0.083) showed an increase in number of ROIs in rmTBI compared to sham controls. When evaluating the percentage area occupied by these microbleeds in males, the corpus callosum (**sham:** 0.095%±0.075; **rmTBI:** 3.440%±0.890; p=0.002), hippocampus (**sham:** 0.109%±0.040; **rmTBI:** 1.130%±0.464; p=0.029) and the thalamus (**sham:** 0.165%±0.050; **rmTBI:** 0.838±0.356; p=0.049) presented an increase compared to sham controls. In females, although some animals showed marked effects on some regions, only the cortex showed a consistent increase in percentage area occupied by microbleeds (**sham:** 0.196%±0.054; **rmTBI:** 1.033%±0.247; p=0.005). Finally, to discern if these increases in area were due to more microbleeds or larger microbleeds the average microbleed size was evaluated. In males, this measurement revealed that the corpus callosum (**sham:** 96.00±75.9; **rmTBI:** 5695±1372; p=0.001), hippocampus (**sham:** 110.2±48.30; **rmTBI:** 1287±363.5; p=0.013) and thalamus (**sham:** 256.7±70.37; **rmTBI:** 862.5±349.0; p=0.063) had larger microbleeds compared to shams. In the case of females, the cortex (**sham:** 321.1±115.2; **rmTBI:** 1725±391.3; p=0.004) and hippocampus (**sham:** 278.9+138.9; **rmTBI:** 2353+1462; p=0.097) showed this pattern

of increased size compared to sham controls. This data suggests that both males and females show clear signs of active microvascular damage at PID1 caused primarily by larger but not more abundant microbleeds and that the main regions affected in males are the corpus callosum, hippocampus and thalamus and in females the cortex and hippocampus.

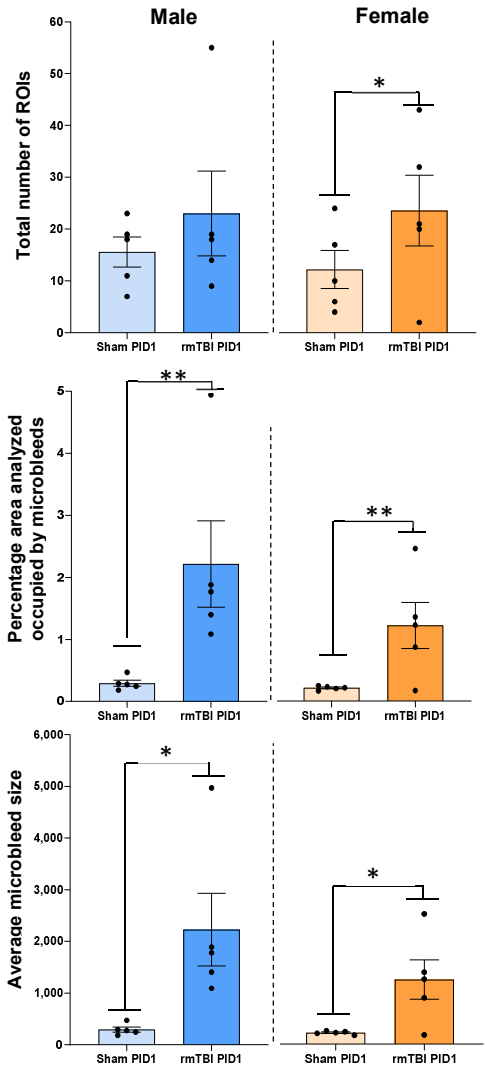

Figure 41. Males and females in the rmTBI group showed increased overall levels of extravasated fibrinogen at PID1. Males showed an overall increase in percentage area occupied by microbleeds and also in microbleed average size. Females presented an increase in number of ROIs (i.e. number of microbleeds), percentage area occupied by microbleeds and also in microbleed average size. Unpaired one-tail t-test was used for group comparison in each sex. *p<0.1; **p<0.05. N=5 per group and sex.

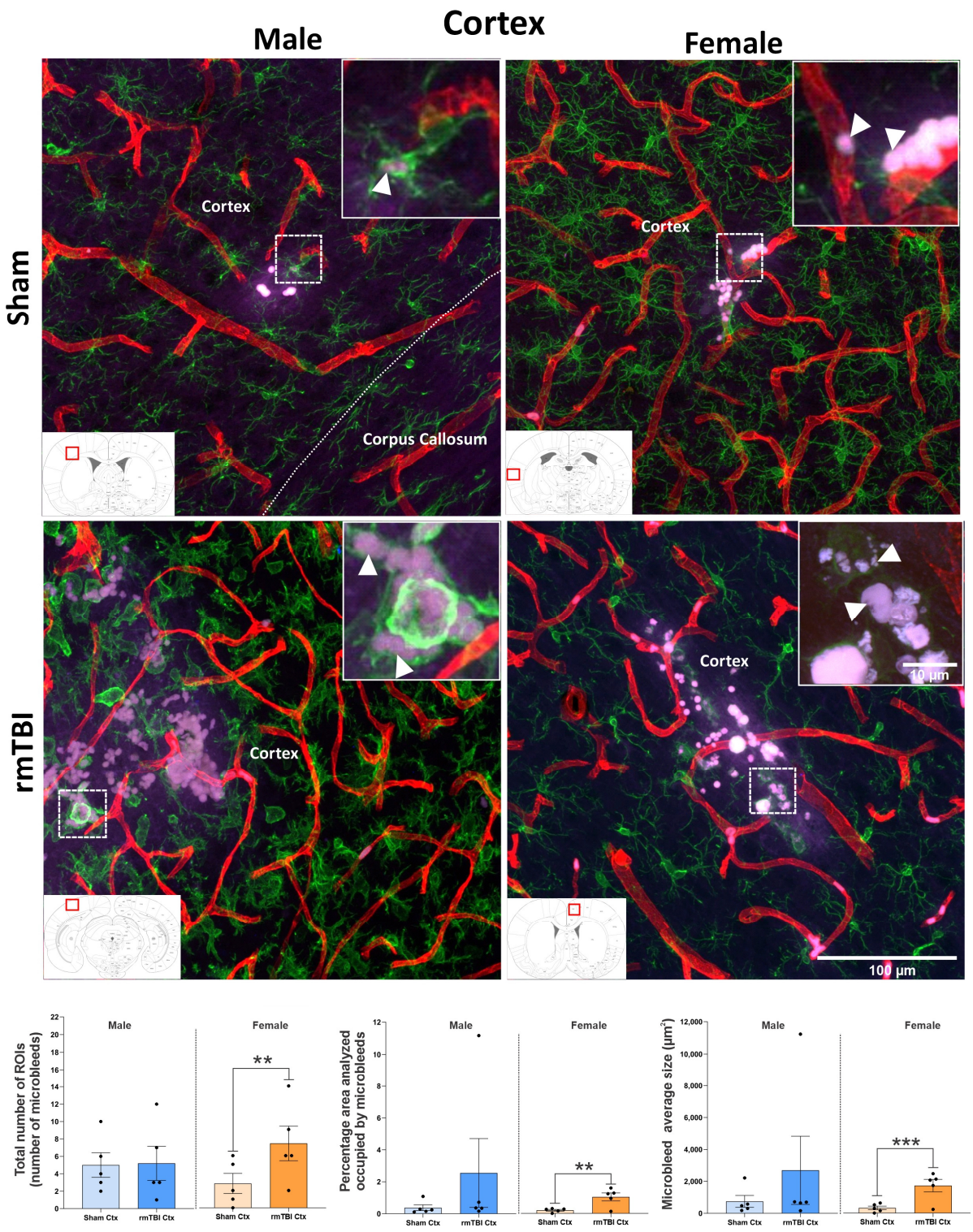

Figure 42. Only females in the rmTBI group showed an increase in fibrinogen extravasation in the cortex at PID1. Although males had some clear examples of microbleeds, no group differences in this brain region were observed. Females displayed an increase in number of ROIs (number of microbleeds), percentage area occupied by microbleeds and microbleed average size. Unpaired one-tail t-test was used for group comparison in each sex. *p<0.1; **p<0.05; ***p<0.01. N=5 per group and sex.

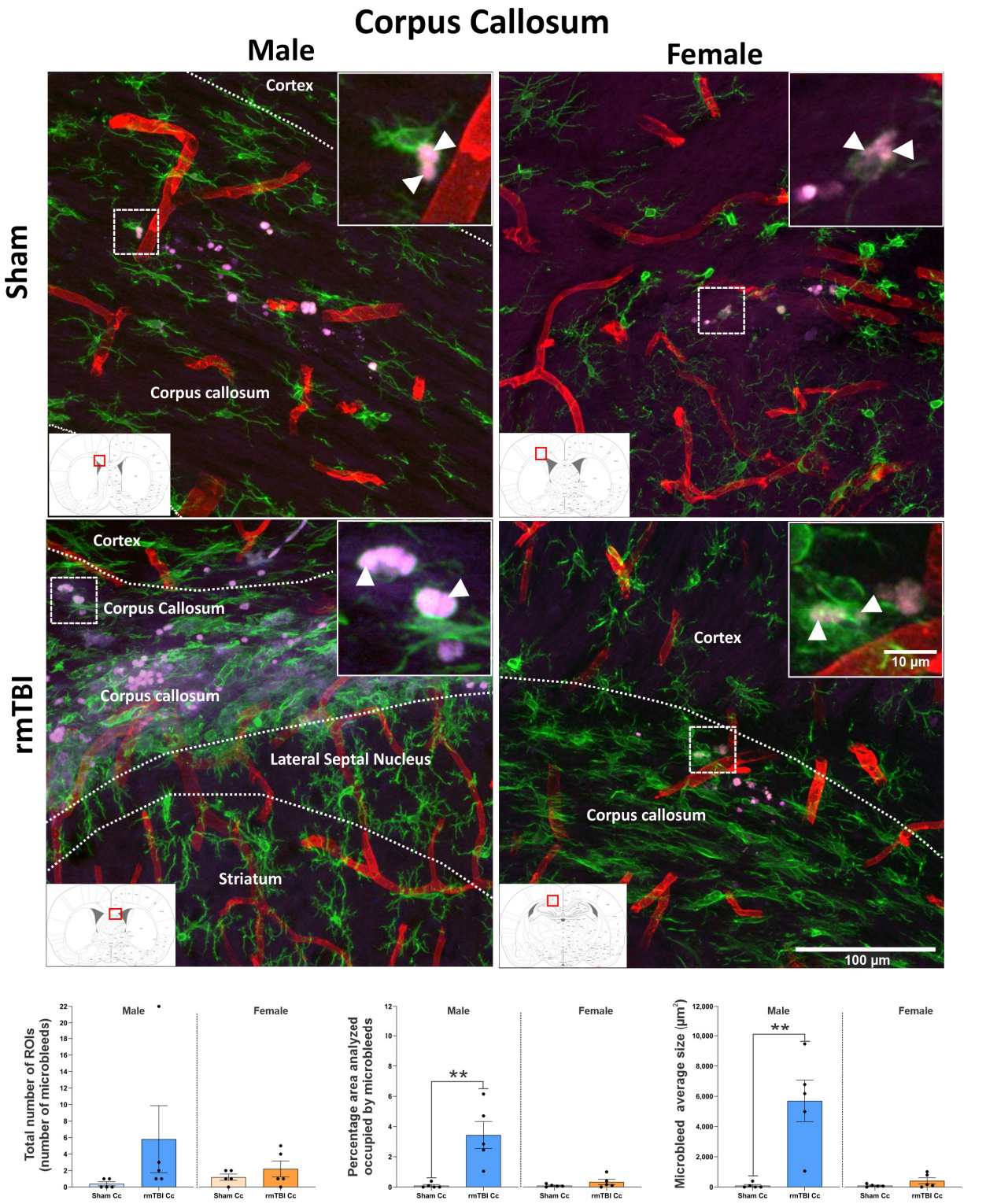

Figure 43. Only males in the rmTBI group showed an increase in fibrinogen extravassation in the corpus callosum at PID1. Results revealed an increase in percentage area analyzed occupied by microbleeds and microbleed average size in males but no differences in females. Unpaired one-tail t-test was used for group comparison in each sex. *p<0.1; **p<0.05. N=5 per group and sex.

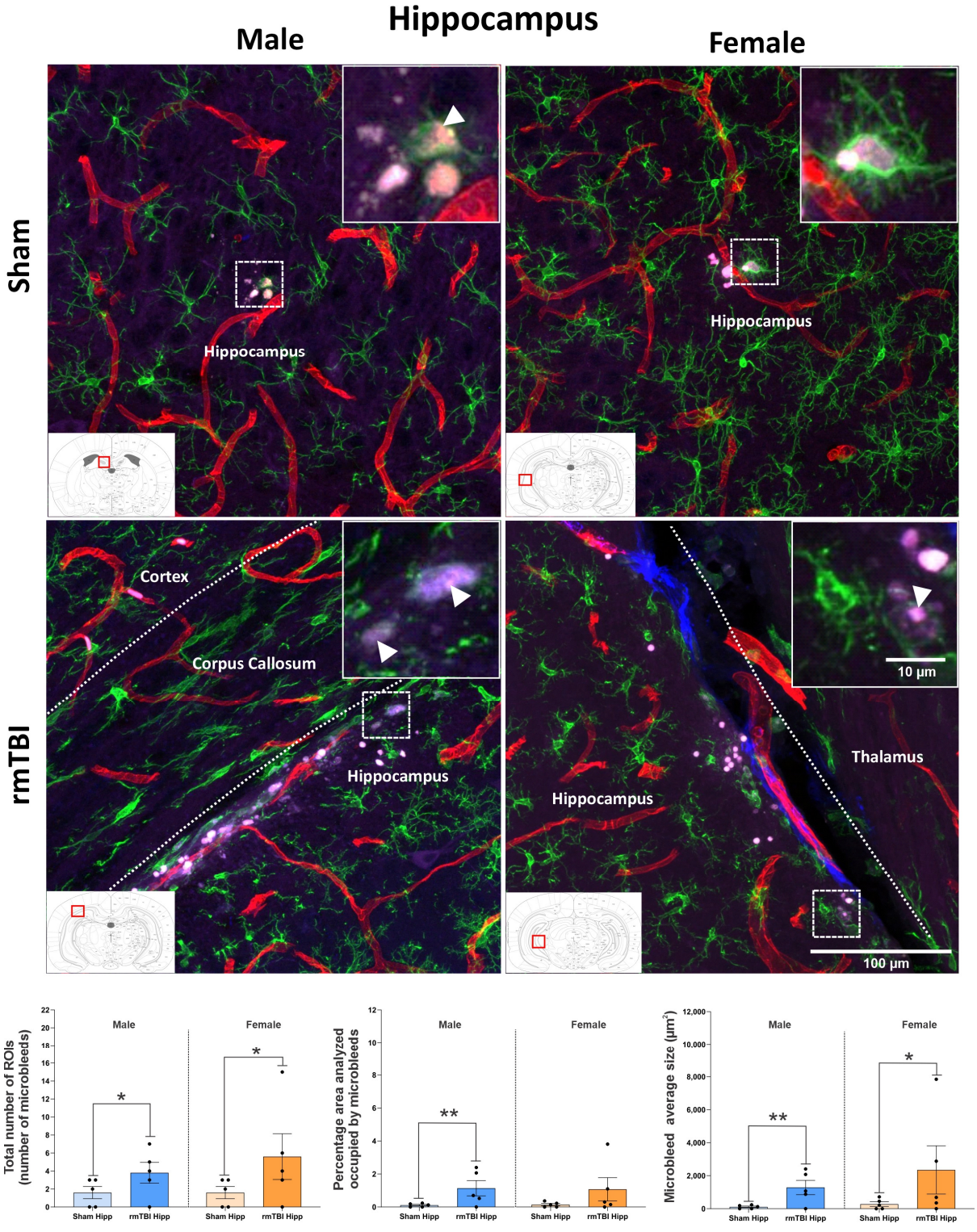

Figure 44. Both males and females in the rmTBI group showed an increase in fibrinogen extravasation in the hippocampus at PID1. All measurements in males show increases in fibrinogen extravasation. Females show an increase in number of ROIs and microbleed average size. Unpaired one-tail t-test was used for group comparison in each sex. *p<0.1; **p<0.05. N=5 per group and sex.

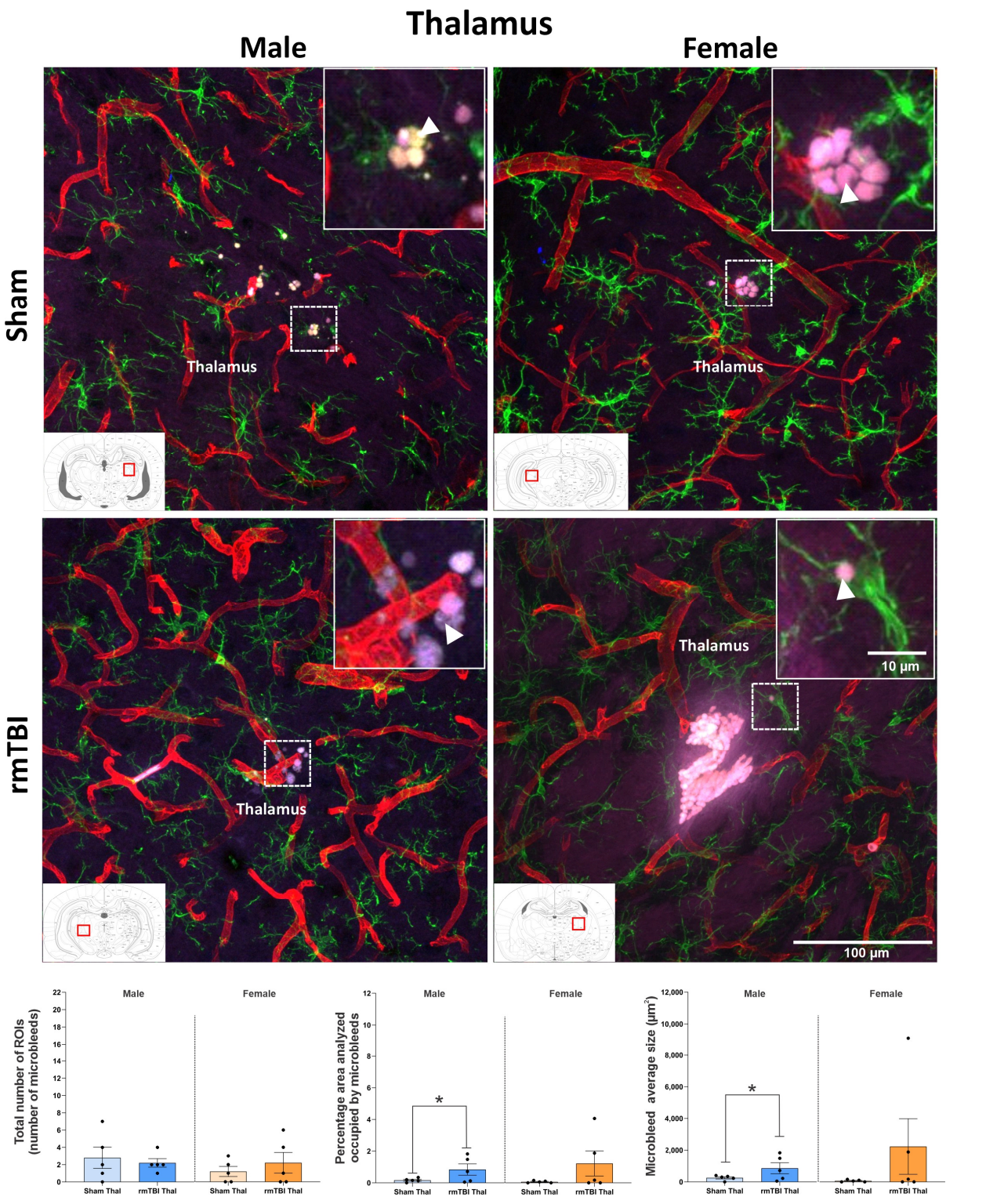

Figure 45. Only males in the rmTBI group showed an increase in fibrinogen extravasation in the thalamus at PID1. Data in males showed an increase in percentage area analyzed occupied by microbleeds and microbleed average size. Females did not show any difference despite some clear examples of large microbleeds in the rmTBI group. Unpaired one-tail t-test was used for group comparison in each sex. *p<0.1; **p<0.05. N=5 per group and sex.

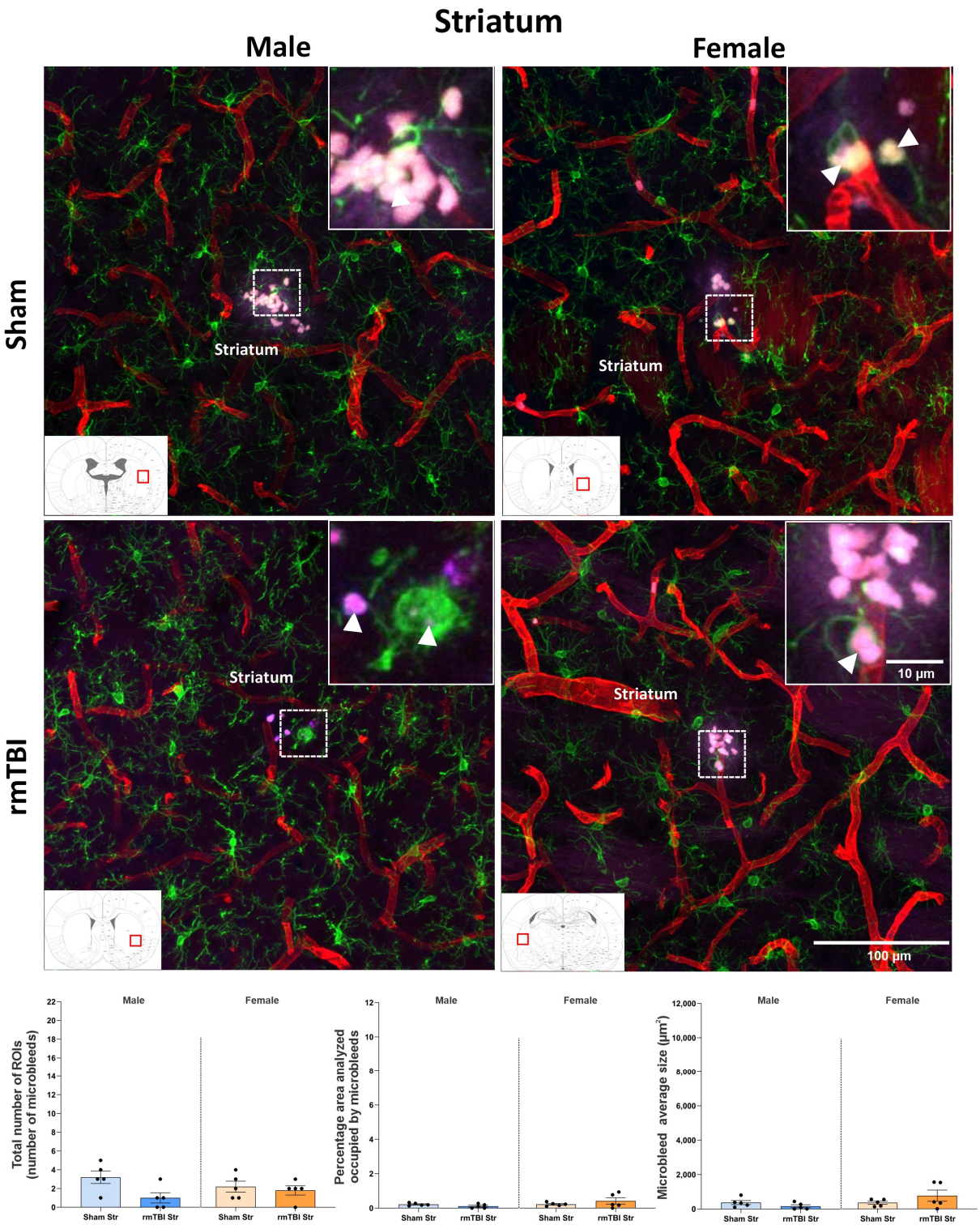

Figure 46. No differences in fibrinogen extravasation were observed in the striatum at PID1. Data in this brain region showed that there were no differences in any of the measurements in nether males or females between shams and rmTBI groups. Unpaired one-tail t-test was used for group comparison in each sex. *p<0.1; **p<0.05. N=5 per group and sex.

4.3.6. Males but not females show small differences in levels of extravasated fibrinogen at PID7.

Fibrinogen extravasation was also evaluated at PID7 to see if similar signs of active microbleeds in rmTBI animals as those detected at PID1 were observed. When looking at the overall total number of ROIs no differences between sham and rmTBI groups in either males or females were observed (**sham male:** 8.200±4.283; **rmTBI male:** 6.000±1.140; p= 0.3165; **sham female:** 4.800±0.2000; **rmTBI female:** 4.000±1.581; p=0.3146). Interestingly, when looking at percentage area analyzed occupied by microbleeds a small increase in males was observed (**sham:** 0.215%±0.080; **rmTBI:** 0.784%±0.320; p=0.061) but no group differences were detected in females (**sham:** 0.362%±0.065; **rmTBI:** 0.549±0.246; p=0.242). Finally, when evaluating the average microbleed size, males showed an increase in microbleed size in the rmTBI group **(sham:** 216.4± 80.73; **rmTBI:** 789.3±321.8; p= 0.0613), but no differences were observed in females (**sham:** 364.9±65.97; **rmTBI:** 552.5±247.5; p=0.2424) (**Fig. 47**). This suggest that to a certain degree, overall microvascular damage in terms of active microbleeds in males was more persistent than in females, however the evidence is not robust enough to provide this conclusion. In a similar way, the regional evaluation revealed that while some individuals presented clear signs of microvascular damage, there were no consistent differences between sham controls and rmTBI groups in neither males nor females in any of the measures analyzed (i.e. number of ROI, percentage area occupied by microbleeds or average microbleed size) (**Fig. 48**). Please note that again, the scales in the graphs at PID7 are matched with the scales on PID1 graphs to allow for a direct visual comparison. These result indicate that active

microbleeds associated with rmTBI are a transient event that is rapidly solved in ~6 days by the physiological mechanism of vascular contention and repair in the brain.

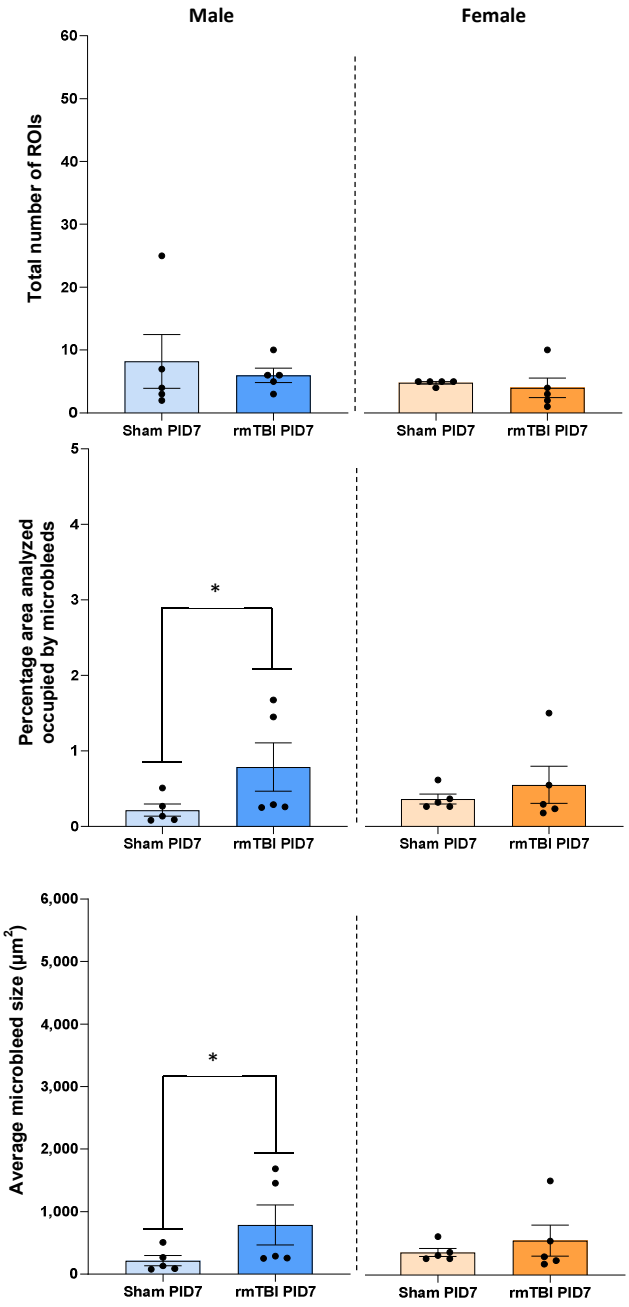

Figure 47. Only males in the rmTBI group showed an overall increase in fibrinogen extravasation at PID7. Similar to what we observed when evaluating hemosiderin deposits at PID7, we only saw a small increase in percentage area occupied by microbleeds and microbleed average size in males. Females showed no differences at this time point between experimental groups. Unpaired one-tail t-test was used for group comparison in each sex. *p<0.1; **p<0.05. N=5 per group and sex.

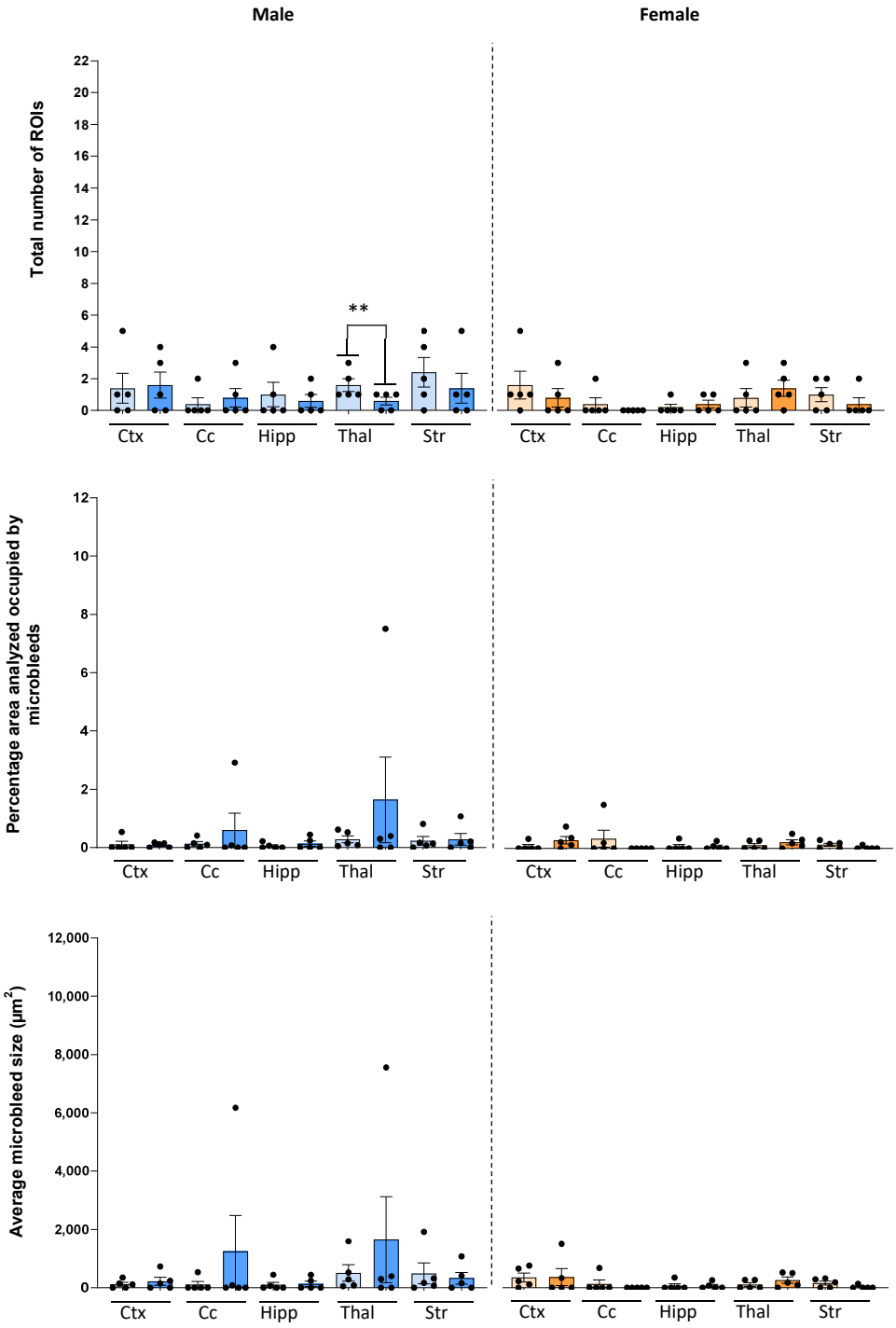

Figure 48. No regional differences in extravasated fibrinogen at PID7. Although there were some animals showing differences, this analysis reveled no relevant changes in microvascular damage in any region between in rmTBI and sham animals. Unpaired one-tail t-test was used for group comparison in each region for each sex. *p<0.1; **p<0.05. N=5 per group and sex.

4.3.7. Microglial cell aggregation and level of activation in microbleeds is increased only in males in the rmTBI group at PID1.

Chronic interaction between microglia and extravasated fibrinogen can be a mechanism for injury amplification in the secondary injury phase of mTBI. To test if microglial cells were presenting differences in reaction depending on the experimental condition, Iba1 positive cells in the vicinity of microbleeds were assessed. In addition, this assessment would test if the increase in microvascular damage observed at PID1 in the rmTBI groups was confirmed with increased microglia reaction. Specifically, microglia aggregation in the perilesional regions (i.e. in the ROIs) and level of activation of these cells based on their morphological features was tested. For microglia aggregation, average area occupied by Iba1+ cells in perilesional regions was measured, and the average circularity index of these Iba1+ cells was computed to determine if they had a more ramified morphology (associated with surveilling microglia and closer to a value of 0) or a more amoeboid morphology (associated with activated microglia and closer to a value of 1). When evaluating the overall aggregation of Iba1+ cells results revealed that male rmTBI animals had a higher average area occupied by these cells accounting for ~11% of total area analyzed (**sham**: 6.368±1.369; **rmTBI:** 10.63±1.076; p=0.0200) **(Fig. 49)**. This increase almost doubled the ~6% level observed in sham controls. Only a trend but no differences were identified on females (**sham:** 7.525±0.7853; **rmTBI:** 9.642±1.466; p=0.1194). When we evaluated the level of microglial activation by measuring the morphological features of these cells, males in the rmTBI group showed a higher circularity index compared to sham controls (**sham:** 0.1252±0.01457; **rmTBI:**

0.1651±0.02199; p=0.0844), indicating a more amoeboid-like morphology of microglial cells in this group compared to sham controls. On the other hand, females showed no difference in this measurement of microglia activation (**sham:** 0.1155±0.01669; **rmTBI:** 0.1514±0.02430; p=0.1291) **(Fig. 49)**

However, this overall analysis does not take into account the potential microglia differences between brain regions, so it is important to evaluate this possible differences controlling for brain region. When performing this regional analysis, it was observed that microglia in the corpus callosum, hippocampus and the thalamus of males in the rmTBI group presented increased aggregation accounting for a ~7% (**sham cc:** 7.970±1.796; **rmTBI cc:** 14.51±2.225; p=0.0257), ~4% (**sham hipp:** 5.405±1.102; **rmTBI hipp:** 8.962±0.9671 p=0.0207) and ~5% (**sham thal:** 5.601±0.6135; **rmTBI thal:** 10.71±3.109; p=0.0728) increase respectively. On the other hand, females only showed regional differences in the hippocampus, with rmTBI animals displaying a ~5% increase in microglia aggregation compared to sham animals (**sham:** 6.222±1.122; **rmTBI:** 11.10±1.554; p=0.0172) **(Fig. 50)**. The evaluation of microglia circularity revealed that in males these cells in the cortex (**sham:** 0.1020±0.006176; **rmTBI:** 0.1503±0.02157; p=0.0318), corpus callosum (**sham:** 0.08875±0.01039; **rmTBI:** 0.1591±0.03078; p=0.0311) and hippocampus (**sham**: 0.1144±0.01186; **rmTBI:** 0.1615±0.01255; p=0.0130) had a higher circularity index, indicating a more amoeboid-like morphology and therefore suggesting that they were more active compared to sham controls. Similar to previous results,

females showed no differences between groups in microglia activation in any of the brain regions evaluated **(Fig. 50)**.

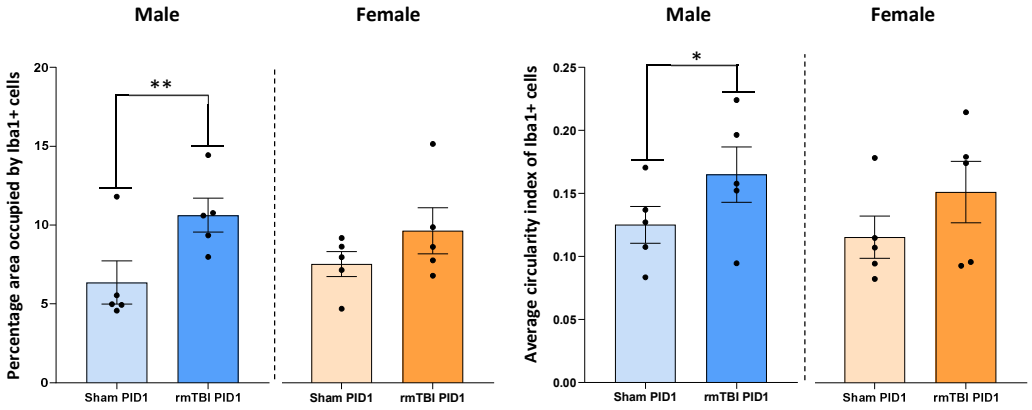

Figure 49. Microglial cells in the male rmTBI group showed an overall increase in aggregation and level of activation at PID1. Analysis of microglia in the vicinity of microbleeds at PID1 showed increased microglia aggregation in rmTBI males but not in females. In addition, also rmTBI males but not females showed increased average circularity index in these cells indicating an increase in the activation level of these cells in this experimental group. Unpaired one-tail t-test was used for group comparison in for each sex. *p<0.1; **p<0.05. N=5 per group and sex.

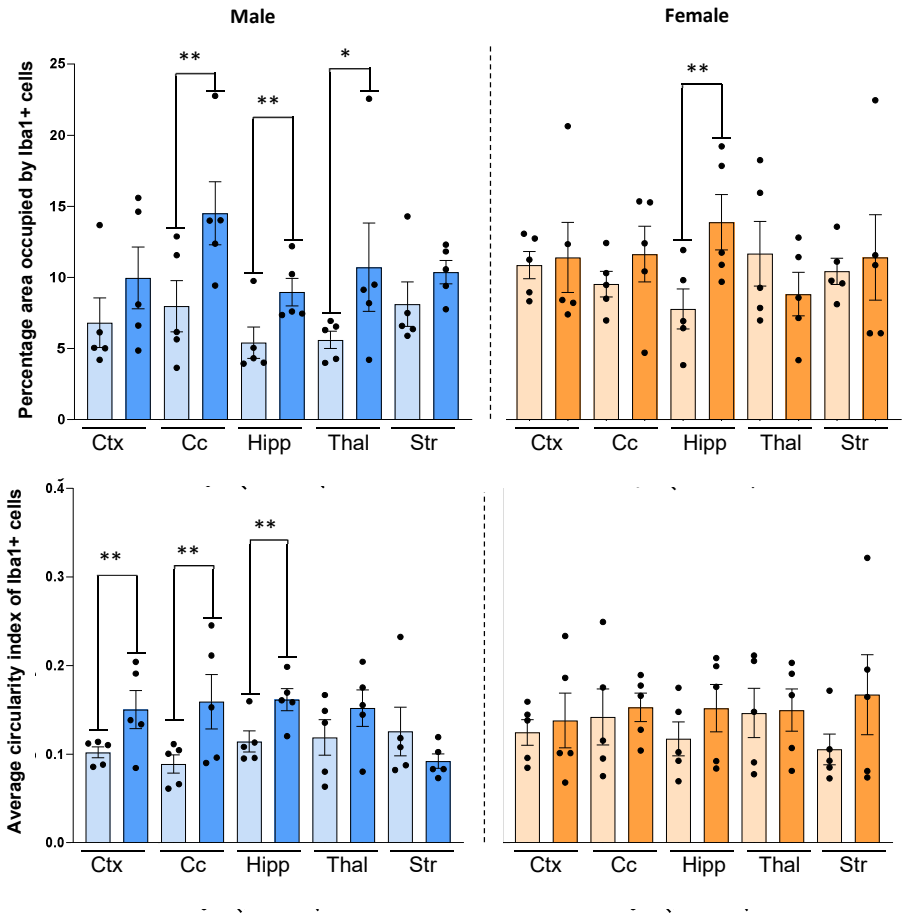

Figure 50. Males in the rmTBI group showed more areas with increased microglia aggregation and activation than females. Analysis of microglia on the different brain regions evaluated revealed that in rmTBI males these cells showed increased aggregation in the corpus callosum, hippocampus and thalamus. In females only the hippocampus showed this pattern. When evaluating the level of activation of this cells by evaluating the circularity index, it was observed that in males in the rmTBI group this measurement was increased in the cortex, corpus callosum and hippocampus. Females showed no differences between rmTBI and sham animals in circularity index. Unpaired one-tail t-test was used for group comparison in for each sex. *p<0.1; **p<0.05. N=5 per group and sex. The reader is advised to consult the imputation method for "missing values" in the *Microglia analysis* paragraph of the methods section in this chapter to better interpret these results.

4.3.8. Microglia aggregation but not level of activation is increased in rmTBI animals in both sexes at PID7

The level of microglia aggregation and activation was also assessed at PID7 to evaluate if these cells were altered at this time point even if the rmTBI effects on microvascular damage were no longer as clear as at PID1. When evaluating overall

average area occupied by Iba1+ cells, we saw an increase in both males and females in the rmTBI group compared to sham controls. This increases corresponded to a ~3% in males (**sham:** 5.794±0.6312; **rmTBI:** 8.915±0.5636; p=0.003) and a ~2% in females (**sham:** 6.756±1.135; **rmTBI**: 8.801±0.6110; p=0.067) **(Fig. 51)**. This suggest that overall, even though signs of active microvascular damage were similar between sham and rmTBI groups at this time point, animals that underwent concussive events showed a higher level of aggregated microglia in the vicinity of microbleeds. However, when assessing the circularity index of these Iba1+ cells we saw no group differences in either sex **(Fig. 51)**. The low number of microbleeds identified at PID7 caused a significant amount of "missing values" according to the methodological approach used to acquire microbleed ROIs. This made regional evaluation of microglia at PID7 impractical and therefore only the overall effects are presented.

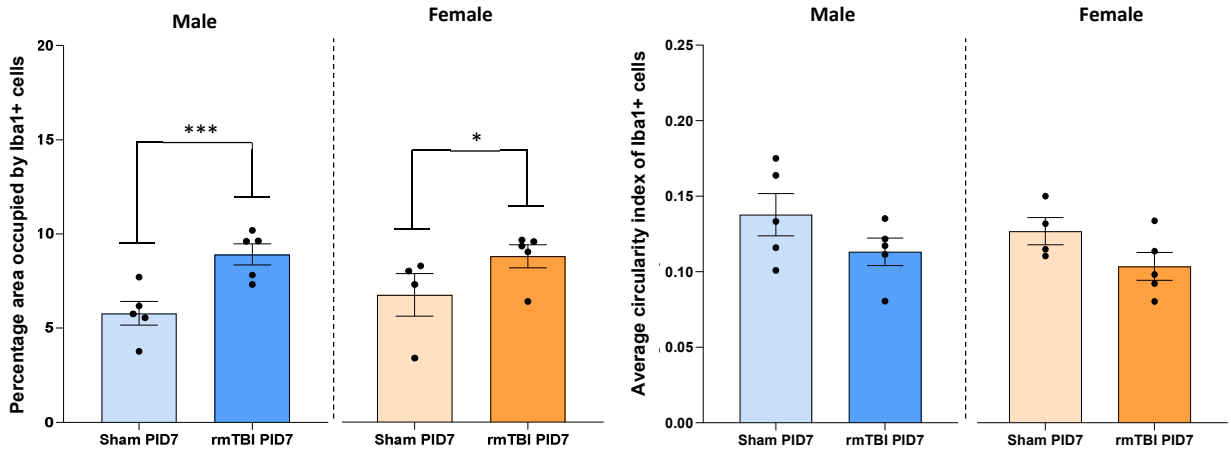

Figure 51. Males and females in the rmTBI group show signs of microglia aggregation in microbleeds at PID7. Analysis of perilesional microglia at PID7 shows that there is increased cell aggregation but not activation in the rmTBI groups of both sexes compared to sham controls. This suggest some potential residual signs of microvascular damage in the rmTBI group at this time point.

4.4. Discussion

In this chapter, using the NAP it was first shown that the ACHI model of rmTBI is associated with acute sensorimotor deficits (Meconi et al., 2018b; Pinar et al., 2020) similar to what is reported in the human population (Guskiewicz et al., 2001; Echemendia et al., 2017; Galea et al., 2018). This is an important piece of translational information since concussions nowadays are mainly diagnosed based on a set of behavioural manifestations rather than specific biomarkers. Concussions are known as silent injuries because even though there are not clear signs of brain damage, mTBI patients may still experience behavioural alterations (Belanger et al., 2007; Petchprapai and Winkelman, 2007; Iverson, 2010). Recent advancements in human observational studies in mTBI patients and other neurodegenerative diseases combined with increases in resolution of different imaging techniques (e.g. MRI, DTI) has allowed to identify new objective sigs of damage in early stages of this pathologies (Wu et al., 2016). One of these promising subtle but non-irrelevant signs of early damage associated with disease severity are CMBs. In this study, short-term (i.e. PID1) and long-term (PID7) microvascular damage associated with the ACHI model were evaluated. Initially, signs of microvascular damage between sham and age-matched naïve animals were compared to test if the sham procedure was causing methodologically-induced microvascular damage. None of our measurements of microvascular damage were increased in the sham group, indicating that the sham procedure alone was not sufficient to cause detectable microvascular damage. Although some studies have reported stress-induced vascular damage (Esposito

et al., 2001; Menard et al., 2017; Lehmann et al., 2018, 2020), these data suggest that the ACHI sham procedure, while potentially stressful for the animals is not sufficient to cause microvascular damage. Indeed, a previous assessment of corticosterone levels in our lab showed that there is no significant difference between naïve control, sham and rmTBI animals. Before proceeding to discuss the results obtained in this part of the study, it is worth reminding the reader that a priori power analysis determined that this study is currently underpowered for inferential statistics and this fact needs to be considered when interpreting the results.

After ruling out methodologically-induced microvascular damage, the levels of hemosiderin deposits associated with rmTBI were evaluated. It was observed that overall (i.e. all brain regions analyzed combined) males in the short-term time point (i.e. PID1) showed an increase in number and density of hemosiderin deposits, brain extension occupied by hemosiderin deposits and also average hemosiderin deposit size. This indicates that overall, males had larger and more abundant microbleeds compared to sham controls. On the other hand, at the same short-term time point, females showed a less prominent change with only a small overall increase in brain extension occupied by hemosiderin deposits and a higher hemosiderin deposits average size. This indicates that while microbleeds in females were larger, they were not more abundant than in the sham group.

To investigate if there was a regional susceptibility to microvascular damage short-term the levels of hemosiderin deposits in different brain regions we assessed separately.

Specifically, the cortex, corpus callosum, hippocampus, thalamus and striatum were explored. The data showed that in males, although all regions evaluated presented signs of microvascular damage, the regions showing more consistent signs of microvascular damage in terms of hemosiderin deposits were the corpus callosum, hippocampus and thalamus. In females these more susceptible brain regions were the hippocampus and thalamus. It is important to note that this data suggests that as we anticipated, our model induces a diffuse injury since the majority of the damage was not restricted to the cortex and was instead distributed in different subcortical structures (Meconi et al., 2018b). The areas affected match with some of the behavioral deficits reported in the literature. For instance, both the hippocampus and the thalamus are involved in learning and memory, cognitive functions that have been repeatedly reported to be altered after mTBI (Matser et al., 1998; Serra-Grabulosa et al., 2005; Wall et al., 2006). In addition, the clear effect in the corpus callosum of males in the rmTBI group corresponds with reports in humans showing that this area is particularly susceptible to the effects of shearing forces in mTBI (Cloots et al., 2013; Bigler, 2018). Indeed, DTI and MRI studies have consistently identified signs of diffuse axonal injury and diffuse vascular injury in this brain region in mTBI patients (Rutgers et al., 2008; Lo et al., 2009; Aoki et al., 2012; Tian et al., 2014; Wu et al., 2016). While both DAI and DVI are commonly observed together (Tian et al., 2014), it is still believed that the movement of axonal fibers is the cause of vascular disruption. However, a recent study found that microvascular damage occurs first and these events may lead to axonal injury (Griffin et al., 2019). The authors suggest that the imaging observation reported in these other studies are compatible with cerebral microbleeds

indicating that these microvascular events may be driving the axonal degeneration. The fibrinogen-centric injury mechanism described in animal models of multiple sclerosis is in accordance with these observations (Davalos et al., 2012; Ryu et al., 2015b). In MS models, the increased prevalence of cerebral microbleeds leads to the accumulation of extravasated fibrinogen in the parenchyma as its insoluble form, fibrin. This accumulation of fibrin triggers the generation of clusters of chronically activated microglia that progressively lead to axonal injury and degeneration through different mechanisms such as local release of pro-inflammatory cytokines, microglia phagocytosis of myelin and inhibition of oligodendrocyte differentiation (Petersen et al., 2018). This suggests again, that cerebral microbleeds may precede axonal damage and potentially trigger it or exacerbate it. Unfortunately, this study did not systematically evaluate axonal damage in areas close to cerebral microbleeds. However, some preliminary evidence suggesting that areas closer to microbleeds also show signs of axonal damage in our model have been obtained **(Fig. 52)** and it is something that will be pursued in future experiments.

To evaluate if fibrinogen was also playing a role the ACHI model of rmTBI, the levels of extravasation of this protein were also assessed. It is important to note that while Prussian blue staining allows the evaluation of old and potentially already resolved microvascular damage by detecting the iron signature left by these events it can not detect more recent and active microbleeds (Liu et al., 2014; Sumbria et al., 2016). For this reason, detection of fibrinogen extravasation in this study was also used to allow investigation of

active microvascular damage. **Figure 53**, provides a visual comparison of the same microbleed stained in serial sections with Prussian blue and fibrinogen. Note how not all the extravasated blood contents (brownish pigment) are fully labelled with the characteristic bright blue pigment of Prussian blue staining. However, since this microbleed is still active, everything is detectable in the florescence image displaying fibrinogen, WGA and Iba1 **(Fig. 53)**. Before proceeding to discuss the results of our fibrinogen extravasation analysis it is important to keep in mind that the fibrinogen positive signal observed is mixed with RBCs autofluorescence. This happens because every time there is a rupture of a blood vessel wall, fibrinogen leaks and starts the clotting cascade. Therefore, if the vessel rupture is large enough to allow the passage of RBCs, these cells will be accompanied by fibrinogen and thus the resulting purplish color.

The evaluation of fibrinogen extravasation revealed that short-term both males and females showed a clear overall increase in area occupied by microbleeds and average size of microbleeds and, although a trend can be observed, no changes in number of ROIs was found. It is worth mentioning that due to the methodology used in the fibrinogen analysis, the evaluation of number of ROIs is not too sensitive (i.e. a very small microbleed and a very large one will be each counted as one ROI), and therefore area occupied by microbleeds and average microbleed size should receive more importance when interpreting these results.

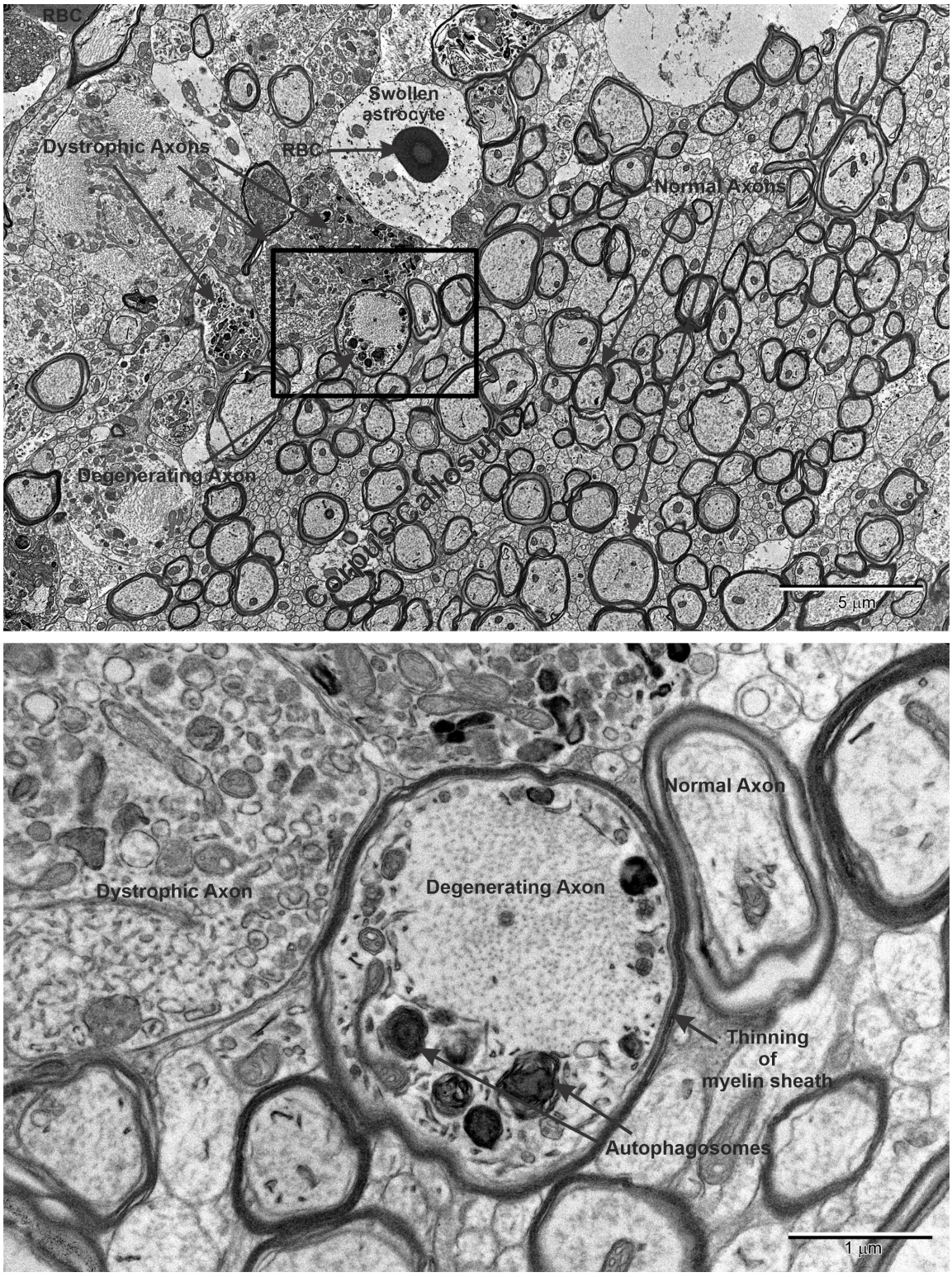

Figure 52. Evidence of axonal damage in the vicinity of a microbleed. Preliminary data shows that axonal damage can de detected in proximity to microvascular damage in the ACHI model or rmTBI. We can observe an oligodendrocyte undergoing autophagy in a degenerating axon. Image shows a region of the corpus callosum from a rmTBI male animal at PID1. Image provided by Dr. Patrick Nahirney.

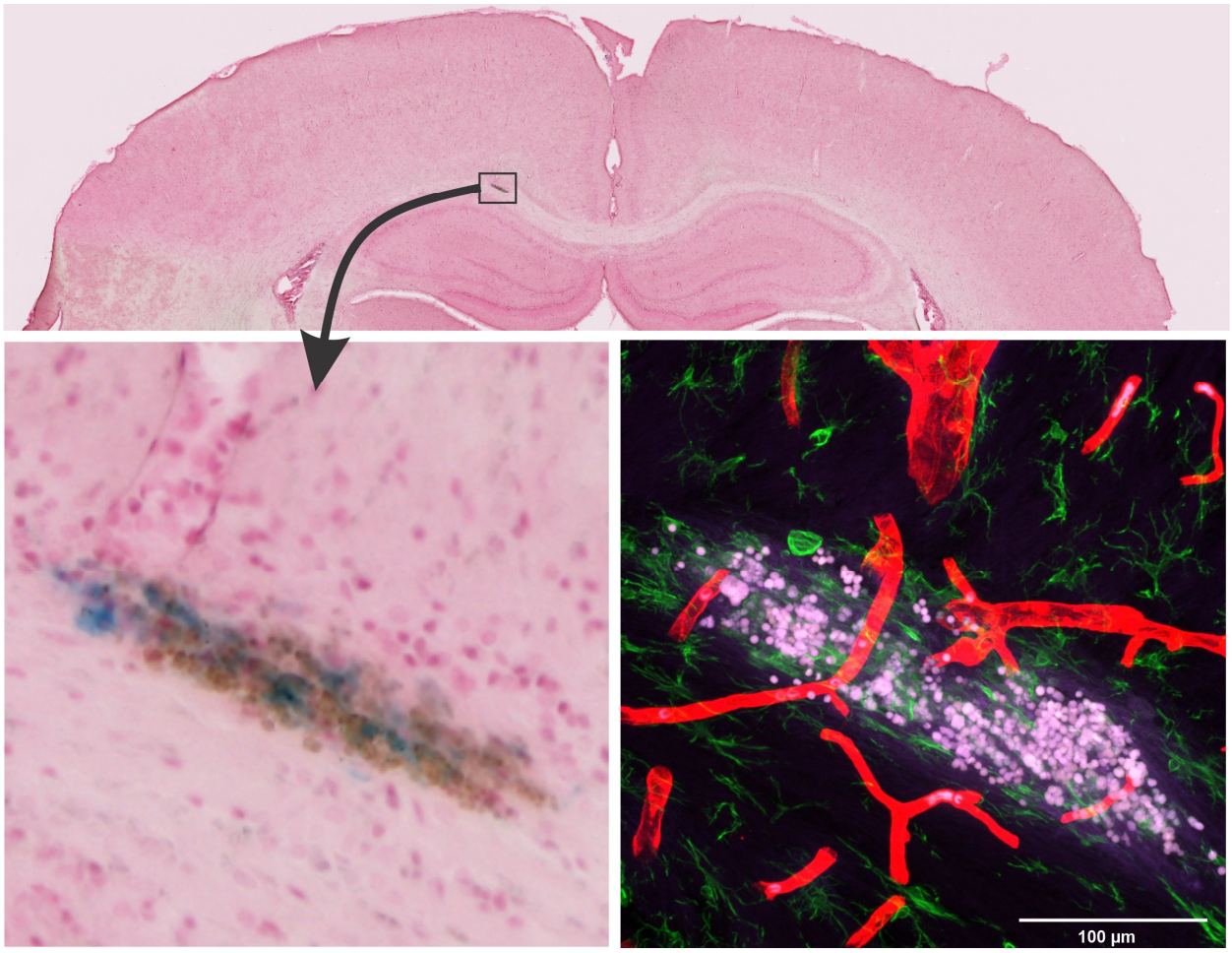

Figure 53. Prussian blue staining and fibrinogen immunolabeling provide complementary evidence when evaluating microvascular damage. Prussian blue labels the iron traces left by vascular injuries that are at least 2-3 days old. In contrast, fibrinogen immunostaining allows visualizing vascular injuries shortly after they occur.

When performing a regional assessment, males showed that only the hippocampus had an increased number of ROIs. In females this pattern was observed in the cortex and hippocampus. When looking at percentage area occupied by microbleeds, males showed that the corpus callosum, hippocampus and thalamus presented an increase in this measurement. In females, although some individuals showed clear signs of microvascular damage in different regions, only the cortex showed a consistent increase

in percentage area occupied by microbleeds. The evaluation of microbleed average size showed that in males the corpus callosum and the thalamus had larger microbleeds while in females the regions with larger microbleeds were the cortex and hippocampus. This data indicates that similarly to what we observed when evaluating hemosiderin deposits, rmTBI animals of both sexes showed increased signs of microvascular damage and similar regions showed an increased susceptibility to microbleed occurrence when performing fibrinogen extravasation analysis. These results also indicate that fibrinogen can potentially be play a role in vascular damage induced inflammation in rmTBI. This could provide an interesting therapeutic target in very early phases on this injury and TBI research could leverage the rich literature already available in other disease models with a vascular and fibrinogen component such as MS and AD.

To know if these observed increases in microvascular damage observed 1 day after the last injury (PID1) were also present at a longer time point (i.e. 7 days after the last injury or PID7) hemosiderin deposit and fibrinogen extravasation analysis were also performed at this time point. Due to the nature of the Prussian blue staining, we were expecting to see an even more clear difference because if there were microbleeds that occurred late during the injury paradigm (i.e. 3rd and 4th day of impacts) and were not yet detectable at the short-term time point (PID1) we would be able to detected them at PID7.

However, to our surprise the data showed that at PID7 overall there were no differences between the rmTBI and the sham group in levels of hemosiderin deposits in number, density or percentage area occupied. Although in males there was a significant

increase in hemosiderin deposit average size suggesting some potential residual effects, it was considered that the evidence is not robust enough to reach this conclusion. Similarly, the regional analysis of hemosiderin deposits showed no relevant differences in any region except for some discrete increases in hemosiderin deposit average size in the cortex and hippocampus in males and in the cortex in females. Although it has been reported that hemosiderin deposits increase with age, the exact mechanism of why this occurs is still not fully understood. It is possible that more spontaneous vascular damage events start occurring but is also plausible that this accumulation of hemosiderin deposits happens because the processes in charge of clearing this excess iron from the brain parenchyma starts functioning less efficiently. However, a combination of these two possibilities cannot be ruled out. In this case, because animals in this study were very young (~PND36-37) it is possible that the blood contents leaked by microbleeds got cleared from the brain parenchyma rapidly, preventing the formation of hemosiderin deposits that can be visualized with Prussian blue staining. This would explain why we do not see differences in hemosiderin deposits between sham and rmTBI animals at PID7. In agreement with these results, when looking at the levels of fibrinogen extravasation at PID7, the clear differences observed in the short-time point were absent then. In this case, because fibrinogen staining labels recent microbleeds, we were expecting the majority of the microbleeds to be resolved at this time point and therefore no differences between sham and rmTBI groups were anticipated. There was only a potential but not robust overall increase in percentage area occupied by microbleeds and microbleed average size in males, and no differences in females.

Taken together, these results suggest that the microvascular damage associated with the ACHI model and injury paradigm is a temporary event that can be visualized acutely but is resolved 7 days after the last impact leaving no evident traces of microvascular damage. These results are is in accordance with a recent study in rodents (Wu et al., 2021) and with reports in humans where signs of progressing vascular damage in mTBI patients are no longer detectable at longer time-points (Rutgers et al., 2008; Homnick et al., 2012). In contrast, there are other imaging studies reporting that subtler forms of vascular damage such as microbleeds, can still be detected after 6-12 months in human mTBI patients (Rostowsky et al., 2018; Studerus-Germann et al., 2018; Einarsen et al., 2019).

In this study, Iba1 staining was used for two reasons. First it provided an internal control of vascular damage that allowed to rule out methodologically-induced vascular damage in the form of perfusion artifacts. Iba1 provides this control, because artificial signs of microvascular damage that may occur during transcardial perfusions do not have enough time to elicit a detectable microglia reaction. In addition, Iba1 labelling allowed evaluating and comparing the overall response of this resident immune cells in the vicinity of microbleeds in sham and rmTBI groups. Microglia cells will be referred to when describing Iba1+ cells in this section, however it is important to point out that other cell types like macrophages are also Iba1. Therefore, it can not be conclusively said that this evaluation included only microglia cells. To evaluate microglia reaction to microbleeds two measurements were obtained: microglia aggregation by evaluating area

occupied by Iba1+ signal, and microglia activation by measuring the circularity index of these cells. When microglia become activated their morphological features transition from a highly ramified morphology to a more amoeboid and circular shape (Heindl et al., 2018; Yew et al., 2019). Highly complex cells have a lower circularity index closer to 0, and more amoeboid cells have a higher circularity index closer to 1 (perfect circle). When evaluating the overall microglia aggregation and activation at PID1, males in the rmTBI group showed increases in both of these measurements. Females on the other hand, showed no changes compared to sham controls. This fits with the evaluation of microvascular damage, where males showed more evident and consistent differences while females changes were less prominent. Again, a regional analysis was also performed. Males showed that the corpus callosum, hippocampus and thalamus had an increase in microglia aggregation compared to sham controls. In females only the hippocampus showed this difference. When evaluating the circularity index, we saw that in males this measurement of microglia activation was increased in the cortex, corpus callosum and hippocampus. On the other hand, females showed no differences.

The microglia reaction in close proximity to microbleeds was also assessed at PID7. This was done to determine if there were differences in microglia reaction in perilesional sites at this time point even though signs of microvascular damage were no longer as evident as at PID1. Both males and females in the rmTBI group showed an overall increase in microglia aggregation around microbleeds. In contrast neither sex showed differences in the level of microglia activation.

One thing to take into consideration when evaluating microglia aggregation is that the relevance of the observed increase in area occupied by Iba1+ at both PID1 and PID7 could be obscured by the increased area of microbleed size. In other words, it makes sense that the larger the microbleed the larger the microglia aggregation. This point is important especially when males in the rmTBI group at PID1 showed a larger area occupied by microbleeds. In this case it would be more appropriate to say that the increase of microglia aggregation is a confirmation of increased microvascular damage in this group more than there was an excessive clustering of microglia. The same interpretation could be applied to males at PID7. On the other hand, at PID7 the fact that there is no clear difference in microbleeds between sham and rmTBI female animals, but there is an increase in microglia aggregation suggest that there could be a true increase in microglia clustering in females independent of microbleed size. This could indicate that residual presence of microglia around microvascular damage sites is observed in females at PID7.

Finally, there are some points to consider in the regional microglia analysis (the points described below do not have an impact on the overall analysis). Equipment and resource limitations guided in part the specific methodology used in this study for fibrinogen and Iba1 immunofluorescence analysis. As mentioned in the methodology section, the unavailability of a motorized confocal microscope that would have allowed a whole slide analysis similar to the Prussian blue evaluation, forced us to use an event-driven analysis. This means that the 12 stained slices per animal were manually and

systematically scanned and standard size imaging windows (ROI) were acquired with a confocal microscope every time extravascular fibrinogen positive signal was observed interacting with Iba1 positive cells. Therefore, all ROIs contained microbleeds and only if a microbleed was present an ROI was imaged. The implication of this is that there were some animals that showed no microbleeds (and thus no ROIs) in some specific regions creating a missing at random scenario. Due to the small sample in this study, using a listwise deletion (just ignoring missing values from analysis) would have greatly impacted our power and results would have not been informative. That is why it was decided to use an adapted multivariate normal imputation method (Schafer, 1997; Sullivan et al., 2017). See *Microglia analysis* for more detailed information. For this regional analysis a value based on the group mean and standard deviation was generated for each missing value. We acknowledge that this data processing can have an influence over the final results but, given the alternatives we considered that overall this approach was superior. For instance, we could have assigned a value of 0 to these animals, but this would imply that no microglia aggregated around microbleeds for that animal in that region (because there were no ROIs) and that the microglia circularity index for that animal was that of a highly ramified cell characteristic of surveilling microglia. This imputation approach could artificially increase group differences by reducing the variability and mean of the transformed group. Alternatively, we could have provided these null animals a value equal to the mean of the group, however this decision can also bias result interpretation accentuating differences between groups by greatly reducing the variability of the group in animals showing no microbleeds in a specific region.

Finally, the other alternative approach would have been to only include in the analysis those animals that showed ROIs in the brain region evaluated (listwise deletion). While this is probably the most appropriate and conservative approach, the fact that some regions showed a big disparity in occurrence of microbleeds (e.g. 100% of rmTBI males showed at least 1 ROI in the corpus callosum while this percentage was only 40% for sham controls) combined with the low number of animals used in this study would have made this analysis highly sensitive to the variability of the animals that presented microbleeds in that region and therefore made our analysis biased and not very informative. The final decision of using multivariate normal imputation method was taken considering all these trade-offs and we decided that it creates the most balanced approach available. However, this fact needs to be taken into account when reaching conclusions.

CHAPTER 5: GENERAL DISCUSSION

5.1. Summary of major findings

The aim of this study was to evaluate the microvascular damage associated with rmTBI in juvenile male and female rats. This study is the first to show with great precision a whole-brain systematic approach for post-mortem histological visualization of microvascular damage associated with rmTBI in the ACHI model. Methodological approaches employed were thoroughly validated on multiple angles prior to addressing our main experimental questions, and convergent evidence revealed that microvascular damage occurs in the ACHI model of mTBI. First, a series of common techniques used to label the brain vasculature and to evaluate vascular damage in rodents were presented. These approaches were validated using two different models of vascular damage (stab wound injury and laser microablation) as positive controls. This permitted selection of the most suitable techniques to evaluate microvascular damage in the ACHI model of rmTBI and it also helped define the histological staining patterns of real vascular damage to avoid evaluating staining artifacts. Intracardiac injection of WGA was shown to be an excellent approach to visualize the brain vasculature with great detail. In addition, detection of hemosiderin deposits using Prussian blue and labelling of fibrinogen extravasation were selected as the most suitable approaches available to evaluate microvascular damage in the ACHI model.

The results presented in this dissertation indicate that there is an acute increase in microvascular damage in animals following rmTBI that is manifested as increases in hemosiderin deposits and extravasation of fibrinogen and RBCs. Although both sexes in the rmTBI group presented a certain degree of microvascular damage when evaluated one day after the last impact, males consistently showed more severe signs than females. These observations are supported by increases in perilesional microglia responses at this short-term time point, only observable in males (females only showed a trend). In addition, the regional analysis revealed that in males of the rmTBI group, the corpus callosum, hippocampus and thalamus were the regions that presented more consistent signs of microvascular damage. Although, in rmTBI females, it was harder to clearly pinpoint individual brain regions that consistently showed higher signs of microvascular damage, and the data suggests that the cortex, hippocampus and thalamus may be more affected in this sex.

The data also indicates that this initial acute increase in microvascular damage associated with rmTBI is a temporary event, since 7 days after the last concussive event, hemosiderin deposits and fibrinogen extravasation levels are no longer discernable from the basal levels of microvascular damage observed in sham controls. Despite this, some signs of increased microglia clustering at this time point suggested potential traces of microvascular damage.

Although this study may be affected by a relative low sample size that may cause some comparisons to be underpowered and thus reduce the possibility to make robust

conclusions, I think that an overall association between the rmTBI injury paradigm employed in this study and microvascular damage is proven with the data presented **(Fig. 54)**. I consider this study to be a good initial stepping stone that can pave the path for future experiments aiming at expanding and complementing the observations presented here.

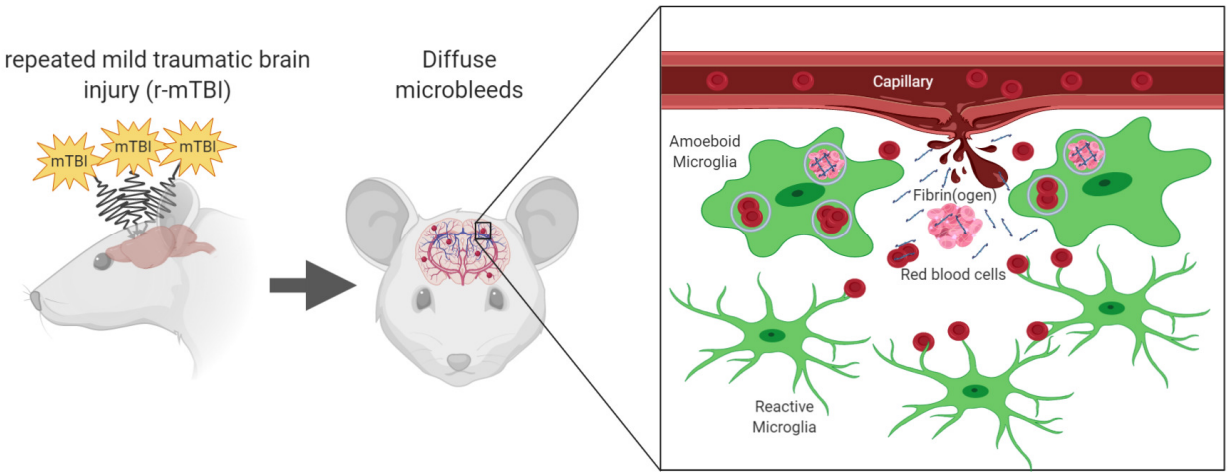

Figure 54. Visual summary of microvascular damage and rmTBI. Results indicate that after rmTBI using the ACHI model there is an acute increase in microvascular damage in the form of diffuse microbleeds. This is reflected as increases in extravasation of fibrinogen and RBCs that are captured and phagocytosed mainly by microglial cells and subsequently processed to generate hemosiderin deposits. This acute manifestation of microvascular damage, however, is a temporary event that seems to be resolved 7 days after the last impact (at least using our specific injury paradigm of 8 impacts over 4 days). However, some potential residual effects of microvascular damage in the form of increased perilesional microglia aggregation at this time point were observed and we cannot discard that an evaluation at a more distant time point can reveal long-term alterations. Indeed, maladaptive responses to microvascular damage, including the generation of clusters of chronically activated microglia cells induced by sustained interaction with fibrin deposits can lead to structural damage (e.g. axonal injury, demyelination, etc.) that over time can result in cognitive deficits.

5.2. Limitations

One of the main limitations of this study is the sample size. A priori power analysis indicated that with an alpha of 0.05, a power of 0.8 and a general effect size of 1.2-1.3. (considered to be a large effect using Cohen's and Sawilowsky's criteria), the projected sample size needed was approximately N = 9-10/group. This is an important fact to consider when interpreting the results in this study, since the sample size used (N= 5/group/sex) may render results underpowered for inferential statistics. However, we are currently working on increasing the sample size to overcome this limitation to be able to make more robust claims. It is also important to consider too that a priori power analysis can be very broad and based on a best educated guess. Therefore, the results presented in this study cannot be completely disregarded based only on this criterion.

Another limitation in this study is the use of slightly different methodologies when evaluating hemosiderin deposits and fibrinogen extravasation. The equipment available allowed us to make whole-slice scanning for Prussian blue-stained sections, therefore permitting an unbiased analysis of the full stained tissue. On the other hand, evaluation of fibrinogen extravasation, although systematic, required human visual scanning of the sections to identify microbleeds. This means that this analysis was event-driven and only when a microbleed was present, an image of that region was acquire for analysis. It would have been optimal to do a similar whole-slice scanning in fibrinogen extravasation analysis using a motorized confocal microscope to include for instance measures from regions without microvascular damage.

Related to methodological considerations, it is important to indicate that in this study we used Iba1 as a marker of microglia, however it has been shown that other cells share expression of this marker. A solution for this limitation would be to use a microglia-specific marker like TMEM-119 in future experiments.

Another fact to take into consideration in this study is that our specific rmTBI injury paradigm induces the impacts over 4 days. This specific paradigm was chosen to mimic a 4-day soccer or rugby tournament. However other injury paradigms have also been tested in our lab including, 1 hit over 1 day, 4 hits over 2 days, 8 hits over 1 day and 16 hits over 4 days. These evaluations were made to both fine tune our model to maximize the probability to see effects while maintaining it under the classification of mTBI (i.e. without causing overt damage in the brain like macroscopic tissue loss or large hemorrhages). This was also done to study the effects of the temporal separation between impacts in this injury model. The specific injury paradigm used in this study (i.e. 8 impacts over 4 days) provided a good balance where animals presented acute behavioural deficits without overt structural damage in the brain. However, this paradigm makes it challenging to define the contribution of each specific impact or to define when microvascular injuries occurred. For instance, the two time points used in this study, 1 and 7 days after the last impact, are also day 5 and day 11 after the initial impact, respectively. Although our Prussian blue data suggests that the majority of microvascular injuries occur during the initial days of impacts, with the current methodology we cannot get a better estimate for this.

Additionally, in this study we are currently lacking behavioural correlations with microvascular damage. This means we do not know the behavioural relevance of the microvascular damage observed here. Although it has been repeatedly reported that even subtle forms of vascular damage, especially cerebral microbleeds, are highly correlated with cognitive deficits and that previous publications from our lab indicate that our ACHI model is associated with spatial learning and memory deficits, we still need to provide an accurate correlation with microvascular damage. However, in conjunction with increasing the sample size in this study, we are also currently working on evaluating the behavioural relevance of microbleeds in our model of rmTBI.

Another limitation is that due to our small sample size a direct statistical comparison between males and females was not performed. Therefore, the sex-differences reported in this study are achieved by isolated comparison between experimental groups within the same sex. (i.e. we compared sham males with rmTBI males, and separately sham females with rmTBI females). In addition, neither testosterone nor estrous cycles were monitored in this study, a fact that could explain some of the variability in animals of the same sex in the same experimental group.

Finally, although we have some preliminary data regarding structural alterations associated with the microvascular damage described in this study in the form of axonal alterations, a more systematic and at scale evaluation of structural alterations such as axonal damage, demyelination, neurodegeneration or death of other cell types in the brain like oligodendrocytes and precursor cells should be performed.

5.3. Future steps

As mentioned earlier, one of the main tasks pending for this study is increasing the sample size in order to be able to formulate robust conclusions more confidently this is currently ongoing.

It would also be interesting to use a method that would allow to identify the specific contribution of each impact on microvascular damage. For this, fixable dextrans conjugated with different fluorophores and different molecular sizes could be used. We would inject these fixable dextran solutions prior to each impact and then analyze the combination or absence of specific fluorophores to get an estimate of when microbleeds occurred and how long the increase in vascular permeability lasts for.

This study would also benefit from experiments correlating microvascular damage with more complex behavioral task evaluating common cognitive deficits observed in the human mTBI population such as memory alterations, emotional changes and disturbances in circadian rhythms.

We consider that a critical future experiment should evaluate the structural damage especially axonal injury and demyelination in the vicinity of microbleeds. This is relevant because diffuse vascular injury is commonly accompanied by diffuse axonal injury but to date it is still unclear if axonal shearing leads to microvascular damage, or if it is microbleeds that leads to axonal damage in these perilesional regions. It would also be very interesting to incorporate *in vivo* imaging techniques such as DTI and susceptibility-

weighted MRI scans to make correlation with post-mortem histology and provide a higher translational component to this study.

Finally, related to this translational component, if further investigations with the ACHI keep providing evidence that fibrinogen plays and important role in mTBI pathophysiology, a therapeutic approach based on the monoclonal antibody designed by Dr. Akassoglou research group should be tested. This therapeutic approach specifically prevents the interaction of microglial receptor CR3 with the cryptic fibrin domain, thus blocking the role of fibrinogen on neuroinflammation without altering its hemostatic function.

5.4. Conclusions

In this study, we observed that that the ACHI model of rmTBI is associated with acute increased microvascular damage in juvenile male and female rats in the form of increased hemosiderin deposits and extravasation of blood contents including fibrinogen and RBCs. We hope that this study provides a good starting point for future research evaluating the role of microvascular damage in the ACHI model of mTBI and contributes to the generation of diagnostic, prognostic and therapeutic tools with the final goal of improving the life quality of patients affected by this type of brain injury.

BIBLIOGRAPHY

Adams JH, Graham DI, Murray LS, Scott G (1982) Diffuse axonal injury due to nonmissile head injury in humans: An analysis of 45 cases. Ann Neurol 12:557–563.

Agrawal A, Timothy J, Pandit L, Manju M (2006) Post-traumatic epilepsy: An overview. Clin Neurol Neurosurg 108:433–439 Available at: https://pubmed.ncbi.nlm.nih.gov/16225987/ [Accessed April 6, 2021].

Ahn SJ, Anrather J, Nishimura N, Schaffer CB (2018) Diverse Inflammatory Response after Cerebral Microbleeds Includes Coordinated Microglial Migration and Proliferation. Stroke.

Aoki Y, Inokuchi R, Gunshin M, Yahagi N, Suwa H (2012) Diffusion tensor imaging studies of mild traumatic brain injury: A meta-analysis. J Neurol Neurosurg Psychiatry 83:870–876 Available at: http://jnnp.bmj.com/ [Accessed April 25, 2021].

Arbogast KB, Thibault KL, Pinheiro BS, Winey KI, Margulies SS (1997) A high-frequency shear device for testing soft biological tissues. J Biomech 30:757–759.

Atkin G, Moore S, Lu Y, Nelson RF, Tipper N, Rajpal G, Hunt J, Tennant W, Hell JW, Murphy GG, Paulson H (2015) Loss of F-box Only Protein 2 (Fbxo2) Disrupts Levels and Localization of Select NMDA Receptor Subunits, and Promotes Aberrant Synaptic Connectivity. J Neurosci 35:6165–6178 Available at: http://www.jneurosci.org/cgi/doi/10.1523/JNEUROSCI.3013-14.2015.

Attwell D, Laughlin SB (2001) An energy budget for signaling in the grey matter of the brain. J Cereb Blood Flow Metab 21:1133–1145 Available at: http://journals.sagepub.com/doi/10.1097/00004647-200110000-00001 [Accessed April 6, 2021].

Batista G, Johnson JL, Dominguez E, Costa-Mattioli M, Pena JL (2016) Translational control of auditory imprinting and structural plasticity by eIF2α. Elife 5.

Bazarian JJ, Blyth B, Mookerjee S, He H, McDermott MP (2010) Sex Differences in Outcome after Mild Traumatic Brain Injury. J Neurotrauma.

Bazarian JJ, McClung J, Shah MN, Cheng YT, Flesher W, Kraus J (2005) Mild traumatic brain injury in the United States, 1998-2000. Brain Inj 19:85–91 Available at: https://pubmed.ncbi.nlm.nih.gov/15841752/ [Accessed April 6, 2021].

Belanger HG, Vanderploeg RD, Curtiss G, Warden DL (2007) Recent neuroimaging techniques in mild traumatic brain injury. J Neuropsychiatry Clin Neurosci 19:5–20.

Benarroch EE (2011) Circumventricular organs. Neurology 77:1198–1204 Available at: https://pubmed.ncbi.nlm.nih.gov/21931109/ [Accessed April 8, 2021].

Bennett ML, Bennett FC, Liddelow SA, Ajami B, Zamanian JL, Fernhoff NB, Mulinyawe SB, Bohlen CJ, Adil A, Tucker A, Weissman IL, Chang EF, Li G, Grant GA, Hayden Gephart MG, Barres BA, Giger RJ, Stevens B (2016) New tools for studying microglia in the mouse and human CNS. Proc Natl Acad Sci.

Bigler ED (2018) Structural neuroimaging in sport-related concussion. Int J Psychophysiol 132:105–123 Available at: https://doi.org/10.1016/j.ijpsycho.2017.09.006.

Bigler ED, Anderson C V, Blatter DD, Andersob C V (2002) Temporal lobe morphology in normal aging and traumatic brain injury. AJNR Am J Neuroradiol 23:255–266.

Bijur PE, Haslum M, Golding J (1996) Cognitive outcomes of multiple mild head injuries in children. J Dev Behav Pediatr 17:143–148 Available at: https://pubmed.ncbi.nlm.nih.gov/8783059/ [Accessed April 6, 2021].

Blennow K, Brody DL, Kochanek PM, Levin H, McKee A, Ribbers GM, Yaffe K, Zetterberg H (2016) Traumatic brain injuries. Nat Rev Dis Prim 2 Available at: https://pubmed.ncbi.nlm.nih.gov/27853132/ [Accessed April 6, 2021].

Blennow K, Fredman P, Wallin A, Gottfries C-G, Karlsson I, Långstrom G, Skoog I, Svennerholm L, Wikkelsö C (1993) Protein Analysis in Cerebrospinal Fluid. Eur Neurol 33:129–133 Available at: https://www.karger.com/Article/FullText/116919

[Accessed April 9, 2021].

Blennow K, Hardy J, Zetterberg H (2012a) The Neuropathology and Neurobiology of Traumatic Brain Injury. Neuron 76:886–899 Available at: http://dx.doi.org/10.1016/j.neuron.2012.11.021.

Blennow K, Hardy J, Zetterberg H (2012b) The Neuropathology and Neurobiology of Traumatic Brain Injury. Neuron 76:886–899.

Block ML, Zecca L, Hong JS (2007) Microglia-mediated neurotoxicity: Uncovering the molecular mechanisms. Nat Rev Neurosci.

Bodnar CN, Roberts KN, Higgins EK, Bachstetter AD (2019) A Systematic Review of Closed Head Injury Models of Mild Traumatic Brain Injury in Mice and Rats. J Neurotrauma 36:1683–1706 Available at: https://www.liebertpub.com/doi/abs/10.1089/neu.2018.6127 [Accessed April 6, 2021].

Borowsky IW, Collins RC (1989) Metabolic anatomy of brain: A comparison of regional capillary density, glucose metabolism, and enzyme activities. J Comp Neurol 288:401–413 Available at: https://pubmed.ncbi.nlm.nih.gov/2551935/ [Accessed April 7, 2021].

Burkhalter A, Bernardo KL (1989) Organization of corticocortical connections in human visual cortex. Proc Natl Acad Sci 86:1071–1075 Available at: http://www.pnas.org/cgi/doi/10.1073/pnas.86.3.1071.

Carmody DP, Dunn SM, Boddie-Willis AS, DeMarco JK, Lewis M (2004) A quantitative measure of myelination development in infants, using MR images. Neuroradiology.

Carroll LJ, Cassidy JD, Peloso PM, Borg J, Von Holst H, Holm L, Paniak C, Pépin M (2004) Prognosis for mild traumatic brain injury: Results of the WHO Collaborating Centre Task Force on mild traumatic brain injury. J Rehabil Med.

Castile L, Collins CL, McIlvain NM, Comstock RD (2012) The epidemiology of new

versus recurrent sports concussions among high school athletes, 2005-2010. Br J Sports Med.

Cavaglia M, Dombrowski SM, Drazba J, Vasanji A, Bokesch PM, Janigro D (2001) Regional variation in brain capillary density and vascular response to ischemia. Brain Res 910:81–93 Available at: https://pubmed.ncbi.nlm.nih.gov/11489257/ [Accessed April 7, 2021].

Cernak I, Savic J, Malicevic Z, Zunic G, Radosevic P, Ivanovic I, Davidovic L (1996) Involvement of the Central Nervous System in the General Response to Pulmonary Blast Injury. J Trauma Inj Infect Crit Care 40:100S-104S.

Charidimou A, Shakeshaft C, Werring DJ (2012) Cerebral microbleeds on magnetic resonance imaging and anticoagulant-associated intracerebral hemorrhage risk. Front Neurol SEP Available at: https://pubmed.ncbi.nlm.nih.gov/23015806/ [Accessed April 9, 2021].

Chen Y, Swanson RA (2003) Astrocytes and brain injury. J Cereb Blood Flow Metab 23:137–149 Available at: http://journals.sagepub.com/doi/10.1097/01.WCB.0000044631.80210.3C [Accessed April 8, 2021].

Cheng C, Trzcinski O, Doering LC (2014) Fluorescent labeling of dendritic spines in cell cultures with the carbocyanine dye â€œDiIâ€ Front Neuroanat 8 Available at: http://journal.frontiersin.org/article/10.3389/fnana.2014.00030/abstract.

Cheng WH, Martens KM, Bashir A, Cheung H, Stukas S, Gibbs E, Namjoshi DR, Button EB, Wilkinson A, Barron CJ, Cashman NR, Cripton PA, Wellington CL (2019) CHIMERA repetitive mild traumatic brain injury induces chronic behavioural and neuropathological phenotypes in wild-type and APP/PS1 mice. Alzheimer's Res Ther 11:1–21 Available at: /pmc/articles/PMC6330571/ [Accessed April 6, 2021].

Chu SF, Chiu WT, Lin HW, Chiang YH, Liou TH (2016) Hazard Ratio and Repeat Injury

for Dementia in Patients with and Without a History of Traumatic Brain Injury. Asia-Pacific J Public Heal 28:519–527 Available at: https://pubmed.ncbi.nlm.nih.gov/27614252/ [Accessed April 6, 2021].

Cianchetti FA, Kim DH, Dimiduk S, Nishimura N, Schaffer CB (2013) Stimulus-Evoked Calcium Transients in Somatosensory Cortex Are Temporarily Inhibited by a Nearby Microhemorrhage. PLoS One 8 Available at: https://pubmed.ncbi.nlm.nih.gov/23724147/ [Accessed April 9, 2021].

Cicerone KD, Kalmar K (1995) Persistent postconcussion syndrome: The structure of subjective complaints after mild traumatic brain injury. J Head Trauma Rehabil.

CIHI (2006) Head Injuries in Canada: A Decade of Change (1994-1995 to 2003-2004).

Cipolla MJ (2009) Anatomy and Ultrastructure. Available at: https://www.ncbi.nlm.nih.gov/books/NBK53086/ [Accessed June 16, 2021].

Cloots RJH, Van Dommelen JAW, Kleiven S, Geers MGD (2013) Multi-scale mechanics of traumatic brain injury: Predicting axonal strains from head loads. Biomech Model Mechanobiol 12:137–150 Available at: https://pubmed.ncbi.nlm.nih.gov/22434184/ [Accessed April 6, 2021].

Cole W, Bailie J (2015) Neurocognitive and Psychiatric Symptoms following Mild Traumatic Brain Injury.

Daneman R, Prat A (2015) The blood–brain barrier. Cold Spring Harb Perspect Biol 7 Available at: /pmc/articles/PMC4292164/ [Accessed April 8, 2021].

Davalos D, Grutzendler J, Yang G, Kim J V., Zuo Y, Jung S, Littman DR, Dustin ML, Gan WB (2005a) ATP mediates rapid microglial response to local brain injury in vivo. Nat Neurosci.

Davalos D, Grutzendler J, Yang G, Kim J V., Zuo Y, Jung S, Littman DR, Dustin ML, Gan WB (2005b) ATP mediates rapid microglial response to local brain injury in vivo. Nat Neurosci 8:752–758 Available at: https://pubmed.ncbi.nlm.nih.gov/15895084/

[Accessed April 8, 2021].

Davalos D, Kyu Ryu J, Merlini M, Baeten KM, Le Moan N, Petersen MA, Deerinck TJ, Smirnoff DS, Bedard C, Hakozaki H, Gonias Murray S, Ling JB, Lassmann H, Degen JL, Ellisman MH, Akassoglou K (2012) Fibrinogen-induced perivascular microglial clustering is required for the development of axonal damage in neuroinflammation. Nat Commun.

Davis BM, Salinas-Navarro M, Cordeiro MF, Moons L, Groef L De (2017) Characterizing microglia activation: A spatial statistics approach to maximize information extraction. Sci Rep 7:1–12 Available at: www.nature.com/scientificreports/ [Accessed April 8, 2021].

Devonshire IM, Papadakis NG, Port M, Berwick J, Kennerley AJ, Mayhew JEW, Overton PG (2012) Neurovascular coupling is brain region-dependent. Neuroimage 59:1997–2006.

Dichgans M (2002) Cerebral autosomal dominant arteriopathy with subcortical infarcts and leukoencephalopathy: Phenotypic and mutational spectrum. In: Journal of the Neurological Sciences, pp 77–80. J Neurol Sci. Available at: https://pubmed.ncbi.nlm.nih.gov/12417361/ [Accessed April 9, 2021].

Dixon CE, Clifton GL, Lighthall JW, Yaghmai AA, Hayes RL (1991) A controlled cortical impact model of traumatic brain injury in the rat. J Neurosci Methods 39:253–262.

Dixon CE, Lyeth BG, Povlishock JT, Findling RL, Hamm RJ, Marmarou A, Young HF, Hayes RL (1987) A fluid percussion model of experimental brain injury in the rat. J Neurosurg 67:110–119.

Donnelly B, Medige J (1997) Shear Properties of Human Brain Tissue. J Biomech Eng 119:423.

Duvernoy HM, Risold PY (2007) The circumventricular organs: An atlas of comparative anatomy and vascularization. Brain Res Rev 56:119–147.

Echemendia RJ et al. (2017) The Sport Concussion Assessment Tool 5th Edition (SCAT5). Br J Sports Med.

Eierud C, Craddock RC, Fletcher S, Aulakh M, King-Casas B, Kuehl D, Laconte SM (2014) Neuroimaging after mild traumatic brain injury: Review and meta-analysis. NeuroImage Clin.

Einarsen CE, Moen KG, Håberg AK, Eikenes L, Kvistad KA, Xu J, Moe HK, Tollefsen MH, Vik A, Skandsen T (2019) Patients with Mild Traumatic Brain Injury Recruited from Both Hospital and Primary Care Settings: A Controlled Longitudinal Magnetic Resonance Imaging Study. J Neurotrauma 36:3172–3182 Available at: https://pubmed.ncbi.nlm.nih.gov/31280698/ [Accessed April 8, 2021].

Esposito P, Gheorghe D, Kandere K, Pang X, Connolly R, Jacobson S, Theoharides TC (2001) Acute stress increases permeability of the blood-brain-barrier through activation of brain mast cells. Brain Res 888:117–127.

Ewing-Cobbs L, Barnes M, Fletcher JM, Levin HS, Swank PR, Song J (2004) Modeling of Longitudinal Academic Achievement Scores After Pediatric Traumatic Brain Injury. Dev Neuropsychol 25:107–133 Available at: https://pubmed.ncbi.nlm.nih.gov/14984331/ [Accessed April 6, 2021].

Faul M., Xu L., Wald MM, Coronado VG (2010) Traumatic brain injury in the United States: emergency department visits, hospitalizations and deaths 2002–2006.

Fazekas F, Kleinert R, Roob G, Kleinert G, Kapeller P, Schmidt R, Hartung HP (1999) Histopathologic analysis of foci of signal loss on gradient-echo T2*- weighted MR images in patients with spontaneous intracerebral hemorrhage: Evidence of microangiopathy-related microbleeds. Am J Neuroradiol 20:637–642 Available at: https://pubmed.ncbi.nlm.nih.gov/10319975/ [Accessed April 9, 2021].

Feeney DM, Boyeson MG, Linn RT, Murray HM, Dail WG (1981) Responses to cortical injury: I. Methodology and local effects of contusions in the rat. Brain Res 211:67–77.

Fehily B, Fitzgerald M (2017) Repeated mild traumatic brain injury: Potential mechanisms of damage. Cell Transplant.

Fineman I, Hovda DA, Smith M, Yoshino A, Becker DP (1993) Concussive brain injury is associated with a prolonged accumulation of calcium: a 45Ca autoradiographic study. Brain Res 624:94–102.

Foda MA, Marmarou A (1994) A new model of diffuse brain injury in rats. Part II: Morphological characterization. J Neurosurg 80:301–313.

Fu TS, Jing R, McFaull SR, Cusimano MD (2015) Health & Economic Burden of Traumatic Brain Injury in the Emergency Department. Can J Neurol Sci 43:238–247.

Gadani SP, Walsh JT, Lukens JR, Kipnis J (2015) Dealing with Danger in the CNS: The Response of the Immune System to Injury. Neuron.

Galea OA, Cottrell MA, Treleaven JM, O'Leary SP (2018) Sensorimotor and Physiological Indicators of Impairment in Mild Traumatic Brain Injury: A Meta-Analysis. Neurorehabil Neural Repair 32:115–128 Available at: http://journals.sagepub.com/doi/10.1177/1545968318760728 [Accessed April 25, 2021].

Ganong WF (2000) Circumventricular Organs: Definition And Role In The Regulation Of Endocrine And Autonomic Function. Clin Exp Pharmacol Physiol 27:422–427 Available at: http://doi.wiley.com/10.1046/j.1440-1681.2000.03259.x [Accessed April 8, 2021].

Gao X, Chen J (2011) Mild traumatic brain injury results in extensive neuronal degeneration in the cerebral cortex. J Neuropathol Exp Neurol 70:183–191.

Gao Z, Wang W, Wang Z, Zhao X, Shang Y, Guo Y, Gong M, Yang L, Shi X, Xu X, An N, Wu W (2014) Cerebral microbleeds are associated with deep white matter hyperintensities, but only in hypertensive patients. PLoS One 9 Available at: https://pubmed.ncbi.nlm.nih.gov/24626222/ [Accessed April 8, 2021].

Gennarelli TA (1994) Animate models of human head injury. J Neurotrauma 11:357–368.

Gennarelli TA, Thibault LE, Adams JH, Graham DI, Thompson CJ, Marcincin RP (1982) Diffuse axonal injury and traumatic coma in the primate. Ann Neurol 12:564–574.

Gerrard-Morris A, Taylor HG, Yeates KO, Walz NC, Stancin T, Minich N, Wade SL (2010) Cognitive development after traumatic brain injury in young children. J Int Neuropsychol Soc 16:157–168 Available at: https://pubmed.ncbi.nlm.nih.gov/19849883/ [Accessed April 6, 2021].

Glushakova OY, Johnson D, Hayes RL (2014) Delayed increases in microvascular pathology after experimental traumatic brain injury are associated with prolonged inflammation, blood-brain barrier disruption, and progressive white matter damage. J Neurotrauma 31:1180–1193 Available at: https://pubmed.ncbi.nlm.nih.gov/24564198/ [Accessed April 11, 2021].

Godement P, Vanselow J, Thanos S, Bonhoeffer F (1987) A study in developing visual systems with a new method of staining neurones and their processes in fixed tissue. Development 101:697–713.

Greco T, Ferguson L, Giza C, Prins ML (2019) Mechanisms underlying vulnerabilities after repeat mild traumatic brain injuries. Exp Neurol Available at: https://www.sciencedirect.com/science/article/pii/S0014488619300123?via%3Dihub.

Griffin AD, Turtzo LC, Parikh GY, Tolpygo A, Lodato Z, Moses AD, Nair G, Perl DP, Edwards NA, Dardzinski BJ, Armstrong RC, Ray-Chaudhury A, Mitra PP, Latour LL (2019) Traumatic microbleeds suggest vascular injury and predict disability in traumatic brain injury. Brain 142:3550–3564 Available at: https://academic.oup.com/brain/article/142/11/3550/5581280 [Accessed April 25, 2021].

Guskiewicz KM, Marshall SW, Bailes J, McCrea M, Cantu RC, Randolph C, Jordan BD

(2005) Association between recurrent concussion and late-life cognitive impairment in retired professional football players. Neurosurgery 57 Available at: https://pubmed.ncbi.nlm.nih.gov/16239884/ [Accessed April 6, 2021].

Guskiewicz KM, McCrea M, Marshall SW, Cantu RC, Randolph C, Barr W, Onate JA, Kelly JP (2003) Cumulative Effects Associated with Recurrent Concussion in Collegiate Football Players: The NCAA Concussion Study. J Am Med Assoc.

Guskiewicz KM, Ross SE, Marshall SW (2001) Postural Stability and Neuropsychological Deficits after Concussion in Collegiate Athletes. J Athl Train 36:263–273 Available at: www.journalofathletictraining.org [Accessed April 25, 2021].

Hall RCW, Hall RCW, Chapman MJ (2005) Definition, diagnosis, and forensic implications of postconcussional syndrome. Psychosomatics 46:195–202 Available at: https://pubmed.ncbi.nlm.nih.gov/15883140/ [Accessed April 6, 2021].

Hanske S, Dyrna F, Bechmann I, Krueger M (2017) Different segments of the cerebral vasculature reveal specific endothelial specifications, while tight junction proteins appear equally distributed. Brain Struct Funct 222:1179–1192 Available at: https://pubmed.ncbi.nlm.nih.gov/27435201/ [Accessed April 7, 2021].

Harris W a, Holt CE, Bonhoeffer F (1987) Retinal axons with and without their somata, growing to and arborizing in the tectum of Xenopus embryos: a time-lapse video study of single fibres in vivo. Development 101:123–133.

Hart T, Brenner L, Clark AN, Bogner JA, Novack TA, Chervoneva I, Nakase-Richardson R, Arango-Lasprilla JC (2011) Major and minor depression after traumatic brain injury. Arch Phys Med Rehabil 92:1211–1219 Available at: https://pubmed.ncbi.nlm.nih.gov/21807140/ [Accessed April 6, 2021].

Hartmann DA, Hyacinth HI, Liao FF, Shih AY (2018) Does pathology of small venules contribute to cerebral microinfarcts and dementia? J Neurochem 144:517–526 Available at: /pmc/articles/PMC5869083/ [Accessed April 7, 2021].

Hay JR, Johnson VE, Young AMH, Smith DH, Stewart W (2015) Blood-brain barrier disruption is an early event that may persist for many years after traumatic brain injury in humans. J Neuropathol Exp Neurol.

Haynes RL, Borenstein NS, Desilva TH, Folkerth RD, Liu LG, Volpe JJ, Kinney HC (2005) Axonal development in the cerebral white matter of the human fetus and infant. J Comp Neurol.

Heindl S, Gesierich B, Benakis C, Llovera G, Duering M, Liesz A (2018) Automated Morphological Analysis of Microglia After Stroke. Front Cell Neurosci 12.

Heinzer S, Kuhn G, Krucker T, Meyer E, Ulmann-Schuler A, Stampanoni M, Gassmann M, Marti HH, Müller R, Vogel J (2008) Novel three-dimensional analysis tool for vascular trees indicates complete micro-networks, not single capillaries, as the angiogenic endpoint in mice overexpressing human VEGF165 in the brain. Neuroimage 39:1549–1558 Available at: https://pubmed.ncbi.nlm.nih.gov/18077185/ [Accessed April 7, 2021].

Hendryx PM, Verduyn WH (1995) Diagnosis and treatment strategies for the latent sequelae of head trauma in children. J Cogn Rehabil 13:8-12 5p Available at: https://psycnet.apa.org/record/1996-18123-001 [Accessed April 6, 2021].

Homnick A, Sifri Z, Yonclas P, Mohr A, Livingston D (2012) The temporal course of intracranial haemorrhage progression: How long is observation necessary? Injury 43:2122–2125 Available at: https://pubmed.ncbi.nlm.nih.gov/22658418/ [Accessed April 8, 2021].

Honig MG, Hume RI (1986) Fluorescent carbocyanine dyes allow living neurons of identified origin to be studied in long-term cultures. J Cell Biol 103:171–187.

Honig MG, Hume RI (1989) Dil and DiO: versatile fluorescent dyes for neuronal labelling and pathway tracing. Trends Neurosci 12:333–341.

Hossmann KA (2006) Pathophysiology and therapy of experimental stroke. Cell Mol

Neurobiol 26:1057–1083 Available at: https://pubmed.ncbi.nlm.nih.gov/16710759/ [Accessed April 6, 2021].

Hsu HL, Chen DYT, Tseng YC, Kuo YS, Huang YL, Chiu WT, Yan FX, Wang WS, Chen CJ (2015) Sex differences in working memory after mild traumatic brain injury: A functional MR imaging study. Radiology 276:828–835 Available at: https://pubmed.ncbi.nlm.nih.gov/25919663/ [Accessed April 6, 2021].

Huw Williams W, Cordan G, Mewse AJ, Tonks J, Burgess CNW (2010) Self-reported traumatic brain injury in male young offenders: A risk factor for re-offending, poor mental health and violence? Neuropsychol Rehabil 20:801–812 Available at: https://pubmed.ncbi.nlm.nih.gov/21069616/ [Accessed April 6, 2021].

Iadecola C (2017) The Neurovascular Unit Coming of Age: A Journey through Neurovascular Coupling in Health and Disease. Neuron 96:17–42 Available at: https://pubmed.ncbi.nlm.nih.gov/28957666/ [Accessed April 7, 2021].

Irimia A, Van Horn JD, Vespa PM (2018) Cerebral microhemorrhages due to traumatic brain injury and their effects on the aging human brain. Neurobiol Aging 66:158–164 Available at: /pmc/articles/PMC5924627/ [Accessed April 9, 2021].

Ivancevic VG (2009) New mechanics of traumatic brain injury. Cogn Neurodyn 3:281–293 Available at: /pmc/articles/PMC2727160/ [Accessed April 6, 2021].

Iverson GL (2010) Clinical and methodological challenges with assessing mild traumatic brain injury in the military. J Head Trauma Rehabil 25:313–319 Available at: http://www.ncbi.nlm.nih.gov/pubmed/20220528.

Jacobson K, Derzko Z, Wojcieszyn J, Hon Y, Organisciak D (1981) Lipid Lateral Diffusion in the Surface Membrane of Cells and in Multibilayers Formed from Plasma Membrane Lipids. Biochemistry 20:5268–5275.

Jeter CB, Hergenroeder GW, Hylin MJ, Redell JB, Moore AN, Dash PK (2013) Biomarkers for the Diagnosis and Prognosis of Mild Traumatic Brain Injury/Concussion. J

Neurotrauma.

Jiang M, Sun L, Feng D-X, Yu Z-Q, Gao R, Sun Y-Z, Chen G (2017) Neuroprotection provided by isoflurane pre-conditioning and post-conditioning. Med Gas Res 7:48–55.

Johnson VE, Stewart W, Smith DH (2010) Traumatic brain injury and amyloid-β pathology: A link to alzheimer's disease? Nat Rev Neurosci.

Jones LL, Lu J, Schachtrup C, Lee JK, Akassoglou K, Sachs BD, Zheng B, Lu P (2007) Fibrinogen inhibits neurite outgrowth via beta3 integrin-mediated phosphorylation of the EGF receptor. Proc Natl Acad Sci.

Jorge RE, Robinson RG, Moser D, Tateno A, Crespo-Facorro B, Arndt S (2004) Major Depression Following Traumatic Brain Injury. Arch Gen Psychiatry 61:42–50 Available at: https://jamanetwork.com/journals/jamapsychiatry/fullarticle/481944 [Accessed April 6, 2021].

Kandel E., Schwartz J., Jessel TM (2013) Principles of Neural Science, Fifth Edition | AccessNeurology | McGraw-Hill Medical. Available at: https://neurology.mhmedical.com/book.aspx?bookID=1049 [Accessed April 7, 2021].

Karbowski J (2007) Global and regional brain metabolic scaling and its functional consequences. BMC Biol 5:18 Available at: https://bmcbiol.biomedcentral.com/articles/10.1186/1741-7007-5-18 [Accessed April 7, 2021].

Karbowski J (2011) Scaling of brain metabolism and blood flow in relation to capillary and neural scaling. PLoS One 6:26709 Available at: www.plosone.org [Accessed April 7, 2021].

Karperien A, Ahammer H, Jelinek HF (2013) Quantitating the subtleties of microglial

morphology with fractal analysis. Front Cell Neurosci 7:1–34 Available at: www.frontiersin.org [Accessed April 8, 2021].

Kattula S, Byrnes JR, Wolberg AS (2017) Fibrinogen and Fibrin in Hemostasis and Thrombosis. Arterioscler Thromb Vasc Biol 37:13–21.

Kim BG, Dai H-N, McAtee M, Bregman BS (2008) Modulation of dendritic spine remodeling in the motor cortex following spinal cord injury: effects of environmental enrichment and combinatorial treatment with transplants and neurotrophin-3. J Comp Neurol 508:473–486.

Kirst C, Skriabine S, Vieites-Prado A, Topilko T, Bertin P, Gerschenfeld G, Verny F, Topilko P, Michalski N, Tessier-Lavigne M, Renier N (2020) Mapping the Fine-Scale Organization and Plasticity of the Brain Vasculature. Cell 180:780-795.e25.

Kleiber M (1947) Body size and metabolic rate. Physiol Rev 27:511–541 Available at: https://journals.physiology.org/doi/abs/10.1152/physrev.1947.27.4.511 [Accessed April 7, 2021].

Koizumi H (2004) The concept of "developing the brain": A new natural science for learning and education. In: Brain and Development.

Konno A, Matsumoto N, Okazaki S (2017) Improved vessel painting with carbocyanine dye-liposome solution for visualisation of vasculature. Sci Rep 7:1–9 Available at: www.nature.com/scientificreports [Accessed April 11, 2021].

Konno A, Matsumoto N, Tomono Y, Okazaki S (2020) Pathological application of carbocyanine dye-based multicolour imaging of vasculature and associated structures. Sci Rep 10 Available at: https://pubmed.ncbi.nlm.nih.gov/32724051/ [Accessed April 11, 2021].

Kotapka MJ, Graham DI, Adams JH, Gennarelli TA (1992) Hippocampal pathology in fatal non-missile human head injury. Acta Neuropathol 83:530–534.

Kurland D, Hong C, Aarabi B, Gerzanich V, Simard JM (2012) Hemorrhagic progression

of a contusion after traumatic brain injury: A review. J Neurotrauma 29:19–31 Available at: https://pubmed.ncbi.nlm.nih.gov/21988198/ [Accessed April 11, 2021].

Lamy M, Baumgartner D, Willinger R, Yoganandan N, Stemper BD (2011) Study of mild traumatic brain injuries using experiments and finite element modeling. In: Annals of Advances in Automotive Medicine, pp 125–135 Available at: https://pubmed.ncbi.nlm.nih.gov/22105390/ [Accessed April 6, 2021].

Lee YK, Hou SW, Lee CC, Hsu CY, Huang YS, Su YC (2013) Increased Risk of Dementia in Patients with Mild Traumatic Brain Injury: A Nationwide Cohort Study. PLoS One.

Lehmann ML, Poffenberger CN, Elkahloun AG, Herkenham M (2020) Analysis of cerebrovascular dysfunction caused by chronic social defeat in mice. Brain Behav Immun 88:735–747.

Lehmann ML, Weigel TK, Cooper HA, Elkahloun AG, Kigar SL, Herkenham M (2018) Decoding microglia responses to psychosocial stress reveals blood-brain barrier breakdown that may drive stress susceptibility. Sci Rep 8:11240 Available at: www.nature.com/scientificreports/ [Accessed April 25, 2021].

Leung LY, VandeVord PJ, Dal Cengio AL, Bir C, Yang KH, King AI (2008) Blast related neurotrauma: a review of cellular injury. Mol Cell Biomech 5:155–168.

Li Y, Song Y, Zhao L, Gaidosh G, Laties AM, Wen R (2008) Direct labeling and visualization of blood vessels with lipophilic carbocyanine dye DiI. Nat Protoc 3:1703–1708 Available at: https://www.ncbi.nlm.nih.gov/pmc/articles/pmid/18846097/?tool=EBI [Accessed April 11, 2021].

Liddelow SA et al. (2017) Neurotoxic reactive astrocytes are induced by activated microglia. Nature 541:481–487 Available at:

https://pubmed.ncbi.nlm.nih.gov/28099414/ [Accessed April 8, 2021].

LIGHTHALL JW (1988) Controlled Cortical Impact: A New Experimental Brain Injury Model. J Neurotrauma 5:1–15.

Lin AH, Luo J, Mondshein LH, ten Dijke P, Vivien D, Contag CH, Wyss-Coray T (2005) Global Analysis of Smad2/3-Dependent TGF-β Signaling in Living Mice Reveals Prominent Tissue-Specific Responses to Injury. J Immunol 175:547–554 Available at: http://www.jimmunol.org/content/175/1/547 [Accessed April 25, 2021].

Lindner MD, Plone MA, Cain CK, Frydel B, Francis JM, Emerich DF, Sutton RL (1998) Dissociable long-term cognitive deficits after frontal versus sensorimotor cortical contusions. J Neurotrauma 15:199–216.

Liu S, Grigoryan MM, Vasilevko V, Sumbria RK, Paganini-Hill A, Cribbs DH, Fisher MJ (2014) Comparative Analysis of H&E and Prussian Blue Staining in a Mouse Model of Cerebral Microbleeds. J Histochem Cytochem.

Lo C, Shifteh K, Gold T, Bello JA, Lipton ML (2009) Diffusion tensor imaging abnormalities in patients with mild traumatic brain injury and neurocognitive impairment. J Comput Assist Tomogr 33:293–297 Available at: https://pubmed.ncbi.nlm.nih.gov/19346863/ [Accessed April 25, 2021].

Lou N, Takano T, Pei Y, Xavier AL, Goldman SA, Nedergaard M (2016) Purinergic receptor P2RY12-dependent microglial closure of the injured blood–brain barrier. Proc Natl Acad Sci.

Lowenstein DH, Thomas MJ, Smith DH, McIntosh TK (1992) Selective vulnerability of dentate hilar neurons following traumatic brain injury: A potential mechanistic link between head trauma and disorders of the hippocampus. J Neurosci 12:4846–4853 Available at: https://pubmed.ncbi.nlm.nih.gov/1464770/ [Accessed April 6, 2021].

Mahmmoud RR, Sase S, Aher YD, Sase A, Gröger M, Mokhtar M, Höger H, Lubec G (2015) Spatial and working memory is linked to spine density and mushroom spines.

PLoS One 10.

Marar M, McIlvain NM, Fields SK, Comstock RD (2012) Epidemiology of concussions among united states high school athletes in 20 sports. Am J Sports Med.

Marín-Padilla M (2012) The human brain intracerebral microvascular system: Development and structure. Front Neuroanat 6:1–14 Available at: https://pubmed.ncbi.nlm.nih.gov/22993505/ [Accessed April 7, 2021].

Masel BE, DeWitt DS (2010) Traumatic Brain Injury: A Disease Process, Not an Event. J Neurotrauma.

Mastorakos P, Mihelson N, Luby M, Burks SR, Johnson K, Hsia AW, Witko J, Frank JA, Latour L, McGavern DB (2021) Temporally distinct myeloid cell responses mediate damage and repair after cerebrovascular injury. Nat Neurosci 24:245–258 Available at: https://pubmed.ncbi.nlm.nih.gov/33462481/ [Accessed April 8, 2021].

Matser EJT, Kessels AGH, Jordan BD, Lezak MD, Troost J (1998) Chronic traumatic brain injury in professional soccer players. Neurology 51:791–796 Available at: https://pubmed.ncbi.nlm.nih.gov/9748028/ [Accessed April 6, 2021].

Mayer AR, Quinn DK, Master CL (2017) The spectrum of mild traumatic brain injury. Neurology.

McDonald SJ, Sun M, Agoston D V., Shultz SR (2016) The effect of concomitant peripheral injury on traumatic brain injury pathobiology and outcome. J Neuroinflammation 13:90 Available at: http://jneuroinflammation.biomedcentral.com/articles/10.1186/s12974-016-0555-1 [Accessed April 12, 2021].

McInnes K, Friesen CL, MacKenzie DE, Westwood DA, Boe SG (2017) Mild Traumatic Brain Injury (mTBI) and chronic cognitive impairment: A scoping review. PLoS One 12.

McIntosh TK, Saatman KE, Raghupathi R (1997) Calcium and the pathogenesis of

traumatic CNS injury: Cellular and molecular mechanisms. Neuroscientist 3:169–175.

Mckee AC, Abdolmohammadi B, Stein TD (2018) The neuropathology of chronic traumatic encephalopathy. In: Handbook of Clinical Neurology.

McKee AC, Cantu RC, Nowinski CJ, Hedley-Whyte ET, Gavett BE, Budson AE, Santini VE, Lee HS, Kubilus CA, Stern RA (2009) Chronic traumatic encephalopathy in athletes: Progressive tauopathy after repetitive head injury. J Neuropathol Exp Neurol.

McMahon PJ et al. (2013) Symptomatology and Functional Outcome in Mild Traumatic Brain Injury: Results from the Prospective TRACK-TBI Study. J Neurotrauma.

Meconi A, Wortman RC, Wright DK, Neale KJ, Clarkson M, Shultz SR, Christie BR (2018a) Repeated mild traumatic brain injury can cause acute neurologic impairment without overt structural damage in juvenile rats. PLoS One 13:1–24.

Meconi A, Wortman RC, Wright DK, Neale KJ, Clarkson M, Shultz SR, Christie BR (2018b) Repeated mild traumatic brain injury can cause acute neurologic impairment without overt structural damage in juvenile rats. PLoS One 13 Available at: /pmc/articles/PMC5940222/ [Accessed April 6, 2021].

Menard C et al. (2017) Social stress induces neurovascular pathology promoting depression. Nat Neurosci 20:1752–1760 Available at: https://doi.org/10.1038/s41593-017-0010-3 [Accessed April 25, 2021].

Merlini M, Rafalski VA, Rios Coronado PE, Gill TM, Ellisman M, Muthukumar G, Subramanian KS, Ryu JK, Syme CA, Davalos D, Seeley WW, Mucke L, Nelson RB, Akassoglou K (2019) Fibrinogen Induces Microglia-Mediated Spine Elimination and Cognitive Impairment in an Alzheimer's Disease Model. Neuron.

Merritt VC, Padgett CR, Jak AJ (2019) A systematic review of sex differences in concussion outcome: what do we know? Clin Neuropsychol 0:1–28 Available at:

https://doi.org/10.1080/13854046.2018.1508616.

Miller K, Chinzei K (1997) Constitutive modelling of brain tissue: experiment and theory. J Biomech 30:1115–1121.

Mychasiuk R, Farran A, Angoa-Perez M, Briggs D, Kuhn D, Esser MJ (2014) A novel model of mild traumatic brain injury for juvenile rats. J Vis Exp:51820 Available at: /pmc/articles/PMC4396946/ [Accessed April 6, 2021].

Nahirney PC, Reeson P, Brown CE (2013) Ultrastructural analysis of neurons, glia and capillaries in the peri-infarct zone of an ischemic stroke. Faseb J 27.

Nahirney PC, Reeson P, Brown CE (2016) Ultrastructural analysis of blood-brain barrier breakdown in the peri-infarct zone in young adult and aged mice. J Cereb Blood Flow Metab 36:413–425 Available at: http://journals.sagepub.com/doi/10.1177/0271678X15608396 [Accessed April 7, 2021].

Nahirney PC, Tremblay ME (2021) Brain Ultrastructure: Putting the Pieces Together. Front Cell Dev Biol 9:187 Available at: www.frontiersin.org [Accessed April 8, 2021].

Namjoshi DR, Cheng WH an., McInnes KA, Martens KM, Carr M, Wilkinson A, Fan J, Robert J, Hayat A, Cripton PA, Wellington CL (2014) Merging pathology with biomechanics using CHIMERA (Closed-Head Impact Model of Engineered Rotational Acceleration): a novel, surgery-free model of traumatic brain injury. Mol Neurodegener 9:55 Available at: http://molecularneurodegeneration.biomedcentral.com/articles/10.1186/1750-1326-9-55 [Accessed April 6, 2021].

NCIPC (2003) Report to Congress on Mild Traumatic Brain Injury in the United States: Steps to Prevent a Serious Public Health Problem. Centers Dis Control Prev Natl Cent Inj Prev Control.

Ni J, Auriel E, Martinez-Ramirez S, Keil B, Reed AK, Fotiadis P, Gurol EM, Greenberg

SM, Viswanathan A (2014) Cortical localization of microbleeds in cerebral amyloid angiopathy: An ultra high-field 7T MRI study. J Alzheimer's Dis 43:1325–1330 Available at: /pmc/articles/PMC4386585/ [Accessed April 9, 2021].

Nishimura N, Schaffer CB (2013) Big effects from tiny vessels imaging the impact of microvascular clots and hemorrhages on the brain. In: Stroke. Lippincott Williams & WilkinsHagerstown, MD. Available at: http://stroke.ahajournals.org [Accessed April 8, 2021].

Norden DM, Muccigrosso MM, Godbout JP (2015) Microglial priming and enhanced reactivity to secondary insult in aging, and traumatic CNS injury, and neurodegenerative disease. Neuropharmacology 96:29–41 Available at: https://pubmed.ncbi.nlm.nih.gov/25445485/ [Accessed April 8, 2021].

Noumbissi ME, Galasso B, Stins MF (2018) Brain vascular heterogeneity: Implications for disease pathogenesis and design of in vitro blood-brain barrier models. Fluids Barriers CNS 15 Available at: https://pubmed.ncbi.nlm.nih.gov/29688865/ [Accessed April 7, 2021].

O'Brown NM, Pfau SJ, Gu C (2018) Bridging barriers: A comparative look at the blood-brain barrier across organisms. Genes Dev 32:466–478 Available at: https://pubmed.ncbi.nlm.nih.gov/29692355/ [Accessed April 7, 2021].

O'Leary DDM, Terashima T (1988) Cortical axons branch to multiple subcortical targets by interstitial axon budding: Implications for target recognition and "waiting periods." Neuron 1:901–910.

O'Neil M, Carlson K, Storzbach D, Brenner L, Freeman M, Quinones A, Motu'apuaka M, Ensley M, Kansagara D (2013) Complications of Mild Traumatic Brain Injury in Veterans and Military Personnel: A Systematic Review. Dep Veterans Aff.

Pakulski C, Drobnik L, Millo B (2000) Age and sex as factors modifying the function of the blood-cerebrospinal fluid barrier. Med Sci Monit 6:314–318 Available at:

https://pubmed.ncbi.nlm.nih.gov/11208329/ [Accessed April 9, 2021].

Parry N (2017) Prussian Blue- A Histology Stain For Iron. BitesizeBio.

Patel B, Lawrence AJ, Chung AW, Rich P, MacKinnon AD, Morris RG, Barrick TR, Markus HS (2013) Cerebral microbleeds and cognition in patients with symptomatic small vessel disease. Stroke 44:356–361 Available at: https://pubmed.ncbi.nlm.nih.gov/23321452/ [Accessed April 11, 2021].

Paul J, Strickland S, Melchor JP (2007) Fibrin deposition accelerates neurovascular damage and neuroinflammation in mouse models of Alzheimer's disease. J Exp Med.

Pekna M, Pekny M (2012) The neurobiology of brain injury. Cerebrum 2012:9 Available at: http://www.ncbi.nlm.nih.gov/pubmed/24569830.

Petchprapai N, Winkelman C (2007) Mild traumatic brain injury: determinants and subsequent quality of life. A review of the literature. J Neurosci Nurs 39:260–272 Available at: http://ezproxy.library.dal.ca/login?url=http://search.ebscohost.com/login.aspx?direct=true&db=c8h&AN=2009679738&site=ehost-live.

Petersen MA et al. (2017) Fibrinogen Activates BMP Signaling in Oligodendrocyte Progenitor Cells and Inhibits Remyelination after Vascular Damage. Neuron.

Petersen MA, Ryu JK, Akassoglou K (2018) Fibrinogen in neurological diseases: Mechanisms, imaging and therapeutics. Nat Rev Neurosci.

Petraglia AL, Dashnaw ML, Turner RC, Bailes JE (2014a) Models of mild traumatic brain injury: Translation of physiological and anatomic injury. Neurosurgery 75:S34–S49.

Petraglia AL, Huang JH (2013) Model for traumatic brain injury. Patent 1:0–2.

Petraglia AL, Plog BA, Dayawansa S, Chen M, Dashnaw ML, Czerniecka K, T WC, Viterise T, Hyrien O, Iliff JJ, Deane R, Nedergaard M, Huang JH (2014b) The

spectrum of neurobehavioral sequelae after repetitive mild traumatic brain injury: A novel mouse model of chronic traumatic encephalopathy. J Neurotrauma.

Pinar C, Trivino-Paredes J, Perrault ST, Christie BR (2020) Hippocampal cognitive impairment in juvenile rats after repeated mild traumatic brain injury. Behav Brain Res 387 Available at: https://pubmed.ncbi.nlm.nih.gov/32184155/ [Accessed April 6, 2021].

Polinder S, Cnossen MC, Real RGL, Covic A, Gorbunova A, Voormolen DC, Master CL, Haagsma JA, Diaz-Arrastia R, Von Steinbuechel N (2018) A Multidimensional Approach to Post-concussion Symptoms in Mild Traumatic Brain Injury. Front Neurol 9:1113 Available at: /pmc/articles/PMC6306025/ [Accessed April 6, 2021].

Prange-Kiel J, Wehrenberg U, Jarry H, Rune GM (2003) Para/autocrine regulation of estrogen receptors in hippocampal neurons. Hippocampus 13:226–234.

Prins ML, Alexander D, Giza CC, Hovda DA (2012) Repeated Mild Traumatic Brain Injury: Mechanisms of Cerebral Vulnerability. J Neurotrauma.

Raichle ME, Mintun MA (2006) BRAIN WORK AND BRAIN IMAGING. Annu Rev Neurosci 29:449–476 Available at: http://www.annualreviews.org/doi/10.1146/annurev.neuro.29.051605.112819 [Accessed April 6, 2021].

Ray SK, Dixon CE, Banik NL (2002) Molecular mechanisms in the pathogenesis of traumatic brain injury. Histol Histopathol 17:1137–1152.

Rice RA, Pham J, Lee RJ, Najafi AR, West BL, Green KN (2017) Microglial repopulation resolves inflammation and promotes brain recovery after injury. Glia.

Rieke GK (1987) Thalamic arterial pattern: An endocast and scanning electron microscopic study in normotensive male rats. Am J Anat 178:45–54 Available at: https://pubmed.ncbi.nlm.nih.gov/3825962/ [Accessed April 8, 2021].

Robertson RT, Levine ST, Haynes SM, Gutierrez P, Baratta JL, Tan Z, Longmuir KJ (2015)

Use of labeled tomato lectin for imaging vasculature structures. Histochem Cell Biol 143:225–234.

Romero JR, Beiser A, Himali JJ, Shoamanesh A, DeCarli C, Seshadri S (2017) Cerebral microbleeds and risk of incident dementia: the Framingham Heart Study. Neurobiol Aging 54:94–99 Available at: /pmc/articles/PMC5401784/ [Accessed April 8, 2021].

Rosenberg GA (2014) Blood-Brain Barrier Permeability in Aging and Alzheimer's Disease. J Prev Alzheimer's Dis 1:138–139 Available at: http://www.ncbi.nlm.nih.gov/pubmed/26301207 [Accessed April 9, 2021].

Rosidi NL, Zhou J, Pattanaik S, Wang P, Jin W, Brophy M, Olbricht WL, Nishimura N, Schaffer CB (2011) Cortical Microhemorrhages Cause Local Inflammation but Do Not Trigger Widespread Dendrite Degeneration Block ML, ed. PLoS One 6:e26612 Available at: https://dx.plos.org/10.1371/journal.pone.0026612 [Accessed April 8, 2021].

Rostowsky KA, Maher AS, Irimia A (2018) Macroscale white matter alterations due to traumatic cerebral microhemorrhages are revealed by diffusion tensor imaging. Front Neurol 9 Available at: https://pubmed.ncbi.nlm.nih.gov/30483210/ [Accessed April 8, 2021].

Rutgers DR, Fillard P, Paradot G, Tadié M, Lasjaunias P, Ducreux D (2008) Diffusion tensor imaging characteristics of the corpus callosum in mild, moderate, and severe traumatic brain injury. Am J Neuroradiol 29:1730–1735 Available at: https://pubmed.ncbi.nlm.nih.gov/18617586/ [Accessed April 25, 2021].

Ryu JK et al. (2018) Fibrin-targeting immunotherapy protects against neuroinflammation and neurodegeneration. Nat Immunol.

Ryu JK, Helmrick MJ, Akassoglou K, Vagena E, Galanakis DK, Schachtrup C, Margolis RU, Degen JL (2010) Fibrinogen Triggers Astrocyte Scar Formation by Promoting the Availability of Active TGF- after Vascular Damage. J Neurosci.

Ryu JK, Petersen MA, Murray SG, Baeten KM, Meyer-Franke A, Chan JP, Vagena E, Bedard C, Machado MR, Coronado PER, Prod'homme T, Charo IF, Lassmann H, Degen JL, Zamvil SS, Akassoglou K (2015a) Blood coagulation protein fibrinogen promotes autoimmunity and demyelination via chemokine release and antigen presentation. Nat Commun.

Ryu JK, Petersen MA, Murray SG, Baeten KM, Meyer-Franke A, Chan JP, Vagena E, Bedard C, Machado MR, Coronado PER, Prod'homme T, Charo IF, Lassmann H, Degen JL, Zamvil SS, Akassoglou K (2015b) Blood coagulation protein fibrinogen promotes autoimmunity and demyelination via chemokine release and antigen presentation. Nat Commun.

Saatman KE, Duhaime A-C, Bullock R, Maas AIR, Valadka A, Manley GT (2008) Classification of traumatic brain injury for targeted therapies. J Neurotrauma 25:719–738.

Saijo K, Crotti A, Glass CK (2013) Regulation of microglia activation and deactivation by nuclear receptors. Glia.

Salehi A, Zhang JH, Obenaus A (2017) Response of the cerebral vasculature following traumatic brain injury. J Cereb Blood Flow Metab 37:2320–2339 Available at: https://pubmed.ncbi.nlm.nih.gov/28378621/ [Accessed April 6, 2021].

Schachtrup C, Ryu JK, Helmrick MJ, Vagena E, Galanakis DK, Degen JL, Margolis RU, Akassoglou K (2010) Fibrinogen triggers astrocyte scar formation by promoting the availability of active TGF-β after vascular damage. J Neurosci 30:5843–5854 Available at: https://www.jneurosci.org/content/30/17/5843 [Accessed April 25, 2021].

Schafer JL (1997) Analysis of Incomplete Multivariate Data. Available at: https://books.google.ca/books/about/Analysis_of_Incomplete_Multivariate_Data.html?id=3TFWRjn1f-oC&redir_esc=y [Accessed April 11, 2021].

Schager B, Brown CE (2020) Susceptibility to capillary plugging can predict brain region specific vessel loss with aging. J Cereb Blood Flow Metab 40:2475–2490 Available at: https://pubmed.ncbi.nlm.nih.gov/31903837/ [Accessed June 16, 2021].

Schlessinger J, Axelrod D, Koppel DE, Webb WW, Elson EL (1977) Lateral transport of a lipid probe and labeled proteins on a cell membrane. Science 195:307–309 Available at: http://www.ncbi.nlm.nih.gov/pubmed/556653.

Schmid F, Barrett MJP, Jenny P, Weber B (2019) Vascular density and distribution in neocortex. Neuroimage 197:792–805.

Schrag M, McAuley G, Pomakian J, Jiffry A, Tung S, Mueller C, Vinters H V., Haacke EM, Holshouser B, Kido D, Kirsch WM (2010) Correlation of hypointensities in susceptibility-weighted images to tissue histology in dementia patients with cerebral amyloid angiopathy: A postmortem MRI study. Acta Neuropathol 119:291–302 Available at: https://pubmed.ncbi.nlm.nih.gov/19937043/ [Accessed April 9, 2021].

Schwartz M, Agranoff BW (1981) Outgrowth and maintenance of neurites from cultured goldfish retinal ganglion cells. Brain Res 206:331–343.

Scimemi A (2018) Astrocytes and the Warning Signs of Intracerebral Hemorrhagic Stroke. Neural Plast 2018.

Scopaz KA, Hatzenbuehler JR (2013) Risk Modifiers for Concussion and Prolonged Recovery. Sports Health 5:537–541 Available at: /pmc/articles/PMC3806172/ [Accessed April 6, 2021].

Serra-Grabulosa JM, Junqué C, Verger K, Salgado-Pineda P, Mañeru C, Mercader JM (2005) Cerebral correlates of declarative memory dysfunctions in early traumatic brain injury. J Neurol Neurosurg Psychiatry 76:129–131.

Seto A, Taylor S, Trudeau D, Swan I, Leung J, Reeson P, Delaney KR, Brown CE (2014) Induction of ischemic stroke in awake freely moving mice reveals that isoflurane anesthesia can mask the benefits of a neuroprotection therapy. Front

Neuroenergetics 6 Available at: https://pubmed.ncbi.nlm.nih.gov/24765075/ [Accessed June 16, 2021].

Shulman RG, Rothman DL, Behar KL, Hyder F (2004) Energetic basis of brain activity: Implications for neuroimaging. Trends Neurosci 27:489–495 Available at: https://pubmed.ncbi.nlm.nih.gov/15271497/ [Accessed April 6, 2021].

Shultz SR, McDonald SJ, Vonder Haar C, Meconi A, Vink R, van Donkelaar P, Taneja C, Iverson GL, Christie BR (2016) The potential for animal models to provide insight into mild traumatic brain injury: Translational challenges and strategies. Neurosci Biobehav Rev.

Shultz SR, Sun M, Wright DK, Brady RD, Liu S, Beynon S, Schmidt SF, Kaye AH, Hamilton JA, O'Brien TJ, Grills BL, McDonald SJ (2015) Tibial fracture exacerbates traumatic brain injury outcomes and neuroinflammation in a novel mouse model of multitrauma. J Cereb Blood Flow Metab 35:1339–1347 Available at: http://journals.sagepub.com/doi/10.1038/jcbfm.2015.56 [Accessed April 12, 2021].

Simard JM, Kilbourne M, Tsymbalyuk O, Tosun C, Caridi J, Ivanova S, Keledjian K, Bochicchio G, Gerzanich V (2009) Key role of sulfonylurea receptor 1 in progressive secondary hemorrhage after brain contusion. J Neurotrauma 26:2257–2267 Available at: https://pubmed.ncbi.nlm.nih.gov/19604096/ [Accessed April 11, 2021].

Skrzypiec AE, Shah RS, Schiavon E, Baker E, Skene N, Pawlak R, Mucha M (2013) Stress-Induced Lipocalin-2 Controls Dendritic Spine Formation and Neuronal Activity in the Amygdala. PLoS One 8.

Smith AF, Doyeux V, Berg M, Peyrounette M, Haft-Javaherian M, Larue AE, Slater JH, Lauwers F, Blinder P, Tsai P, Kleinfeld D, Schaffer CB, Nishimura N, Davit Y, Lorthois S (2019) Brain capillary networks across species: A few simple organizational requirements are sufficient to reproduce both structure and function. Front Physiol 10:233 Available at: www.frontiersin.org [Accessed June 16, 2021].

Studerus-Germann AM, Gautschi OP, Bontempi P, Thiran JP, Daducci A, Romascano D, von Ow D, Hildebrandt G, von Hessling A, Engel DC (2018) Central nervous system microbleeds in the acute phase are associated with structural integrity by DTI one year after mild traumatic brain injury: A longitudinal study. Neurol Neurochir Pol 52:710–719 Available at: https://pubmed.ncbi.nlm.nih.gov/30245171/ [Accessed April 8, 2021].

Stuermer C a (1988) Retinotopic organization of the developing retinotectal projection in the zebrafish embryo. J Neurosci 8:4513–4530.

Sullivan TR, Lee KJ, Ryan P, Salter AB (2017) Multiple imputation for handling missing outcome data when estimating the relative risk. BMC Med Res Methodol 17 Available at: https://pubmed.ncbi.nlm.nih.gov/28877666/ [Accessed April 11, 2021].

Sumbria RK, Grigoryan MM, Vasilevko V, Krasieva TB, Scadeng M, Dvornikova AK, Paganini-Hill A, Kim R, Cribbs DH, Fisher MJ (2016) A murine model of inflammation-induced cerebral microbleeds. J Neuroinflammation 13 Available at: /pmc/articles/PMC5006574/ [Accessed April 25, 2021].

Sun DA, Deshpande LS, Sombati S, Baranova A, Wilson MS, Hamm RJ, DeLorenzo RJ (2008) Traumatic brain injury causes a long-lasting calcium (Ca 2+)-plateau of elevated intracellular Ca levels and altered Ca 2+ homeostatic mechanisms in hippocampal neurons surviving brain injury. Eur J Neurosci 27:1659–1672.

Susman M, DiRusso SM, Sullivan T, Risucci D, Nealon P, Cuff S, Benzil D (2002) Traumatic brain injury in the elderly: Increased mortality and worse functional outcome at discharge despite lower injury severity. J Trauma 53.

Takhounts EG, Crandall JR, Darvish K (2003) On the importance of nonlinearity of brain tissue under large deformations. Stapp Car Crash J 47:79–92.

Tate DF, Bigler ED (2000) Fornix and hippocampal atrophy in traumatic brain injury.

Learn Mem 7:442–446.

Taylor CA, Bell JM, Breiding MJ, Xu L (2017) Traumatic Brain Injury–Related Emergency Department Visits, Hospitalizations, and Deaths — United States, 2007 and 2013. MMWR Surveill Summ.

Taylor S, Mehina E, White E, Reeson P, Yongblah K, Doyle KP, Brown CE (2018) Suppressing interferon-γ stimulates microglial responses and repair of microbleeds in the diabetic brain. J Neurosci 38:8707–8722 Available at: /pmc/articles/PMC6596226/ [Accessed April 25, 2021].

Teasdale G, Jennett B (1974) ASSESSMENT OF COMA AND IMPAIRED CONSCIOUSNESS. A Practical Scale. Lancet.

Thanos S, Bonhoeffer F (1987) Axonal arborization in the developing chick retinotectal system. J Comp Neurol 261:155–164.

Thomas R. Frieden, Debra Houry GB (2015) Traumatic Brain Injury In the United States: Epidemiology and Rehabilitation. Centers Dis Control Prev.

Tian Y, Liu J, Kou Z (2014) Diffuse axonal injury after traumatic cerebral microbleeds: an evaluation of imaging techniques. Neural Regen Res 9:1222 Available at: http://www.nrronline.org/text.asp?2014/9/12/1222/135330 [Accessed April 11, 2021].

Tomaiuolo F, Carlesimo GA, Di Paola M, Petrides M, Fera F, Bonanni R, Formisano R, Pasqualetti P, Caltagirone C (2004) Gross morphology and morphometric sequelae in the hippocampus, fornix, and corpus callosum of patients with severe non-missile traumatic brain injury without macroscopically detectable lesions: a T1 weighted MRI study. J Neurol Neurosurg Psychiatry 75:1314–1322.

Tomkins O, Shelef I, Kaizerman I, Eliushin A, Afawi Z, Misk A, Gidon M, Cohen A, Zumsteg D, Friedman A (2008) Blood-brain barrier disruption in post-traumatic epilepsy. J Neurol Neurosurg Psychiatry 79:774–777 Available at:

https://pubmed.ncbi.nlm.nih.gov/17991703/ [Accessed April 8, 2021].

Trivino-Paredes JS, Nahirney PC, Pinar C, Grandes P, Christie BR (2019) Acute slice preparation for electrophysiology increases spine numbers equivalently in the male and female juvenile hippocampus: A DiI labeling study. J Neurophysiol 122:958–969 Available at: https://pubmed.ncbi.nlm.nih.gov/31268808/ [Accessed April 11, 2021].

Ungvari Z, Tarantini S, Kirkpatrick AC, Csiszar A, Prodan CI (2017) Cerebral microhemorrhages: Mechanisms, consequences, and prevention. Am J Physiol - Hear Circ Physiol 312:H1128–H1143 Available at: https://pubmed.ncbi.nlm.nih.gov/28314762/ [Accessed April 8, 2021].

Unterharnscheidt F, Higgins LS (1969) Traumatic lesions of brain and spinal cord due to nondeforming angular acceleration of the head. Tex Rep Biol Med 27:127–166.

Van Wageningen TA, Vlaar E, Kooij G, Jongenelen CAM, Geurts JJG, Van Dam AM (2019) Regulation of microglial TMEM119 and P2RY12 immunoreactivity in multiple sclerosis white and grey matter lesions is dependent on their inflammatory environment. Acta Neuropathol Commun 7 Available at: https://pubmed.ncbi.nlm.nih.gov/31829283/ [Accessed April 11, 2021].

Vaz WLC, Goodsaid-Zalduondo F, Jacobson K (1984) Lateral diffusion of lipids and proteins in bilayer membranes. FEBS Lett 174:199–207 Available at: http://www.sciencedirect.com/science/article/pii/0014579384811576.

Verger K, Junqué C, Jurado M a, Tresserras P, Bartumeus F, Nogués P, Poch JM (2000) Age effects on long-term neuropsychological outcome in paediatric traumatic brain injury. Brain Inj 14:495–503.

Vink R (2018) Large animal models of traumatic brain injury. J Neurosci Res 96:527–535 Available at: http://doi.wiley.com/10.1002/jnr.24079 [Accessed April 6, 2021].

Vinters H V., Gilbert JJ (1983) Cerebral amyloid angiopathy: Incidence and complications

in the aging brain. II. The distribution of amyloid vascular changes. Stroke 14:924–928 Available at: http://ahajournals.org [Accessed April 9, 2021].

Vitali P, Boghen D, Daneault N, Guillon-Létourneau L, Poppe AY (2014) Cerebral Microbleed Causing an Acute Stroke-like Episode in a CADASIL Patient. Can J Neurol Sci 41:661–663 Available at: https://pubmed.ncbi.nlm.nih.gov/25373821/ [Accessed April 9, 2021].

Voormolen DC, Cnossen MC, Polinder S, Von Steinbuechel N, Vos PE, Haagsma JA (2018) Divergent classification methods of post-concussion syndrome after mild traumatic brain injury: Prevalence rates, risk factors, and functional outcome. J Neurotrauma 35:1233–1241 Available at: https://pubmed.ncbi.nlm.nih.gov/29350085/ [Accessed April 6, 2021].

Voss JD, Connolly J, Schwab KA, Scher AI (2015) Update on the Epidemiology of Concussion/Mild Traumatic Brain Injury. Curr Pain Headache Rep.

Wade SL, Michaud L, Brown TM (2006) Putting the pieces together: Preliminary efficacy of a family problem-solving intervention for children with traumatic brain injury. J Head Trauma Rehabil 21:57–67 Available at: https://pubmed.ncbi.nlm.nih.gov/16456392/ [Accessed April 6, 2021].

Wakisaka Y, Chu Y, Miller JD, Rosenberg GA, Heistad DD (2010) Spontaneous intracerebral hemorrhage during acute and chronic hypertension in mice. J Cereb Blood Flow Metab 30:56–69 Available at: https://pubmed.ncbi.nlm.nih.gov/19724290/ [Accessed April 9, 2021].

Walker KR, Tesco G (2013) Molecular mechanisms of cognitive dysfunction following traumatic brain injury. Front Aging Neurosci 5.

Wall SE, Williams WH, Cartwright-Hatton S, Kelly TP, Murray J, Murray M, Owen A, Turner M (2006) Neuropsychological dysfunction following repeat concussions in jockeys. J Neurol Neurosurg Psychiatry 77:518–520 Available at:

/pmc/articles/PMC2077488/ [Accessed April 6, 2021].

Walls JR, Coultas L, Rossant J, Henkelman RM (2008) Three-Dimensional Analysis of Vascular Development in the Mouse Embryo Chan-Ling T, ed. PLoS One 3:e2853 Available at: https://dx.plos.org/10.1371/journal.pone.0002853 [Accessed April 7, 2021].

Weber JT (2012) Altered calcium signaling following traumatic brain injury. Front Pharmacol 3 APR.

Werner C, Engelhard K (2007) Pathophysiology of traumatic brain injury. Br J Anaesth 99:4–9.

Wiederschain GY (2011) The Molecular Probes handbook. A guide to fluorescent probes and labeling technologies. Biochem 76:1276–1276 Available at: http://link.springer.com/10.1134/S0006297911110101.

Wiegman AF, Meier IB, Schupf N, Manly JJ, Guzman VA, Narkhede A, Stern Y, Martinez-Ramirez S, Viswanathan A, Luchsinger JA, Greenberg SM, Mayeux R, Brickman AM (2014) Cerebral microbleeds in a multiethnic elderly community: Demographic and clinical correlates. J Neurol Sci 345:125–130 Available at: https://pubmed.ncbi.nlm.nih.gov/25091451/ [Accessed April 8, 2021].

Wong AD, Ye M, Levy AF, Rothstein JD, Bergles DE, Searson PC (2013) The blood-brain barrier: An engineering perspective. Front Neuroeng 6 Available at: /pmc/articles/PMC3757302/ [Accessed April 6, 2021].

Wu JZ, Pan CS, Wimer BM, Rosen CL (2017) Finite element simulations of the head-brain responses to the top impacts of a construction helmet: Effects of the neck and body mass. Proc Inst Mech Eng Part H J Eng Med 231:58–68 Available at: /pmc/articles/PMC5308880/ [Accessed April 6, 2021].

Wu X, Kirov II, Gonen O, Ge Y, Grossman RI, Lui YW (2016) MR imaging applications in mild traumatic brain injury: An imaging update. Radiology 279.

Wu Y, Wu H, Zeng J, Pluimer B, Dong S, Xie X, Guo X, Ge T, Liang X, Feng S, Yan Y, Chen J-F, Sta Maria N, Ma Q, Gomez-Pinilla F, Zhao Z (2021) Mild traumatic brain injury induces microvascular injury and accelerates Alzheimer-like pathogenesis in mice. Acta Neuropathol Commun 9:74 Available at: https://actaneurocomms.biomedcentral.com/articles/10.1186/s40478-021-01178-7 [Accessed April 25, 2021].

Wyss-Coray T, Rogers J (2012) Inflammation in Alzheimer disease-A brief review of the basic science and clinical literature. Cold Spring Harb Perspect Med.

Xiong B, Li A, Lou Y, Chen S, Long B, Peng J, Yang Z, Xu T, Yang X, Li X, Jiang T, Luo Q, Gong H (2017) Precise Cerebral Vascular Atlas in Stereotaxic Coordinates of Whole Mouse Brain. Front Neuroanat 11:128 Available at: http://journal.frontiersin.org/article/10.3389/fnana.2017.00128/full [Accessed April 7, 2021].

Xiong Y, Mahmood A, Chopp M (2014) Animal models of traumatic brain injury. Nat Rev Neurosci 14:128–142.

Yang B, Tse KM, Chen N, Tan L Bin, Zheng QQ, Yang HM, Hu M, Pan G, Lee HP (2014) Development of a finite element head model for the study of impact head injury. Biomed Res Int 2014.

Yew WP, Djukic ND, Jayaseelan JSP, Walker FR, Roos KAA, Chataway TK, Muyderman H, Sims NR (2019) Early treatment with minocycline following stroke in rats improves functional recovery and differentially modifies responses of peri-infarct microglia and astrocytes. J Neuroinflammation 16:6 Available at: https://jneuroinflammation.biomedcentral.com/articles/10.1186/s12974-018-1379-y [Accessed April 25, 2021].

Zamolodchikov D, Strickland S (2016) A possible new role for Aβ in vascular and inflammatory dysfunction in Alzheimer's disease. Thromb Res.

Zhang J, Yang Y, Sun H, Xing Y (2014) Hemorrhagic transformation after cerebral infarction: Current concepts and challenges. Ann Transl Med 2:81 Available at: /pmc/articles/PMC4200641/ [Accessed April 11, 2021].

Zhu XH, Qiao H, Du F, Xiong Q, Liu X, Zhang X, Ugurbil K, Chen W (2012) Quantitative imaging of energy expenditure in human brain. Neuroimage 60:2107–2117 Available at: /pmc/articles/PMC3325488/ [Accessed April 7, 2021].

Zlokovic B V. (2008) The Blood-Brain Barrier in Health and Chronic Neurodegenerative Disorders. Neuron 57:178–201 Available at: https://pubmed.ncbi.nlm.nih.gov/18215617/ [Accessed April 8, 2021].

Zlokovic B V. (2009) Blood-Brain Barrier and Neurovascular Mechanisms of Neurodegeneration and Injury. In: Encyclopedia of Neuroscience, pp 265–271. Elsevier Ltd.

APPENDIX A. Detailed protocol for Prussian blue stained whole-slice segmentation

A1. Image segmentation protocol

1. Open whole-slice image in ImageJ.

Each animal consists of 12 sections that are divided into 4 slides (3 sections per slide). Each of these 3 sections from the same slide are saved as a whole-slice image (acquired with StereoInvestigator) into its corresponding folder (Slide1, Slide2, etc.)

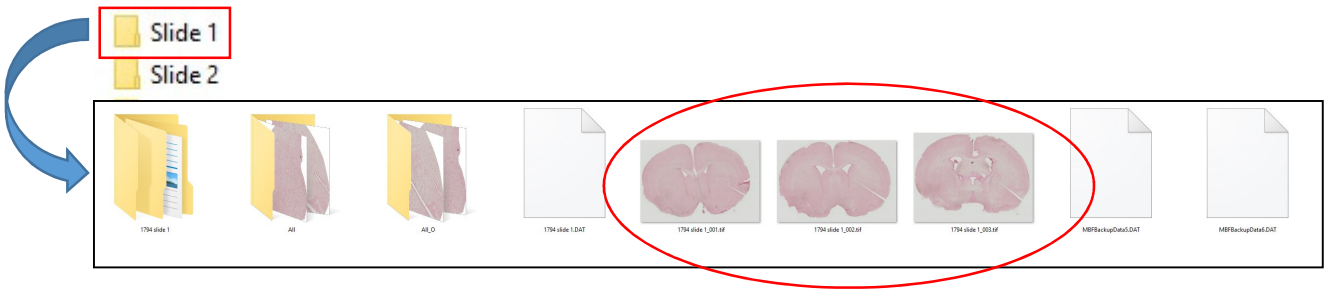

For an unknown reason the images acquired with StereoInvestigator are compressed in a format that ImageJ can not open using the *drag&drop* function even though the images are saved as .tiff files. Therefore, the *Bioformats* plugin has to be used to open them.

1.1. *File* > *Import* > *Bio-Formats*

1.2. Browse and select the image to be opened. Use the default settings in the *Bio-Formats Import Options* window and click *OK*. (Depending on the specifications of the computer employed to perform this, it might take between 2-8 min to open the image).

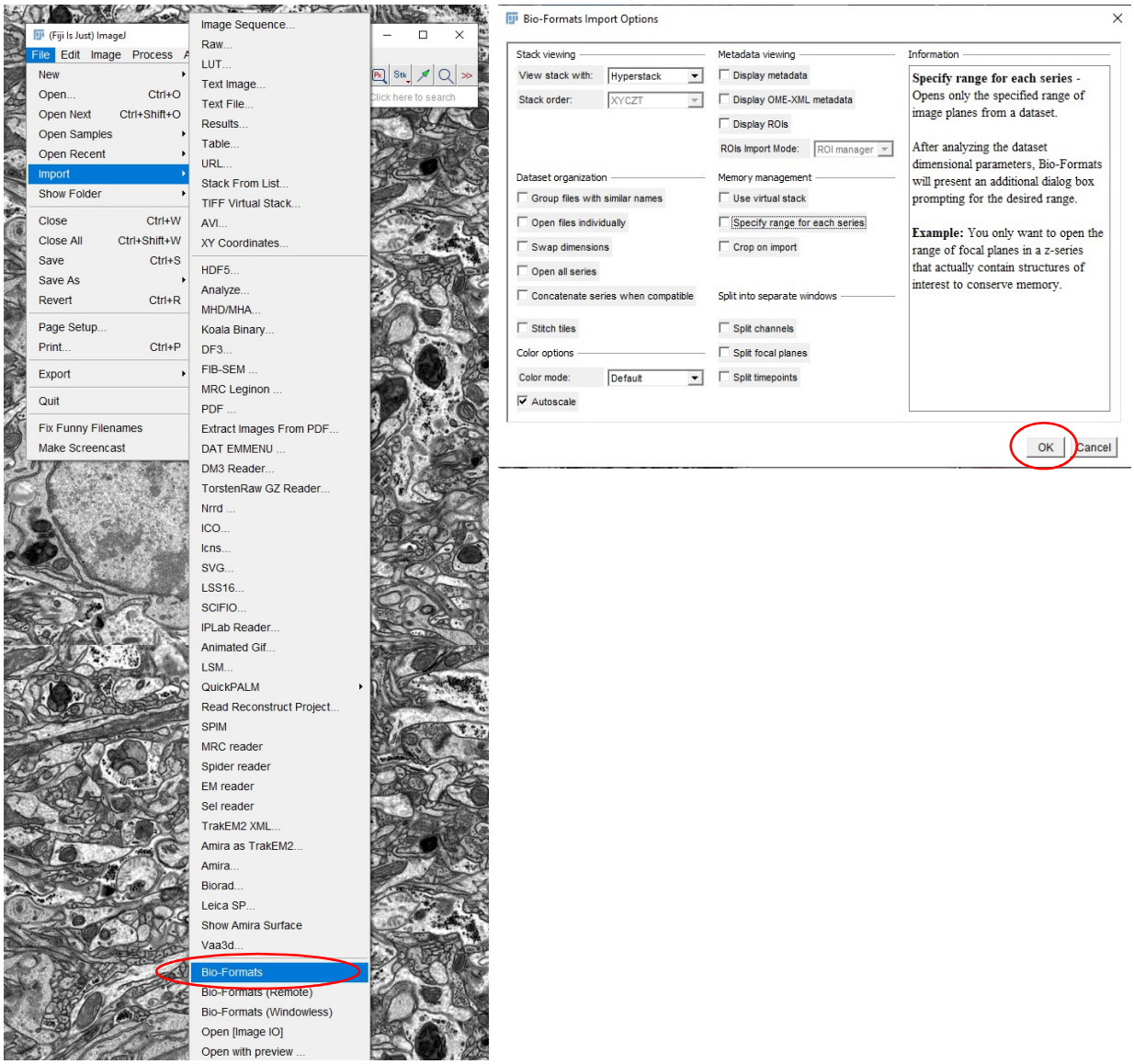

2. Convert into RGB Color and duplicate image.

When an image is opened with *Bio-Formats*, it usually generates a hyper-stack with one slider for the channels and on slider for the z-dimension (not all images have both sliders). This protocol does not employ this image type so first the imported image has to be converted into *RGB Color* and then it has to be duplicated. The duplication step is important because it is less efficient to import an image every time it has to be

segmented (a new image will be needed per each region segmented), therefore the initially imported image should be duplicated. After this, the originally imported image can be closed and only the *RGB Color* version can remain open. It is recommended to have a duplicated *RGB Color* image as a "reservoir" and then duplicate this "reservoir" for each segmented region.

2.1. *Image* > *Type* > *RGB Color*

2.2. *Image* > *Duplicate (shortcut: Ctrl + Shift + D)*

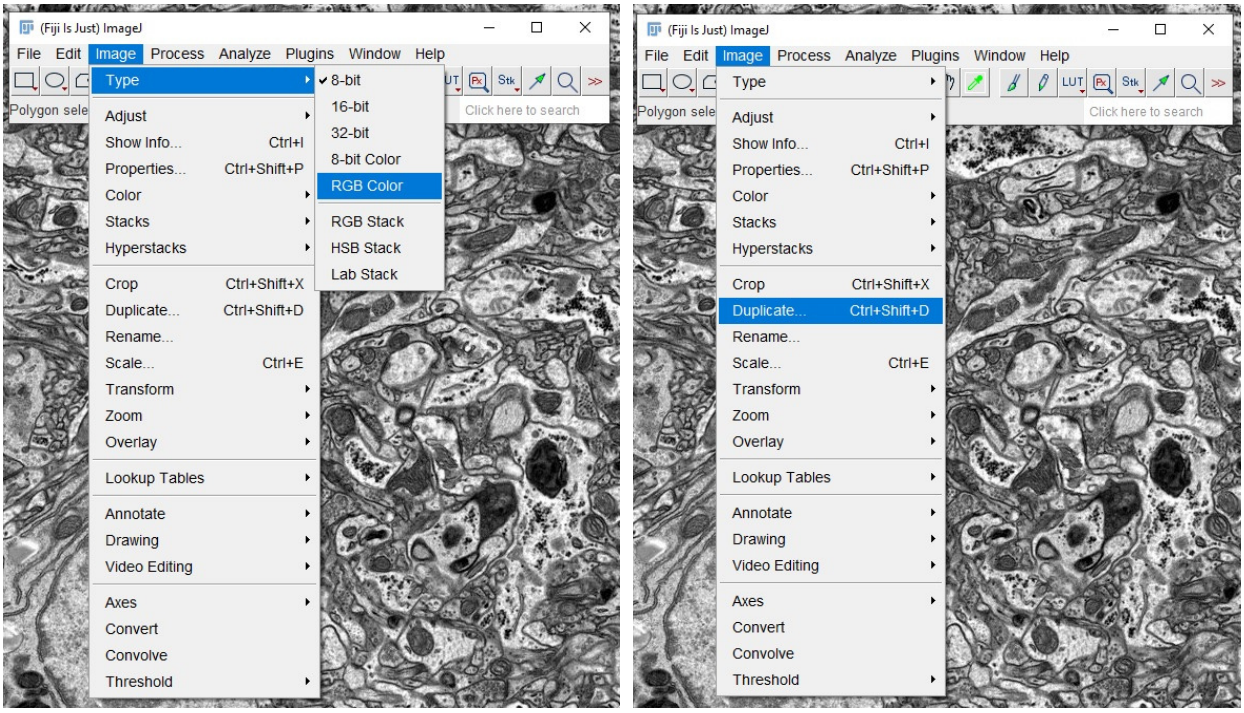

3. Trace region of interest and segment it.

Then, the *Polygon selections* tool has to be selected in the tool bar to start tracing the region of interest. For this dissertation, the regions assessed were cortex, corpus callosum (although parts of the external capsule were also included), hippocampus, striatum, and thalamus. Once the region is traced, the selection has to be cropped and the outside of the image cleared.

3.1. Click on *Polygon selections* and with the guidance of a brain atlas trace the region of interest.

3.2. Right-click to close the contour of the selection. Be aware that if the tracing is done to fast and a "double click" is accidentally triggered, the contour will be closed before the tracing is completed. The "+"(plus) and "-"(minus) signs in the keyboard can be used to move around and zoom in and out of the image while tracing.

3.3. Save the segmented file as .tiff (File > Save As >Tiff)

Polygon selection tool

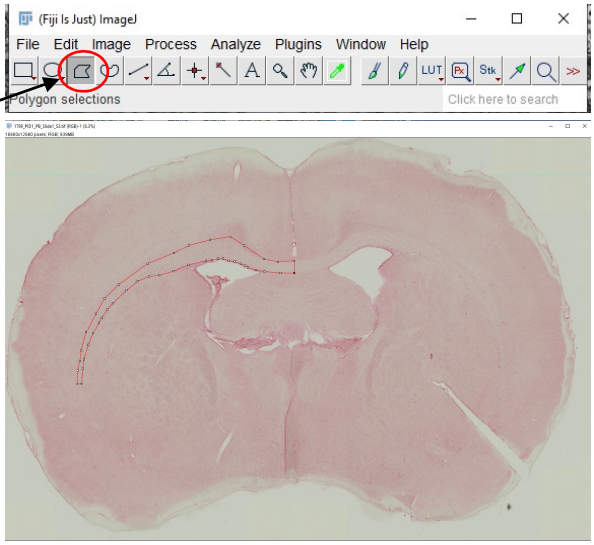

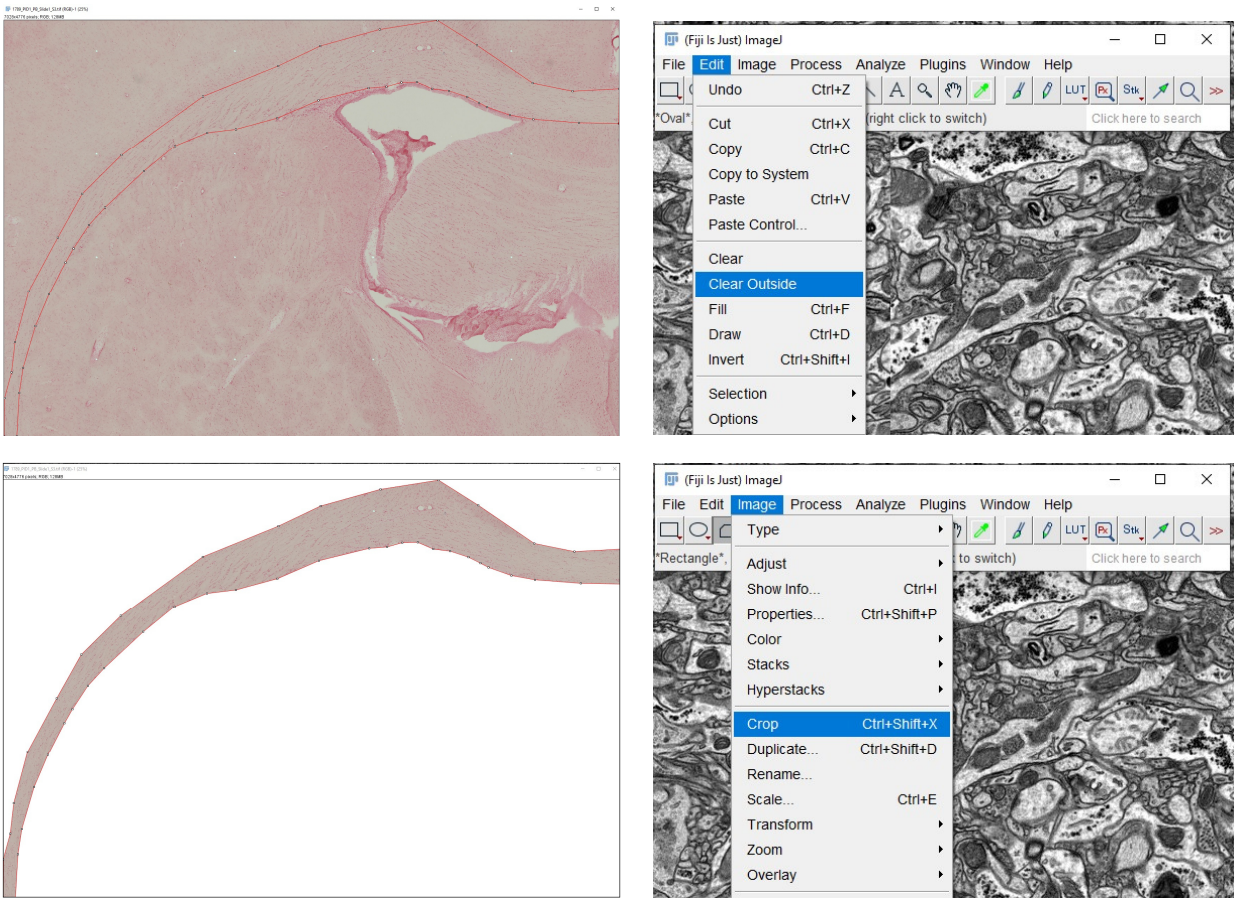

Before saving the segmented image, it is recommended to create a folder with the name “All” in the same directory where the whole-slice image is saved and where all the segmented regions can be saved.

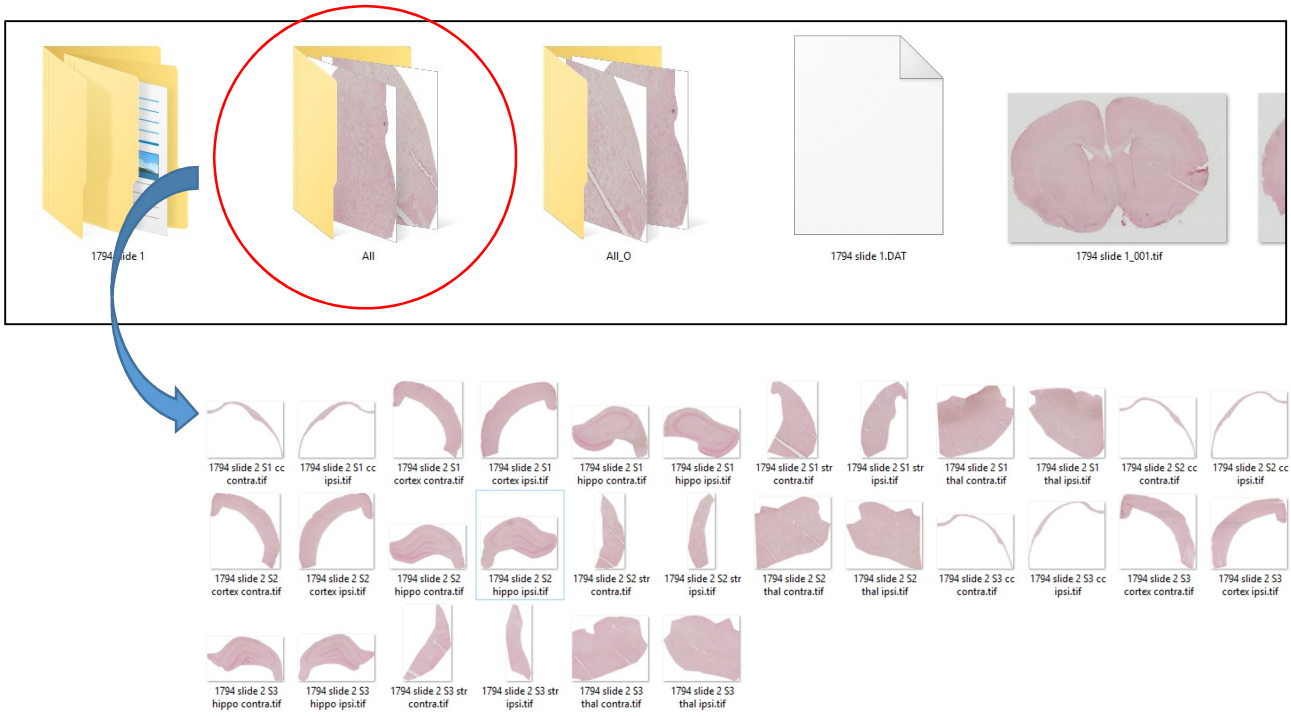

The segmented images should to be saved as .tiff with the following format:

Animal ID + Slide number + Section Number + Region Code

1794 slide 1 S1 cc

Animal ID: 1792, 1802, 1807, etc.

Slide number: The folder where the whole-slice image is saved (slide 1, slide 2, slide 3, etc.)

Section number: The slice that is currently being segmented (S1, S2 or S3)

Region codes:

hipp for Hippocampus

thal for Thalamus

cc for corpus callosum

str for Striatum and Pallidum

ctx for Cortex

Tips: It is a very mechanical and repetitive task, therefore, it is recommended to create your own shortcuts and even macros in ImageJ to speed up the process. For instance, a shortcut for the *Clear Outside* function can be created. The symbol, letter or character in your keyboard should be assigned to the desired command.

Plugins > Shortcuts > Add Shortcut

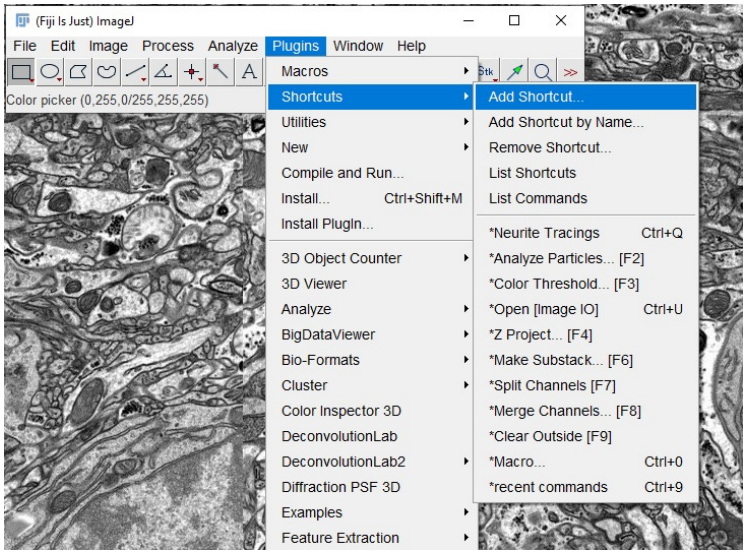

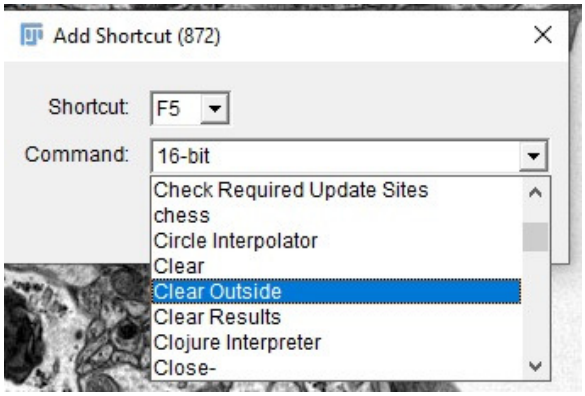

Macros can be used to concatenate commands. For instance, a very simple macro to save the segmented file as a .tiff without having to repeat every time the *File > Save as > Tiff* sequence could be generated (this could be also set as shortcut). With the *Record…* command, ImageJ will translate into macro code every action performed. So if the *File > Save as > Tiff* sequence is performed the *Record…* function is active, a macro of that sequence will be generated. After this *Create* has to be selected to make the macro. The commands saved in a macro will be performed every time *Run* is selected. In this case *Run*, will save the currently selected image as .tiff with the name provided.

Plugins > Macros > Record…

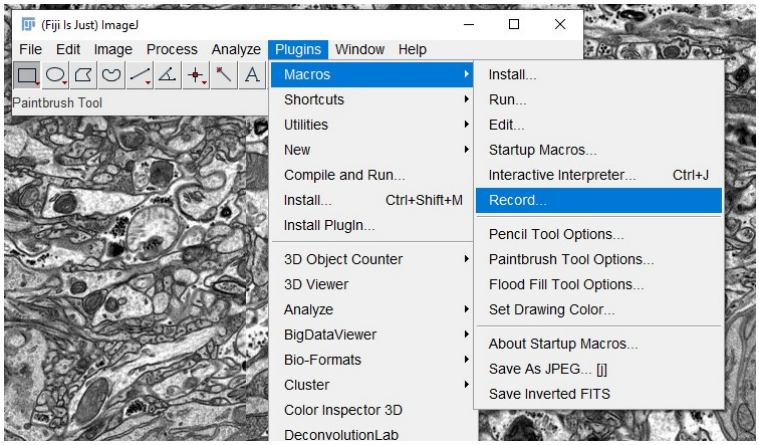

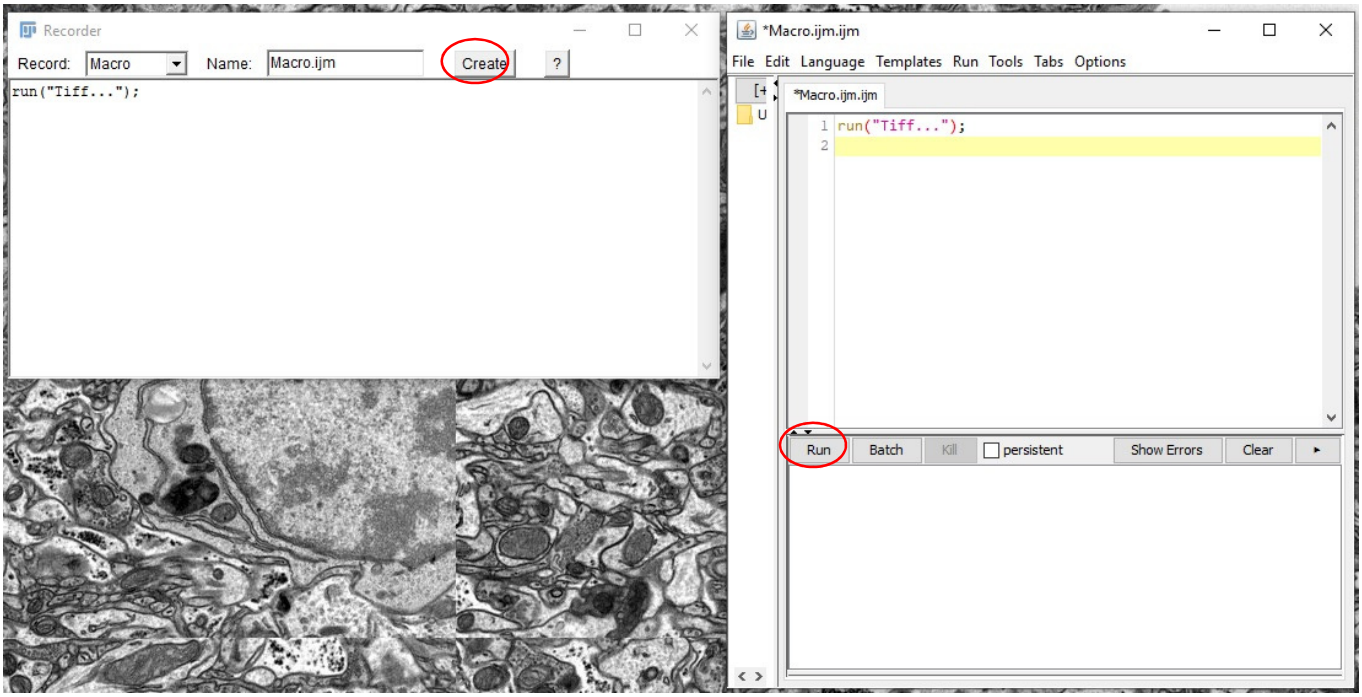

A2. Region of interest segmentation Reference

This a set of images stained with nuclear fast red that provide segmentation reference to show the segmentation limits of the regions of interest. It is acknowledged that they are approximate and may not be 100% accurate, but are kept consistent between animals.

Slide 1 – Section 1

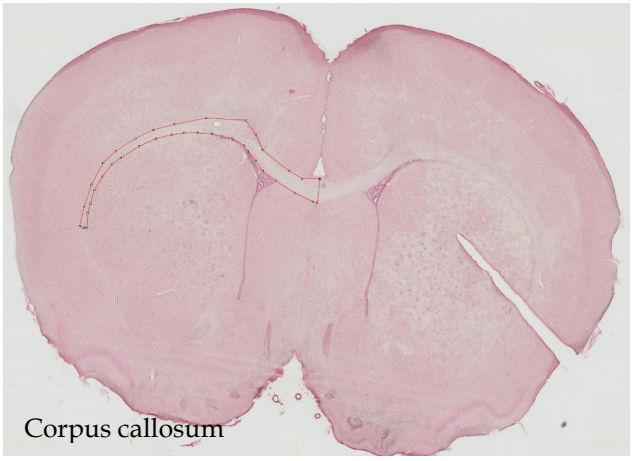

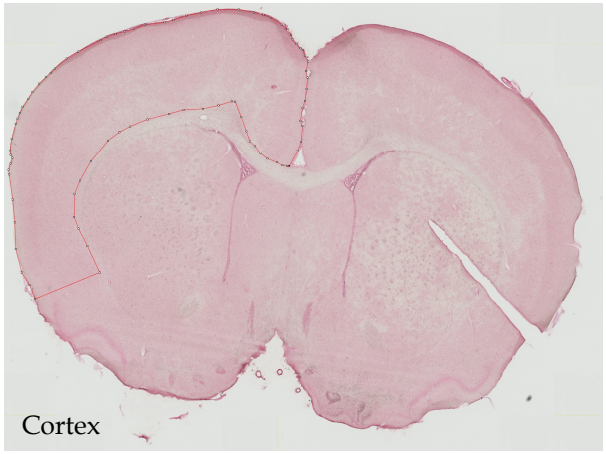

Slide 1 – Section 2

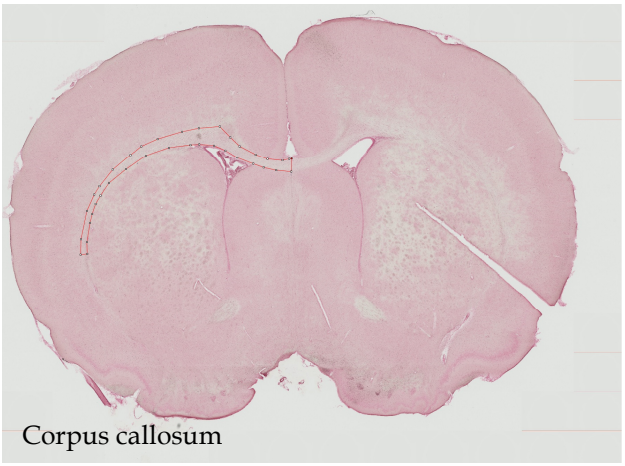
Corpus callosum

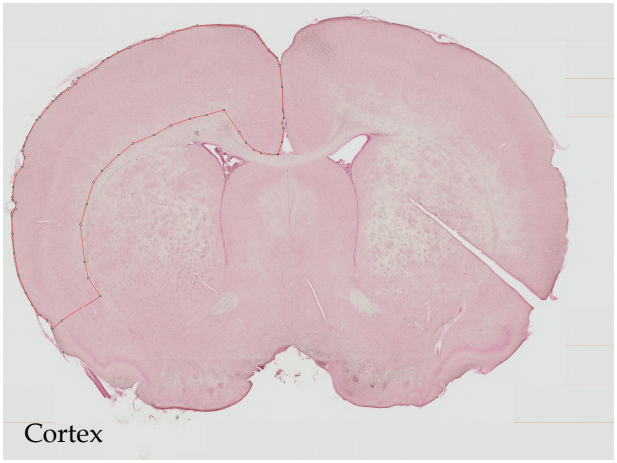
Cortex


Striatum

Slide 1 – Section 3

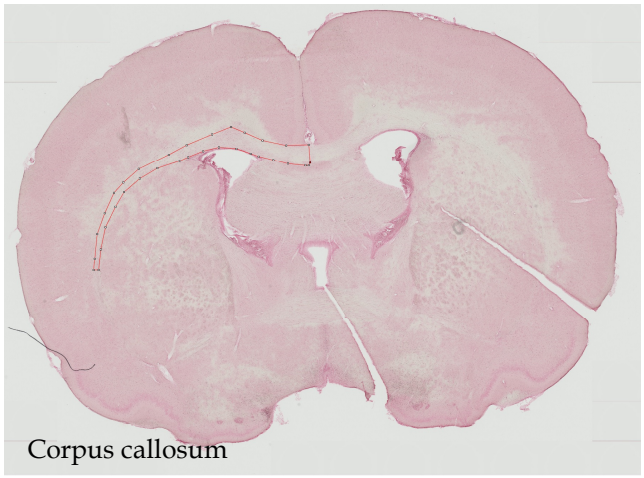

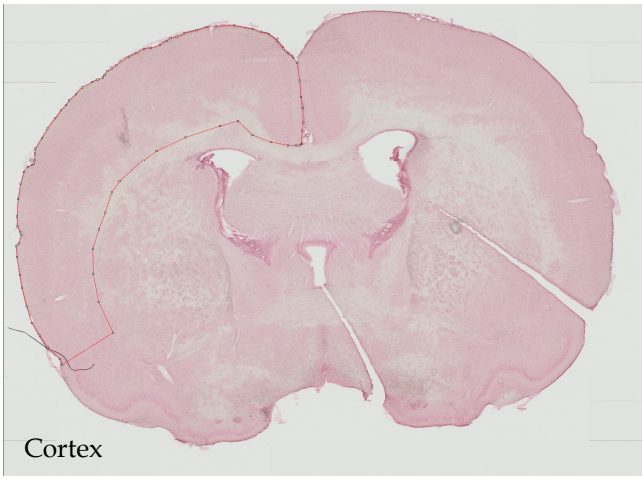

.

Slide 2 – Section 1

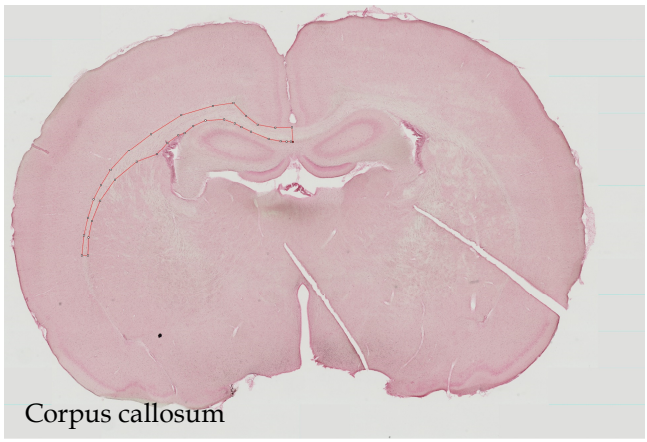
Corpus callosum


Cortex

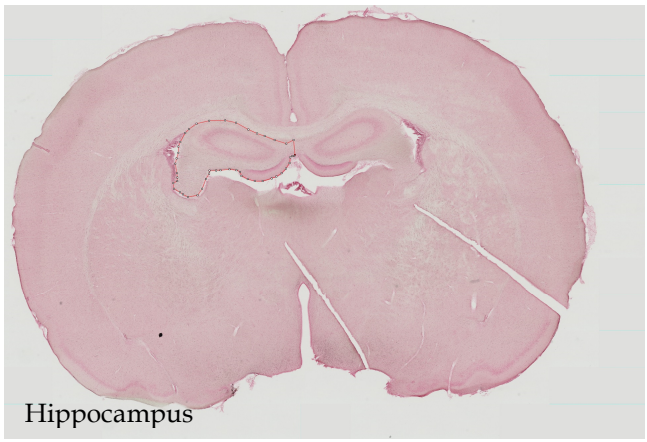
Hippocampus

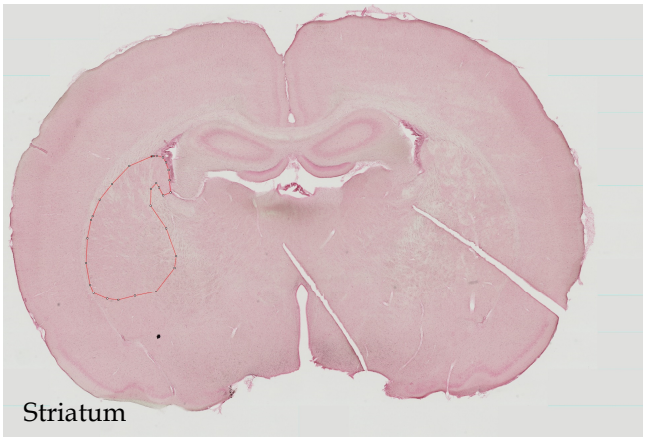
Striatum

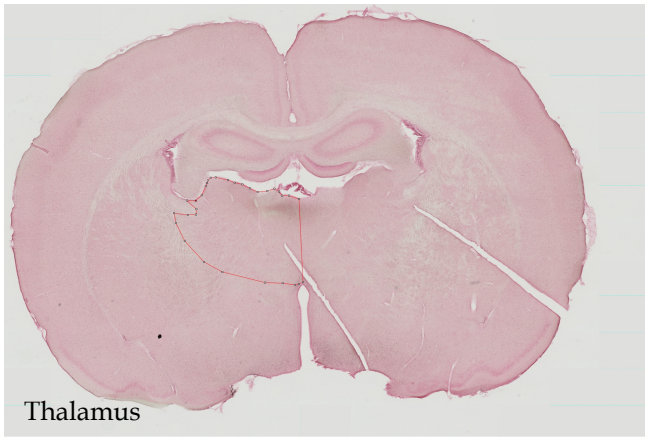
Thalamus

Slide 2 – Section 2


Corpus callosum

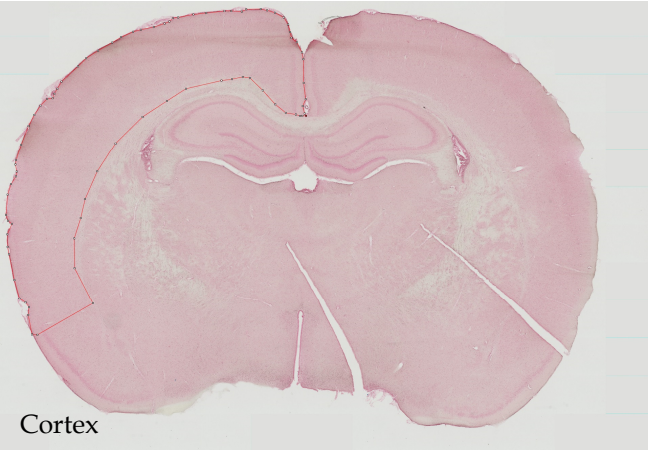
Cortex

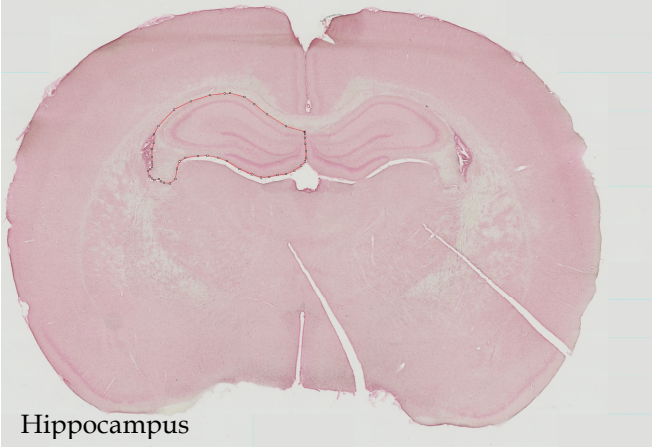
Hippocampus


Striatum

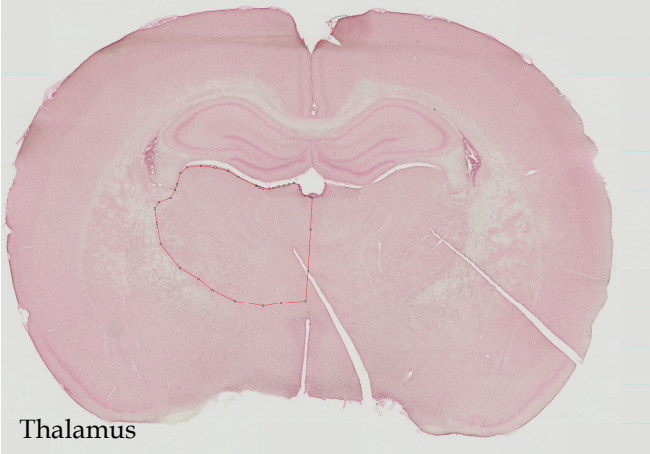
Thalamus

Slide 2 – Section 3

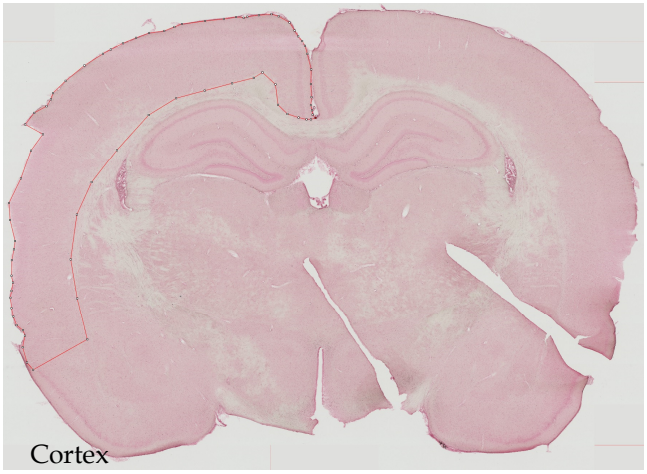

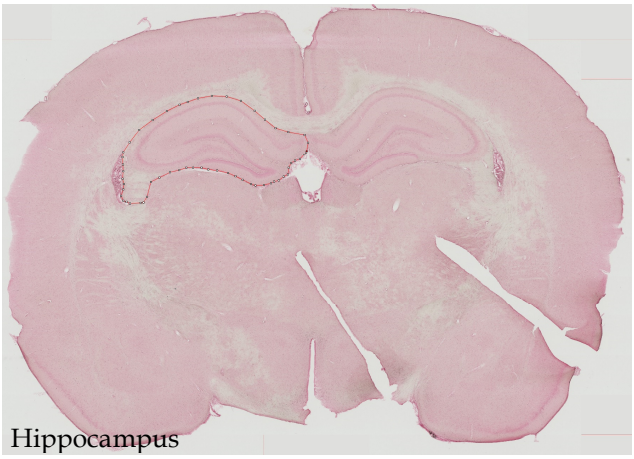

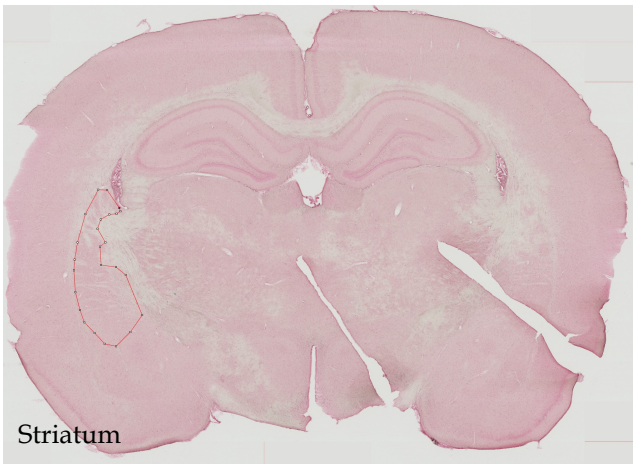

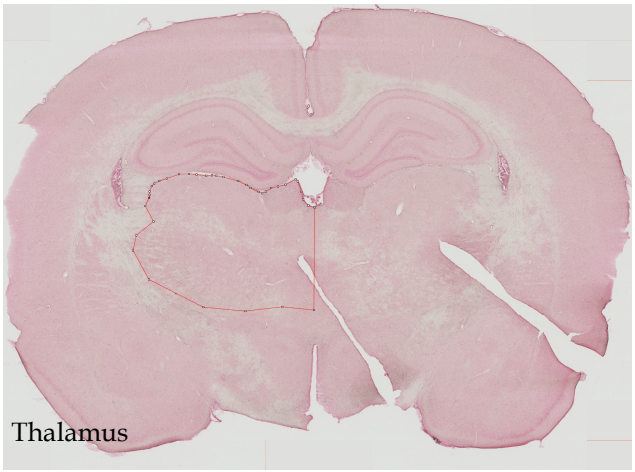

Slide 3 – Section 1


Corpus callosum


Cortex

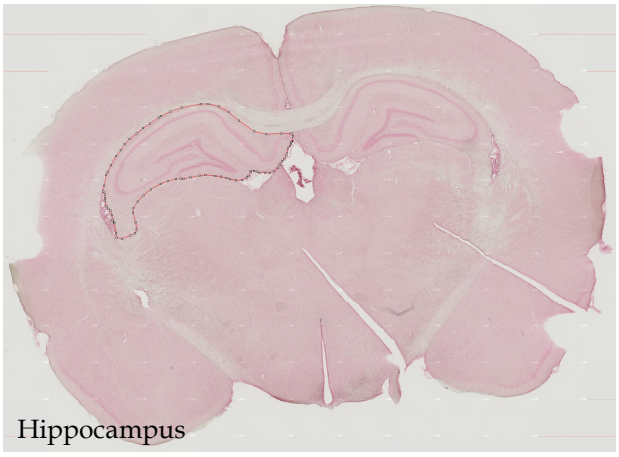
Hippocampus


Striatum

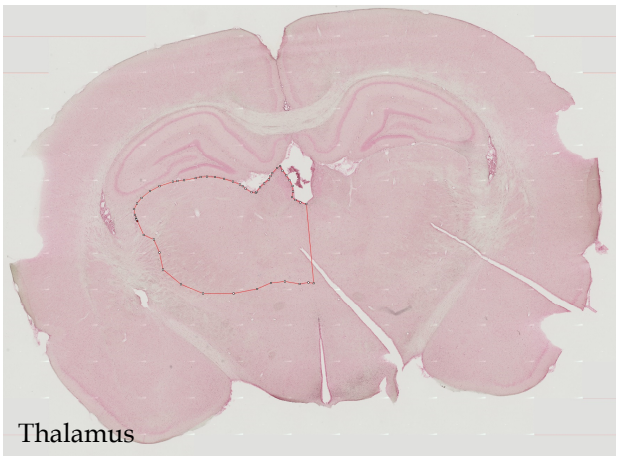
Thalamus

Slide 3 – Section 2

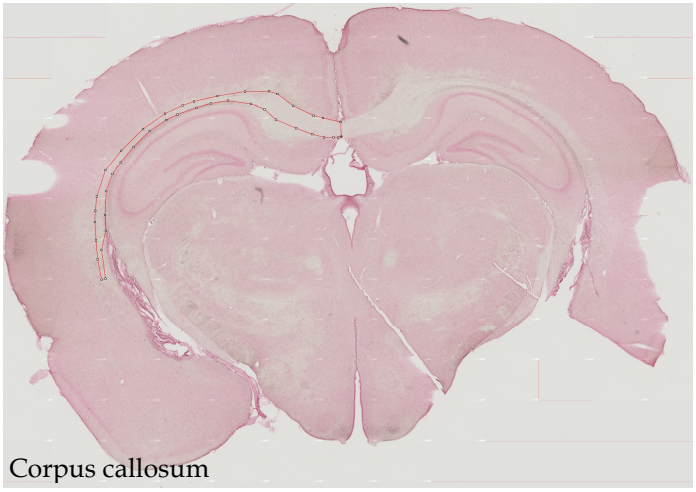
Corpus callosum

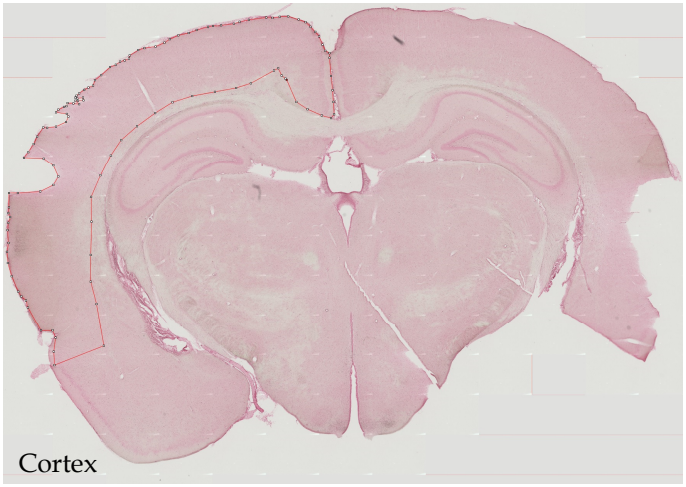
Cortex

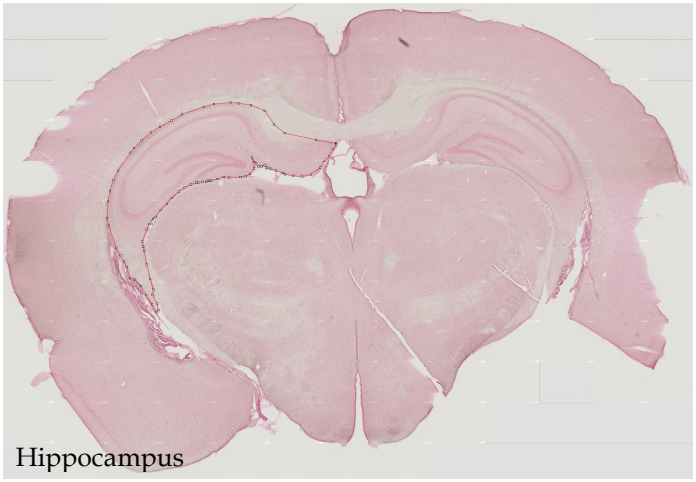
Hippocampus

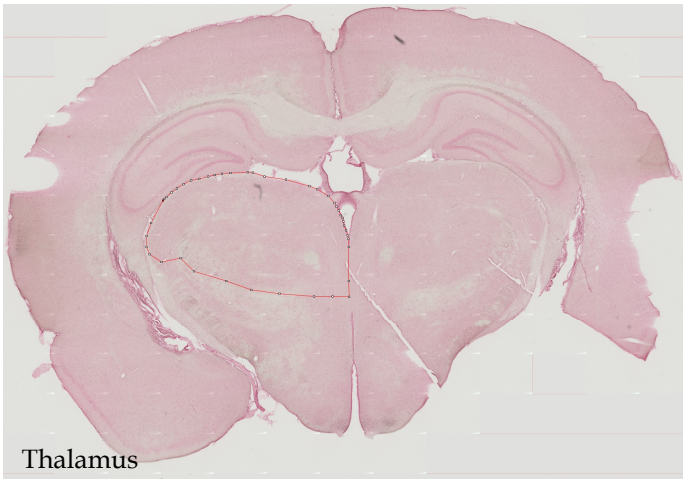
Thalamus

Slide 3 – Section 3

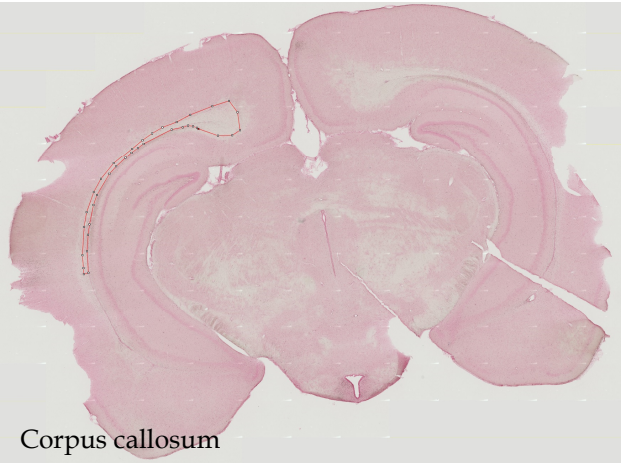

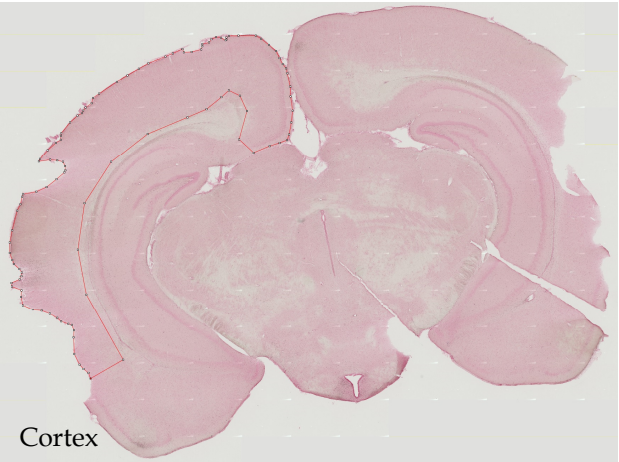

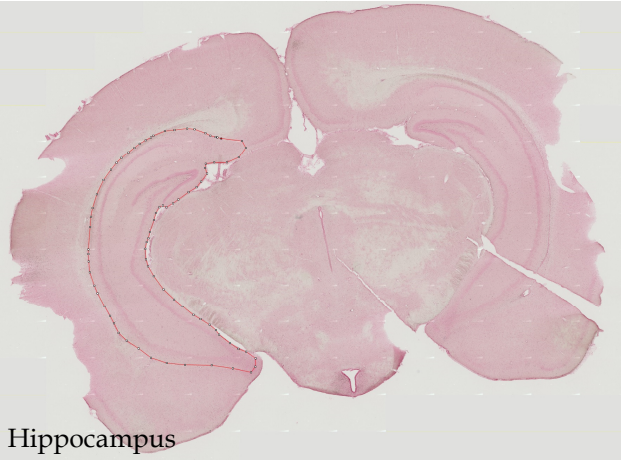

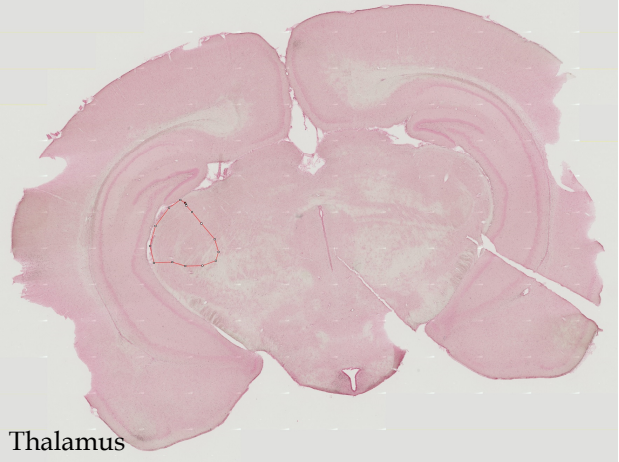

Slide 4 – Section 1

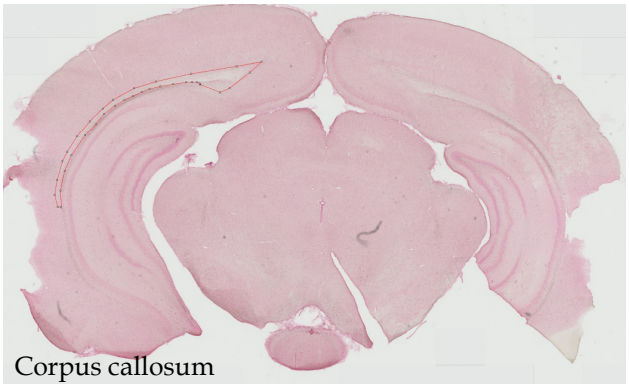
Corpus callosum

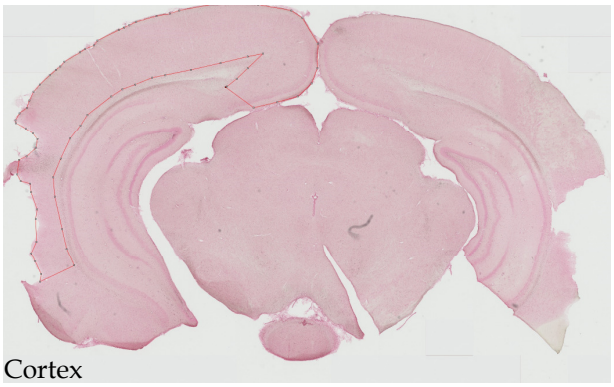
Cortex

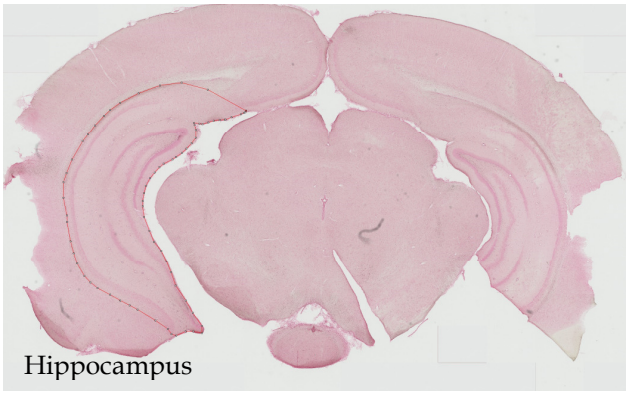
Hippocampus

Slide 4 – Section 2

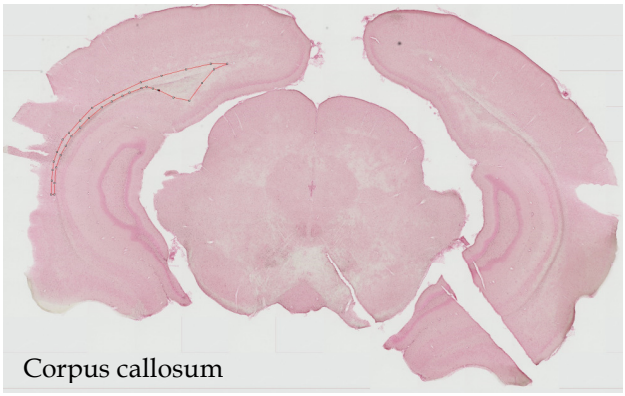
Corpus callosum

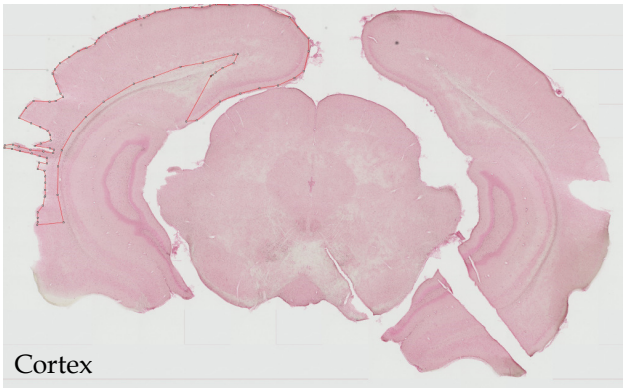
Cortex

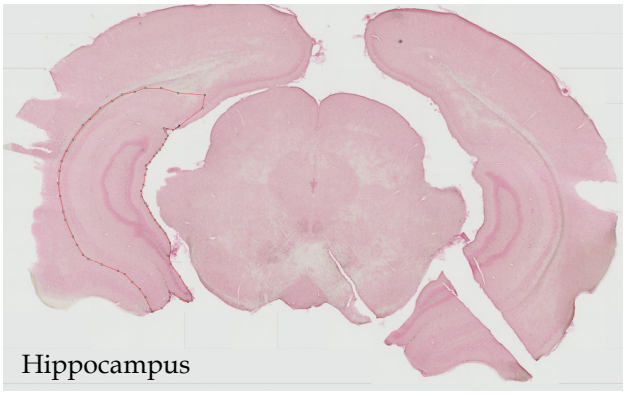
Hippocampus

Slide 4 – Section 3

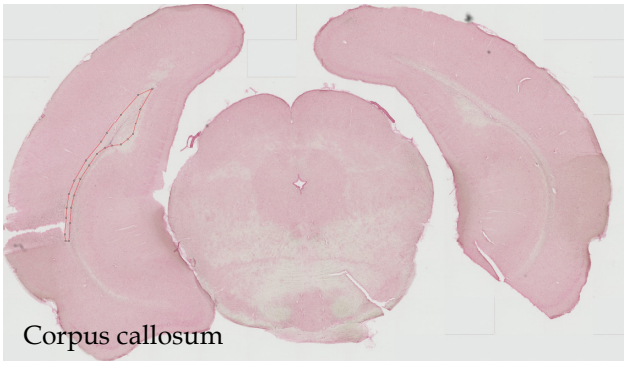
Corpus callosum

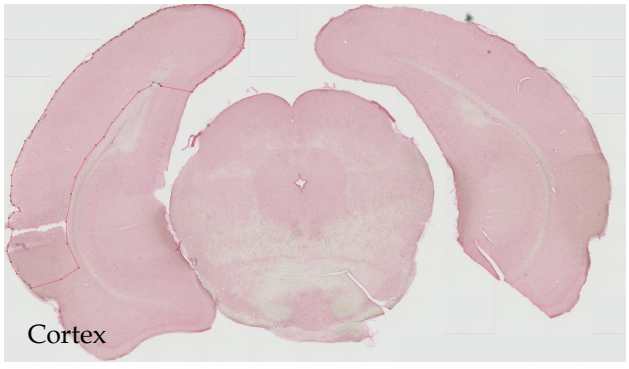
Cortex

APPENDIX B. Macros used for hemosiderin deposit, fibrinogen extravasation and microglia analysis

B1. Hemosiderin deposits analysis macro for Prussian blue stained sections

B1.1 Analysis of blue particles

```
i1 = getTitle();
run("Duplicate...", " ");
// Color Thresholder 2.0.0-rc-68/1.52g
// Autogenerated macro, single images only!
min=newArray(3);
max=newArray(3);
filter=newArray(3);
a=getTitle();
run("HSB Stack");
run("Convert Stack to Images");
selectWindow("Hue");
rename("0");
selectWindow("Saturation");
rename("1");
selectWindow("Brightness");
rename("2");
min[0]=125;
max[0]=190;
filter[0]="pass";
min[1]=30;
max[1]=254;
filter[1]="pass";
min[2]=10;
max[2]=250;
filter[2]="pass";
```

```
for (i=0;i<3;i++){
selectWindow(""+i);
setThreshold(min[i], max[i]);
run("Convert to Mask");
if (filter[i]=="stop")  run("Invert");
}
imageCalculator("AND create", "0","1");
imageCalculator("AND create", "Result of 0","2");
for (i=0;i<3;i++){
selectWindow(""+i);
close();
}
selectWindow("Result of 0");
close();
selectWindow("Result of Result of 0");
rename(a);
// Colour Thresholding----------
run("Analyze Particles...", "size=5-Infinity circularity=0.30-1.00 show=Masks display exclude include summarize add");
run("Maximum...", "radius=20");
run("Outline");
run("Dilate")
run("Invert LUT");
i2 = getTitle();
imageCalculator("AND create", i1, i2);
```

B1.2. Total area analyzed measurement

```
run("8-bit");
run("Auto Threshold", "method=Triangle white");
run("Fill Holes");
run("Create Selection");
run("Measure");
# If images on white background use "method=Triangle"
# If images on black background use "method=Triangle white"
```

B2. Fibrinogen analysis macro

```
Original_ImageTitle=getTitle()
run("Z Project...", "projection=[Max Intensity]");
run("Duplicate...");
ImageTitle=getTitle()
run("Split Channels");
selectWindow(Original_ImageTitle);
close();
selectWindow(ImageTitle+" (green)");
close();
selectWindow(ImageTitle+" (blue)");
BlueImage=getTitle();
run("Duplicate...");
Image_Analysis=getTitle();
selectWindow(ImageTitle+" (red)");
RedImage=getTitle();
run("Merge Channels...", "c1=&RedImage c3=&BlueImage create");
selectWindow(Image_Analysis);
run("Threshold...");
```

B3. Microglia analysis macro

```
for (i = 0; i < 60; i++) {
Original_ImageTitle=getTitle();
filep = "E:/Microglia_Threshold/1822/"; # path to file will be specific in your machine
run("Z Project...", "projection=[Max Intensity]");
ImageTitle=getTitle();
run("Split Channels");
selectWindow(Original_ImageTitle);
close();
selectWindow(ImageTitle+" (blue)");
close();
selectWindow(ImageTitle+" (red)");
close();
selectWindow(ImageTitle+" (green)");
setAutoThreshold("Li dark");
run("Convert to Mask");
thres_image=getTitle();
selectWindow(thres_image);
run("Options...", "iterations=3 count=5 do=Open");
run("Analyze Particles...", "size=40-Infinity show=Masks display summarize add");
analized = getTitle();
saveAs("jpeg", filep+analized);
selectWindow(analized);
close();
selectWindow(ImageTitle+" (green)");
close();
roiManager("save", filep+analized+".zip");
close("ROI Manager");
}
```

APPENDIX C. Evaluation of autofluorescence

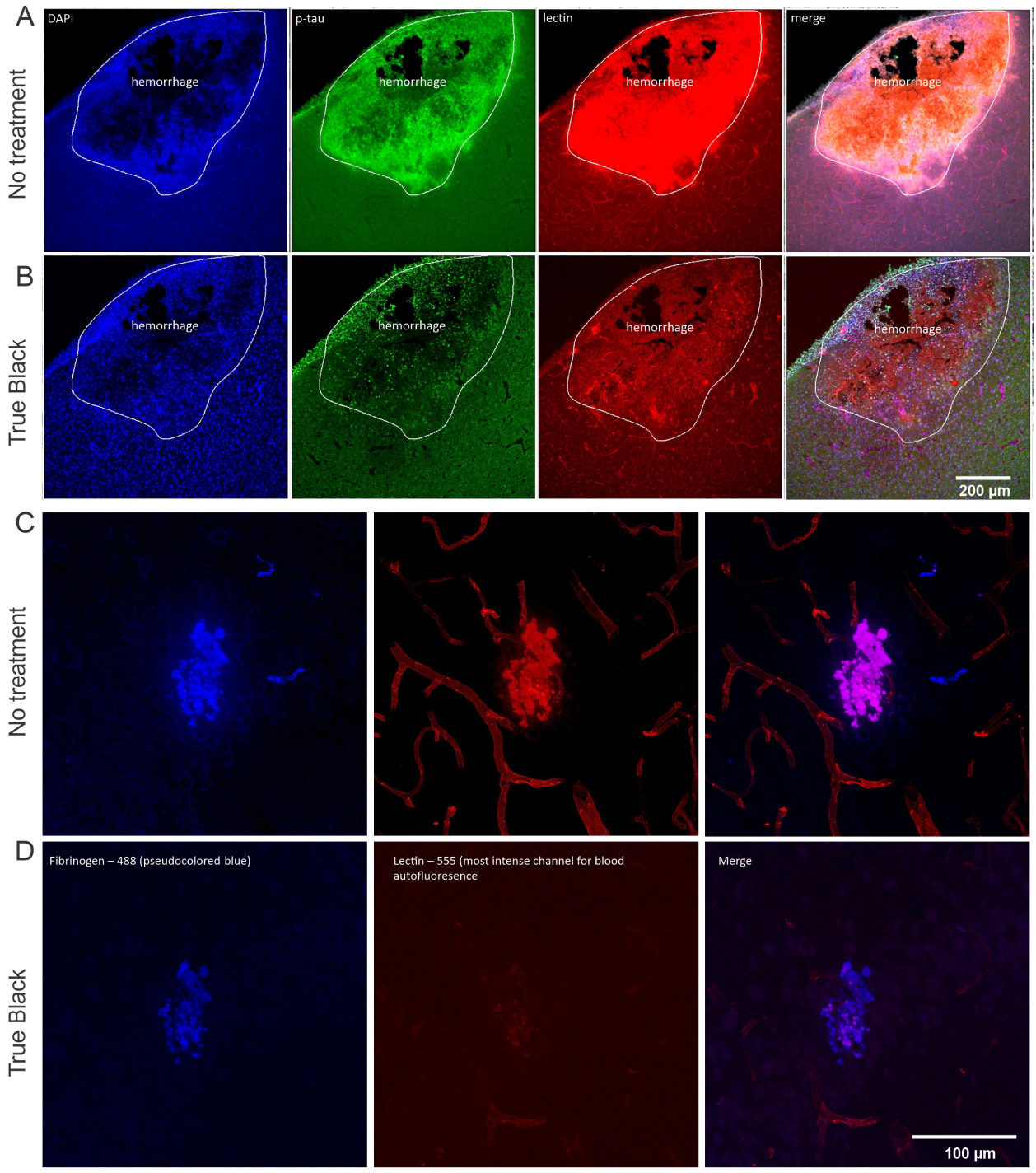

C1. Treatment of blood autofluorescence using True Black. (A, B) positive control of cerebral hemorrhage used to evaluate the usage of True black to quench autofluorescence. We can see how True black treatment **(B)** greatly reduces blood and tissue autofluorescence and allows a better visualization of the other fluorescence channels. **(C, D)** A similar treatment was used for sections analysed for presence of leaked

fibrinogen and we can see how again, True Black reduces autofluorescence caused by RBCs. Note that repetitive confocal imaging of this microbleed caused photobleaching of the WGA channel, thus reducing vessel visualization.

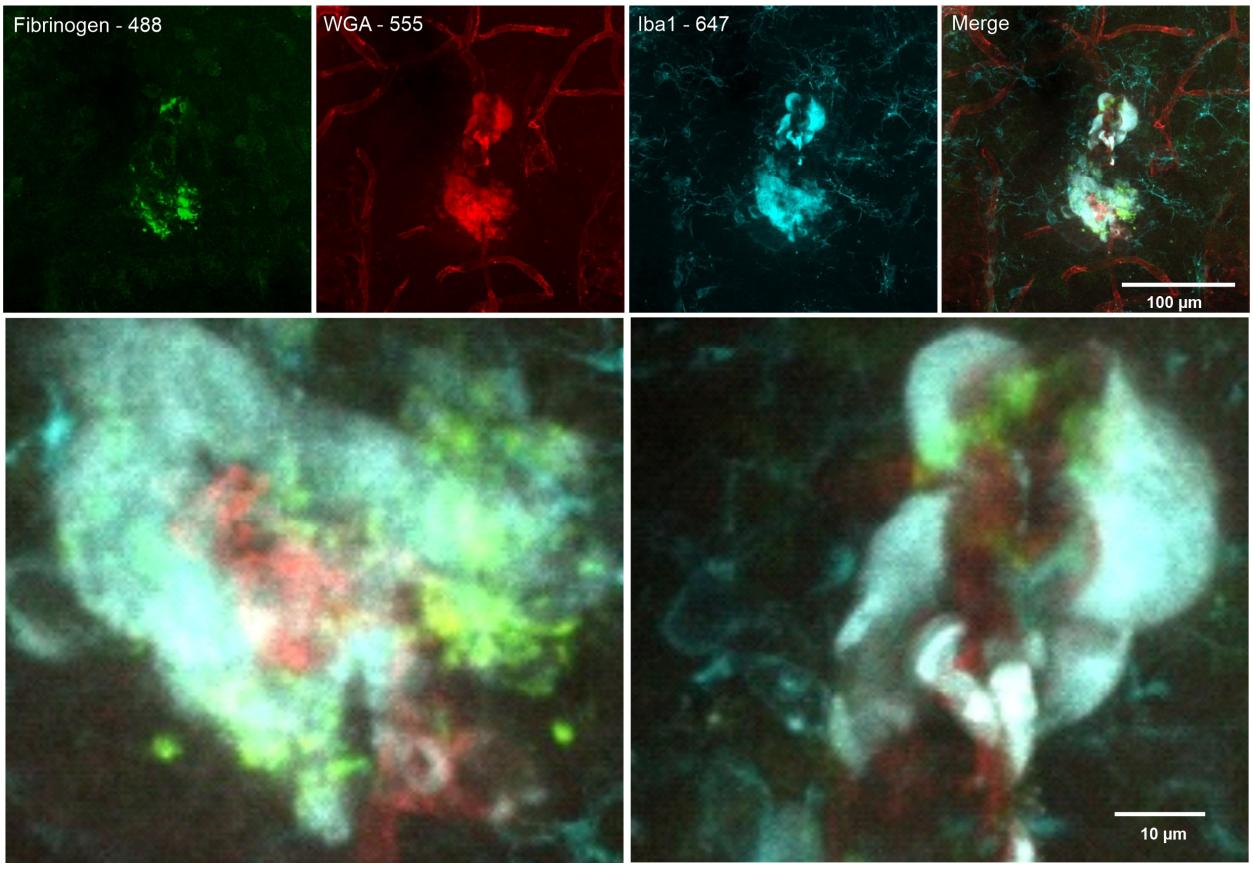

C2. Leaked fibrinogen can be differentiated from RBCs autofluorescence in microbleeds. (Top panel) We can observe the common "puncta" patter staining of leaked fibrinogen in a microbleed independent of autofluorescence from RBCs. We have to keep in mind that microglia and macrophages have lectin receptors, therefore fluorescent WGA can also bind to these receptors and increase the signal overlap on different channels for these cells. **(bottom panel)** We can see two images with merged fluorescent channels at a higher magnification depicting differences from green (fibrinogen – Alexa488), red (mainly WGE – Alexa555, but also potential RBC autoflorescence and WGA bound to microglia) and far red channels (Iba1 – Alexa647).

APPENDIX D. Assessment of naïve controls

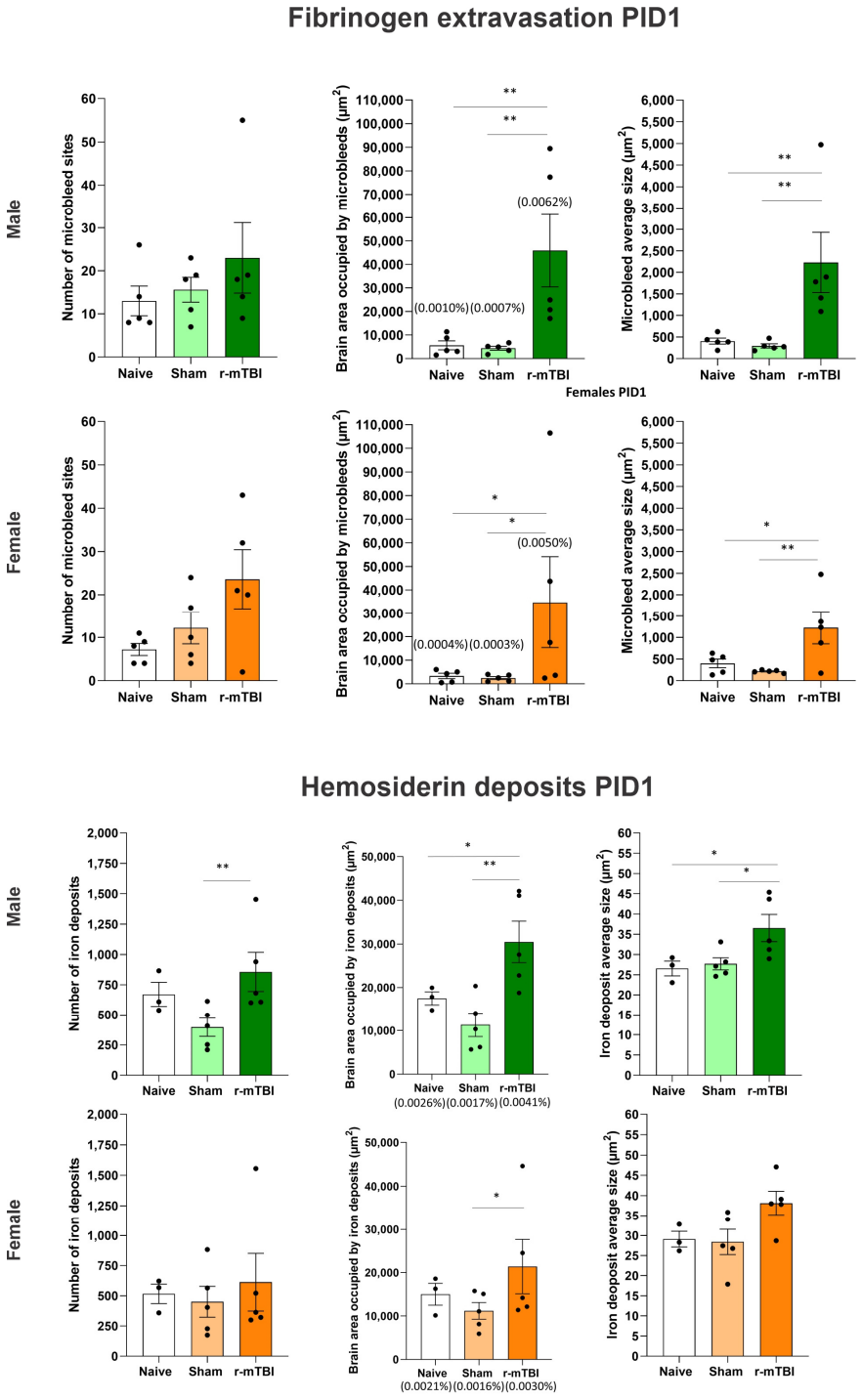

D1. Naïve and sham animals presented equivalent results in all the measures used to evaluate fibrinogen extravasation and hemosiderin deposits. These results suggest that the ACHI procedure was not artificially creating signs of microbleeds in sham animals. It is possible that the non-significant reduction observed in sham animals compared to naïve could be explained by increased handling, but with these results this is only speculation *p<0.1; **p<0.05.